Aus dem Max von Pettenkofer-Institut für Hygiene und Medizinische Mikrobiologie
Lehrstuhl für Medizinische Mikrobiologie und Krankenhaushygiene
der Ludwig-Maximilians-Universität München

Leitung: Prof. Dr. Sebastian Suerbaum

Analysis of the *Helicobacter pylori* CagA translocation process and its inhibition by novel small molecule inhibitors

Dissertation
zum Erwerb des Doktorgrades der Naturwissenschaften
an der Medizinischen Fakultät der
Ludwig-Maximilians-Universität München

vorgelegt von
Clara Madalena Lettl
aus Augsburg

2021

Mit Genehmigung der Medizinischen Fakultät
der Universität München

Betreuer: Prof. Dr. Rainer Haas
Zweitgutachter: Prof. Dr. Andreas Ladurner

Dekan: Prof. Dr. med. Thomas Gudermann
Tag der mündlichen Prüfung: 16.03.2022

Eidesstattliche Versicherung

Ich, Clara Madalena Lettl, erkläre hiermit an Eides statt, dass ich die vorliegende Dissertation mit dem Thema

Analysis of the *Helicobacter pylori* CagA translocation process and its inhibition by novel small molecule inhibitors

selbständig verfasst, mich außer der angegebenen keiner weiteren Hilfsmittel bedient und alle Erkenntnisse, die aus dem Schrifttum ganz oder annähernd übernommen sind, als solche kenntlich gemacht und nach ihrer Herkunft unter Bezeichnung der Fundstelle einzeln nachgewiesen habe.
Ich erkläre des Weiteren, dass die hier vorgelegte Dissertation nicht in gleicher oder in ähnlicher Form bei einer anderen Stelle zur Erlangung eines akademischen Grades eingereicht wurde.

Augsburg, 19.03.2022 Clara Lettl

Teile dieser Arbeit wurden veröffentlicht unter folgenden Titeln:

- **Lettl C**[§], Schindele F[§], Testolin G, Bär A, Rehm T, Brönstrup M, Schobert R, Bilitewski U, Haas R, Fischer W (2020): Inhibition of Type IV Secretion Activity and Growth of *Helicobacter pylori* by Cisplatin and Other Platinum Complexes. *Front. Cell. Infect. Microbiol*. 10:788

- **Lettl C**, Haas R, Fischer W (2021): Kinetics of CagA type IV secretion by *Helicobacter pylori* and the requirement for substrate unfolding. *Mol. Microbiol*. (online verfügbar seit 14.06.2021)

- Steiner TM[§], **Lettl C**[§], Schindele F, Goebel W, Haas R, Fischer W, Eisenreich W (2021): Substrate usage determines carbon flux via the citrate cycle in *Helicobacter pylori*. *Mol. Microbiol.* (online verfügbar seit 23.06.2021)

Weitere Publikationen im Promotionszeitraum, die nicht in dieser Arbeit enthalten sind:

- Moteshareie H, Hajikarimlou M, Mulet Indrayanti A, Burnside D, Paula Dias A, **Lettl C**, Ahmed D, Omidi K, Kazmirchuk T, Puchacz N, Zare N, Takallou S, Naing T, Hernández RB, Willmore WG, Babu M, McKay B, Samanfar B, Holcik M, Golshani A (2018): Heavy metal sensitivities of gene deletion strains for ITT1 and RPS1A connect their activities to the expression of URE2, a key gene involved in metal detoxification in yeast. *PLOS ONE* 13 (9):e0198704

- Honold A, **Lettl C**, Schindele F, Illarionov B, Haas R, Witschel M, Bacher A, Fischer M (2019): Inhibitors of the Bifunctional 2-*C*-Methyl-D-erythritol 4-Phosphate Cytidylyl Transferase/2-*C*-Methyl-D-erythritol-2,4-cyclopyrophosphate Synthase (IspDF) of *Helicobacter pylori*. *HCA* 102 (3):e1800228

- **Lettl C**, Fischer W (2020): Export von Gefahrgut: *Helicobacter pylori* und sein CagA-Protein. *Biospektrum* 26 (6):597–599

([§] geteilte Erstautorenschaft)

Table of contents

Abstact

Secretion systems are a prerequisite of many pathogenic bacteria to colonize the host and to induce severe diseases. The human gastric pathogen *Helicobacter pylori* uses the Cag type IV secretion system (CagT4SS) to inject its effector protein, the cytotoxin-associated gene A (CagA) into eukaryotic cells. Upon translocation, CagA interacts with a plethora of proteins, thus hijacking cellular signaling cascades. This aberrant cell reprogramming is a major cause of the development of severe malignant disorders of the stomach.

Concerning the rapid emergence of *H. pylori* strains that are resistant to commonly used antibiotics, novel treatment strategies are urgently needed. Targeting bacterial secretion systems is a promising strategy to develop new therapeutics that inhibit the delivery of virulence factors or the spread of antibiotic resistance. Indeed, in case of several type III secretion systems (T3SS), the inability to translocate or secrete the effector proteins due to mutations or chemical inhibition was proven to be sufficient to prevent or clear an infection. While CagA translocation-deficient *H. pylori* strains are still able to colonize the stomach, the delivery of CagA is associated with severe disease progression. Hence, inhibiting CagT4SS activity is an auspicious approach to prevent the development of malignant disorders and might furthermore be used to boost antibiotic treatment regimens.

In the last decades, huge progress was made, deciphering the structure of the CagT4SS and characterizing the cargo protein CagA, but little is known about the secretion process itself. To further analyze CagA translocation, a split-luciferase-based reporter assay was developed, which represents the first possibility to monitor CagT4SS activity *in vitro* in real time. In addition, the assay was adapted to conduct endpoint measurements. Due to the high sensitivity and time resolution, the reporter assay could be implemented to get novel insights into the kinetics and mode of action of the secretion process: Beside a fast onset of CagA translocation observed within less than 15 min after co-incubation with the host cells, the oncoprotein delivery was soon saturated and only a minor part of the total available bacterial CagA pool got injected. Furthermore, various experiments indicated, that unfolded protein is required for the translocation via the secretion apparatus. Finally, CagB was identified as a novel factor involved in Cag type IV secretion activity, whose exact function has to be further investigated.

In addition to the functional investigation on the CagT4SS, two groups of inhibitors directly interfering with CagA translocation were characterized: The commonly used anti-cancer drug cisplatin was shown to block T4SS activity via a protein interaction-based mechanism that might be distinct from its growth-arresting activities. Furthermore, small molecule compounds targeting the quinone-binding pocket of the respiratory chain complex I were not only species-specific and highly potent inhibitors of *H. pylori* growth, but also directly interfered with CagA translocation, most likely due to the immediate depletion of bacterial ATP levels.

Zusammenfassung

Für zahlreiche bakterielle Pathogene ist die Fähigkeit, Effektorproteine mittels Sekretionssystemen in Wirtszellen zu translozieren, eine wesentliche Voraussetzung zur Kolonisierung und zur Verursachung schwerer Krankheitsverläufe. Etwa die Hälfte der Weltbevölkerung ist mit *Helicobacter pylori* infiziert, einem Bakterium, das ausschließlich den menschlichen Magen besiedelt und dort mittels eines Typ IV-Sekretionssystems (T4SS) das Oncoprotein CagA (Cytotoxin-assoziiertes Gen A) in die Epithelzellen injiziert. In den Wirtszellen interagiert CagA mit einer Vielzahl an zellulären Proteinen und führt dadurch zu veränderten Signalwegen, was wiederum die Entwicklung von bösartigen Tumoren begünstigt. Auch wenn Behandlungsmöglichkeiten mit dem Ziel der Eradikation der Bakterien bisher noch zur Verfügung stehen, so erfordert die enorme Entwicklung von Resistenzen die Suche nach neuen, innovativen Ansätzen. Bakterielle Sekretionssysteme sind ein vielversprechender Angriffspunkt neuartiger Therapeutika, da so die Virulenz der jeweiligen Pathogene geschwächt werden kann. Inhibitoren von Typ III-Sekretionssystemen konnten zum Beispiel schon erfolgreich eingesetzt werden, um Infektionen im murinen Modell zu verhindern. Zwar können auch *H. pylori*-Stämme, die kein CagA translozieren, den human Magen kolonisieren, jedoch sind diese Stämme deutlich weniger pathogen, d. h. das Risiko Magenkarzinome zu verursachen ist wesentlich geringer. Die Entwicklung von CagT4SS-Inhibitoren ist daher ein möglicher Ansatz, um schwere Krankheitsverläufe zu verhindern, aber auch um bestehende antibiotische Behandlungen zu unterstützen.

In den letzten Jahren wurden viele neue Erkenntnisse über die Struktur und Funktion des Sekretionsapparats und des Effektorproteins CagA erlangt, doch der Translokationsprozess an sich ist noch weitgehend unerforscht. Daher wurde in dieser Arbeit ein Lumineszenz-basierter Assay entwickelt, der es zum ersten Mal ermöglicht, *in vitro* die Translokation von CagA in Echtzeit zu detektieren. Das System wurde zudem für zahlreiche Endpunktmessungen adaptiert. Aufgrund der hohen Sensitivität und zeitlichen Auflösung des Assays konnten neue Erkenntnisse hinsichtlich der Kinetik und der Funktionsweise der Translokation gewonnen werden. So konnte gezeigt werden, dass bereits innerhalb kürzester Zeit nach Beginn der Infektion *in vitro* große Mengen CagA in die Wirtszellen gebracht werden, doch ist dieser Prozess rasch gesättigt und es wird nur ein minimaler Anteil der gesamten zur Verfügung stehenden CagA-Menge transloziert. Des Weiteren können wohl nur entfaltete Proteine mittels des CagT4SS transportiert werden. Schließlich wurde CagB als ein neuer Faktor identifiziert, der auf bislang unbekannte Weise in den Sekretionsprozess involviert ist.

Parallel zur funktionalen Charakterisierung der CagA-Translokation wurden zwei Substanzklassen, die direkt inhibitorisch auf das T4SS wirken, untersucht. Es konnte gezeigt werden, dass Cisplatin und weitere Platinkomplexe, deren DNA-Bindekapazität häufig zur Tumortherapie eingesetzt wird, unmittelbar über Protein-basierte Wechselwirkungen die

CagA-Translokation hemmen, wobei dieser Effekt auf das Typ IV-System wohl unabhängig von Wachtumsinhibition und DNA-Interaktion ist. Für eine Gruppe von Substanzen, die in der Chinon-Bindetasche des Komplexes I der Atmungskette binden, konnte zum einen die hohe Potenz gegenüber *H. pylori* und die Speziesspezifität gezeigt und erklärt werden, zum anderen wurde der neu entwickelte Translokationsassay angepasst, um die direkte Wirkung dieser Inhibitoren auf die CagA-Translokation zu belegen. Verschiedene Experimente deuten darauf hin, dass der unmittelbare Effekt auf die Typ IV-Sekretionsmaschinerie wohl in dem drastischen Rückgang des bakteriellen ATP Levels begründet ist.

1 Introduction

1.1 One century of antibiotic treatment and the rise of antimicrobial resistance

In the early 20th century, Paul Ehrlich believed in the existence of a “magic bullet”, a chemical compound that would kill pathogens without harming the human body. Indeed, in 1929 Alexander Fleming incidentally identified bactericidal and bacteriolytic properties of penicillin a secondary metabolite isolated from a mold of the genus *Penicillium* (Fleming, 1929). In the following decades this, and other antibiotics saved the lives of millions of people dramatically changing the leading cause of death. In 1900 pneumonia, tuberculosis, diarrhea and enteritis accounted for almost half (45.4 %) of all deaths in the US, 100 years later, in 1997, only 4.5 % of all deaths were caused by infectious diseases (mainly pneumonia, influenza and HIV). In contrast, heart diseases, cancer and stroke are now the leading causes of death. (Dodds, 2017; Centers for Disease Control and Prevention, 1999)

While the mortality due to infectious diseases is in general declining, antimicrobial resistance is on the rise, representing a major challenge of today’s health care. In his Nobel lecture in 1945 already, Alexander Fleming warned that underdosing and misusing penicillin bears the risk of developing resistance (Fleming, 1945).

Antimicrobial resistance in general can be classified in two groups: The genus- or species-specific intrinsic resistance, and the strain-specific acquired resistance (Van Duijkeren *et al.,* 2018). Lack or inaccessibility of the target, independency of the inhibited pathway, or efficient export and inactivation systems are the main reasons for intrinsic resistance (Van Duijkeren *et al.,* 2018; Arzanlou *et al.,* 2017). Gram-negative bacteria for example are in general less susceptible to many drugs, since the lipopolysaccharide (LPS)-containing outer membrane presents a penetration barrier (Arzanlou *et al.,* 2017). On the other hand, *Mycoplasma* spp. that have no cell wall are intrinsically resistant to β-lactam antibiotics, such as the above-mentioned penicillin (Taylor-Robinson and Bébéar, 1997).

Acquired resistance implies the incorporation of foreign resistance genes or spontaneous mutation. Again, up-regulation of multidrug efflux pumps or decreased influx and thus lower concentrations at the target site play a major role. Enzymatic drug inactivation reactions might account for resistance, too. Moreover, alterations of the target sites themselves by mutations or chemical modifications might occur. (Van Duijkeren *et al.,* 2018)

Today, we know, that uncompleted treatment regimens or too low dosing are the driving forces for the emergence of antimicrobial resistance. Furthermore, prophylactic or non-therapeutic antibiotic use in farm animals are causative for increasing resistance rates (Dodds, 2017).

According to the world health organization (WHO) at least 700,000 people per year die due to infections with drug-resistant microorganisms globally (WHO, 2019). At the same time the WHO raises concerns regarding declining efforts of the global pharmaceutical industry to develop new antibiotics, insufficient clinical pipelines, and missing innovation (WHO, 2019).

Thus, intensive research is needed to extend our spectrum of available antibiotics and to improve therapeutic strategies. In contrast to the broad-spectrum antibiotics commonly used so far, novel antibiotics should be highly species-specific, thus being harmless for the patient and his commensal microbiome and extending the original idea of Paul Ehrlich.

Additionally, a promising approach to circumvent the emergence of resistant strains is the identification and development of pathoblockers, *i.e.* of inhibitors targeting important virulence factors of the pathogens instead of killing them (Dickey *et al.,* 2017). Indeed, for some T3SS it was already shown that the inability to translocate or secrete the effector proteins due to mutations or chemical inhibition is sufficient to prevent or clear an infection (Pendergrass and May, 2019). Deeper knowledge on the respective pathogens, their virulence factors and their resistance behavior is crucial to develop new therapeutic strategies.

A bacterium that is in the focus of current research and development for novel antibiotics is the human pathogen *Helicobacter pylori*. Even though consensus treatment strategies are available, antibiotic resistance rates towards the therapeutically used antibiotics are increasing to an alarming level worldwide, causing dramatic decreases in treatment efficacy (Fallone *et al.,* 2016). Especially the clarithromycin-containing regimens, commonly used so far, are now frequently insufficient for successful eradication (Savoldi *et al.,* 2018). Consequently, clarithromycin-resistant *H. pylori* strains were listed on the WHO´s priority list for research and development of new antibiotics in 2017 (Tacconelli *et al.,* 2018).

1.2 The gastric pathogen *H. pylori*

Already prior to the out of Africa migration of anatomically modern humans 60,000 years ago, *H. pylori* colonized the human stomach. Indeed, genome analysis could prove a co-evolution for more than 100,000 years. (Moodley *et al.,* 2012)

In the early 1980s, B. J. Marshall and J. R. Warren identified the link between an *H. pylori* infection and the development of gastric diseases (Warren and Marshall, 1983; Marshall and Warren, 1984; Marshall *et al.,* 1985). Since 1994, *H. pylori* is the first and only bacterium classified as a human carcinogen (IARC Working Group on the Evaluation of Carcinogenic Risks to Humans, 1994). Accounting for more than 800,000 new cases of gastric cancer per year (2018), *H. pylori* is clearly the most important infectious cause of cancer (De Martel *et al.,* 2020). Worldwide approximately 50 % of the human population is chronically infected with the pathogen, albeit with major regional variations (Hooi *et al.,* 2017).

1.2.1 Transmission, epidemiology and associated diseases

The spiral-shaped, highly motile, microaerophilic ε-proteobacterium exclusively colonizes the human gastric mucosa. In most cases, *H. pylori* is acquired during childhood and persists life-long, if not eradicated by antibiotic treatment. Details of transmission are not understood completely, but oral-oral, gastro-oral and fecal-oral routes are the most likely ones (Kayali *et*

al., 2018). Furthermore, primarily in developing countries, infections caused by contaminated drinking water are discussed (Aziz *et al.,* 2015). In general, *H. pylori* is passed intra-familiar, as vertical transmission from mother to child is the main cause of infection (Weyermann *et al.,* 2009; Osaki *et al.,* 2015; Mamishi *et al.,* 2016). Even though improved sanitation, the access to clean water and a higher socioeconomic status are associated with declining infection rates, approximately 4.4 billion people were colonized by *H. pylori* in 2015 (Hooi *et al.,* 2017). Although infections are prevalent worldwide, clear differences regarding the bacterial dissemination are observed between continents (*e.g*. Africa 70.1 %, Oceania 24.4 %), countries (*e.g*. Nigeria 87.7 %, Switzerland 18.9 %), and even between population groups within the same country (*e.g*. Alaskan native population 75 %, non-Hispanic whites in the US 18.4-26.6 %) (Hooi *et al.,* 2017). Overall, *H. pylori* infections are predominately found in rural developing areas (>80 % dissemination), while infection rates in urban developed zones are considerably lower (<40 %) (Kayali *et al.,* 2018).

There is a huge discrepancy between infection prevalence and gastric cancer incidence: for example, many individuals in sub-Saharan regions, India and Bangladesh are infected with the bacterium, while severe pathologies are comparably rare (Holcombe, 1992; Miwa *et al.,* 2002). Indeed, the clinical course of an *H. pylori* infection is strongly influenced by the genetic predisposition of the respective human host, by microbial factors of the colonizing strains (see section 1.3.3) and by lifestyle factors like smoking or diet (Suerbaum and Michetti, 2002; Atherton, 2006).

The initial, acute phase of infection is mostly asymptomatic. Although an acute immune response (*e.g.* interleukin-8 (IL-8) secretion) is induced, it is mostly not sufficient for bacterial clearance, resulting in a chronic infection. (Dixon, 2001)

In the course of disease, almost all infected subjects develop a chronic gastritis. While this remains asymptomatic in most cases (80-90 %), at the same time it is significantly associated with a higher risk to develop severe diseases (Dooley *et al.,* 1989; Suerbaum and Michetti, 2002). Antral-predominant gastritis, which is the most common *H. pylori* induced inflammation, is a predisposition to develop duodenal ulcer (Suerbaum and Michetti, 2002; Atherton, 2006). Corpus-predominant or pan gastritis on the other hand increases the risk for gastric ulcer and gastric cancer, that is the third leading cause of cancer-related death (Atherton, 2006; Bray *et al.,* 2018). Additionally, a rather rare complication almost exclusive for *H. pylori* infections is primary gastric non-Hodgkin's lymphoma. Mucosa-associated lymphoid tissue (MALT) is absent in a healthy stomach, but is induced upon *H. pylori* infection (Genta *et al.,* 1993), this in turn is the main reason (72-98 %) for such malignant lymphoma (Parsonnet *et al.,* 1994; Wotherspoon, 1998). It is worth mentioning, that an early diagnosis and a subsequent eradication of *H. pylori* can lead to the remission of MALT lymphoma (Stolte *et al.,* 2002), underlining the importance of effective treatment strategies.

Altogether, approximately 10 % of infected individuals develop peptic ulcer disease, 1-3 % gastric adenocarcinoma, and <0.1 % MALT lymphoma (Wroblewski *et al.,* 2010). Thus, *H. pylori* infections account for about 5.5 % of the global cancer burden (Parkin, 2006).

1.2.2 Treatment strategies and challenges

Already in the 1990s, the awareness of the health hazard connected to an *H. pylori* infection prompted efforts to develop a vaccine. Even though experiments in mouse models initially seemed quite promising, immunization turned out not to be sufficient to completely protect against an *H. pylori* infection: vaccination of mice could only reduce bacterial load, but rarely achieved sterilizing immunity (Sutton and Chionh, 2013). Meanwhile, several attempts of prophylactic and therapeutic vaccinations failed, since they did not translate well from the animal model to the human situation (Sutton and Boag, 2019). A major challenge in the development of novel immunization strategies is the intrinsic ability of *H. pylori* to escape the host immune system. The bacterium can evade and sophisticatedly manipulate the innate and the adaptive immune response: for example, pathogen-associated molecular patterns (PAMPs) like LPS or flagellin are evolved to circumvent recognition by Toll-like receptors (TLRs) that would trigger a pro-inflammatory response (Cullen *et al.,* 2011; Andersen-Nissen *et al.,* 2005). Simultaneously, anti-inflammatory signaling cascades via TLR2 and TLR9 or C-type lectin receptors are preferentially activated (Salama *et al.,* 2013). In addition, two secreted virulence factors, the vacuolating cytotoxin (VacA) and the γ-glutamyl transpeptidase (GGT), actively suppress the adaptive immune response by interfering with T-cell proliferation and activation (Gebert *et al.,* 2003; Schmees *et al.,* 2007). Further virulence factors that protect *H. pylori* from elimination by the immune system are discussed in section 1.3.2.

A characteristic feature of the bacterium that is not only involved in immune evasion but also in the development of drug resistance, is its immense genetic diversity and volatility.

This is on the one hand caused by an extremely elevated mutation rate due to the absence of many enzymes involved in DNA damage repair, the presence of several hyper-mutable genes subjected to slipped-strand mispairing-mediated variation and numerous repetitive sequences allowing intragenomic deletions or rearrangements (Björkholm *et al.,* 2001; Suerbaum and Josenhans, 2007; Salaün *et al.,* 2004; Aras *et al.,* 2003). On the other hand, *H. pylori* is naturally competent and possesses conjugation systems for horizontal gene transfer (Hofreuter *et al.,* 1998; Fischer *et al.,* 2010). Together, this enables an in-host microevolution and adaption that plays a major role in the success of establishing a chronic colonization of the human stomach (Suerbaum and Josenhans, 2007). Yet, it was shown, that during the acute phase of infection, the overall mutational rate of the bacteria is even increased, accumulating changes in genes encoding outer membrane proteins (OMPs) and allowing for a fast adaption to the respective environment (Linz *et al.,* 2014).

Besides the absence of a prophylactic vaccination, several antibiotic treatment strategies are available, although resistances to the commonly used drugs are emerging. In general, only symptomatic individuals are subjected to diagnosis and subsequent therapy. Once a complete elimination is achieved, reinfection rates are low ensuring a long lasting benefit of the treatment (Suerbaum and Michetti, 2002). A successful *H. pylori* eradication requires the consequent taking of up to four different drugs for 7 to 14 days. The combination of several antibiotics lowers the risk of antimicrobial resistance development. Currently, first line quadruple therapies including a proton-pump inhibitor (PPI) in combination with bismuth, metronidazole and tetracycline or in combination with amoxicillin, metronidazole and clarithromycin are recommended. In areas with low clarithromycin resistance rates, triple therapies consisting of a PPI combined with clarithromycin and amoxicillin or metronidazole are used. As a second line therapy option, combinations with levofloxacin or rifabutin are available. (Fallone *et al.,* 2016; Malfertheiner *et al.,* 2017)

PPIs like omeprazole increase the gastric pH, thereby enhancing the solubility and bioavailability of the co-administered antibiotics. Bismuth salts, *e.g*. ranitidine bismuth citrate, inhibit gastric acid secretion, and additionally have antibacterial effects against *H. pylori* (Lambert and Midolo, 1997). So far, the exact mode of action of bismuth salts on the bacteria is not understood, but it is assumed that several mechanisms play together including interference with bacterial membrane integrity, ATP synthesis and adherence (Alkim *et al.,* 2017). Clarithromycin is a macrolide antibiotic interfering with translation by binding to the 23S rRNA of the 50S ribosomal subunit. Several resistance mechanisms are known, amongst others increased drug efflux or point mutations in the 23S rRNA (Dinos, 2017), the latter being the main reason for resistance in *H. pylori* (Versalovic *et al.,* 1997). Like clarithromycin, tetracycline inhibits protein biosynthesis: it binds to the 16S rRNA of the 30S ribosomal subunit and prevents aminoacyl-tRNA binding. Again, increased drug efflux is a reason for resistance, but for *H. pylori* mutations at the target site, the 16S rRNA, are more relevant (Arslan *et al.,* 2017). Amoxicillin is a bactericidal broad-spectrum β-lactam antibiotic. Its interaction with penicillin-binding proteins (PBPs) causes the inhibition of cell wall synthesis. The production of β-lactamases and mutations in the PBPs are potential mechanisms of *H. pylori* to gain resistance against amoxicillin (Tseng *et al.,* 2009; Rimbara *et al.,* 2008). The nitroimidazole antibiotic metronidazole causes DNA damage and acts as a mutagen. Metronidazole must be activated by intracellular nitroreductases, for example by the oxygen-insensitive NADPH nitroreductase RdxA (Arslan *et al.,* 2017). Several resistance mechanisms are described for metronidazole, with *rdxA* inactivation being the predominant one (Wang *et al.,* 2001).

The two drugs used as backups in second line treatment regimens target DNA replication and mRNA synthesis. Levofloxacin inhibits gyrase activity and belongs to the third generation of fluoroquinolones. Rifabutin, that is closely related to rifampicin, blocks the DNA-dependent

RNA polymerase. In both cases, mutations in the target gene – *gyrA* or *rpoB* respectively – can confer resistance. (Arslan *et al.,* 2017)

To combat the enormous emergence of resistance, susceptibility-guided treatment strategies are reasonable. They are especially recommended if first and second line therapies failed or in regions with high prevalence for clarithromycin resistance (Malfertheiner *et al.,* 2017).

1.3 Virulence factors of *H. pylori* – Targets for pathoblockers

The natural habitat of *H. pylori*, the human stomach, is very hostile and was for many years considered to be sterile. A multitude of virulence factors enable the bacteria to establish the persistent colonization under harsh conditions. Other virulence factors are directly linked to the clinical outcome of an infection. The risk to develop severe gastric diseases for example is significantly higher if the colonizing strains produce the protein toxins CagA or VacA, or if the bacteria express certain adhesins (Chang *et al.,* 2018). Thus, disarming the pathogen by targeting its virulence factors is a promising approach to complement existing therapeutic regimens.

The virulence factors of *H. pylori* can be classified in three categories (Chang *et al.,* 2018) and are discussed in the following sections.

1.3.1 Virulence factors involved in establishing a colonization

Once inside the human stomach, *H. pylori* is exposed to harsh acidic conditions, *i.e*. pH 2 in the lumen of the stomach. To protect themselves, the bacteria produce high amounts of Ni^{2+}-dependent urease. This enzyme converts urea to ammonia and CO_2, thus buffering the bacterial cytosol and periplasm and generating a protective neutral layer around the bacteria. (Montecucco and Rappuoli, 2001)

Nevertheless, animal experiments using Mongolian gerbils could show that the bacteria can only survive for a limited time (about 30 min) at pH 2 (Schreiber *et al.,* 2005). Hence, *H. pylori* must quickly pass the acidic lumen and get through the thick mucus layer to finally reach the stomach mucosa. Up to six unipolar flagella enable the bacteria to overcome gastric peristalsis and once they reach the mucus, they can corkscrew through the viscous environment due to their helical shape (Spohn and Scarlato, 2001; Hazell *et al.,* 1986). Again, urease activity plays an important role, since the elevated local pH alters mucus viscosity (Celli *et al.,* 2009). The directed movement from the gastric lumen to the final habitat, the gastric mucosa, is guided by chemotaxis: various gradients, from amino acids like glutamine, to mucin, urea and bicarbonate are sensed by the bacteria (Spohn and Scarlato, 2001). Finally, the bacteria tightly adhere to the gastric epithelial cell layer via a repertoire of OMPs which act as adhesins, to prevent moving back into the gastric lumen and to establish a stable colonization. A sophisticated modulation of these OMPs allows the rapid adaption to changing environmental conditions. (Bonsor and Sundberg, 2019)

The interaction of the blood group antigen-binding adhesin A (BabA) with its cellular receptor Lewis b (Le^b), for example, is highly pH-dependent. At pH 6, BabA binds with high affinity, but with decreasing pH the affinity strongly declines, resulting in a more than 20,000 fold reduction at pH 2 (Bugaytsova *et al.,* 2017). Hence, on the one hand the bacteria can tightly adhere to epithelial cells, but on the other hand can detach and escape from mucosal debris that is shed into the gastric lumen to swim back to the gastric epithelial layer. Additionally, the alteration of OMP patterns is a powerful strategy to avoid an eliminating immune response (Bonsor and Sundberg, 2019).

Other important bacterial adhesins with known interaction partners are for example the sialic acid-binding protein A (SabA) that recognizes sialylated glycans (Mahdavi *et al.,* 2002) or AlpA and AlpB (adherence-associated lipoproteins A and B), that strongly bind the extracellular matrix component laminin (Senkovich *et al.,* 2011).

Two further OMPs – OipA (outer inflammatory protein A) and HopQ (*Helicobacter* outer membrane protein Q) – will be discussed in the following sections.

In several studies the essentiality of urease activity (Eaton and Krakowka, 1994), flagellar movement (Eaton *et al.,* 1996), helical shape (Bonis *et al.,* 2010), chemotaxis (Terry *et al.,* 2005) and adhesion (De Jonge *et al.,* 2004) for successful colonization was proven. Consequently, several approaches to identify inhibitors of these virulence factors are under investigation (Ménard *et al.,* 2014; Tarsia *et al.,* 2018; Masetti *et al.,* 2020).

1.3.2 Virulence factors enabling immune escape

An *H. pylori* infection triggers a chronic inflammation (gastritis), *i.e.* for example the infiltration of immune cells in the mucosa, the secretion of pro-inflammatory cytokines and an elevated production of reactive oxygen species (ROS) and antimicrobial peptides. Thus, avoiding the elimination by the host immune system is directly connected to a successful colonization and essential to maintain the long-term persistence. Crucial features are the enormous genetic versatility, the low immunogenicity of PAMPs like LPS and flagellin and the secretion of VacA and GGT mentioned above. Additionally, the bacteria have evolved various virulence factors to avoid damage caused by ROS and reactive nitrogen intermediates produced by cells of the gastric mucosa in response to an *H. pylori* infection (Wang *et al.,* 2006; Davies *et al.,* 1994). Antioxidant enzymes that are secreted to the supernatant include superoxide dismutase (SOD) and catalase (Mori *et al.,* 1997). SOD scavenges superoxide by converting it to H_2O_2, which in turn is decomposed to H_2O and O_2 by catalase (Wang *et al.,* 2006). Furthermore, *H. pylori* constitutively produces the arginase RocF that competes with cellular nitric oxide (NO) synthetases for the substrate L-arginine and thus inhibits the production of harmful NO (Gobert *et al.,* 2001). RocF not only disarms part of the innate immune defense, but additionally interferes with the adaptive immune system by blocking T-cell proliferation (Zabaleta *et al.,* 2004). Notably, arginase and urease activity are directly connected, since the first one

hydrolyzes L-arginine to urea and ornithine and urea is then further converted to buffer the acidic environment as described above (Zabaleta *et al.,* 2004).

Finally, a unique and very sophisticated way to manipulate the immune response is the T4SS-dependent injection of CagA into various types of host cells. A more detailed description of CagA and the CagT4SS is given in section 1.4.

Amongst other effects, CagA translocation causes the inhibition of antimicrobial peptide expression by gastric epithelial cells. Human β-defensin 3 for example would be highly active against the bacteria, but its production is suppressed in a CagA translocation-dependent manner (Bauer *et al.,* 2012). Furthermore, CagA subverts the behavior of various specialist immune cells to the benefit of the pathogen. *In vitro* experiments using human granulocytes and differentiated HL-60 cells revealed that leukocyte migration is strongly impaired by translocated and subsequently phosphorylated CagA (Busch *et al.,* 2015).

Ex vivo studies from mice demonstrated that even though *H. pylori* is recognized by antigen-presenting cells, the bacteria circumvent an eliminating immune response for example by negatively modulating dendritic cells (DCs). The translocation of CagA into DCs was sufficient to suppress pro-inflammatory cytokine release and simultaneously promoted the production of anti-inflammatory IL-10. Additionally Cag type IV secretion activity interfered with DC maturation. (Tanaka *et al.,* 2010; Kaebisch *et al.,* 2014)

While *H. pylori* is equally phagocytosed by neutrophils independent of the presence of the cytotoxin (Odenbreit *et al.,* 2001), it was recently shown that CagA-positive strains have higher survival rates (Behrens, 2020). Notably, this effect was strongly dependent on the interaction of the adhesin HopQ with human carcinoembryonic antigen-related cell adhesion molecules (CEACAMs) that will be discussed in section 1.4.4.

As mentioned for virulence factors essential for successful colonization (1.3.1), several virulence factors enabling the escape from the host immune response are promising targets for pathoblockers, since they are necessary to establish a chronic infection (Seyler *et al.,* 2001; Chevalier *et al.,* 1999; Wüstner *et al.,* 2017) or directly associated with a severe disease progression (see 1.3.3).

1.3.3 Virulence factors directly linked to disease induction

The clinical outcome of an *H. pylori* infection is strongly dependent on the genetic composition of the respective infecting strains. Various virulence factors, partly already mentioned in 1.3.1 and 1.3.2, directly trigger the course of disease. A small selection is discussed in this chapter.

Patients infected with strains producing certain variants of the cytotoxin VacA have an elevated risk to develop gastric adenocarcinoma or peptic ulcer disease (Chang *et al.,* 2018). VacA is a cytotoxin that acts on a variety of host cells including gastric epithelial cells and immune cells. Once internalized into epithelial cells, it disrupts many different cellular processes and induces the eponymous formation of cytoplasmic vacuoles. While most strains encode an intact *vacA*

open reading frame, sequence variations as well as different expression levels determine the cancerogenicity. (McClain *et al.,* 2017)

The two OMPs BabA and OipA are associated with a severe pathogenesis (Chang *et al.,* 2018). In case of BabA, the exact mechanisms are not yet understood, but it is discussed, whether BabA can affect other virulence factors like the CagT4SS or OipA. Furthermore it is unclear whether BabA expression levels are cause or consequence of an elevated inflammation. (Fujimoto *et al.,* 2007)

OipA is one of the most important markers for the severity of gastric inflammation and subsequent clinical outcome (Yamaoka *et al.,* 2002). The 5´ region of the *oipA* gene is characterized by repetitive CT dinucleotides, whereby full-length protein synthesis is only possible if the number of these repeats allows an in frame transcript (Yamaoka *et al.,* 2000). The *oipA* "on" status, *i.e*. production of functional OipA, directly correlates with high bacterial load, elevated IL-8 secretion and neutrophil infiltration (Yamaoka *et al.,* 2002). Furthermore, *oipA* "on" is typically associated with a *cagA*-positive genotype (Ando *et al.,* 2002). So far, the cellular counterpart of this adhesin is unidentified.

Another central virulence factor of *H. pylori* is the high-temperature requirement A (HtrA) protease. To the current knowledge, HtrA is produced by any strain and essential for bacterial viability (Tegtmeyer *et al.,* 2016). It is very likely, that certain sequence polymorphisms are associated with an increased risk to develop gastric adenocarcinoma, but further research is needed (Chang *et al.,* 2018; Yeh *et al.,* 2019). HtrA is a serine protease and chaperone initially identified in *Escherichia coli* that is widely conserved amongst prokaryotes and eukaryotes (Strauch and Beckwith, 1988; Pallen and Wren, 1997). Intracellular HtrA is involved in the protein quality control and thus a crucial mechanism to maintain homeostasis under thermal, acidic, osmotic or antibiotic stress conditions (Zarzecka *et al.,* 2019). In case of *H. pylori*, HtrA is a bifunctional protein. Besides its intracellular function as chaperone and protease, it can be secreted and subsequently cleaves E-cadherins, which causes the loss of cell-cell adherens junctions and thus the disruption of the epithelial barrier (Hoy *et al.,* 2010). It is postulated, that HtrA activity enhances CagA translocation into epithelial cells (Harrer *et al.,* 2017). Due to its central role in *H. pylori* viability and virulence, HtrA is an intensively studied target for novel inhibitors (Perna *et al.,* 2015; Tegtmeyer *et al.,* 2016; Rai *et al.,* 2018).

Finally, a high risk marker for the development of gastric adenocarcinoma, MALT lymphoma and peptic ulcer disease is the oncoprotein CagA in combination with a functional T4SS (Chang *et al.,* 2018). Translocated and phosphorylated CagA mediates a plethora of downstream processes involved in the malignant transformation of gastric cells. Targeting CagA translocation is a promising approach to develop pathoblockers since it only affects virulence but not viability of *H. pylori*. Furthermore, due to the uniqueness of the CagT4SS, such compounds would be species-specific. Indeed, they would even discriminate between highly virulent (CagA translocation positive) and less virulent (CagA translocation negative)

strains. This could be worthwhile, since there is some evidence that *H. pylori* infections in children might be associated with protection against allergic or chronic inflammatory disorders (Salama *et al.,* 2013).

A more detailed introduction into CagA and the CagT4SS is given in the following sections.

1.4 Disarming the pathogen by understanding its effector protein translocation

1.4.1 Type IV secretion systems – Overview and prototypical architecture

T4SS are highly versatile molecular nanomachineries found in a wide range of gram-positive and gram-negative bacteria as well as in some archaea. They can be functionally classified in (1) conjugative T4SSs that enable the contact-dependent transfer of DNA between microorganisms, (2) systems involved in DNA uptake from the extracellular space during transformation and (3) T4SSs that secrete or transfer effector molecules. Based on their molecular architecture they can further be divided into type IVA and type IVB secretion systems. T4ASSs are closely related to the VirB/D4 system discussed below, while T4BSSs are only distantly related. Examples for T4BSSs are the Dot/Icm (defect in organelle trafficking and intracellular multiplication) system of the intracellular pathogens *Coxiella burnetii* and *Legionella pneumophila*. (Wallden *et al.,* 2010)

The first identified and one of the best characterized T4SS is the VirB/D4 apparatus of *Agrobacterium tumefaciens* (Ward *et al.,* 1988; Li and Christie, 2018). Via this secretion system the phytopathogen injects single-stranded T-DNA copies as well as several cargo proteins into the host cells and thus induces tumor formation in the infected plants. The VirB/D4 T4SS is built up by twelve proteins, namely VirB1-VirB11 and VirD4. Closely related homologs of most of those proteins can be found in T4SS of other species (Wallden *et al.,* 2010), for example in the R388 conjugative plasmid encoded T4SS of *E. coli* for whom the molecular structure was solved using electron microscopy (Low *et al.,* 2014).

The prototypical T4SS consists of an outer membrane core complex (OMCC), an inner membrane complex (IMC) associated with three ATPases and an extracellular pilus. A schematic structure of the secretion apparatus is depicted in Figure 1.1.

The three putatively hexameric cytoplasmic ATPases are interacting with each other and together provide the energy for pilus biogenesis and substrate delivery. VirD4, the only protein not encoded on the *virB* operon, acts as type IV coupling protein and recruits DNA to further transfers it to the “traffic ATPase” VirB11 and the secretion apparatus. VirB11 and the third ATPase VirB4 are directly associated with the IMC. Electron microscopy studies revealed that VirB4 is tightly inserted into the inner membrane and organized as adjacent hexameric barrels. (Christie *et al.,* 2014; Li and Christie, 2018; Low *et al.,* 2014; Wallden *et al.,* 2010)

The IMC, composed of 12 copies of VirB3 and VirB8 and 24 copies of VirB6, forms a channel across the inner membrane, that is one postulated route for substrate transport (Bergé *et al.,* 2017; Li and Christie, 2018; Low *et al.,* 2014). VirB10 is a central component of the T4SS,

connecting the IMC and the OMCC and building up the periplasmic stalk as well as the outer membrane channel (Bergé *et al.,* 2017). In a 1:1:1 ratio, VirB10, VirB7 and VirB9 assemble to the 14-fold symmetry of the OMCC (Low *et al.,* 2014). VirB7 is a lipoprotein, that anchors in the outer membrane and interacts with the periplasmic VirB9 via its N-terminus (Bergé *et al.,* 2017).

A tubular pilus forms the extracellular part of the VirB/D4 secretion system that enables donor-host contact and possibly constitutes a channel to transfer T4SS substrates to the recipient cell. It is built up by the major pilus component, the pilin VirB2, and a minor pilus component, the putative adhesin VirB5. (Wallden *et al.,* 2010; Li and Christie, 2018)

Finally, the periplasmic muramidase VirB1 breaks down peptidoglycans, thus facilitating the T4SS assembly (Bergé *et al.,* 2017).

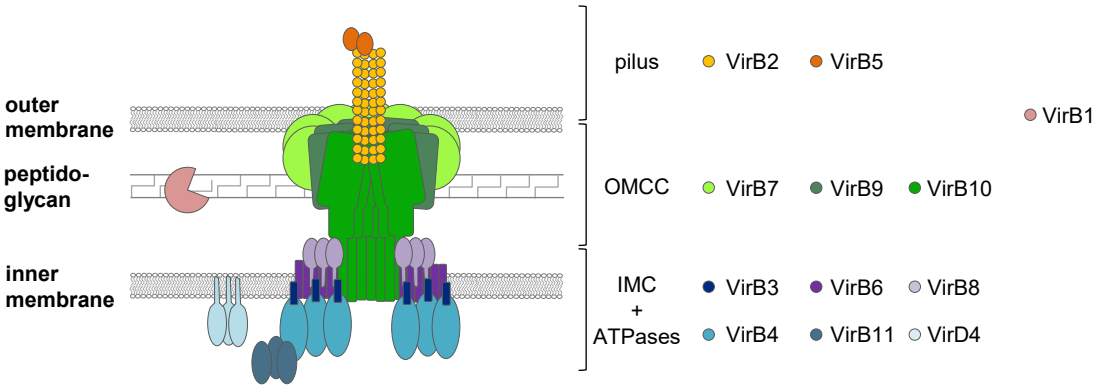

Figure 1.1 Architecture of a prototypical T4SS. With a minimal set of twelve proteins, the VirB/D4 system is structured in an IMC associated with three cytosolic ATPases, an OMCC that spans both membranes and the periplasm and an extracellular pilus. Except for the pilus subunits VirB2/VirB5 and the peptidoglycan hydrolase VirB1, the model considers copy numbers and symmetries of the respective protein subcomplexes. Notably, negative stain electron microscopy data indicated, that VirD4 might be at least transiently organized as two dimers between the VirB4 barrels and not as a hexamer (Redzej *et al.,* 2017). Figure adapted from Waksman and Orlova, 2014; Bergé *et al.,* 2017.

1.4.2 Type IV secretion systems – *H. pylori*

H. pylori encodes up to four different T4SSs: the Tfs3 and Tfs4 systems that are putatively conjugative secretion systems with yet unknown function, the ComB system that renders the bacteria naturally competent and the *cag* pathogenicity island (*cag*PAI) encoded T4SS that delivers the CagA effector protein into eukaryotic host cells. While the ComB DNA uptake system is part of the core genome of *H. pylori*, the other three T4SSs are located on genomic islands and are variably present in different strains. *Tfs3* and *tfs4* can be integrated at different genomic positions, while the *cag*PAI is usually integrated at a specific locus albeit with varying arrangement within the island. (Fischer *et al.,* 2020)

The CagT4SS is clearly the most intensively studied and best characterized T4SS of *H. pylori*. Recently cryo-electron microscopy and *in situ* cryo-electron tomography studies gave new insights into the structure of the complex nanomachinery (Chung *et al.,* 2019; Hu *et al.,* 2019).

Furthermore, the OMP HopQ was identified as an important adhesin involved in CagA translocation (Königer *et al.,* 2016; Javaheri *et al.,* 2016). Besides studies on the apparatus, the oncoprotein CagA itself and the consequences of its translocation are still in the focus of current research.

1.4.3 Molecular architecture of the CagT4SS

The roughly 30 proteins of the secretion apparatus as well as the effector protein CagA are encoded on an about 37 kb genomic island, the *cag*PAI (Figure 1.2). The gene arrangement within the island is highly conserved and the encoded proteins have high sequence similarity between different strains, thus most likely the *cag*PAI was only once acquired during the evolution of *H. pylori*. The island, framed by 31 bp direct repeats, is typically located between a gene coding for a Sel1 repeat-containing protein (*hp0519*) and a glutamate racemase-encoding gene (*hp0549*). (Fischer, 2011)

Figure 1.2 Gene arrangement of the *cag*PAI. The genetic organization of the 29 genes is shown for *H. pylori* strain 26695. The island is integrated between *hp0519* and *hp0549* and flanked by a left junction (LJ) and a right junction (RJ), *i.e*. by 31 bp direct repeats. In addition to the T4SS components and the effector protein CagA, the *cag*PAI of some strains including 26695 encodes a putative DNA helicase (*hel*). Figure adapted from Fischer, 2011.

The *cag*PAI encoded proteins, their (putative) function and subcellular localization are listed in Table 1.1 - Table 1.3. Notably, the CagT4SS is strongly involved in IL-8 induction, which is mainly independent of CagA translocation. Consequently, several components of the secretion system are only required for IL-8 induction but not for CagA translocation. There is evidence, that the CagT4SS not only delivers the oncoprotein into the host cells, but is additionally involved in the trans-kingdom transfer of DNA and peptidoglycan (Varga *et al.,* 2016; Viala *et al.,* 2004). Furthermore, independent studies showed that LPS inner core heptose metabolites, specifically ADP-L-*glycero*-β-D-*manno*-heptose, are translocated into eukaryotic host cells in a CagT4SS-dependent manner and that this is the main trigger for IL-8 secretion (Stein *et al.,* 2017; Gall *et al.,* 2017; Zimmermann *et al.,* 2017; Pfannkuch *et al.,* 2019).

In the following tables, the *cag*PAI encoded proteins essential for CagA translocation and IL-8 induction are classified as secretion apparatus components “SA”, while those that are supportive, but not essential for both phenotypes are nominated supportive components “SC”. Proteins involved in CagA translocation only are classified as translocation factors “TF”.

Table 1.1 *Cag*PAI encoded proteins with defined localization within the T4SS. (Fischer, 2011; Cover *et al.,* 2020) Except the coupling protein Cagβ, all components are essential for CagA translocation and IL-8 induction.

Gene	Protein	Localization	Classification	Function/homologies
hp0522	Cagδ/Cag3	OMCC	SA	
hp0524	Cagβ/Cag5	IMC	TF	Coupling protein/ATPase, VirD4
hp0525	Cagα/VirB11	IMC	SA	"Traffic" ATPase, VirB11
hp0527	CagY	OMCC	SA	VirB10
hp0528	CagX	OMCC	SA	VirB9
hp0532	CagT	OMCC	SA	VirB7
hp0537	CagM	OMCC	SA	
hp0544	CagE	IMC	SA	ATPase, VirB3/VirB4 (*)

(*) VirB3 and VirB4 are produced as a single protein in *H. pylori* (Kutter *et al.,* 2008).

Table 1.2 *Cag*PAI encoded proteins with putative function and localization within the T4SS. (Cover *et al.,* 2020; Fischer, 2011; Pham *et al.,* 2012)

Gene	Protein	Localization	Classification	Function/homologies
hp0523	Cagγ/Cag4	PP	SA	Peptidoglycan hydrolase, VirB1
hp0526	CagZ	C, IM	TF	Cagβ stabilization
hp0529	CagW	IM	SA	VirB6
hp0530	CagV	IM	SA	VirB8
hp0531	CagU	IM	SA	
hp0538	CagN	PP, IM	SC	
hp0539	CagL	PP, S	SA	VirB5
hp0540	CagI	PP, S	SA	
hp0541	CagH	IM	SA	
hp0542	CagG	PP	SC, TF	
hp0543	CagF	IM, C	TF	Secretion chaperon
hp0545	CagD	IM, PP, S	SC, TF?	
hp0546	CagC	IM, OM, S	SA	Pilus subunit, VirB2

C: cytoplasmic, IM: inner membrane, OM: outer membrane, PP: periplasmic,
S: surface-exposed or supernatant
CagD: conflicting data regarding IL-8 induction and CagA translocation

Table 1.3 *Cag*PAI encoded proteins with unknown function. So far, all those proteins were classified as not essential (NE) for either CagA translocation or IL-8 induction, except for CagB, where no data is available. The putative localization is assigned based on sequenze prediction. (Fischer, 2011)

Gene	Protein	Localization	Classification
hp0520	Cagζ/Cag1	IM	NE
hp0521	Cagε/Cag2	C	NE
hp0534	CagS	C	NE
hp0535	CagQ	IM	NE
hp0536	CagP	IM	NE
NA	CagB	C	No data

NA: not annotated, C: cytoplasmic, IM: inner membrane

Even though the CagT4SS is evolutionary related to the above described T4SS and contains homologs of all 12 VirB/D4 proteins, most of them share only low similarity with typical components of other T4SS. Yet, several proteins essential for CagT4SS activity are unique for this system. (Fischer, 2011)

Furthermore, the *cag*PAI encodes several putative open reading frames with so far unknown function. Together, they form the distinct architecture of the CagT4SS, that is in general classified as a type IVA system, but shares several characteristic features with the Dot/Icm system of *L. pneumophila* (Figure 1.3). First of all, the CagT4SS has an extraordinary diameter of the OMCC (41 nm), which is twice the diameter of prototypical VirB/D4 systems (*E. coli* pKM101: 17 nm, *Xanthomonas citri*: 22.5 nm, Figure 1.3 C) (Chung *et al.,* 2019; Chandran *et al.,* 2009; Sgro *et al.,* 2018). So far, only the Dot/Icm system of *L. pneumophila* was shown to have similar dimensions (40 nm, Durie *et al.,* 2020). The larger diameter is caused by the incorporation of multiple copies of proteins that are part of the OMCC, but lack homologs in prototypical T4SS (Cag3 and CagM) and by additional domains of VirB-homologous proteins (Frick-Cheng *et al.,* 2016; Sheedlo *et al.,* 2020). In total the OMCC of the *H. pylori* CagT4SS consists of 154 protein subunits, while the minimized, prototypical systems are only built up of 42 protein subunits (Sheedlo *et al.,* 2020). A second structural difference is the presence of a periplasmic ring (PR) consisting of parts of CagX (residues 32-130, 261-323) and CagY (residues 1469-1603), similar structures are not found in the prototypical system (Sheedlo *et al.,* 2020). Astonishingly there is a change in symmetry between the outer membrane complex (CagT/Cag3/CagM/CagY/CagY) and the PR (CagY/CagX) from 14-fold to 17-fold symmetry (Chung *et al.,* 2019; Sheedlo *et al.,* 2020). Again, this phenomenon was also described for the Dot/Icm T4SS of *L. pneumophila*, that has a 13-fold symmetry of the outer membrane disk and a 18-fold symmetry of the PR (Durie *et al.,* 2020).

The two enlarged T4SSs not only resemble each other regarding the architecture of the OMCC, but also regarding the symmetry of the IMC and the cytoplasmic components: while the IMC and the three ATPases of the prototypical type IVA systems (*e.g*. the R388 encoded system) form an asymmetric unit, a symmetric arrangement of IMC and ATPases was observed for the CagT4SS and the Dot/Icm T4SS (Hu *et al.,* 2019; Chetrit *et al.,* 2018). (Figure 1.3 D)

Besides these structural similarities, the proteins of the two large secretion systems are highly divergent on sequence level (Cover *et al.,* 2020).

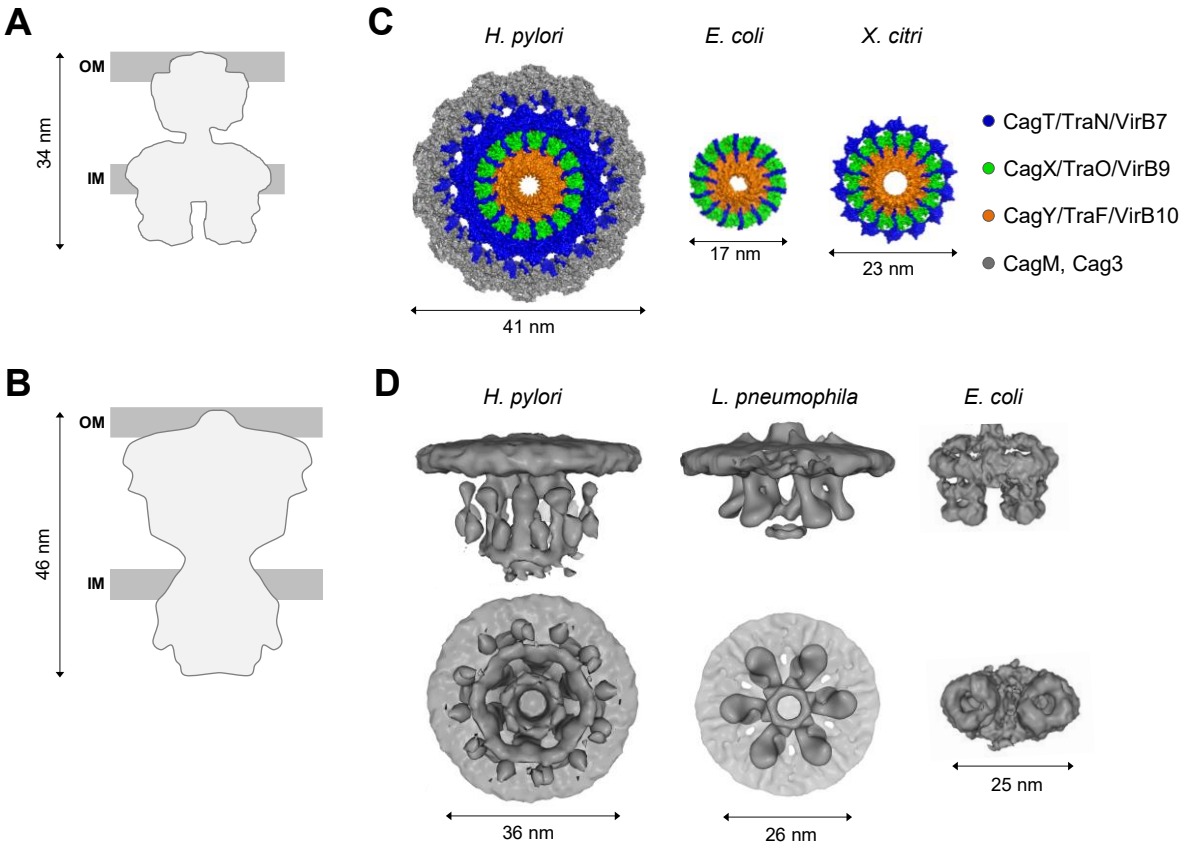

Figure 1.3 Comparison of the molecular architecture of different T4SS. (A) Silhouette of the T4SS encoded by the R388 conjugative plasmid of *E. coli* based on its electron microscopy structure (VirB3-10 only, Low *et al.,* 2014). (B) Putative silhouette of the CagT4SS combining cryo-electron microscopy and cryo-electron tomography data from different studies (Sheedlo *et al.,* 2020; Hu *et al.,* 2019). (C) Comparison of the OMCCs of the CagT4SS of *H. pylori* (PDB 6X6S, Sheedlo *et al.,* 2020), the pKM101 encoded T4SS of *E. coli* (PDB 3JQO, Chandran *et al.,* 2009), and the VirB/D4 system of *X. citri* (PDB 6GYB, Sgro *et al.,* 2018). All structures are shown as top view. (D) Comparison of the IMC and the organization of the cytoplasmic components. The 3D-structures solved by cryo-electron tomography are shown as side view (upper row) and bottom view (lower row). Additionally, parts of the inner membrane are depicted in case of the CagT4SS and the Dot/Icm system of *L. pneumophila*. The structure of the *E. coli* complex was generated in a system lacking the ATPases VirB11 and VirD4. (Source: EMD-0634 (Hu *et al.,* 2019), EMD-7612 (Chetrit *et al.,* 2018), EMD-2567 (Low *et al.,* 2014)).

1.4.4 Non *cag*PAI encoded factors involved in CagA translocation

In the last decades, several non *cag*PAI encoded proteins, were associated with increased T4SS activity. The interaction of the adhesin BabA with Le^b for example was shown to augment CagA translocation and subsequent pro-inflammatory cytokine release (Ishijima *et al.,* 2011). Meanwhile, several independent studies could prove, that the HopQ-CEACAM interaction plays a fundamental role in T4SS-mediated CagA translocation and inflammation (Belogolova *et al.,* 2013; Königer *et al.,* 2016; Javaheri *et al.,* 2016; Zhao *et al.,* 2018; Behrens *et al.,* 2020). To the current knowledge, all *H. pylori* wild-type (wt) strains express one of two different *hopQ* alleles (Cao and Cover, 2002). Using transposon insertion mutagenesis, HopQ was identified to impact CagA translocation activity, but not adhesion to epithelial cells (Belogolova *et al.,* 2013). Recently, human CEACAMs were determined as the host cell receptors of HopQ (Königer *et al.,* 2016; Javaheri *et al.,* 2016; Behrens *et al.,* 2020). X-ray crystal structures revealed the binding of HopQ to the N-terminal variable immunoglobulin (IgV) domain of CEACAM 1 and 3. Via this IgV domains, CEACAMs usually homo- or heterodimerize, which is prohibited upon HopQ binding. (Bonsor *et al.,* 2018)

1.4.5 CagA – Effector and oncoprotein

Many pathogenic bacteria use their T4SS to inject a set of different effector proteins into the recipient cells. An outstanding example are the more than 300 proteins that are transferred via the Dot/Icm apparatus by *L. pneumophila*, yet with mainly redundant functions within the host cell. Thus, deletions of single effector proteins rarely result in altered phenotypes. (Schroeder, 2017)

In contrast, CagA is the only known protein translocated by the CagT4SS and strains that inject CagA are more virulent than strains that do not. Within the host cells, CagA acts as a promiscuous non-physiological “scaffold/hub protein” that interacts with multiple proteins and thus alters cell signaling (Hatakeyama, 2017). CagA was first identified in 1993, as the *H. pylori* antigen associated with the development of peptic ulcer disease (Tummuru *et al.,* 1993). Two years later, it could be confirmed that *cagA*-positive strains are associated with an increased risk to develop gastric cancer (Blaser *et al.,* 1995). Since then, several epidemiological studies and animal experiments proved this finding.

X-ray crystallography revealed, that CagA has a unique structure that lacks similarity with any other known protein. The major part (70 %) of the protein shows a distinct folding, while the C-terminal part is intrinsically disordered. Consequently, structural data are only available for the N-terminal domains of CagA. (Hayashi *et al.,* 2012; Kaplan-Türköz *et al.,* 2012)

Full-length CagA has a variable size of 120-145 kDa, depending on polymorphisms in the C-terminal region (Tummuru *et al.,* 1993; Covacci *et al.,* 1993; Hatakeyama, 2017).

A graphic illustration of CagA is depicted in Figure 1.4.

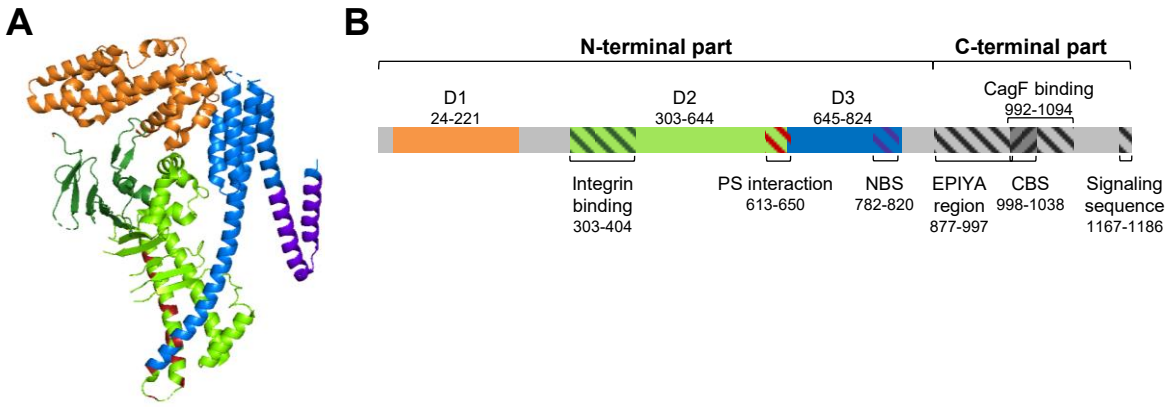

Figure 1.4 Structure of the effector protein CagA. (A) X-ray structure of the N-terminal domains of CagA (PDB 4DVY, Hayashi *et al.,* 2012). The domains and interaction sites are color coded as in (B). (B) Scheme of the functional regions of the CagA protein. A detailed description is given in the text. The amino acid numbering refers to *H. pylori* strain 26695. Grey sections indicate regions with unknown folding. (Hayashi *et al.,* 2012; Kaplan-Türköz *et al.,* 2012; Schindele *et al.,* 2016)

The N-terminal part of the protein has an average weight of 100 kDa, average dimensions of 11x8x5.5 nm^3, and can be subdivided in three domains (Figure 1.4, Hayashi *et al.,* 2012): The first domain (D1) consists of ten α-helices and is structurally isolated from the remaining protein. Is has only a minimal interacting interface with the second N-terminal domain, hence it is supposed to be highly mobile in solution. Since the first N-terminal amino acids (residues 1-17 strain P12, *i.e*. residues 1-23 strain 26695) of CagA were determined to be dispensable for its translocation, a translocation signal at the very N-terminus can be excluded. On the other hand, a D1-truncated version of CagA was only poorly translocated, *i.e.* 5 % of full-length CagA, as determined by a recently developed β-lactamase-dependent translocation reporter assay. This was partly explained by a reduced but not abolished interaction with the chaperone CagF. (Schindele *et al.,* 2016)

Another study revealed, that D1 is the only domain of CagA, that cannot fold spontaneously (Woon *et al.,* 2013).

Domains D2 and D3 build the protease resistant N-shaped structural core of CagA. It is dominated by α-helices, but contains a single-layer β-sheet in D2. (Hayashi *et al.,* 2012)

Domain D2 contains two functional sites: a cluster of basic amino acids (Hayashi *et al.,* 2012) and an integrin β1 interaction site at the surface-exposed part of the β-sheet (Kaplan-Türköz *et al.,* 2012). The cluster of basic amino acids can bind to the acidic membrane phospholipid phosphatidylserine (PS, Hayashi *et al.,* 2012). Usually, PS is clustered at the inner leaflet of the cytoplasmic membrane of eukaryotic cells, but it is transiently externalized to the cell surface upon *H. pylori* binding. CagA-PS interaction is discussed to be involved in CagA translocation. Furthermore, it was shown that in polarized epithelial cells, CagA is attached to the inner leaflet via PS binding. (Murata-Kamiya *et al.,* 2010)

Finally, domain D3 contains an “N-terminal binding sequence” (NBS) which interacts with its counterpart, the “C-terminal binding sequence” (CBS), located in the C-terminal disordered part of CagA (Bagnoli *et al.,* 2005; Hayashi *et al.,* 2012). There is experimental evidence that upon NBS-CBS binding, the intrinsically disordered C-terminus undergoes an “induced folding” that enhances the pathogenic potential of CagA by strengthening the interaction with PAR-1 (polarity regulating serine/threonine kinase partitioning defective-1) and subsequently SHP-2 (Src homology region 2 domain-containing phosphatase-2) discussed below (Hayashi *et al.,* 2012).

The three N-terminal domains are connected and intersected by short disordered sequences that display flexible intramolecular linkers, but might also act as interaction and modification sites (Hayashi *et al.,* 2012).

The intrinsically disordered C-terminal part of CagA is decisive for cancer development, since it contains several motifs that directly interact with host cell proteins and thereby trigger aberrant downstream signaling.

Upon delivery into human cells, CagA is tyrosine-phosphorylated by kinases of the Src (sarcoma) family at repetitive elements of glutamic acid-proline-isoleucine-tyrosine-alanine (EPIYA) motifs in the C-terminal region (Selbach *et al.,* 2002). The sequential arrangement of the EPIYA repeats is highly dependent on the origin of the respective *H. pylori* strain and determines its virulence potential (see 1.4.6). While CagA of Western *H. pylori* strains contain EPIYA-A, EPIYA-B and one or several EPIYA-C motifs, EPIYA-A/B/D is characteristic for CagA of East Asian strains (Figure 1.5). The classification of the respective motifs (A-D) is based on the flanking regions. (Higashi *et al.,* 2002)

In addition to the tyrosine phosphorylation-dependent alteration in cell signaling, the EPIYA repeat region was shown to be essential for the membrane-targeting of CagA in non-polarized epithelial cells *in vitro* (Higashi *et al.,* 2005).

16 amino acid-spanning CM motifs comprise the second class of repetitive elements that are located directly adjacent to the last EPIYA-C or -D (Figure 1.5, Ren *et al.,* 2006). Via this amino acid sequences, CagA multimerizes phosphorylation-independently within the mammalian host cells. CM motifs are conserved between different *H. pylori* strains, but the Western version (CM^W) and the East Asian variant (CM^E) differ in five residues (Lu *et al.,* 2008). Since parts of the EPIYA-C motif are equivalent to a CM sequence, multiple copies of EPIYA-C in Western *H. pylori* strains result in increased numbers of CM elements in the respective CagA variants (Ren *et al.,* 2006).

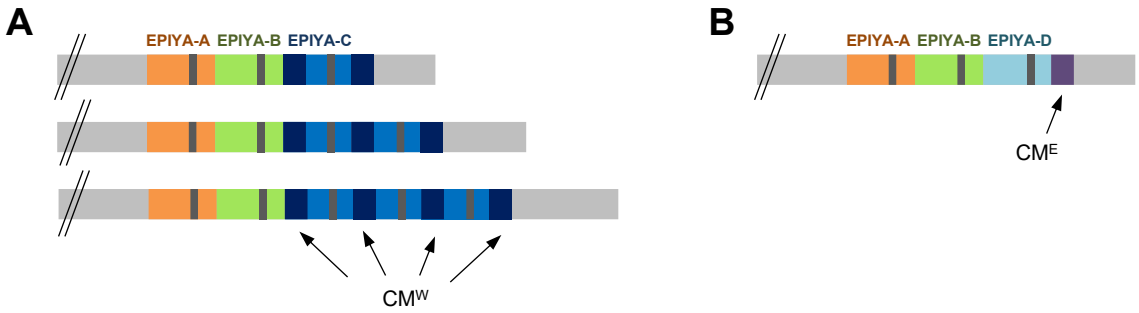

Figure 1.5 Schematic composition of the C-terminal part of CagA. (A) The EPIYA repeat region of Western CagA typically comprises an EPIYA-A and -B segment and a variable number of EPIYA-C segments. In contrast, prototypical East Asian CagA (B) has EPIYA-A, -B and -D segments. The tyrosine phosphorylation motif within each EPIYA segment is indicated in dark grey. Western and East Asian CagA differ in the number and sequence of the CagA-multimerization (CM) motifs: East Asian CagA has one CM motif directly adjacent to the EPIYA-D motif (CM^E). In contrast, Western CagA has at least two CM motifs (CM^W), one within the EPIYA-C segment and one adjacent. Multiple copies of EPIYA-C result in additional CM^W repeats. (Hatakeyama, 2017)

Further important elements of the C-terminal part of CagA are the above-mentioned CBS, as well as a further interaction site for the chaperone CagF, that is located closely to the C-terminus and essential for efficient CagA translocation (Pattis *et al.,* 2007).

The lack of an N-terminal signaling sequence (see above) and the consensus that effector proteins of T4SSs are in general recognized via a C-terminal signal sequence raised the question regarding the secretion signal of CagA. Translocation data obtained by a β-lactamase-dependent reporter assay as well as by phosphotyrosine-specific immunoblots indicated that a minimal length of the C-terminal region (>9 residues) rather than a distinct sequence of charged amino acids determines CagA translocation efficiency. (Schindele *et al.,* 2016)

1.4.6 CagA – Interaction with host cell proteins and the risk to develop cancer

Once inside the host cell, CagA is interacting with more than 20 cellular proteins, yet the exact sequential timing, the interconnections and the consequences are mainly unknown. The EPIYA repeat region in the C-terminal part accounts for most of the interactions relevant for severe pathogenesis, while the N-terminal part of the protein is mainly involved in intracellular localization, *i.e*. tethering to the plasma membrane. But *in vitro* experiments indicated that only full-length CagA can induce a severe tumorigenic phenotype. Meanwhile, a few phosphorylation-independent interactions of the N-terminal part of CagA with host cell proteins were identified and characterized. (Buti *et al.,* 2011; Backert *et al.,* 2010)

The first N-terminal domain D1 of CagA interferes with pro-apoptotic signaling cascades by inducing the proteasomal degradation of tumor suppressors and thus significantly promotes the survival of infected cells (Hatakeyama, 2017): intracellular CagA binds the apoptosis stimulating protein of p53 2 (ASPP2) via D1, which in turn recruits p53 and induces

proteasome-mediated degradation of p53 (Buti *et al.,* 2011). Furthermore, CagA can interact with the gastric tumor suppressor RUNX2 (Runt-related transcription factor 2) via WW motifs within D1 that bind to the PPXY sequence counterpart of RUNX2. As a consequence, RUNX2 is ubiquitinated by a so far unidentified E3 ubiquitin ligase and subsequently degraded. (Tsang *et al.,* 2010).

Beside the N-terminal D1, the above-mentioned CM motifs in the C-terminal part of CagA contribute to phosphorylation-independent effects of CagA on cell signaling. They are decisive for promoting an epithelial-to-mesenchymal-transition resembling phenotype and are also nominated CRPIA (conserved repeat responsible for phosphorylation-independent activity). Via these sequence motifs, CagA binds and occupies the catalytic center of the microtubule affinity regulating kinase (MARK = PAR-1) and mimics its natural substrates, *i.e*. proteins involved in the establishment and maintenance of cell polarity and proteins involved in filamentous actin organization. (Saadat *et al.,* 2007; Nesić *et al.,* 2010; Hatakeyama, 2017)

In addition, the CM motifs can bind the hepatocyte growth factor receptor c-Met resulting in a cancer-promoting inflammatory response and enhanced cellular motility and invasiveness (Churin *et al.,* 2003; Suzuki *et al.,* 2009).

As discussed above, CagA variants harbor different numbers and kinds of CM motifs, depending on their EPIYA repeat region composition. This strongly influences the pathologic potential of the respective CagA variant, since in Western strains the number of CM elements directly correlates with the amount of bound PAR-1 and the East Asian CM motif has a higher affinity for PAR-1 than the Western CM, which is thus associated with an increased risk for severe disease development (Lu *et al.,* 2008).

Inside the eukaryotic host cell, CagA is tyrosine-phosphorylated by kinases of the Src family. *In vitro* experiments revealed a hierarchic process, whereby phosphorylation is initiated by c-Src that targets the EPIYA-C or -D motif. Subsequently, c-Abl (Abelson murine leukemia viral oncogene homolog 1) phosphorylates EPIYA-A or -B. (Mueller *et al.,* 2012)

As a consequence, CagA can interact with SH2-domain (Src homology 2 domain)-containing phosphatases (SHP) that selectively recognize phosphorylated tyrosine and that are important signal transducers. By interacting and deregulating SHPs, CagA interferes and alters cellular signaling, and thus promotes inflammation and cancer development.

As an example, SHP-2, that is a *bona fide* oncoprotein, is binding to phosphorylated tyrosine in the EPIYA-C or -D motif (Higashi *et al.,* 2002). It is well known, that dysregulation or mutations of SHP-2 are involved in cancer development (Mohi and Neel, 2007). CagA-SHP-2 binding leads for example to aberrant activation of the Ras-Erk pathway and down-regulation of focal adhesion kinase (FAK) activity and thus alters cell morphogenesis and motility (Hatakeyama, 2017). CagA variants with multiple EPIYA-C

repeats or the East Asian variants with an EPIYA-D motif stronger interact with SHP-2 resulting in a higher risk for cancer development (Higashi *et al.,* 2002).
A second phosphorylation-dependent effect that should be mentioned, is the activation of C-terminal Src kinase (CSK) by phosphorylated EPIYA-A, -B, or -C. CSK inhibits other Scr kinases like the above-described c-Scr and thus downregulates CagA phosphorylation. It is discussed, that this feedback loop prevents excess CagA toxicity and cell damage and represents a prerequisite for persistent colonization. (Tsutsumi *et al.,* 2003)

1.4.7 Small molecule inhibitors – First attempts to interfere with CagT4SS activity

So far, few attempts to develop small molecule inhibitors directly targeting the T4SS-dependent translocation of CagA were reported. One study identified small peptidomimetics that interfered *in vitro* with T4SS-associated pilus formation and effector molecule translocation by a yet unknown mechanism (Shaffer *et al.,* 2016). Others focused on the inhibition of the VirB11 ATPase Cagα (Hilleringmann *et al.,* 2006; Sayer *et al.,* 2014; Arya *et al.,* 2019), but there is concern that Cagα inhibition might not be selective, but also block other (bacterial) ATPases (Shaffer *et al.,* 2016).
In *Brucella abortus*, a gram-negative mammalian pathogen, promising type IV secretion inhibition was achieved with a group of novel inhibitors interfering with VirB8 dimerization (Paschos *et al.,* 2011; Smith *et al.,* 2012). Several analogs of those inhibitors were highly active against the pKM101 plasmid encoded conjugative T4SS in *E. coli*, too. Interestingly in the same study it was shown, that beside a low similarity on sequence level, several VirB8 homologs from different species including the CagV protein of *H. pylori* share high structural similarities and can heterodimerize with each other. (Casu *et al.,* 2016)
Further research is needed to identify specific inhibitors of the CagT4SS and CagA translocation.

1.5 Aims of the thesis

60-70 % of *H. pylori* isolates from Western countries and almost all isolates from East Asia carry a functional CagT4SS and the corresponding effector protein CagA (Hatakeyama, 2017). The oncoprotein is a major risk factor for a severe disease progression and the development of gastric cancer. Deeper knowledge on the translocation process is fundamental to develop novel treatment strategies that are urgently needed, due to the emergence of antibiotic resistance and the increasing failure rates of eradication therapies. Even though in the recent years huge progress was achieved solving the structure of CagA and the CagT4SS, it is still unknown how CagA is transferred through the apparatus and across the host plasma membrane.

So far, CagA translocation is mainly analyzed by immunoblots detecting phosphorylated and thus intracellular CagA. Recently a novel β-lactamase-dependent translocation reporter system was developed, that facilitates quantitative measurements independently of CagA phosphorylation. This assay was proven to be applicable for high-throughput screening of translocation inhibitors. (Schindele *et al.,* 2016)

Even though the assay improved detection limits of CagA translocation and significantly shortened the experimental procedure time, the N-terminal β-lactamase fusion partially interfered with CagA protein synthesis and thus limited the applications of the system.

In the present work, a novel translocation reporter assay should be developed that is based on a split-luciferase complementation system. The assay should be used to monitor CagA translocation kinetics in real time to obtain new insights into the injection process. Furthermore, the new reporter system should be employed to address the question whether CagA is transported in a folded or unfolded manner.

To get new insights into the mode of action of the CagT4SS the split-luciferase complementation system should further be used to characterize *cag*PAI encoded proteins with yet unknown function.

In the second part of this thesis, recently identified inhibitors of the CagA translocation process should be characterized: First, the mode of action of the anti-cancer drug cisplatin on CagT4SS activity and bacterial viability should be elucidated. Second, various small molecule compounds, that belong to the group of respiratory chain complex I inhibitors, should be investigated concerning their impact on *H. pylori* growth and CagA translocation. In this context, the subcellular targets of three selected novel small molecule inhibitors should be identified. Furthermore, intensive studies regarding species specificity and structure-activity relationships should be conducted. Finally, the therapeutic potential should be evaluated by investigating the emergence of resistance, the *in vitro* cytotoxicity against eukaryotic cells, and the impact on the growth of selected species of the commensal human gut microbiome.

2 Material

2.1 Bacterial strains

2.1.1 *H. pylori* strains

H. pylori strains generated and used in the present work are listed in Table 2.1.

Table 2.1 List of *H. pylori* strains

	ID	Description	Source/ Reference
P12[HiBiT-CagA]	CLH40/41	WSP953[pCL3], marker free	This work
P12[HiBiT-CagA] Δ*cagT*	CLH42	CLH40[pJP95], Cm^R	This work
P12 $T27N^{NuoB}$	CLH50	$T27N^{NuoB}$, spontaneous mutation	This work
P12 $T27A^{NuoB}$, $V133M^{NuoD}$	CLH63	$T27A^{NuoB}$, $V133M^{NuoD}$, spontaneous mutations	This work
P12[HiBiT-CagA] Δ*hopQ*	CLH100	CLH40[pFS10], Erm^R	This work
P12[TEM-CagA] Δ*flaA*	CLH101	RNP3[pRH121], Cm^R	This work
P12[TEM-CagA] Δ*flaA, recA::flaA*	CLH111	CLH101[pCL6], Cm^R, Kan^R	This work
P12 Δ*cagζ*	CLH119	WSP80[pCL7], Erm^R	This work
P12 Δ*cagε*	CLH121	WSP80[pCL8], Erm^R	This work
P12 Δ*cagQ/R*	CLH123	WSP80[pCL9], Erm^R	This work
P12 Δ*cagB*	CLH127	WSP80[pCL11], Erm^R	This work
P12[HiBiT-Cagζ]	CLH128	CLH119[pCL12], marker free	This work
P12[HiBiT-Cagε]	CLH130	CLH121[pCL13], marker free	This work
P12[HiBiT-CagQ]	CLH132	CLH123[pCL15], marker free	This work
P12[HiBiT-CagR]	CLH134	CLH123[pCL16], marker free	This work
P12[HiBiT-CagB]	CLH139	CLH127[pCL17], marker free	This work
P12[HiBiT-Ub-CagA]	CLH147	WSP953[pCL19], marker free	This work
P12[HiBiT-$Ub^{I3G, I13G}$-CagA]	CLH153	WSP953[pCL20], marker free	This work
P12[HiBiT-CagA] Δ*flaA*	CLH166	CLH40[pRH121], Cm^R	This work
P12[HiBiT-CagA] Δ*flaA, recA::flaA*	CLH168	CLH166[pCL6], Cm^R, Kan^R	This work
P12[HiBiT-GFP-CagA]	CLH172	WSP953[pCL21], marker free	This work
P12[HiBiT-DHFR-CagA]	CLH175	WSP953[pCL23], marker free	This work

	ID	Description	Source/ Reference
P12[DHFR-CagA]	CLH185	WSP953[pCL24], marker free	This work
P12 T27A^{NuoB}	CLH194	T27A^{NuoB}, spontaneous mutation	This work
P12[DHFR-CagA-HiBiT]	CLH195	CLH185[pCL26], Cm^{R}	This work
P12 V133M^{NuoD}	CLH198	V133M^{NuoD}, spontaneous mutation	This work
P12[HiBiT-CagA] Δ*cagζ*	CLH201	CLH40[pCL7], Erm^{R}	This work
P12[HiBiT-CagA] Δ*cagB*	CLH216	CLH41[pCL11], Erm^{R}	This work
P12 [DHFR-CagA/HiBiT-CagA]	CLH219	CLH185[pCL27], Kan^{R}	This work
P12[HiBiT-CagA] Δ*cagB, recA::cagB* (*cagA* promotor)	CLH230	CLH216[pCL28], Kan^{R}	This work
P12[HiBiT-CagA] Δ*cagQ*	CLH240	CLH41[pCL9], Erm^{R}	This work
P12[HiBiT-CagA] Δ*cagB, recA::cagB* (*cagB* promotor)	CLH251	CLH216[pCL31], Kan^{R}	This work
P12[HiBiT-CagA] V133M^{NuoD}	CLH273	CLH41 transformed with PCR CL5/CL6, template CLH198	This work
B8[HiBiT-CtkA]	StNH21	B8[pWS725], Kan^{R}	S. Niedermaier
P12 GFP	LJH11	WSP12[pCH7c], Cm^{R}	L. Jimenez-Soto
P12 Δ*cagH*	WSP696	WSP80[pWS423], Erm^{R}	W. Fischer
P12[TEM-CagA]	RNP3	WSP12[pWS486, pEG21, pCW1, pJP62], marker free	R. Nair
P12[TEM-CagA] Δ*cagT*	WSP1172	RNP3[pJP95], Cm^{R}	W. Fischer
P12	WSP12	wt, clinical isolate	W. Fischer
G27[HiBiT-CagA]	WSP1472#2	G27[pCL3], marker free	W. Fischer
G27[HiBiT-CagA], Δ*cagB*	WSP1472#3	G27[pCL3] Δ*cagB*, marker free	W. Fischer
P12 Δ*cagA*	WSP649	WSP12[pWS373], Kan^{R}	W. Fischer
P12 Δ*cagA* (1-257)	WSP953	WSP80[pWS556], Erm^{R}	W. Fischer
P12 strep	WSP80	Str^{R}	W. Fischer
P12[TEM-CagA] Δ*hopQ*	WSP1229	RNP3[pFS10], Erm^{R}	W. Fischer

2.1.2 *E. coli* and other bacterial strains

All further bacterial strains used and generated in the present work are listed in Table 2.2.

Table 2.2 List of further bacterial strains used in the present work

	Genotype/description	**Growth conditions**	**Source/ Reference**
E. coli TOP10	F- *mcrA*, Δ(*mrr-hsdRMS-mcrBC*), Φ80*lacZ*Δ*M15*, Δ*lacO74*, *recA1*, *ara*Δ*139*, Δ(*ara-leu*)*7697*, *galU*, *galK*, *rpsL*(Str^R), *endA1*, *nupG*	see 3.1.10 and 3.1.12	Thermo Fisher
E. coli S17 λpir	*RP4-2*(*Km::Tn7*,*Tc::Mu-1*), *pro-82*, *LAMpir*, *recA1*, *endA1*, *thiE1*, *hsdR17*, *creC510*	as *E. coli* TOP10	B. Sedlmaier-Erlenfeld
E. coli TOP10 Δ*ndh2* (CLE23)	as TOP10, pKD46, Δ*ndh2::FRT-aph*, Km^R	as *E. coli* TOP10	This work
E. coli (BW25113)	parental strain for the Keio Collection, F- Δ(*araD-araB*)*567*, Δ*lacZ4787*(*::rrnB-3*), λ-, *rph-1*, Δ(*rhaD-rhaB*)*568*, *hsdR514*	as *E. coli* TOP10	Baba *et al.,* 2006
E. coli Δ*tolC* (JW5503-1)	as BW25113, Δ*tolC832::FRT-aph*, Kan^R	as *E. coli* TOP10	Baba *et al.,* 2006
E. coli Nissle 1917 (mutaflor)		as *E. coli* TOP10	B. Stecher
Enterococcus faecalis (OG1RF)		as *E. coli* TOP10	B. Stecher ATCC 47077
Staphylococcus aureus	*Staphylococcus aureus* subsp. *aureus* Rosenbach	as *E. coli* TOP10	ATCC 29213
Campylobacter jejuni	C31	as *H. pylori*	W. Fischer
Lactobacillus reuteri	I49	see 3.1.10	B. Stecher DSM 32035
Clostridium scindens		as *L. reuteri*	B. Stecher
Eubacterium rectale		as *L. reuteri*	B. Stecher
Bacteroides vulgatus		as *L. reuteri*	B. Stecher ATCC 8482
Bacteroides thetaiotaomicron		as *L. reuteri*	B. Stecher ATCC 29148
Akkermansia muciniphila	YL44	as *L. reuteri*	B. Stecher DSM 26127
Bilophila wadsworthia		as *L. reuteri* (+ 10 mM taurine)	B. Stecher

2.2 Cell lines

Cell lines used and generated in the present work are listed in Table 2.3.

Table 2.3 Cell lines and culture conditions

	Description	Culture conditions	Reference
AGS	Human gastric epithelial adenocarcinoma cell line	RPMI/10 % FCS 37 °C, 5 % CO_2	ATCC® CRL-1739
NCTC clone 929 (L929)	Murine fibroblast cell line	DMEM/10 % FCS/ 2 mM L-glutamine/ 1 mM sodium pyruvate 37 °C, 5 % CO_2	ATCC® CCL-1
AGS [HaloTag-LgBiT] = AGS[LgBiT]	AGS cells stably transfected with pCS1956B02 Reporter cell line for split-luciferase complementation assay Single cell clone-derived	RPMI/10 % FCS 37 °C, 5 % CO_2 0.5 mg/ml hygromycin	This work

2.3 Plasmids

Vectors used in the present work are listed in Table 2.4.

Table 2.4 List of plasmids

	Description	Cloning strategy	Resistance	Source/ Reference
pCL3	Marker free insertion of *HiBiT-cagA* (N-terminal) in *cagA* locus	pUC19 (*Sph*I/*Eco*RI) + PCR WS821/WS822 + PCR WS265/JP67 template WSP12	Amp^R	This work
pCL6	Complementation of *flaA* in *recA* locus, *flaA* promotor	pJP99 (*Xho*I/*Kpn*I) + PCR CL45/CL46, template WSP12	Kan^R, Amp^R	This work
pCL7	Deletion of *cagζ*, *cagζ::rpsL-erm*	PCR WS103/CL56, template HP2kb05_F13 (*Sal*I) + *rpsL-erm* cassette	Erm^R, Kan^R	This work
pCL8	Deletion of *cagε*, *cagε::rpsL-erm*	PCR WS118/CL55, template HP2kb05_F13 (*Sal*I) + *rpsL-erm* cassette	Erm^R, Kan^R	This work
pCL9	Deletion of *cagQ/R*, *cagQ/R::rpsL-erm*	PCR WS404/WS405, template HP2kb04_P16 (*Bam*HI/*Sal*I) + *rpsL-erm* cassette	Erm^R, Kan^R	This work
pCL11	Deletion of *cagB*, *cagB::rpsL-erm*	PCR WS850/WS849, template HP2kb08_K23 (*Bam*HI/*Sal*I) + *rpsL-erm* cassette	Erm^R, Kan^R	This work

	Description	Cloning strategy	Resistance	Source/ Reference
pCL12	Marker free insertion of *HiBiT-cagζ* (N-terminal) in *cagζ* locus	Religation PCR WS846/WS851, template HP2kb05_F13 (*Nde*I)	Kan^R	This work
pCL13	Marker free insertion of *HiBiT-cagε* (N-terminal) in *cagε* locus	Blunt end ligation PCR CL47/CL51, template HP2kb05_F13	Kan^R	This work
pCL15	Marker free insertion of *HiBiT-cagQ* (N-terminal) in *cagQ/R* locus	Blunt end ligation PCR CL49/CL62, template HP2kb04_P16	Kan^R	This work
pCL16	Marker free insertion of *HiBiT-cagR* (N-terminal) in *cagQ/R* locus	Blunt end ligation PCR WS852/WS853, template HP2kb04_P16	Kan^R	This work
pCL17	Marker free insertion of *HiBiT-cagB* (N-terminal) in *cagB* locus	Blunt end ligation PCR CL50/CL54, template HP2kb08_K23	Kan^R	This work
pCL19	Marker free insertion of *HiBiT-ubiquitin-cagA* (N-terminal) in *cagA* locus	PCR CL63/WS265, template pCL3 (*Sal*I/*Bam*HI) + PCR CL64/CL65, template pGEM-Ub_#17	Amp^R	This work
pCL20	Marker free insertion of *HiBiT-ubiquitin$^{I3G, I13G}$-cagA* (N-terminal) in *cagA* locus	Blunt end ligation PCR CL67/CL68, template pCL19	Amp^R	This work
pCL21	Marker free insertion of *HiBiT-gfp-cagA* (N-terminal) in *cagA* locus	pCL19 (*Sal*I/*Bam*HI) + PCR CL69/CL70, template pWS130	Amp^R	This work
pCL23	Marker free insertion of *HiBiT-dhfr-cagA* (N-terminal) in *cagA* locus	pCL19 (*Sal*I/*Bam*HI) + PCR CL71/CL72, template pCMV6-Kan/Neo-*dhfr*	Amp^R	This work
pCL24	Marker free insertion of *dhfr-cagA* (N-terminal) in *cagA* locus	Religation PCR WS242/CL71, template pCL23 (*Xho*I/*Sal*I)	Amp^R	This work
pCL26	Fusion of a C-terminal *HiBiT* tag to *cagA*	pWS336 (*Kpn*I/*Xba*I) + PCR WS237/CL76, template WSP12	Cm^R, Amp^R	This work
pCL27	Insertion of *HiBiT-cagA* in *recA* locus, *cagA* promotor	pJP99 (*Xho*I/*Kpn*I) + PCR JP28/JP67, template CLH41	Kan^R, Amp^R	This work
pCL28	Complementation of *cagB* in *recA* locus, *cagA* promotor	pJP99 (*Nde*I/*Kpn*I) + PCR CL89/CL90, template CLH41	Kan^R, Amp^R	This work
pCL31	Complementation of *cagB* in *recA* locus, *cagB* upstream region	pJP99 (*Xho*I/*Kpn*I) + PCR WS242/CL90, template CLH41	Kan^R, Amp^R	This work

	Description	Cloning strategy	Resistance	Source/ Reference
pCS1956B02	Expression vector for *haloTag-lgBiT* (CMV promotor)		Hyg^R, Amp^R	Promega
pFS10	Deletion of *hopQ*, *hopQ::rpsL-erm*		Erm^R	Bonsor *et al.,* 2018
pGEM®-T Easy	Cloning vector		Amp^R	Promega
pGEM-Ub_#17	Template for murine *ubiquitin* (allelic variant corresponding to P0CG50)	pGEM®-T Easy + PCR CL64/CL65, template murine genomic DNA	Amp^R	This work
pJP95	Deletion of *cagT*, *cagT::cat*		Cm^R	Fischer *et al.,* 2001
pKD4	Template for *aph*-cassette, ori R6K γ		Kan^R, Amp^R	Datsenko and Wanner, 2000
pKD46	Helper plasmid for chromosomal deletions in *E. coli*, encoding lambda Red genes (*exo, bet, gam*); temperature-sensitive replicon; arabinose-inducible promoter		Amp^R	Datsenko and Wanner, 2000
pCMV6-Kan/Neo-*dhfr*	Template for murine *dhfr*		Kan^R	Origene (MR201752)
pRH121	Deletion of *flaA*, *flaA::cat*		Cm^R	Haas *et al.,* 1993
pUC19	Cloning vector		Amp^R	Thermo Fisher
pWS130	Template for *gfp*		Cm^R	Hohlfeld *et al.,* 2006
pJP99	*recA* integration vector		Kan^R, Amp^R	Püls *et al.,* 2002
pWS336	*cagA* reconstitution plasmid, (*cagA* 3′ region, codons 847-1214)		Cm^R, Amp^R	Schindele *et al.,* 2016
pWS556	Deletion of 5′ *cagA* (bases 1-770 replaced by r*psL-erm*)		Erm^R	W. Fischer

	Description	Cloning strategy	Resistance	Source/ Reference
HP2kb05_F13	gene bank plasmid, (WSP12 551966-554178)		Kan^R	Fischer *et al.,* 2010
HP2kb04_P16	gene bank plasmid, (WSP12 572052-574286)		Kan^R	Fischer *et al.,* 2010
HP2kb08_K23	gene bank plasmid, (WSP12 583621-585666)		Kan^R	Fischer *et al.,* 2010

2.4 Primers

Oligonucleotides used in the present study are listed in Table 2.5.

Table 2.5 List of primers (ordered from Metabion)

	Sequence (5′ → 3′)	Restriction enzyme/ modifications/tags
CL3	TGGCTTCATCATTTGCTG	
CL4	CCACTTCATACCATTGAGC	
CL5	TGACAAACACCCCTATTTG	
CL6	CATTGGTTGAGCCAATCA	
CL7	AGAGCCCCTAGCTTTTAT	
CL8	GCTATAAATGCGTTTGCC	
CL9	TATTTAAGCGGTTGCTCG	
CL10	GTTTCTAAATTGATGCCCG	
CL11	GCTACCCCAAAAGAAGAA	
CL12	CCACTTCAAAGCTGAGTAAT	
CL13	GGGCTTGCCTCTAATAAC	
CL14	GTTTTGCTTGCGTTCAAC	
CL15	GCAAATCACGGTGTATGT	
CL16	CGATGAAATAGCCCACTT	
CL17	CTGGGGTGTATCTAGTCA	
CL18	GGCAAGAGCGAGATTTC	
CL19	GTCGTAAAGACTTTGCGAT	

	Sequence (5′ → 3′)	**Restriction enzyme/ modifications/tags**
CL20	AGGCTGAAATCAAGACAATG	
CL21	TAGAGCAGCAAGAAAACG	
CL22	CGCCTTATTGTGTCGTAAG	
CL35*	CGGTGCCCTGAATGAACTGC	
CL36*	GCCGATTGTCTGTTGTGCCC	
CL37**	TTGACTACGCCATTGAAAAAGATTGTGAT TGTCGGCGGCGGTGTAGGCTGGAGCTGCTTC	
CL38**	AAGTTTCGTTAGCTCGTTGTGGGCCGCA GCAGAGATACGTCATATGAATATCCTCCTTAG	
CL39**	TATATCACTCTCACAAATTCGCTC	
CL40**	ATGGCTGGAAATACTTAAGGATTCGG	
CL45	ACCGCTCGAGATCGATAAAGCCCTTT AAAATTTCAAACTTTAACCG	*Xho*I
CL46	GCGGTACCATCCAACACAATAACCGCCTATAATAAAAAG	*Kpn*I
CL47	*GTGTCTGGTTGGCGACTTTTCAAGAAAA TTAGC*CTGATACAAAGAGGATTGAGTAG	*HiBiT* tag
CL49	*GTGTCTGGTTGGCGACTTTTCAAGAAAA TTAGC*CTGCTTCCTACTAAAACACGC	*HiBiT* tag
CL50	*GTGTCTGGTTGGCGACTTTTCAAGAA AATTAGC*CTGGAAAACAAATCAATAGGAC	*HiBiT* tag
CL51	CATTTTATAGGTCGCTTGTG	5'-phosphate
CL54	CATTTTGTTTCCCATGTGGATC	5'-phosphate
CL55	ACCGGTCGACCAATCCTCTTTGTATCATTT	*Sal*I
CL56	ACCGGTCGACATTGATTGTGTCAGCCATAG	*Sal*I
CL62	CATTTCACAATAGCATACCTAAAGC	5'-phosphate
CL63	TAGTCGACGCTAATTTTCTTGAAAAGTCGCCAACC	*Sal*I
CL64	TAGTCGACATGCAGATCTTCGTGAAGACCC	*Sal*I
CL65	ATGGATCCAACCCACCTCTCAGGCGAAG	*Bam*HI
CL67	ACAGGCAAGACCGGTACCCTGGAGGTCGA	
CL68	CAGGGTCTTCACGAAACCCTGCATGTCGAC	5'-phosphate
CL69	TAGTCGACAGTAAAGGAGAAGAACTT	*Sal*I
CL70	TTGGATCCATTTTGTATAGTTCATCCAT	*Bam*HI

	Sequence (5′ → 3′)	**Restriction enzyme/ modifications/tags**
CL71	TAGTCGACATGGTTCGACCATTGAACTG	*Sal*I
CL72	TTGGATCCAAGTCTTTCTTCTCGTAGACTT	*Bam*HI
CL76	GGGGTACCTTA*GCTAATTTTCTTGAAAAGTCGC CAACCAGACAC*AGATTTTTGGAAACCACCTT	*Kpn*I, *HiBiT* tag
CL89	ATCATATGGAAAACAAATCAATAGG	*Nde*I
CL90	TAGGTACCCTACTTGTCCCAACCATT	*Kpn*I
JP28	ACCGCTCGAGGGTAAAAATGTGAATCGT	*Xho*I
JP67	GGCCGAGCTCGGTACCTTAAGATTTTTGGAAACCAC	*Sac*I, *Kpn*I
UB110	AACGATGAAGCTTCTAGCTTGCTA	
UB111	GTGCTTATTCSTNAGATACCGTCAT	
WS103	GGGGATCCGTCGACAAAGAGACTAAAGATTGA	*Bam*HI/*Sal*I
WS118	GCGGATCCTGTCGACATCCCAAATGCAATGGATTG	*Bam*HI/*Sal*I
WS237	AATCTAGAGCAAACGATAGAC	*Xba*I
WS242	ACCGCTCGAGCATATGTTCTCCTTACTAACTAGTTTC	*Xho*I, *Nde*I, *Spe*I
WS265	CAGGATCCGACTAACGAAACCATTAACC	*Bam*HI
WS404	GCGGATCCTCTCAAGTAAGACTCTAGTG	*Bam*HI
WS405	ACCGGTCGACTTTAGTAGGAAGCATTTCAC	*Sal*I
WS821	AGCTGCATGCTGTAAAAAATTTCATGCGTTTC	*Sph*I
WS822	CCGGATCCCC*GCTAATTTTCTTGAAAAGTCGCCAA CCAGACACCAT*ATGTTCTCCTTACTAACTAGTTTC	*Bam*HI, *HiBiT* tag
WS846	ACTGCAT*ATGGTGTCTGGTTGGCGACTTTTCAAGA AAATTAGC*CTGGCTGACACAATCAATACAAC	*Nde*I, *HiBiT* tag
WS849	ACGTGTCGACTGATTTGTTTTCCATTTTGTTTC	*Sal*I
WS850	AGGGATCCGGTTGGGACAAGTAGGTT	*Bam*HI
WS851	ACGTCATATGGTTACCTCCATAAGGTATATTC	*Nde*I
WS852	*GTGTCTGGTTGGCGACTTTTCAAGAAAAT TAGC*CTGTTTTTGATACTATTGAATCC	*HiBiT* tag
WS853	CATGGGATCTGCTTTGGT	5'-phosphate

*, ** sequences obtained from Datsenko and Wanner, 2000 and Yun *et al.,* 2005, respectively.
Recognition sites of restriction enzymes are underlined, *HiBiT* tag sequences are shown in italic.

2.5 Antibodies

Antisera used for immunoblotting, immunoprecipitation, or enzyme-linked immunosorbent assay (ELISA) are listed in Table 2.6.

Table 2.6 List of antibodies

	Antigen/Description/ Origin	**Application/Dilution or final concentration**	**Source/Reference (ID/order number)**
α-CagA	CagA (EPIYA region, polyclonal)/rabbit	Western blot/1:5000	Schindele *et al.,* 2016 (AK299)
α-CagA	CagA (C-terminal, polyclonal)/rabbit	Western blot/1:5000	Odenbreit *et al.,* 2000 (AK257)
α-CagT	CagT (polyclonal)/rabbit	Western blot/1:5000	Fischer *et al.,* 2001 (AK270)
α-FlaA	FlaA (polyclonal)/rabbit	Western blot/1:5000	Haas *et al.,* 1993 (AK183)
α-HopQ	HopQ (polyclonal)/rabbit	Western blot/1:5000	Königer *et al.,* 2016 (AK298)
α-PTyr	Phosphorylated tyrosine (monoclonal)/mouse	Western blot/1:5000 Immunoprecipitation/1:250	Santa Cruz Biotechnology (PY99, sc-7020)
α-mouse-POX	Murine IgG (polyclonal), POX-coupled/goat	Western blot/1:10000	Sigma-Aldrich (A9917)
Protein A-AP	Immunoglobulins/Protein A alkaline phosphatase (AP) conjugate/*S. aureus*	Western blot/1:5000	Sigma-Aldrich (P7488)
α-IL-8	Human IL-8 (monoclonal)/ mouse	ELISA (capture antibody)/ 3 µg/ml	BD Pharmingen (554716)
α-IL-8 biotin	Human IL-8 (monoclonal), biotin conjugated/mouse	ELISA (detection antibody)/ 0.5 µg/ml	BD Pharmingen (554718)

2.6 Inhibitors and reference antibiotics

Unless indicated otherwise, stock solutions of all small molecule inhibitors were prepared in DMSO and stored at -20 °C. Stock concentrations were adjusted to not exceed a final concentration of 0.5 % (v/v) solvent in the respective experiment. An appropriate control (only solvent) was included in all experiments.

#14, #16, #17 and analogs were kindly provided from BASF or bought from LGC standards. Further complex I and III inhibitors listed in Table 4.3 were obtained from BASF, too.

Cisplatin was obtained from Sigma-Aldrich, transplatin and transpalladium from Alfa Aesar. All further platin complexes were kindly provided by Prof. Schobert (University of Bayreuth).

Stock solutions of L-cysteine (Serva), L-methionine (Merck) and L-alanine (Roth) were prepared in ddH_2O and mixed with cisplatin (6.3 mM in DMSO), to test the impact of different amino acids on the inhibitory effect of cisplatin. The cisplatin-amino acid mixtures were stored at -20 °C until further use.
Carbonyl cyanide m-chlorophenyl hydrazine (CCCP, DMSO), rotenone (DMSO), antimycin A (ethanol), rifampicin (DMF), and methotrexate (DMSO) were obtained from Sigma-Aldrich. Metronidazole (DMSO) was purchased from Cayman Chemical. As indicated, DMSO, DMF or ethanol was used to prepare the respective stock solutions.
Further antibiotics that were used for cloning, too, are listed in Table 2.7.

2.7 Buffers

Anode I	300 mM Tris 10 % (v/v) methanol pH 10.4
Anode II	25 mM Tris 10 % (v/v) methanol pH 10.4
Cathode buffer	25 mM Tris 40 mM 6-aminocaproic acid 10 % (v/v) methanol pH 9.6
DNA electrophoresis loading dye (6x)	20 % (v/v) glycerol 50 mM EDTA 0.05 % (w/v) bromophenol blue 0.5 % (w/v) N-lauroylsarcosine pH 8.0
N3 buffer	3 M potassium acetate pH 5.5
PBS*	1 mM phenylmethylsulfonyl fluoride (PMSF) 1mM sodium vanadate 1 µM leupeptin 1 µM pepstatin in D-PBS

P1 buffer	50 mM Tris 10 mM EDTA 100 mg/ml RNase (Roche) pH 8.0
P2 buffer	200 mM NaOH 1 % (w/v) SDS
Radioimmunoprecipitation (RIPA) buffer	50 mM Tris/HCl 100 mM NaCl 1 mM EDTA 1 % (v/v) Nonidet P-40 0.25 % (w/v) sodium deoxycholate pH 7.4
SDS sample buffer (2x)	100 mM Tris/HCl 4 % (w/v) SDS 0.2 % (w/v) bromophenol blue 20 % (v/v) glycerol 10 % (v/v) β-mercaptoethanol pH 6.8
SDS running buffer	25 mM Tris 250 mM glycine 20 % (w/v) SDS pH 8.3
Stripping buffer	25 mM glycine 1 % (w/v) SDS pH 2
TAE	40 mM Tris 20 mM acetic acid 1 mM EDTA pH 8.0
TBS-T	150 mM NaCl 200 mM Tris/HCl 0.05 % (v/v) Tween® 20 pH 7.5

TfbI	30 mM potassium acetate 100 mM RbCl 10 mM $CaCl_2$ 50 mM $MnCl_2$ 15 % (v/v) glycerol pH 5.2 (with acetic acid)
TfbII	10 mM MOPS 75 mM $CaCl_2$ 10 mM RbCl 15 % (v/v) glycerol pH 6.5 (with acetic acid)

2.8 Media supplements, sera and antibiotics

Vitamin mix	100 g/l α-D-glucose 10 g/l L-glutamine 26 g/l L-cysteine 1.1 g/l L-cystine 0.15 g/l L-arginine 0.1 g/l cocarboxylase 20 mg/l iron(III)nitrate 3 mg/l thiamine 13 mg/l P-aminobenzoic acid 0.25 g/l nicotinamide adenine dinucleotide (NAD) 10 mg/l vitamin B12 1 g/l adenine 20 mg/l guanine 0.5 g/l uracil
Horse serum	HyClone, Thermo Fisher (heat inactivated, 56 °C, 20 min)
Fetal calf serum (FCS)	Life Technologies (heat inactivated, 56 °C, 20 min)
Cholesterol (250x)	Life Technologies

Table 2.7 List of antibiotics used for cloning

	Solvent	**Final concentration serum plates (*H. pylori*)**	**Final concentration LB-plates (*E. coli*)**
Ampicillin	ddH_2O		100 µg/ml
Chloramphenicol	ethanol	6 µg/ml	30 µg/ml
Erythromycin	ethanol	10 µg/ml	250 µg/ml
Kanamycin	ddH_2O	8 µg/ml	50 µg/ml
Streptomycin	ddH_2O	250 µg/ml	

D-PBS, media and media supplements used for cell culturing were all purchased from Life Technologies. Hygromycin solved in ddH_2O (50 mg/ml) was obtained from Life Technologies, too.

To test the effect of different sera and sera fractions on CagA translocation and *H. pylori* growth, sera were treated as following:

In general, all tested sera were initially heated at 56 °C for 20 min to inactivated complement factors. Merck Millipore Amicon™ Ultra Centrifugal Filter Units (100 kDa, Merck) were used for size exclusion fractionation. Samples were centrifuged at 4000 rpm (Megafuge 3.0 R, Thermo Scientific) until an eight times concentration was obtained.

Furthermore, FCS was boiled for 20 min to denature proteins or proteinase K (0.5 mg/ml, Roche) treated for 1 h at 56 °C and subsequently boiled for 20 min.

To separate extracellular vesicles, FCS was 1:1 diluted in D-PBS and centrifuged for 16 h at 100000 rpm in an ultracentrifuge (rotor: TLA 100.3, Optima^{TM} MAX-XP, Beckman Coulter). The soluble fraction was transferred to a new tube and the insoluble membrane fraction was suspended in the respective volume of D-PBS.

2.9 Kits, reagents, and enzymes

If not indicated otherwise, chemicals and reagents were purchased from Roth, Merck, Sigma-Aldrich or VWR. All kits used in the present work are listed in Table 2.8. Restriction enzymes and their respective buffers were all purchased from NEB. Further enzymes are specified in the respective sections.

Table 2.8 Kits used in this study

	Supplier (order number)
ATP Bioluminescence Assay Kit CLS II	Sigma-Aldrich (11699695001)
BacLight™ Bacterial Membrane Potential Kit	Thermo Fisher (B34950)
DNeasy Blood & Tissue Kits	Qiagen (69504)
Experion RNA StdSens Analysis Kit	Bio-Rad (7007103)
Illustra GFX™ PCR DNA and Gel Band Purification Kit	Thermo Fisher (GE28-9034-70)
LiveBLAzer™ FRET-B/G Loading Kit with CCF4-AM	Thermo Fisher (K1095)
Nano-Glo® HiBiT blotting system	Promega (N2410)
Nano-Glo® Live Cell Assay System	Promega (N2011)
RNase-free DNase Set	Qiagen (79254)
RNeasy Plus Mini Kit	Qiagen (74134)
TaKaRa Ex Taq® DNA polymerase	TaKaRa (RR001C)
TURBO DNA-*free*™ Kit	Thermo Fisher (AM1907)
Cell Proliferation Reagent WST-1	Sigma-Aldrich (5015944001)

2.10 Consumables

Plasticware and other consumables were in general purchased from VWR, Greiner Bio-One, Corning, Thermo Fisher or Omnilab. Tissue culture-treated plates and flasks were bought from Omnilab, except for black, clear flat bottom 96-well plates (VisionPlate 96-well) that were obtained from 4titude.

3 Methods

3.1 Microbiological methods

3.1.1 Cultivation of *H. pylori*

H. pylori streaked from freezer stocks (Table 3.1) were grown for 3 days on serum plates (Table 3.2) under microaerobic atmosphere (85 % N_2, 10 % CO_2, 5 % O_2) at 37 °C (MI22N, Scholzen). For optimal bacterial fitness and to prevent overgrowth, strains were transferred to fresh agar plates every day and kept at 37 °C under microaerobic atmosphere or 10 % CO_2. To avoid accumulation of mutations that might interfere with experimental outcome, *H. pylori* was only passaged four to five times.

Table 3.1 Freezing medium used for long term storage of bacteria at -80 °C

	Final amount
Brucella broth (BD, 28 g/l)	70 %
FCS	10 %
Glycerol	20 %

Table 3.2 Composition of “serum plates”

	Final concentration
GC agar (Oxoid)	36 g/l
Horse serum	8 %
Vitamin mix	1 %

Liquid cultures of *H. pylori* were performed in Brucella broth/10 % FCS (heat inactivated) (BB/FCS) at 37 °C under microaerobic atmosphere in an anaerobic pot or at 10 % CO_2 under gentile agitation.

3.1.2 Measuring the optical density of bacterial suspensions

The optical density at 550 nm (OD_{550}) is commonly used to estimate the number of bacterial cells/ml. In case of *H. pylori*, an OD_{550} of 0.1 correlates with approximately $3x10^7$ cfu/ml. To determine the OD_{550}, bacteria were diluted in D-PBS, transferred to a 1 ml cuvette, and OD_{550} was measured in a spectrophotometer (DR2000, Hach).

3.1.3 Genetic manipulation of *H. pylori*

A transformation protocol modified from Haas *et al.* (1993) was used for genetic manipulation of *H. pylori*. Bacteria grown on plates were diluted to an OD_{550} of 0.1-0.2 in 1 ml BB/FCS and

incubated at 37 °C, 10 % CO_2 under gentile agitation for 2 h. Next, plasmid DNA, genomic DNA or PCR products were added, and cultures were grown for further 4 h taking advantage of *H. pylori`s* natural competence for taking up foreign DNA and it`s highly active recombination system. Bacteria were harvested by centrifugation at 4000 rpm for 5 min (Mikro 120, Hettich) and spread on serum plates containing the respective antibiotic (see Table 2.7). After 3-5 days cultivation at 37 °C under microaerobic atmosphere, single colonies were picked and further tested for successful transformation.

To obtain marker-free mutants, the streptomycin susceptibility counterselection strategy was used (Dailidiene *et al.,* 2006). Therefor a streptomycin resistant recipient strain was first transformed with an *rpsL-erm* cassette-containing deletion plasmid. Resulting erythromycin resistant and at the same time streptomycin sensitive clones were subsequently transformed with the corresponding plasmid encoding the tagged gene variant to reintroduce it into the original locus.

3.1.4 Determination of MIC values

The minimal inhibitory concentration (MIC) is defined as the lowest compound concentration that completely inhibits growth. Broth microdilution assay (see 3.1.12) was used to determine MIC values in liquid cultures. Additionally, MICs were evaluated for growth on serum plates supplemented with the respective compounds and antibiotics. Thus, inhibitors were added to the hot agar prior to solidification or compounds were spread on the already solid agar surface. All substances were tested in two-fold dilutions. *H. pylori* P12 (OD_{550} = 0.1, 5 µl) was spotted on the agar and grown for 2 days at 37 °C, 10 % CO_2 to obtain MIC values.

3.1.5 Disk diffusion test

To compare the sensitivity of different *H. pylori* mutants to selected small molecule inhibitors, the zones of inhibition were determined via disk diffusion tests.

To do so, bacteria were harvested, the OD_{550} was adjusted to 0.1 and 100 µl of the respective strains were plated on non-selective serum plates. Sterile paper disks (Ø 0.6 cm) were placed on the agar and 15 µl of the compound of interest diluted to the indicated concentration in BB medium were applied. Bacteria were grown under standard conditions for 3-4 days and the zones of inhibition were measured.

3.1.6 Evaluating the rate of spontaneous emergence of resistance

A protocol adapted from Björkholm *et al.* (2001) was used to determine the spontaneous emergence of resistance. Thus, an *H. pylori* liquid culture was started with a low amount of bacteria ($6x10^5$ cfu) in a small volume of BB/FCS (50 µl) and grown for 12 h at 37 °C, 10 % CO_2 under gentile agitation in a 96-well plate. The culture volume was subsequently increased to 500 µl and finally to 10 ml in a cell culture flask (T25). After 2-3 days, bacteria in the

stationary growth phase were harvested (4000 rpm, 20 min, Megafuge 16R, Thermo Scientific) and resuspended in 1 ml BB/FCS. Next, 100 µl were spread on serum plates supplemented with the indicated concentration of the compound of interest (this corresponds to 1 ml of the original culture). In parallel, the total number of cfu/ml was determined. Plates were incubated for 5-6 days at 37 °C, 10 % CO_2 and colonies were counted. Resistance rates were computed by dividing by the viable count. The median was calculated from at least five independent experiments with three independent cultures each, thus occasional jackpot cultures have no influence on the statistics.

Due to the minimal amount of bacteria used to inoculate the liquid cultures, the presence of resistant mutants in the initial samples was considered to be rather unlikely. To further prove this assumption, $6x10^6$ cfu, *i.e.* ten times the inoculum, were plated on selective plates without liquid culturing. In general, in five independent experiments, less than ten (rifampicin) and less than three (all other tested compounds) mutants per plate were observed.

3.1.7 Testing for cross resistance

H. pylori P12 wt and NuoB or NuoD mutant strains were collected from serum plates and OD_{550} was adjusted to 0.1. 5 µl bacteria were spotted on serum plates supplemented with the indicated concentrations of the compounds. Growth was checked after 2-3 days incubation and pictures were taken using a SLR camera (Canon).

3.1.8 Motility assay

Bacterial motility was assessed testing the swarming behavior on soft agar plates (Table 3.3). Briefly, *H. pylori* grown on serum plates were harvested, diluted to an OD_{550} of 30 and 5 µl bacterial suspension were spotted on the soft agar. The diameter of the area of spreading was measured after 5-6 days incubation under microaerobic atmosphere, 37 °C.

Table 3.3 Soft agar plates

	Final concentration
BB	28 g/l
FCS	8 %
Vitamin mix	1 %
BactoAgar	4 g/l

3.1.9 Time-to-kill kinetics monitoring

Antibiotics can in general be classified as bactericidal or as bacteriostatic. Whereas the latter ones only block bacterial growth, bactericidal agents kill the target organism. Frequently, this classification is concentration-dependent and species-specific.

The method of choice to discriminate between bactericidal and bacteriostatic is a killing kinetics assay that gives information about time-dependent killing, too. An agent is classified as bactericidal under the defined testing conditions if its killing efficiency is at least 99.9 % (*i.e.* a ≥3 $\log_{10}$ cfu/ml reduction in colony count from the initial inoculum) (French, 2006). Otherwise, it is bacteriostatic.

To monitor killing kinetics, *H. pylori* liquid cultures were inoculated to an initial OD_{550} of 0.05 and test compounds were added to the indicated concentration. Cultures were incubated at 37 °C, 10 % CO_2 under gentile agitation. At distinct time points (0 h, 0.5 h, 1 h, 2 h, 4 h, 8 h and 24 h) aliquots were plated to determine the viable count.

3.1.10 Cultivation of other bacteria

E. coli was grown on LB-plates (Lennox-L agar 32 g/l, Life Technologies) at 37 °C. Lennox-L broth (20 g/l, LB, Invitrogen) was used for liquid cultures. For long term storage, bacteria were resuspended in freezing medium (see Table 3.1) and frozen at -80 °C. *L. reuteri* was grown in Anaerobic Akkermansia Medium as described previously (Eberl *et al.,* 2019). All other bacterial species were cultivated as indicated in Table 2.2. Growth curves of strictly anaerobic species were performed and kindly provided by D. Ring and Prof. Dr. B. Stecher.

3.1.11 Genetic manipulation of *E. coli*

3.1.11.1 Generation of chemically competent *E. coli*

Chemically competent cells were generated according to the protocol modified from D. Hanahan (1983). Briefly, 10 ml preculture were inoculated with *E. coli* (TOP 10) from the glycerol freezer stock and grown overnight at 37 °C, 200 rpm. The next day, 200 ml main cultures were inoculated to an OD_{550} of 0.15-0.2 and incubated at 37 °C, 200 rpm until a final OD_{550} of 0.5-0.6. Cultures were cooled down on ice for 5 min and bacteria were subsequently harvested at 4 °C, 4000 rpm for 15 min (Megafuge 16R, Thermo Scientific). Next, pellets were resuspended in 2/5 volume ice cold buffer TfbI (see 2.7) and rest on ice for 5 min. After harvesting by centrifugation, cells were resuspended in 1/25 volume ice cold buffer TfbII (see 2.7) and 50 µl aliquots were immediately frozen in liquid nitrogen. Chemically competent *E. coli* were stored at -80 °C.

3.1.11.2 Transformation of chemically competent *E. coli*

50 µl competent cells were thawed on ice and incubated with 10 µl ligation mixture or 1 µl plasmid DNA for 30 min on ice to allow attachment of DNA to the RbCl-treated cell membranes.

Following, bacteria were heat shocked at 42 °C for 90 s in a water bath to open membrane pores and allow DNA uptake. 1 ml LB was added, and cells were incubated at 37 °C for 1 h before spreading on selective plates (see 2.8). After one day cultivation at 37 °C, single colonies were picked and further tested for successful transformation.

3.1.11.3 One-step inactivation of chromosomal genes in *E. coli*

The knockout of chromosomal genes in *E. coli* was performed according to the one-step inactivation protocol established by Datsenko and Wanner in 2000. This method is based on the Red recombinase system which allows gene disruption by transformation with linear DNA fragments. The bacteriophage-derived λ Red system encodes three proteins, one of them, Gam, inhibits the bacterial RecBCD exonuclease V thus preventing degradation of the linear DNA. The other two proteins, Exo and Bet, promote recombination. All three are provided on the λ Red helper plasmid pKD46 under the control of an arabinose inducible P_{araB} promoter. pKD46 is a low copy number plasmid with a temperature-sensitive replicon which is easily eliminated if bacteria are grown at 37 °C without antibiotic selection pressure.

The DNA for targeted gene-replacement is generated by PCR using primers with 36- to 50-nt extensions that are homologous to the flanking regions of the gene of interest and a resistance cassette encoding template plasmid (pKD4). Using this system, targeted gene knockout can in theory be performed in any *E. coli*.

Briefly, *E. coli* (TOP10) carrying the λ Red helper plasmid pKD46 were grown at 30 °C to an OD_{550} of 0.6 in LB supplemented with 100 µg/ml ampicillin and 10 mM L-arabinose and made chemically competent as described above.

50 µl of these freshly prepared cells were then transformed with 4-6 µg *Dpn*I digested, purified and enriched PCR product (3.3.4) as described for plasmid transformation.

Transformants were checked for successful gene replacement via PCR.

3.1.12 Growth curves and broth microdilution assay

Bacteria grown on plates were diluted to an OD_{550} of 0.075 or 0.15 in BB/FCS (*H. pylori*) or LB (*E. coli*) and subcultured in 96-well plates (clear, flat-bottom). Plates were sealed with a gas permeable membrane (Breathe-Easy® sealing membrane, Diversified Biotech) and incubated at 37 °C, 200 rpm in a plate reader (*E. coli*: Fluostar (BMG Labtech), *H. pylori*: Clariostar (BMG Labtech)). In case of *H. pylori*, CO_2 levels were adjusted to 10 % using an atmospheric control unit (BMG Labtech). OD_{550} was automatically measured every 5 min until the stationary phase was reached. To evaluate antimicrobial activity of selected small molecule inhibitors *in vitro*, the same experimental setup was performed, but additionally the respective compounds were added to the corresponding concentrations. Inhibitors were tested in serial two-fold or ten-fold dilutions.

Growth curves were processed using the MARS Data Analysis software 3.30 applying a curve smoothing factor of 21 and IC_{50} values were calculated from five independent experiments using Graph Pad Prism 5.01. The lowest compound concentration that showed complete growth inhibition in five independent experiments was determined as the MIC.

3.1.13 Evaluation of the effects of platin compounds on bacterial fitness

To evaluate the viability after cisplatin treatment, *H. pylori* grown on plates were harvested and OD_{550} was adjusted to 0.1. Bacteria were incubated for 2 h in D-PBS/10 % FCS (PBS/FCS) or BB/FCS supplemented with 100 µM cisplatin in DMSO or DMSO only at 37 °C, 10 % CO_2 in the presence of AGS cells. 5 µl culture were spotted on serum plates and growth was checked after 24 h incubation.

3.2 Cell culture

3.2.1 Cultivation and storage of cell lines

AGS and L929, both adherent cell lines, were grown in T75 cell culture flasks under standard conditions (see Table 2.3). To harvest cells for further experiments or subculturing, cells were washed once with D-PBS and trypsinized using 0.05 % Trypsin-EDTA. The enzyme activity was stopped by diluting with culture medium.

Considering an approximate doubling time of 20-24 h for AGS as well as for L929, cells were splitted to the desired confluency using the guiding values for culturing listed in Table 3.4.

Table 3.4 Guiding values for cell culturing

	Number of cells (confluent)	**Volume [ml]**
T75 flask	$9.4x10^6$	10
T25 flask	$3.1x10^6$	5
6-well plate/well	$1.2x10^6$	2
12-well plate/well	$5x10^5$	1.5
96-well plate/well	$4.5x10^4$	0.2

For long term storage, approximately $3x10^6$ cells were resuspended in 1 ml freezing medium (45 % RPMI/50 % FCS/5 % DMSO). Samples were frozen at a controlled rate of cooling (-1°C/min) in cryogenic tubes using the Nalgene Mr. Frosty Cryo 1 °C Freezing Containers at -80 °C for at least 24 h. Afterwards, stocks were transferred to liquid nitrogen tanks.

To thaw cells, freezer stocks were gently thawed in warm water, cells were washed ones with pre-warmed culture medium (900 rpm, 5 min, Megafuge 3.0 R, Thermo Scientific) and seeded into T75 cell culture flasks.

3.2.2 Generation of an AGS cell line expressing the HaloTag-LgBiT fusion protein

In order to measure the translocation of HiBiT-tagged proteins to eukaryotic host cells *in vitro*, a cell line stably expressing the HaloTag-LgBiT fusion protein was generated. Therefore, AGS cells were transfected with pCS1956B02, a vector purchased form Promega, allowing for stable integration and subsequent expression of the target protein under the control of a strong CMV (cytomegalovirus) promotor. A more detailed description of the recombinant fusion protein is given in section 4.1.

Prior to transfecting, the hygromycin concentration suitable for AGS cell selection was determined. Therefor, AGS cells were seeded in 6-wells and grown to 80-90 % confluency. Next hygromycin (0.1 mg/ml - 1 mg/ml) was added, medium was replaced every 2-3 days and fresh antibiotic was added. The lowest concentration that completely blocked growth and killed all cells after one week of incubation was 0.5 mg/ml.

The day before transfection, AGS cells were seeded in a 6-well and grown to 80-90 % confluency. Next, 4 µg plasmid DNA were diluted in 250 µl Opti-MEM (without serum). In parallel 10 µl lipofectamine 2000 (Life Technologies) were gently diluted in 250 µl Opti-MEM and incubated for 5 min at RT. Afterwards the diluted DNA and the diluted lipofectamine 2000 were combined, gently mixed by inversion and incubated for 20 min at RT. This mixture was then added to the respective 6-well and samples were incubated at 37 °C, 5 % CO_2 for 24 h before 0.5 µg/ml hygromycin was added. The medium containing the selective antibiotic was replaced every 2-3 days.

Successful transfection was confirmed by staining an aliquot of cells with a fluorescent, chloroalkane linker-containing dye. Briefly, cells were seeded in 8-well µ-slides (IBIDI). Once 80-90 % confluent, cells were stained overnight with the TMR-ligand that irreversible binds the HaloTag-LgBiT protein via a chloroalkane linker (1:1000 diluted, Promega #G299A, λ_{ex} = 552 nm, λ_{em} = 578 nm). The next day, cells were washed twice with D-PBS and analyzed by fluorescence microscopy (TCS SP5, Leika). Equally stained AGS wt cells served as control. ImageJ 1.48v was used to process the data.

HaloTag-LgBiT expressing cells were cultured in RPMI/10 % FCS supplemented with 0.5 µg/ml hygromycin. The day before infection experiments with *H. pylori*, this medium was replaced by RPMI/10 % FCS without antibiotics.

Fluorescence activated cell sorting (FACS) was used to develop single cell clone-derived cell lines. Thus, transfected AGS cells grown in T25 cell culture flasks were stained overnight with R110-ligand (1:1000 diluted, Promega #G322A, λ_{ex} = 498 nm, λ_{em} = 528 nm). After washing twice with D-PBS, cells were detached (see 3.2.1) and pressed through a cell strainer. Individual cells with strong R110 staining were transferred to a 96-well plate using the FACS-Aria™ III at the CyTUM-MIH core facility (TU Munich). Cells were grown in RPMI/10 % FCS supplemented with 0.5 mg/ml hygromycin and the appropriate volume of a 100x penicillin-

streptomycin stock (Life Technologies). Clones were subsequently splitted to larger culture flasks and finally frozen for further experiments.

3.2.3 Evaluation of cytotoxicity

Proliferation and viability of eukaryotic cells treated with small molecule inhibitors was assessed using the WST-1 cell proliferation assay (Roche/Sigma-Aldrich).

WST-1 is a tetrazolium salt that is cleaved to formazan by the “succinate-tetrazolium reductase” system which is only functional in metabolically active cells (Hörper, 1997). The amount of formazan dye can be photometrically determined and correlates directly with the amount of metabolically active cells per well.

Briefly, murine L929 fibroblasts seeded into 96-well plates ($3.0x10^5$ cells/well, black, clear flat-bottom, 4titude) were cultured in Phenol red-free medium (see Table 2.3) for 24 h at 37 °C, 5 % CO_2. Next, test compounds or DMSO were added to the respective concentrations and incubation was continued for 3 days. WST-1 reagent was added according to the manufacturer’s protocol and plates were kept at 37 °C, 5 % CO_2 for 1 h. The absorbance at 450 nm and 690 nm (reference wavelength) was recorded in a plate reader (Clariostar, BMG Labtech). For evaluation, the difference of A_{450nm} and A_{690nm} was calculated, and the blank control (only medium and WST-1) was subtracted. Percental viability was normalized to the untreated control.

3.3 Molecular biology methods – Working with nucleic acids

3.3.1 Isolation of genomic DNA from bacteria

The DNeasy Blood & Tissue Kits (Qiagen) was used to extract whole genomic DNA from bacterial samples. Briefly, bacteria grown on agar plates were pelletized (4500 rpm, 5 min, Mikro 120, Hettich) and resuspended in 180 µl buffer ATL. 20 µl proteinase K were added and samples were incubated at 56 °C, 800 rpm for at least 3 h (Thermomixer compact, Eppendorf) until complete lysis. Next, 200 µl buffer AL were added, samples were vortexed and incubated for 10 min at 70 °C. After addition of 200 µl ethanol and subsequent vortexing, the mixture was applied to a silica-membrane. The spin-column was centrifuged at 8000 rpm for 1 min (Mikro 120). Membrane-bound DNA was first washed with 500 µl buffer AW1 (8000 rpm, 1 min, Mikro 120) and next with 500 µl AW2 (14000 rpm, 3 min, Mikro 120). To avoid ethanol carryover, samples were ones more spun down (14000 rpm, 1 min, Mikro 120). Finally, 200 µl ddH_2O were applied to the column, samples were incubated for 1 min and genomic DNA was eluted at 8000 rpm, 1min (Mikro 120). Genomic DNA was stored at -20 °C.

3.3.2 Plasmid isolation from *E. coli*

Plasmid DNA from *E. coli* was purified by alkaline lysis followed by isopropanol precipitation. Bacteria grown on plates were collected in D-PBS and harvested by centrifugation (4500 rpm, 5 min, Mikro 120, Hettich). Pellets were resuspended in 250 µl buffer P1 (see 2.7) and bacteria were lysed by adding 250 µl buffer P2 (see 2.7). To neutralize and stop alkaline lysis, 350 µl N3 (see 2.7) were added and samples were mixed by inversion. Cell debris were removed by centrifugation (14000 rpm, 10 min, Mikro 120) and the supernatant was transferred to a new collection tube. Nucleic acids were precipitated by adding 650 µl isopropanol and incubation at -20 °C for 20 min. Next, plasmids were harvested by centrifugation at 14000 rpm for 10 min (Mikro 120), once washed with 500 µl 70 % ethanol and dried using a vacuum centrifuge (DNA110, Savant). Plasmids were solved in 50 µl ddH_2O and stored at -20 °C.

3.3.3 Polymerase chain reaction (PCR)

To specifically amplify DNA via PCR, the *TaKaRa Ex Taq* DNA polymerase was used, that has 3'-to-5' exonuclease proofreading activity. The general reaction mixture and the standard cycling protocol are shown in Table 3.5 and Table 3.6. Annealing temperatures were adjusted to the primer pairs used and elongation times were adapted to the respective amplicon size. PCRs were performed on the peqstar thermocycler (Peqlab Biotechnologie GmbH).

Table 3.5 Master mix composition for one reaction (*TaKaRa Ex Taq* DNA polymerase)

	Volume [µl]	**Final concentration**
10x Ex Taq™ Buffer (Mg^{2+} free)	5.0	1x
TaKaRa Ex Taq™ (5 U/µl)	0.1	0.01 U/µl
dNTP mixture (2.5 mM each dNTP)	4.0	0.2 mM each dNTP
$MgCl_2$ (25 mM)	6.0	3 mM
Forward primer (10 µM)	1.0	0.2 µM
Reverse primer (10 µM)	1.0	0.2 µM
Template	1.0-5.0	
	Add ddH_2O to a final volume of 50 µl	

Table 3.6 PCR cycling conditions

	Temperature [°C]	Time [min]
Initial denaturation	94	10
30-35 cycles	94	0.5
	48-54	0.5
	68	1/kb
Final elongation	68	10
Storage	10	

To generate PCR products suitable for blunt-end ligation, target DNA was first amplified by *TaKaRa Ex Taq* DNA polymerase using one 5'-phosphorylated primer. Next, nucleic acids were purified (3.3.6) and *Dpn*I treated for 0.5 h to remove methylated template DNA (3.3.7). 0.1 µl Pfu polymerase (stock 2.5 U/µl, Stratagene) and 4 µl dNTPs (stock 2.5 mM each dNTP) were added directly to the restriction enzyme mixture (50 µl) and sample was incubated at 72 °C for 30 min (Thermomixer compact, Eppendorf) to generate blunt-end PCR products.

3.3.4 Quantification and enrichment of DNA

Nucleic acid concentrations were measured using a NanoDrop spectrophotometer (ND-1000, Peqlab Biotechnologie GmbH). The ratios of the absorbance at 260 nm and 280 nm (A_{260}/A_{280}) and at 260 nm and 230 nm ($A_{260}/_{230}$) were taken to access purity of nucleic acid samples. Values of about 1.8 (A_{260}/A_{280}) and 2.0-2.2 ($A_{260}/_{230}$) are generally considered to indicated pure DNA samples.

To enrich digested and purified PCR products solved in ddH_2O, samples were mixed with buffer N3 (10 % (v/v), see 2.7) and isopropanol (70 % (v/v)). Nucleic acids were precipitated at -20 °C for 20 min. Samples were spun down at 14000 rpm for 10 min (Mikro 120, Hettich) and afterwards washed with 500 µl 70 % ethanol. After complete drying using a vacuum centrifuge (DNA110, Savant), nucleic acids were finally solved to the desired concentration in ddH_2O and stored at -20 °C.

3.3.5 Gel electrophoresis

Amplified PCR products were visualized using gel electrophoresis. Thus, samples were mixed with DNA electrophoresis loading dye (see 2.7) and subjected to an agarose gel (1-2 % agarose (w/v) in TAE buffer). GeneRuler 1 kb or 100 bp DNA ladder (Thermo Fisher) was used for determination of sizes. Nucleic acid molecules were separated by applying an electric field. Afterwards gels were stained either in an ethidium bromide bath to visualize bands using an

ultraviolet transilluminator (GelDoc™ XR, BioRad) or using methylene blue and subsequent destaining with water to excise target nucleic acids from the agarose gels.

3.3.6 Purification of DNA fragments

DNA fragments from PCR mixtures, restriction enzyme digests or DNA-containing agarose gel bands were isolated via the Illustra GFX™ PCR DNA and Gel Band Purification Kit according to the manufactures protocol. Briefly, 50 µl sample were mixed with 500 µl capture buffer, thoroughly mixed by vortexing and loaded on a column. In case of DNA-containing agarose gel bands, 10 µl capture buffer were added per 10 mg gel. Samples were incubated at 56 °C until the agarose was completely melted and then transferred to the column. After centrifugation (1 min, 14000 rpm, Mikro 120, Hettich) the flow through was discarded and the column-bound DNA was washed with 500 µl washing buffer. To avoid ethanol carryover, samples were ones more spun down (14000 rpm, 1 min, Mikro 120). Finally, 50 µl ddH_2O were applied to the column, samples were incubated for 1 min and DNA was eluted at 14000 rpm, 1 min (Mikro 120). DNA was stored at -20 °C.

3.3.7 Restriction enzyme digestion

Plasmids and DNA fragments were digested using enzymes from NEB. Reactions were mixed as listed in Table 3.7 using the restriction enzyme specific 10x buffer provided by the manufacturer. Digestions were incubated at 37 °C for 1 h in case of analytic samples and at least 3 h in case of preparative ones.

Table 3.7 Restriction enzyme digestion mixtures

	Analytic digestion	**Preparative digestion**
10x buffer [µl]	1	5
Restriction enzyme(s) [µl]	0.5	1
Plasmids/DNA fragments [µl]	5	40
	Add ddH_2O to a final volume of 10 µl	Add ddH_2O to a final volume of 50 µl

3.3.8 Ligation

Sticky end and blunt end ligations were performed using the T4 DNA ligase (NEB). Therefore, 7 µl insert were mixed with 1 µl vector, 1 µl 10x ligase buffer and 1 µl enzyme and incubated at 4 °C overnight. In case of blunt end ligations, 5 µl PCR product were mixed with 3 µl ddH_2O, 1 µl 10x ligase buffer and 1 µl ligase.

3.3.9 Sequencing and *in silico* cloning

DNA samples were sequenced by GATC Biotech using Lightrun sequencing service. Thus, 5 µl of purified PCR product or plasmid DNA (20-80 ng/µl) were mixed with 5 µl primer (10 µM) and sent to GATC/Eurofins Genomics. Sequences were analyzed using CLC Main Workbench 7. This software was also used to design plasmids *in silico* and for general sequence analysis. RNAseq data were generated and evaluated by GeneWiz. IGV 2.8.12 was used to visualize and analyze the data.

3.3.10 Isolation of bacterial RNA

Total RNA was isolated from *H. pylori* cultivated for 2 h at 10 % CO_2, 37 °C in PBS/FCS at an OD_{550} of 0.1 in a total volume of 30 ml. Additionally, samples were prepared from bacteria directly taken from serum plates. After harvesting the cells (4000 rpm, Megafuge 16R, Thermo Scientific, 20 min, 4 °C), pellets were flash frozen in liquid nitrogen and stored at -80 °C until further processing.

The RNeasy Kit (Qiagen) was used to isolate total bacterial RNA. Thus, bacterial pellets were suspended in 700 µl buffer RLT containing 1 % β-mercaptoethanol. Lysis matrix B 2 ml tubes with 0.1 mm silica beads (MP biomedicals) were used to mechanically disrupt the cells in a precellys 24 tissue homogenizer (40 s, 5500 rpm, Bertin Technologies). After removing cell debris by centrifugation (12000xg, 5 min, 4 °C), the supernatant was mixed with an equal volume of pre-cooled 70 % ethanol. Subsequently, the samples were transferred to RNeasy spin columns and centrifuged for 15 s at 9000xg, 4 °C to bind the RNA to the silica membrane. To remove DNA, an on-column DNase I digestion was performed (#79254, Qiagen). Thus, columns were firstly washed with 350 µl buffer RW1 (15 s, 9000xg, 4 °C) and then 80 µl DNase I in buffer RDD (10 µl DNase I + 70 µl RDD) was applied to the spin column membrane. Samples were incubated for 15 min at RT before washing again with 350 µl RW1. Next, membranes were washed twice with 500 µl buffer RPE (9000xg, 4 °C, 15 s and 2 min, respectively). Finally, remaining ethanol was removed by centrifugation for 1 min at full speed and RNA was eluted in 40 µl RNase free H_2O (1 min, 9000xg, 4 °C).

To obtain DNA free samples appropriate for RNA sequencing, a second DNase digestion was performed using the TURBO DNA-*free* kit. Thus, 40 µl of the RNA sample were mixed with 4 µl 10x Turbo DNase buffer and 2 µl DNase were added. Samples were incubated at 37 °C for 30 min. To stop the DNase digestion, 9.2 µl inactivation reagent were added and samples were kept for 5 min at RT before centrifugation for 1.5 min at 10000xg, 4 °C. Finally, the sample was transferred to a fresh tube and stored at -80 °C for further use.

3.3.11 Quality control of RNA samples

To assess purity and amount of isolated bacterial RNA, sample were subjected to three quality control analyses. First, concentrations and A_{260}/A_{280} were determined using a NanoDrop

spectrophotometer (ND-1000, Peqlab Biotechnologie GmbH). Values of about 1.8-2.2 (A_{260}/A_{280}) were generally considered to indicated samples appropriate for RNAseq experiments. Second, PCRs using primers UB110/UB111 were performed to exclude DNA contaminations. Finally, RNA samples were checked with the Experion RNA Analysis Kit (Experion RNA StdSens, BioRad) according to the manufacturer's protocol and RQI values were determined (Experion Automated Electrophoresis System, BioRad).

3.4 Methods to monitore effects on the respiratory chain

3.4.1 Oxygen consumption measurements

To monitor oxygen consumption of bacteria and eukaryotic cells over time, OxoPlates (OP96U, Presence) were used. Via an integrated optical sensor at the bottom of each well of these 96-well U-bottom plates, the dissolved oxygen concentration can be easily measured in a fluorescence plate reader. The optical sensor consists of two immobilized fluorophore species, both exited at 550 nm. The fluorescence intensity of the oxygen sensing fluorophore is reduced by increasing oxygen concentrations and can be detected at 650 nm (I_{650}). The second fluorophore serves as internal, oxygen-insensitive standard and emits light at 590 nm (reference wavelength, I_{590}). (John *et al.,* 2003)

Every batch of OxoPlates was calibrated using oxygen-free water (cal0) and air-saturated water (cal100) according to the manufacturer's instructions. Therefor oxygen-free water was generated by dissolving 0.15 g Na_2SO_3 in 15 ml ddH_2O in a tightly closed 15 ml conical tube. To prepare the air-saturated calibration standard, 20 ml ddH_2O were filled in a 50 ml conical tube and shaken vigorously for 2 min. Afterwards the tube was opened and gently moved for 1 min to avoid oversaturation of the water. Both calibration standards were measured in quadruplicates using 200 µl/well cal100 and 300 µl/well cal0. Prior to measuring, OxoPlates were incubated with the respective samples for 1 h at 37 °C to allow equilibration of the sensors. To avoid oxygen intake during pre-incubation and measurement, cal0 samples were sealed with an adhesive film.

To measure oxygen consumption of bacteria treated with small molecule inhibitors, *H. pylori* or *E. coli* grown on plates were diluted to an OD_{550} of 1 in nutrient-free buffer (D-PBS), OxoPlates were filled with 140 µl bacterial suspension per well and incubated for 10 min at 37 °C in a 10 % CO_2 incubator. Next test compounds were added, and incubation was continued for further 10 min. Oxygen consumption was monitored in a prewarmed plate reader (Fluostar, BMG Labtech) at 37 °C for 20-30 min using the time-resolved mode (integration start: 0 µs, integration time: 500 µs). I_{650} and I_{590} were recorded every 2 min and in the third cycle (*i.e.* after 4 min) 4 µl pyruvate (250 mM stock in D-PBS) were injected.

The partial oxygen pressure (pO_2) was calculated as percentage of oxygen saturated air using the following equation:

pO_2 [% air saturation] = 100 x [$(I_{650}/I_{590})_{cal0}$ / $(I_{650}/I_{590})_{sample}$ - 1] / [$(I_{650}/I_{590})_{cal0}$ / $(I_{650}/I_{590})_{cal100}$ - 1]

To monitor the oxygen consumption of eukaryotic cells, L929 cells were harvested as described above (3.2.1) and washed twice with D-PBS. In the meantime, OxoPlates were pre-incubated with 70 µl D-PBS at 37 °C to allow equilibration of the optical sensor. Next, $1x10^6$ cells/70 µl and the test compounds were added to each well and incubated for 10 min at 37 °C. Oxygen consumption was monitored for up to 1 h as described for bacterial samples.

3.4.2 ATP content measurements

The ATP Bioluminescence Assay Kit CLS II was used to determine the ATP content of *H. pylori* treated with small molecule inhibitors. Thereby the emission of light is detected that is generated by the luciferase from *Photinus pyralis* (American firefly) when converting luciferin to oxyluciferin in an ATP-dependent manner.

Briefly, 450 µl *H. pylori* (OD_{550} 0.15 in BB/FCS) were incubated with the respective compounds for 5 min at 37 °C, 10 % CO_2 and subsequently harvested by centrifugation (8000xg, 5 min). The supernatant was discarded, and the cell pellet was resuspended in 75 µl cold 100 mM Tris/HCl, 4 mM EDTA (pH 7.6). The samples were boiled for 2 min and centrifuged for 1 min at 10000xg, 4 °C to remove cell debris. 50 µl of the ATP-containing supernatant were transferred to a 96-well plate (black, clear flat bottom, Corning) and measurement was immediately started in a plate reader (Clariostar, BMG Labtech). Bioluminescence was recorded with 1 s delay after automatic injection of 50 µl luciferase reagent per well using a signal integration time of 10 s. ATP contents were calculated as percentage of the untreated control after subtracting the blank value (100 mM Tris/HCl, 4 mM EDTA).

The same experimental setup was applied to monitor the ATP content of bacteria incubated for different time frames in PBS/FCS.

3.4.3 Membrane potential staining

Symmetric cyanine dyes as for example 3,3-diethyloxacarbocyanine iodide ($DiOC_2(3)$) enable the highly sensitive and accurate measurement of bacterial membrane potentials via flow cytometry. In its monomeric state, $DiOC_2(3)$ emits green fluorescence (λ_{ex} = 488 nm, λ_{em} = 530 nm), but aggregates are formed in cells with intact membrane potential due accumulation of the dye at hyperpolarized membranes. Those aggregates emit red fluorescence (λ_{ex} = 488 nm, λ_{em} > 600 nm). Using high concentrations of $DiOC_2(3)$ all bacteria are in general stained green. Thus, the ratio of red to green fluorescence, *i.e.* potential-sensitive to potential independent fluorescence, is a measure for bacterial membrane potential. (Novo *et al.,* 1999)

BacLight™ Bacterial Membrane Potential Kit was used to access the membrane potential of *H. pylori* treated with small molecule inhibitors. 100 µl bacteria (OD_{550} 0.075 in PBS/FCS) were incubated for the indicated time with the respective compounds at the particular concentrations at 37 °C, 10 % CO_2. CCCP, an ionophore, was used as control for destruction of membrane potential. Next, 12.5 µl of the bacterial suspension were transferred to 200 µl D-PBS supplemented with 1 mM EDTA and 15 µM $DiOC_2(3)$ and stained for 30 min at 37 °C, 10 % CO_2. Red and green fluorescence was measured by flow cytometry using PE- and FITC-settings (BD FACSCanto™ II, BD). Results were evaluated using FlowJo10.0. For quantitative evaluation, the PE-A/FITC-A median of the unstained sample was first subtracted, and samples were subsequently normalized to the DMSO-treated control.

3.4.4 Isotopologue profiling

Isotopologue profiling is an advanced technique that enables the study of the central metabolic pathways in living organisms under defined conditions. Labeled precursors, in this case carbon substrates containing ^{13}C, are metabolized by *H. pylori* and the resulting ^{13}C-excess and isotopologue patterns allow a reconstruction of the functional metabolic pathways.

For ^{13}C labeling experiments, *H. pylori* P12 grown on plates were diluted to an OD_{550} of 0.1 in BB/FCS and precultured for 8 h under microaerobic atmosphere at 37 °C under agitation. Next, main cultures (50 ml) were inoculated to a final OD_{550} of 0.05 and supplemented with 10 mM [U-$^{13}C_6$]D-glucose (Sigma-Aldrich). Cultures were grown overnight under microaerobic atmosphere at 37 °C under agitation. Following the overnight culture, bacteria were treated for 5 min with the respective inhibitors. Therefor the 50 ml cultures were firstly incubated for 2 h, 37 °C, 10 % CO_2 under agitation to equilibrate to the atmospheric conditions during treatment. Next, compounds were added, and incubation was continued for 5 min. Afterwards, samples were immediately cooled down on ice, bacterial pellets were harvested at 4000 rpm, 4 °C for 20 min (Megafuge 3.0 R, Thermo Scientific). Pellets were inactivated by freezing (30 min, dry ice) and subsequent boiling for 20 min. Pellets were stored at -80 °C for further analysis. All samples were prepared in duplicates.

The subsequent preparation of cytosolic metabolites and protein-bound amino acids as well as the analysis via gas chromatography/mass spectrometry (GC/MS) was performed by Thomas Steiner in the lab of Prof. Eisenreich, TU Munich.

In addition, isotopologue profiling was performed with the P12 V133M^{NuoD} mutant strain. Due to severe growth defects of these bacteria, precultures were inoculated to an OD_{550} of 0.2 and main cultures to an OD_{550} of 0.1, respectively. All further steps were performed as described for the wt strain.

Experiments were evaluated using the absolute ^{13}C-excess values of the respective metabolites or calculating the percentage of ^{13}C-surplus compared to the untreated control using the following equation:

$\Delta^{13}C$ surplus = ($^{13}C\text{-excess}_{sample}$ - $^{13}C\text{-excess}_{untreated\ control}$)/ $^{13}C\text{-excess}_{untreated\ control}$ x 100

3.5 Molecular biology and biochemistry methods

3.5.1 SDS-PAGE and immunoblotting

SDS-PAGE and subsequent Western blotting was used to detect protein synthesis in *H. pylori* as well as for semi-quantitative analysis of CagA translocation in AGS cells (see also section 3.6.1).

3.5.1.1 Sample preparation and SDS-PAGE gel electrophoresis

In general, bacterial samples were diluted to a final OD_{550} of 20 in D-PBS and the appropriate volume of 2x SDS sample buffer (see 2.7) was added. Samples were boiled for 10 min and spun down for 5 min at 14000 rpm (Mikro 120, Hettich). 5-10 µl of the cooled down mixture were loaded on an SDS-PAGE gel (Table 3.8) using the Mini-PROTEAN® (Bio-Rad) system. A pre-stained protein ladder (#26612/26616/26619, Thermo Fisher) was used for molecular weight determination. Electrophoresis was performed in SDS running buffer (see 2.7). Firstly, 90-100 V were applied for 10-20 min to allow samples to enter the stacking gel, next runs were continued at up to 140 V until the required separation was achieved.

Table 3.8 SDS-PAGE gel composition (for one gel), volume in [µl]

	Stacking gel	**Resolving gel**		
	4 %	**6 %**	**10 %**	**12 %**
ddH_2O	680	2600	1900	1600
30% Acrylamide/Bis-acrylamide 29:1	170	1000	1700	2000
Tris/HCl (1.5 M, pH 8.8)		1300	1300	1300
Tris/HCl (0.5 M, pH 6.8)	130			
SDS (10 %)	10	50	50	50
APS 25 % (w/v) in dH_2O	10	50	50	50
TEMED	1	4	2	2

3.5.1.2 Blotting

Proteins separated by SDS-PAGE were transferred to polyvinylidene difluoride (PVDF) or nitrocellulose membranes by semi-dry transfer at 1.25 mA/cm^2 for 90 min. The blotting sandwich was mounted using a three-buffer system (see 2.7): Two thin whatman papers

moisted with anode II were placed on top of two thick filter papers soaked with anode I buffer. Next, a PVDF membrane, activated in methanol and equilibrated in anode II, or a nitrocellulose membrane only equilibrated in anode II was added. The SDS-PAGE-gel was loaded on top and the sandwich was completed by two thin and two thick whatman papers, each soaked with cathode buffer.

3.5.1.3 Probing and developing

After successful transfer, membranes were blocked at least 1 h at RT in 5 % milk in TBS-T (see 2.7) to prevent non-specific binding of detection antibodies. Membranes were incubated with the respective primary antibody (Table 2.6) overnight at RT with gentle agitation. The next day, membranes were washed at least five times for 5 min with TBS-T. Then, the secondary antibody or protein A-AP was added for 1 h at RT and after additional washing steps, blots were developed: In case of horse radish peroxidase (POX)-coupled secondary antibodies, membranes were incubated for 5 min in 2 ml chemiluminescence substrate mixture and bands were visualized on an X-ray film. In case of protein A-AP development, blots were incubated in 5 ml developing solution (Table 3.9) until bands of interest were visible and the reaction was stopped by adding tap water.

Table 3.9 AP-developing solution

	Volume [ml]
Tris/HCl, (0.1 M, pH 9.6)	9
$MgCl_2$ (1 M)	0.07
BCIP (5 mg/ml in DMF)	0.1
NBT (1 mg/ml in 0.1 MTris/HCl)	1

3.5.1.4 Stripping

Using the POX system, PVDF membranes can be subsequently re-probed with different primary antibodies since the chemiluminescence developing does not leave a stain on the membrane. This allows for example to detect the protein of interest and a loading control on the same blot. After successfully developing for the first target, membranes were incubated for 10-30 min in stripping buffer (see 2.7) to remove primary and secondary antibodies. Afterwards, membranes were washed three times with TBS-T and a second time blocked in 5 % milk/TBS-T. Probing and developing was conducted as described above.

3.5.2 Bioluminescence-based assays to analyze protein synthesis

The NanoLuc luciferase complementation system that is in detail described in the result's section (4.1), can be used to analyze the expression of HiBiT-tagged proteins qualitatively using a modified Western blot protocol (3.5.2.1) or quantitatively via a lysate assay using a plate reader (3.5.2.2). Both systems are based on the high affinity of the HiBiT tag to the LgBiT fragment, generating a fully functional NanoLuc luciferase.

3.5.2.1 HiBiT blotting system

The Nano-Glo® HiBiT blotting system was used to detect HiBiT-tagged proteins immobilized on nitrocellulose membranes. This method is similar to a common immunoblot, but HiBiT-tagged target proteins are detected in an antibody-free manner by luciferase complementation. Thus, in the present work, blots developed by this method are labeled "α-HiBiT".

Briefly, bacterial lysates were generated, and samples were separated on an SDS-PAGE gel as described (3.5.1). As recommended by the manufacturer's protocol, proteins were blotted on a nitrocellulose membrane for optimal accessibility of the HiBiT tag and to reduce background autoluminescence caused by binding of the furimazine substrate to the membrane that is more pronounced in case of PVDF membranes. After successful transfer, membranes were incubated for at least 10 min in TBS-T to solubilize the HiBiT tag and wash away transfer buffers. Membranes were transferred to a 50 ml conical tube containing 3 ml 1x Nano-Glo® blotting buffer (10x Nano-Glo® blotting buffer diluted in ddH_2O) and recombinant LgBiT protein (1:200). Blots were incubated overnight at 4 °C under gentile agitation to achieve optimal binding of HiBiT and LgBiT. The next day, samples were equilibrated to RT and 6 µl 500x Nano-Glo® luciferase assay substrate were added. After 5 min incubation, bands were visualized using a chemiluminescence imager (ChemiDoc™ MP, BioRad). Pictures were processed using Image Lab 5.2.1.

3.5.2.2 HiBiT lysate assay

A modified protocol of the Nano-Glo® HiBiT blotting system was developed for highly sensitive detection and relative quantification of HiBiT-tagged protein expression using a plate reader. Thus, a defined amount of bacteria was lysed in cold RIPA buffer (see 2.7) on ice. 20 µl lysate were mixed with 20 µl 2x master mix (Table 3.10) in a 96-well plate (white, flat bottom). Plates were automatically shaked for 10 s at 300 rpm, double orbital by the plate reader (Clariostar, BMG Labtech) and luminescence was measured after 10 min incubation (10 s integration time, gain 4095, focal height 9.5 mm, top optics, 470 nm (80 nm bandwidth)).

Table 3.10 2x master mix for the HiBiT lysate assay

	Dilution
10x assay buffer	1:10
LgBiT	1:100
Substrate	1:200
	Add ddH_2O to the final volume

(all components are included in the Nano-Glo® HiBiT blotting system kit)

3.5.3 Subcellular localization of HiBiT-tagged proteins

To determine the subcellular localization of proteins, the respective *H. pylori* mutants synthesizing a HiBiT-tagged variant of the target protein were suspended in 4 ml D-PBS supplemented with the protease inhibitors PMSF, leupeptin and pepstatin (see also PBS*, 2.7) to a final OD_{550} of 0.5. Samples were kept on ice and lysed by ultrasonication. Unbroken cells and cell debris were removed by centrifugation (30 min, 5000 rpm, Megafuge 3.0 R, Thermo Scientific, 4 °C). 800 µl of the clarified supernatant were mixed with 200 µl RIPA buffer and kept on ice until further analysis (“before fractionation samples”). 3 ml of the remaining supernatant were transferred to an ultracentrifuge tube and fractionated for 1.5 h at 100000 rpm, 4 °C (rotor: TLA 100.3, Optima™ MAX-XP, Beckman Coulter). Afterwards, 800 µl of the supernatant fraction were mixed with 200 µl RIPA buffer. The pellet was once washed with cold D-PBS and finally solved in 3 ml D-PBS supplemented with 20 % RIPA buffer by gentile ultrasonication.

The three fractions (“before fractionation”, supernatant and pellet) were processed as followed: An aliquot of 20 µl was 1:1 mixed with the 2x HiBiT master mix (Table 3.10) and luminescence was measured as described.

Additionally, 500 µl sample were mixed with 2 ml cold aceton and proteins were precipitated overnight at -20 °C. The next day, samples were centrifuged for 15 min at maximal speed, 4 °C (5424 R, Eppendorf). The supernatants were discarded and the pellets were washed twice with 500 µl cold methanol. After complete drying, the pellet was solved in 25 µl PBS/ 0.2 % SDS and an equal amount of 2x SDS sample buffer was added. Samples were analyzed by SDS-PAGE and subsequent immunoblotting as described.

3.6 Analysis of *in vitro* infections

3.6.1 CagA phosphorylation assay

After translocation to the host cell, CagA is tyrosine-phosphorylated by cellular kinases. Thus, detecting phosphorylated tyrosines by Western blotting is a commonly used tool to study CagA translocation.

Briefly, AGS cells were seeded in a 6-well plate (see 3.2.1) and infected with the respective *H. pylori* strains for 4 h at a multiplicity of infection (MOI) of 100 in PBS/FCS at 5 % CO_2, 37 °C. Alternatively, bacteria were cultured in PBS/FCS at 10 % CO_2, 37 °C for 2 h prior to the infection and subsequently co-incubated with the AGS cells at an MOI of 60. Samples were cooled down on ice and unbound bacteria and cell debris were removed by washing twice with cold D-PBS. 500 µl D-PBS supplemented with protease and phosphatase inhibitors (PBS*, see 2.7) were added and cells were detached using a cell scraper. After harvesting at 4500 rpm, 4 °C for 5 min (5424 R, Eppendorf), samples were resuspended in 25 µl PBS*. 25 µl 2x SDS sample buffer were added and samples were boiled for 10 min.

Subsequent Western blots were performed as described (3.5.1). To detect phosphorylated CagA, membranes were incubated with a phosphotyrosine-specific primary antibody (PY99, 1:5000). Blots were developed using α-mouse-POX (1:10000). CagA was used as a loading control, therefor membranes were stripped (3.5.1.4) and re-probed with AK299 (1:5000). Protein A-AP (1:5000) was used for developing.

3.6.2 Immunoprecipitation of phosphorylated CagA

To analyze poorly translocated CagA variants, phosphorylated CagA was enriched by immunoprecipitation. Infection of AGS cells seeded in T75 cell culture flasks was performed as described (3.6.1) using the preculture including protocol.

After washing twice with D-PBS, cells and adherent bacteria were harvested in PBS* and centrifuged for 5 min at 4500 rpm, 4 °C (5424 R, Eppendorf). Pellets were resuspended in 500 µl RIPA* (RIPA buffer supplemented with protease inhibitors (see PBS*)) and lysed via ultrasonication. Unbroken cells and cell debris were removed by centrifugation (10 min, 4 °C, 14000 rpm, 5424 R). An aliquot of the supernatant was mixed with the respective volume of 2x SDS sample buffer and boiled for 10 min. The remaining supernatant was incubated overnight at 4 °C with the phosphotyrosine-specific antibody PY99 while rotating (1:250). The next day, protein G agarose (Roche) was added (50 µl/450 µl sample) and incubation was continued for 2 h at 4 °C. Protein G agarose was pelletized and washed three times with cold RIPA* (30 s, 14000 rpm, 4 °C, 5424 R). Finally, 50 µl of 2x SDS sample buffer were added and samples were boiled for 10 min.

3.6.3 Adherence assay

The adhesion of *H. pylori* to AGS cells was assessed via flow cytometry using GFP expressing or DAPI stained bacteria.

Firstly, bacteria were pre-incubated in PBS/FCS at 37 °C, 10 % CO_2 at an OD_{550} of 0.1 for 2 h to ensure optimal fitness. In case of GFP-producing *H. pylori* strains, AGS cells seeded in 12-well plates were directly infected with an MOI of 60 at 5 % CO_2, 37 °C. Non-fluorescent strains were stained for 5 min with 4′,6-diamidino-2-phenylindole dihydrochloride (DAPI, 5 µg/ml) and washed twice with PBS/FCS prior to infection.

After 1 h infection, samples were chilled on ice and unbound bacteria and cell debris were removed by washing twice with cold D-PBS. Cells were gently detached with 500 µl 2 mM EDTA in D-PBS at RT. Next, 1 % FCS was added to block EDTA, samples were kept on ice and immediately analyzed by flow cytometry (BD FACSCanto™ II, BD). Using FITC- (GFP) and Pacific Blue- (DAPI) settings the amount of cell-bound bacteria was determined. Results were normalized to the average fluorescence of the bacteria themselves, thus, in parallel, an aliquot of bacteria from the preculture was analyzed by flow cytometry regarding GFP expression or DAPI staining. Median fluorescence values were used for quantification.

3.6.4 Induction of the hummingbird phenotype

Translocation and subsequent phosphorylation of CagA is directly associated with an altered morphology of AGS cells. A spreading and elongated growth is characteristic for this so-called hummingbird phenotype and was first described by Segal *et al.* (1999). To investigate the induction of the hummingbird, AGS cells were infected with an MOI of 60 in PBS/FCS at 5 % CO_2, 37 °C for 2-4 h. Cell morphology was checked by light microscopy (DM IRB, Leika) and pictures were taken using a spot insight camera (#18.0, Diagnostic Instruments).

3.6.5 TEM-1 β-lactamase-dependent quantification of CagA translocation

The recently developed TEM-1 β-lactamase-dependent translocation assay was used to quantify CagA translocation to eukaryotic host cells *in vitro* (Schindele *et al.,* 2016). Thereby, the translocation of a TEM-1 β-lactamase-CagA fusion protein (TEM-CagA) via the T4SS is determined in a ratiometric manner. This assay is suitable for high-throughput screenings scanning for CagA translocation inhibitors.

In general, *H. pylori* P12[TEM-CagA] was pre-incubated for 2 h at 37 °C, 10 % CO_2 in PBS/FCS at an OD_{550} of 0.075. To test the impact of inhibitors, the respective compounds were added to the appropriate concentration during the last 30 min of preculture. Next, AGS cells, seeded in 96-well plates (4titude) were infected with 200 µl bacterial culture in duplicates (*i.e.* MOI 100). After 2.5 h infection at 37 °C, 5 % CO_2, supernatants were removed, and cells were loaded with 45 µl substrate solution (Table 3.11). Blue and green fluorescences were measured after 2 h incubation at RT in the dark in a Clariostar plate reader (BMG Labtech)

using bottom optics. Samples were excited at 405 nm (10 nm bandwidth) and emission was detected with 460 nm (20 nm bandwidth) and 530 nm (15 nm bandwidth) filters. 45 µl substrate solution without cells or bacteria were measured as blank and gains were adjusted to obtain blank values of about 300 (blue fluorescence) and 200 (green fluorescence) as recommended by the manufacturer. Blank values were subtracted and CagA translocation was calculated as the ratio of blue to green fluorescence. The relative amount of translocated CagA was determined as followed: 100 x ($ratio_{sample}$ - $ratio_{negative\ control}$) / ($ratio_{positive\ control}$ - $ratio_{negative\ control}$), using P12[TEM-CagA] as positive and the translocation-deficient P12[TEM-CagA] Δ*cagT* strain as negative control.

Table 3.11 Substrate solution for the TEM-CagA translocation reporter assay (one reaction)

	Volume [µl]
Solution A (CCF4-AM)	0.05
Solution B	0.5
Solution C	7.78
Probenecid (0.5 M in 1 M NaOH)	0.25
D-PBS	41.4

(Solutions A-C are included in the LiveBLAzer™ FRET-B/G Loading Kit with CCF4-AM)

As indicated, the CagA translocation reporter assay was also performed using brain heart infusion (BHI, BD), BB, BB/FCS or PBS/FCS mixed with the respective amount of BB.

3.6.6 IL-8 ELISA

Upon infection with *cag*PAI-positive *H. pylori* strains, AGS cells secrete chemokines, such as IL-8. A sandwich ELISA was used to quantify IL-8 in supernatants from *in vitro* infections (see 3.6.1). As control, AGS cells were treated for 4 h with 20 ng/ml recombinant human TNF-α (Preprotech).

Immunoabsorbent 96-well plates (Nunc) were coated overnight at 4 °C with 50 µl capture antibody per well (3 µg/ml in 100 mM Na_2HPO_4, pH 9.0). Plates were washed four times with PBS/0.05 % Tween-20 and blocked for 2-4 h at RT with 100 µl PBS/FCS per well. After additional washing, 100 µl sample or IL-8 standard (BD Pharming) diluted in PBS/FCS were added, and plates were incubated overnight at 4 °C. The next day, plates were extensively washed and 100 µl detection antibody (0.5 µg/ml in PBS/FCS) were applied for 1 h at RT. In the meantime, the streptavidin-biotin-peroxidase conjugate (Biozol) was prepared in 50 mM Tris pH 7.6. Again, plates were washed four times before incubating for 1 h with 100 µl

conjugate/well. Before adding the TMB substrate solution (100 µl/well, BD Biosciences), plates were washed six times. POX activity was stopped after 30 min incubation at RT in the dark by 50 µl 1 M H_2SO_4/well. Absorbance was measured at 450 nm using the Clariostar plate reader (BMG Labtech) and concentrations were calculated after substracting the blank value (PBS/FCS only).

3.6.7 Luciferase complementation-based quantification of CagA translocation

In addition to the TEM-1 β-lactamase-dependent quantification of CagA translocation, a split-luciferase-based assay was developed to determine the amounts of translocated CagA in a highly sensitive and (optional) time-resolved manner. A detailed description of the assay principle can be found in the result section (4.1).

3.6.7.1 Time-resolved method (Real-time assay)

To monitor the translocation of CagA in real time, bacteria producing the HiBiT-CagA fusion protein were diluted to an OD_{550} of 0.1 in PBS/FCS and pre-incubated for 2 h at 37 °C, 10 % CO_2. Next, HaloTag-LgBiT expressing AGS cells seeded in a 96-well plate (4titude) were infected with 40 µl preculture (*i.e.* MOI 25) and 10 µl 5x luciferase substrate (Table 3.12) were added. Measurements were immediately started in a prewarmed Clariostar plate reader (BMG Labtech) with CO_2 levels adjusted to 5 % using an atmospheric control unit (BMG Labtech). Thereby, luminescence at 470 nm (20 nm bandwidth, 10 s integration time, gain 4095, bottom optics, 5.2 mm focal height) was automatically detected every 3-5 min for up to 2.5 h.

Table 3.12 5x master mix for the HiBiT translocation assay (one reaction)

	Volume [µl]
Assay buffer	9.5
Substrate	0.5

(all components are included in the Nano-Glo® live cell assay system kit)

3.6.7.2 Endpoint measurement and total CagA

To measure the amount of translocated HiBiT-CagA at one, defined timepoint, HiBiT-CagA-producing *H. pylori* strains were precultured in PBS/FCS for 2 h at 37 °C, 10 % CO_2 at an OD_{550} of 0.019. HaloTag-LgBiT expressing AGS cells seeded in a 96-well plate (4titude) were infected with 200 µl preculture (*i.e.* MOI 25) at 37 °C, 5 % CO_2 for 2.5 h. Next, supernatants were discarded, and cells were loaded with 40 µl PBS/FCS and 10 µl 5x luciferase substrate (Table 3.12). After 10 min incubation, luminescence was measured as described above

(3.6.7.1). The relative amount of translocated CagA was calculated as percentage of the respective control after subtraction of the background signal (uninfected cells).
Optional, after quantifying the translocated CagA, the amount of "total CagA", *i.e*. the injected CagA and the CagA present in the adherent bacteria was analyzed. Therefor, 50 µl/well cold RIPA buffer was added to each well and samples were lysed at 4 °C for 5-10 min. Next, 20 µl lysate were mixed with 20 µl 2x master mix (Table 3.10) and measured as described (3.5.2.2) using black 96-well plates with flat clear bottom (Corning). For the blank value, luminescence of uninfected cells was measured.
"Total CagA" was calculated considering a dilution factor of five from the original sample.

3.7 *In silico* docking and visualization of protein structures

Crystal and cryo-electron microscopy structures were obtained from the protein data bank (www.rcsb.org) or the protein data bank in Europe (www.ebi.ac.uk/pdbe). PyMOL Molecular Graphics System version 2.3.4 was used to visualize proteins and docking poses, to align proteins with unknown structure to reference backbones, and to measure distances and dimensions. Docking data of small molecule inhibitors into the quinone-binding pocket were kindly provided by Dr. Ahmadreza Mehdipour from the group of Prof. Gerhard Hummer at the Max Planck Institute of Biophysics (Frankfurt a. M.).

3.8 Statistical analysis

All statistical calculations were performed using GraphPad Prism 5. Differences between two independent groups were evaluated via the unpaired Student's t-test, to compare three or more groups, One-way ANOVA and the indicated post test were applied. Significant differences are indicated as follows: ***p<0.001, **p<0.01 and *p<0.05, ns (not significant) p>0.05
If not indicated otherwise, quantitative data shown are means and standard deviations of at least five independent experiments. In case of real-time HiBiT-CagA translocation assays a representative result with means and standard deviations of two technical replicates is depicted.
Linear regression analyses were calculated considering mean values of each Y point. Goodness of fit is indicated as R^2. IC_{50} values were calculated from at least five independent experiments using non-linear regression with variable slope.

4 Results

4.1 Development of a split-luciferase-based CagA translocation reporter assay

One of the major virulence factors of *H. pylori* is the oncoprotein CagA that is translocated into the eukaryotic host cell via the *cag*PAI encoded T4SS. Once inside, CagA is tyrosine-phosphorylated by cellular kinases and thus gets able to hijack host cell proliferation. Even though *H. pylori´*s T4SS is in the focus of extensive research, the exact mechanisms of translocation as well as the architecture of the secretion apparatus are not yet fully understood. But deeper insights are essential for novel treatment strategies that directly target oncoprotein delivery.

For many years, CagA translocation was evaluated in an indirect, semi-quantitative and time-consuming way via Western blotting. Thereby, intracellular, phosphorylated CagA is detected with a phosphotyrosine-specific primary antibody. But this method gives information about the amount of phosphorylated intracellular CagA only, and sensitivity is rather low. Thus, a novel β-lactamase-based CagA translocation assay was developed (Schindele *et al.,* 2016) which allows the direct, fast, and quantitative measurement of T4SS activity using a fluorescence plate reader. With this method, new aspects regarding the impact of *cag*PAI components and CagA sequence on type IV secretion were investigated. Furthermore, the TEM-CagA translocation assay can be used for high-throughput screening of T4SS inhibitors. But on the other hand, probably due to the rather large tag, the TEM-CagA fusion protein is poorly synthesized and thus, characteristic translocation-associated processes like CagA phosphorylation, and the induction of the hummingbird phenotype can hardly be observed. Hence, in the present work, a novel split-luciferase-based CagA translocation assay was developed which needs only a minimal eleven amino acid tag and furthermore also allows the monitoring of CagA translocation in real time, and thus the possibility to investigate secretion dynamics.

4.1.1 Assay principle

Due to its high sensitivity, low signal-to-noise ratio, versatility, easy handling and detection, bioluminescence is a widely used tool for biological assays. It is the generation of light during the oxidation of a photon-emitting substrate catalyzed by a class of enzymes called luciferases. NanoLuc is a genetically modified monomeric subunit (19 kDa) of the luciferase of the deep-sea shrimp *Oplophorus gracilirostris* that was engineered for maximal brightness and stability in eukaryotic cells (Hall *et al.,* 2012). Together with its optimized luciferin substrate, the coelenterazine analog furimazine, it enables stable glow-type luminescence (half-life >2 h) and at the same time a very bright signal intensity with low background autoluminescence (Hall *et al.,* 2012, Figure 4.1).

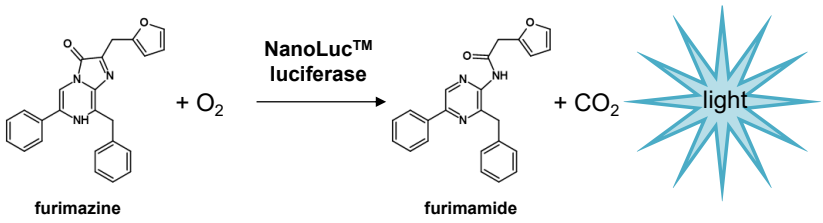

Figure 4.1 Bioluminescent reaction catalyzed by the NanoLuc luciferase. Furimazine, an optimized version of the native substrate coelenterazine, is oxidized in an ATP-independent manner by the NanoLuc luciferase, and blue light (460 nm) is emitted (Hall *et al.,* 2012).

NanoLuc can also be used for split-luciferase complementation assays to detect protein-protein interactions or to measure the production of tagged proteins (Dixon *et al.,* 2016). In the present work, the system was adapted to monitor CagA translocation into gastric cells (AGS) *in vitro*. The principle of the assay is depicted in Figure 4.2.

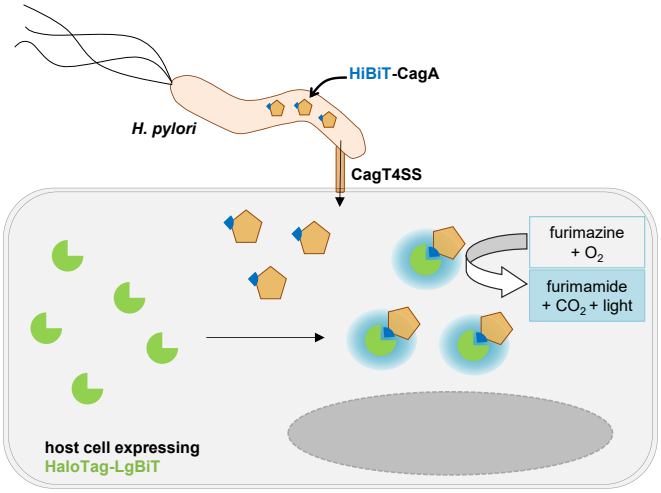

Figure 4.2 Principle of the split-luciferase CagA translocation reporter assay. The HiBiT-CagA fusion protein is translocated via the T4SS into a HaloTag-LgBiT-producing AGS cell. HiBiT and LgBiT together form an active luciferase that catalyzes the oxidation of furimazine. Photons are emitted and HiBiT-CagA translocation can be assessed measuring luminescence.

In principle, NanoLuc is split in two parts – HiBiT and LgBiT – which were genetically designed to have a high affinity to each other (K_D = 700 pM) and together form a functional enzyme that oxidizes furimazine in an ATP-independent manner emitting blue light (460 nm) (Schwinn *et al.,* 2018). The LgBiT is recombinantly synthesized by the host cells as fusion protein with a "HaloTag". This 33 kDa self-labeling protein tag is a modified bacterial haloalkane dehalogenase (EC 3.8.1.5) designed to form a covalent bond with synthetic ligands (Los *et al.,* 2008). Thus, any cell producing this HaloTag can be rapidly and irreversibly stained by dyes comprising a functional chloroalkane linker. The LgBiT protein itself is the larger fragment of the split-luciferase with a molecular weight of 18 kDa. On the other hand, the small 1.3 kDa HiBiT peptide is fused to the N-terminus of the cargo protein CagA. If HiBiT-CagA is injected into the host cell, HiBiT and LgBiT can interact and can form an active luciferase complex. The

emission of light directly correlates with the number of active luciferases and thus the amount of translocated HiBiT-CagA.

4.1.2 Assay development

An *H. pylori* P12 producing the HiBiT-CagA fusion protein was generated using the *rpsL-erm* counterselection system. This cloning strategy enables the marker-free insertion of the eleven amino acid-comprising HiBiT tag ((M)VSGWRLFKKIS) at the N-terminus of CagA, *i.e.* maximal preservation of the natural genetic context.

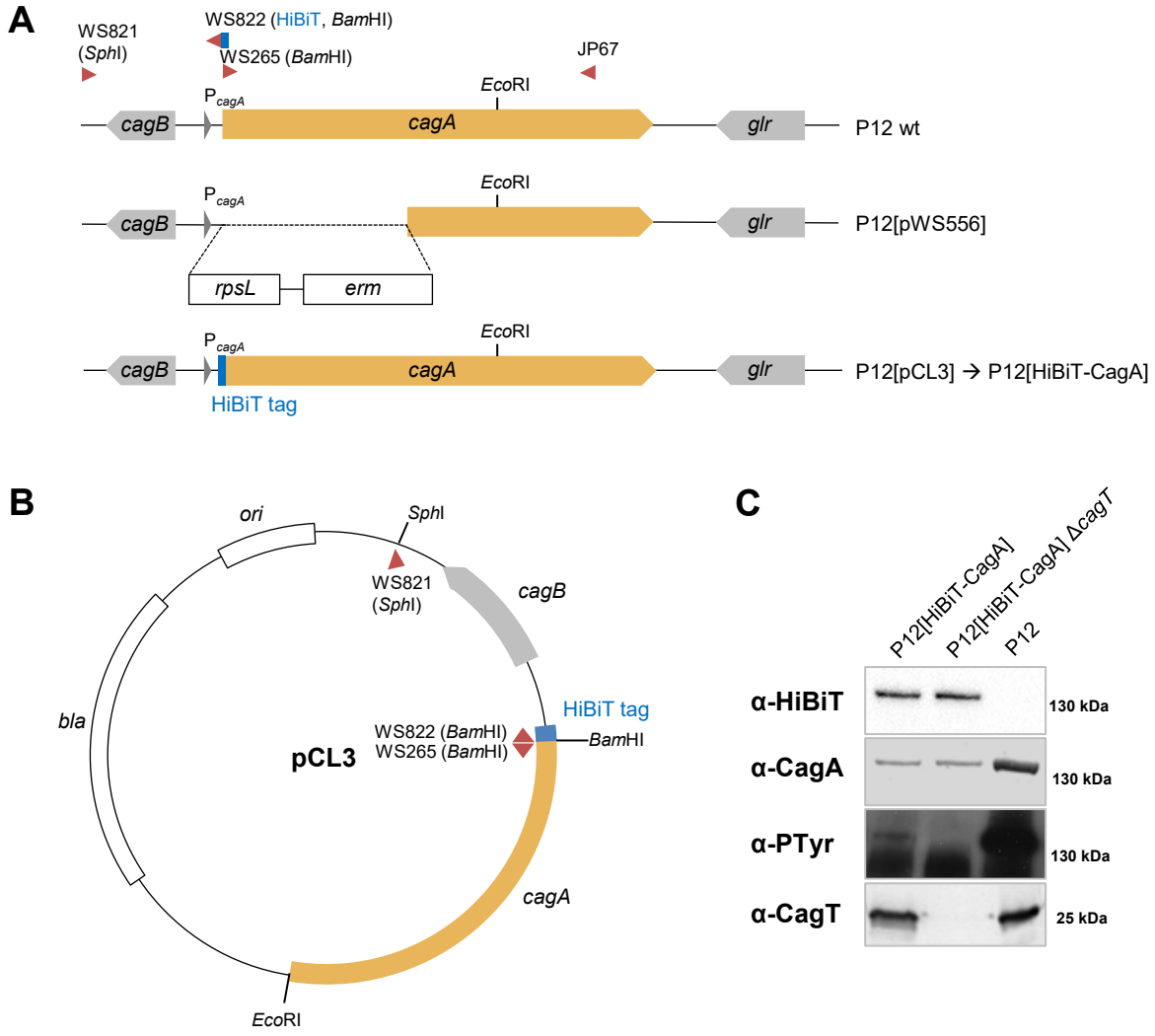

Figure 4.3 Construction of the HiBiT-CagA reporter strain. (A/B) Using the *rpsL-erm* counterselection strategy, an N-terminal HiBiT-CagA fusion was introduced in the *cagA* locus under the control of the *cagA* promotor (P_{cagA}) in a two-step cloning protocol. After partial replacement of 5´*cagA* by an *rpsL-erm* cassette via transformation with pWS556, *HiBiT-cagA´* was reintroduced by homologous recombination using pCL3. The *HiBiT-cagA´*-encoding plasmid pCL3 was generated by ligation of PCR WS821/WS822 (*Sph*I/*Bam*HI) and PCR WS265/JP67 (*Bam*HI/*Eco*RI) in pUC19 (*Sph*I/*Eco*RI). The *HiBiT*-encoding nucleotides (33 bp) were introduced by primer WS822. (C) Western blots to confirm HiBiT-CagA synthesis (α-HiBiT/α-CagA (AK299)) and translocation with subsequent phosphorylation by cellular kinases (α-PTyr (PY99)). As a negative control, a Δ*cagT* mutant was generated, that is T4SS deficient, but produces HiBiT-CagA.

Hence, the first 2 kb at the 5´ end of *cagA* (= *cagA´*) were replaced by an *rpsL-erm* cassette via homologous recombination using plasmid pWS556. In a second transformation step, *HiBiT-cagA´* was reintroduced by homologous recombination using plasmid pCL3. A more detailed scheme of the cloning strategy is depicted in Figure 4.3 A and B. HiBiT-CagA synthesis was proven by Western blot (Figure 4.3 C). A translocation-deficient mutant of the reporter strain was generated by *cagT* deletion using plasmid pJP95 (*cagT::cat*). Translocation of HiBiT-tagged CagA into AGS cells was confirmed by *in vitro* infection and subsequent detection of phosphorylated CagA.

To detect HiBiT-CagA translocation into eukaryotic cells via the split-luciferase complementation assay, the host cell must synthesize the larger NanoLuc counterpart. Therefore, AGS cells were transfected with a *haloTag-lgBiT*-encoding plasmid (pCS1956B02) that carries a hygromycin resistance. To ensure continuously reproducible assay performance, a stably transfected, single cell clone-derived cell line was developed using FACS. To prove that the *haloTag-lgBiT* construct under the control of a strong CMV promotor is well-expressed and the protein is equally distributed within the cytosol, cells were stained with a dye comprising a chloroalkane linker that irreversibly stains HaloTag and thus LgBiT-producing cells (Figure 4.4).

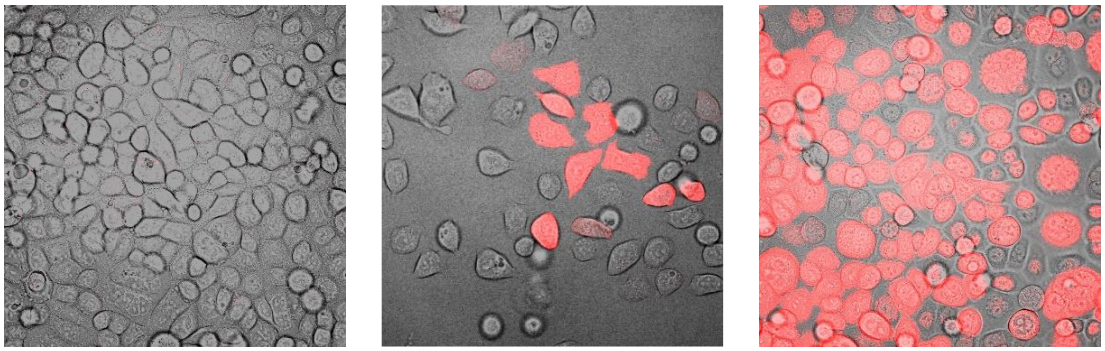

AGS | AGS[HaloTag-LgBiT] (unsorted) | AGS[HaloTag-LgBiT] (sorted)

Figure 4.4 Visualization of the HaloTag-LgBiT production. Transfected AGS cells were stained for HaloTag-LgBiT synthesis using a TMR-chloroalkane linker dye. In the single cell clone-derived, sorted cell line, all cells produced high amounts of HaloTag-LgBiT (right), whereas only a minor fraction of the original unsorted AGS cells (middle) could be stained for the luciferase fragment. Equally treated AGS wt cells showed no labeling (left).

After successfully cloning the HiBiT-CagA reporter strains and establishing the stable cell line, two different protocols of the split-luciferase complementation assay were developed: a real-time assay for CagA translocation dynamics and an endpoint assay comparable to the already existing TEM-CagA reporter assay. Thus, AGS[LgBiT] cells seeded in 96-well plates were infected with the respective reporter strains. In case of the real-time assay, the furimazine substrate was directly added and luminescence was immediately recorded (as relative light units, RLU) in a Clariostar plate reader at optimal infection conditions of 37 °C, 5 % CO_2. On the other hand, for the endpoint assay, cells were incubated for 2.5 h with the bacteria at

37 °C, 5 % CO_2 and the substrate was added after removing the infection supernatant followed by a one-point measurement. In both cases, luminescence was recorded at 470 nm (20 nm bandwidth, 10 s integration time, gain 4095, bottom optics). The results of a typical real-time and endpoint assay are shown in Figure 4.5. In both cases, translocation could be observed in the HiBiT-CagA-producing reporter strain but not in the negative controls (Δ*cagT*/uninfected). Furthermore, after a minimal lag phase, already within the first 15 min of infection a strong and linear increase in translocation could be seen in the real-time assay that reached a plateau after about 1 h infection.

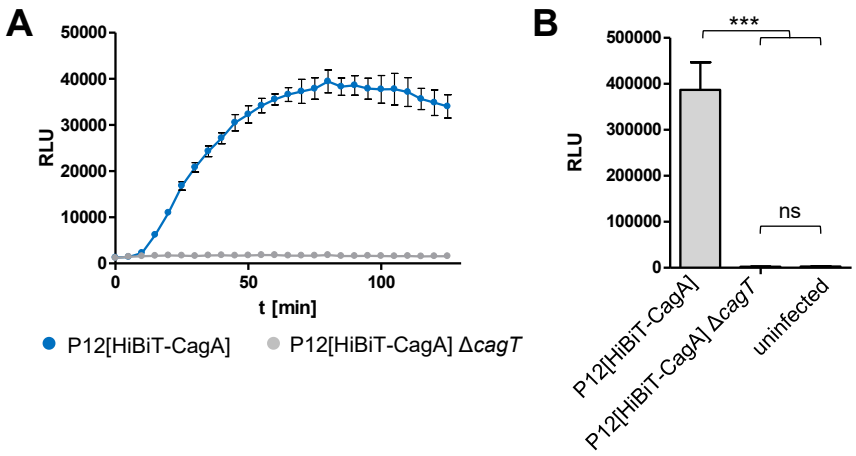

Figure 4.5 Output of the split-luciferase complementation-based CagA translocation assays. (A) AGS[LgBiT] cells were infected with the indicated strains at an MOI of 25 and CagA translocation was monitored in real time by measuring the increase in luminescence. An exemplary real-time assay with means and standard deviations of two technical replicates is shown. (B) AGS[LgBiT] were co-incubated for 2.5 h with the respective strains at an MOI of 25 or left uninfected. HiBiT-CagA translocation was determined via the endpoint protocol. Data shown are means and standard deviations of three independent experiments. (Statistics: One-Way ANOVA, Bonferroni post test, ***p<0.001)

In general, the light intensity is reciprocally correlated with the signal duration. *I.e.* glow-type luminescence in general shows lower absolute values than flash-type luminescence which in turn has higher technical requirements, since the substrate has to be injected just prior to measuring due to the short signal half-life. A characteristic feature of the NanoLuc luciferase when oxidizing furimazine is the production of very bright glow-type luminescence with a signal half-life >2 h (Hall *et al.,* 2012).

The measurement of every single sample of the HiBiT-CagA translocation assay takes at least 10 sec, which, in case of 45 samples (= half a 96-well plate), is nearly 8 min. To examine the decay in signal intensity, endpoint assays were performed and luminescence was monitored every 10 min over a period of time of 1 h (Figure 4.6). A decrease in bioluminescence was observed after 20 min, necessitating the measurement within 10 min after adding the substrate. Nevertheless, measuring up to 96 samples is possible.

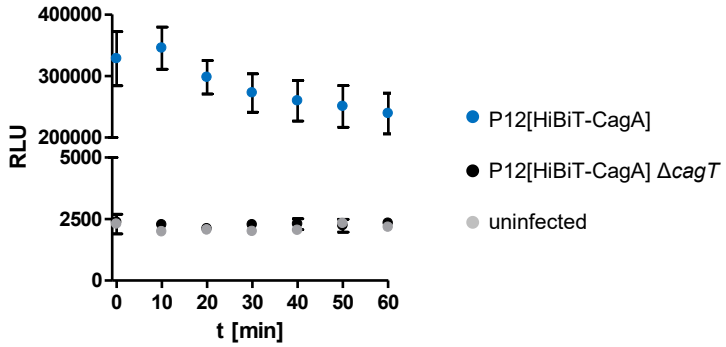

Figure 4.6 Characteristic course or the luminescence signal of an endpoint infection. AGS[LgBiT] cells were co-incubated with the respective strains for 2.5 h at an MOI of 25 and HiBiT-CagA translocation was determined. The maximal signal intensity was detected within the first 10 min after addition of the substrate. Background luminescence (P12[HiBiT-CagA] Δ*cagT*/uninfected) stayed continuously low. A representative result of three independent experiments with means and standard deviations of two technical replicates is shown.

In order to evaluate assay performance and to optimize infection conditions, real-time and endpoint experiments were done with different MOIs (Figure 4.7). Dynamics of T4SS activity, observed in the live assay, were best to be studied at an MOI of 25 or 13, but even at very low MOIs (MOI 2-1), HiBiT-CagA translocation was still detectable in the real-time settings (Figure 4.7 A). The endpoint assay (Figure 4.7 B/C) had a very wide range of detection: The maximal signal intensity was observed at MOI 50, but even at MOI 0.125 a significant translocation could be detected.

In both cases, an increase in the absolute luminescence signal was observed with a rising number of bacteria infecting the cells. At the highest tested bacterial load (MOI 50 and 100 respectively), no further increase in CagA translocation was detected, but assay performance slightly dropped. In case of the real-time assay, this was most likely due to the unfavorable high bacterial density during the preculture. Furthermore, it cannot be excluded that the high bacterial load was interfering with the infection progress itself, suggesting for example a damaging of the host cells. Finally, the substrate furimazine or the amount of LgBiT provided by the host cells could be limiting factors at high MOIs. In case of the endpoint assay, a linear correlation existed between the number of bacteria (MOI) and the amount of CagA translocation (ΔRLU) until an MOI 25 (Figure 4.7 D). Thus, it can be concluded that until MOI 25 neither the substrate furimazine nor the LgBiT protein synthesized by the host cells was a limiting factor for HiBiT-CagA translocation detection.

In sum, the bioluminescence-based assay is several times more sensitive than the already existing TEM-CagA translocation assay that already has a low detection limit (MOI 6, Schindele, 2017). The high sensitivity offers the possibility to study the translocation of poorly synthesized HiBiT-CagA variants and *H. pylori* mutants with severe T4SS defects.

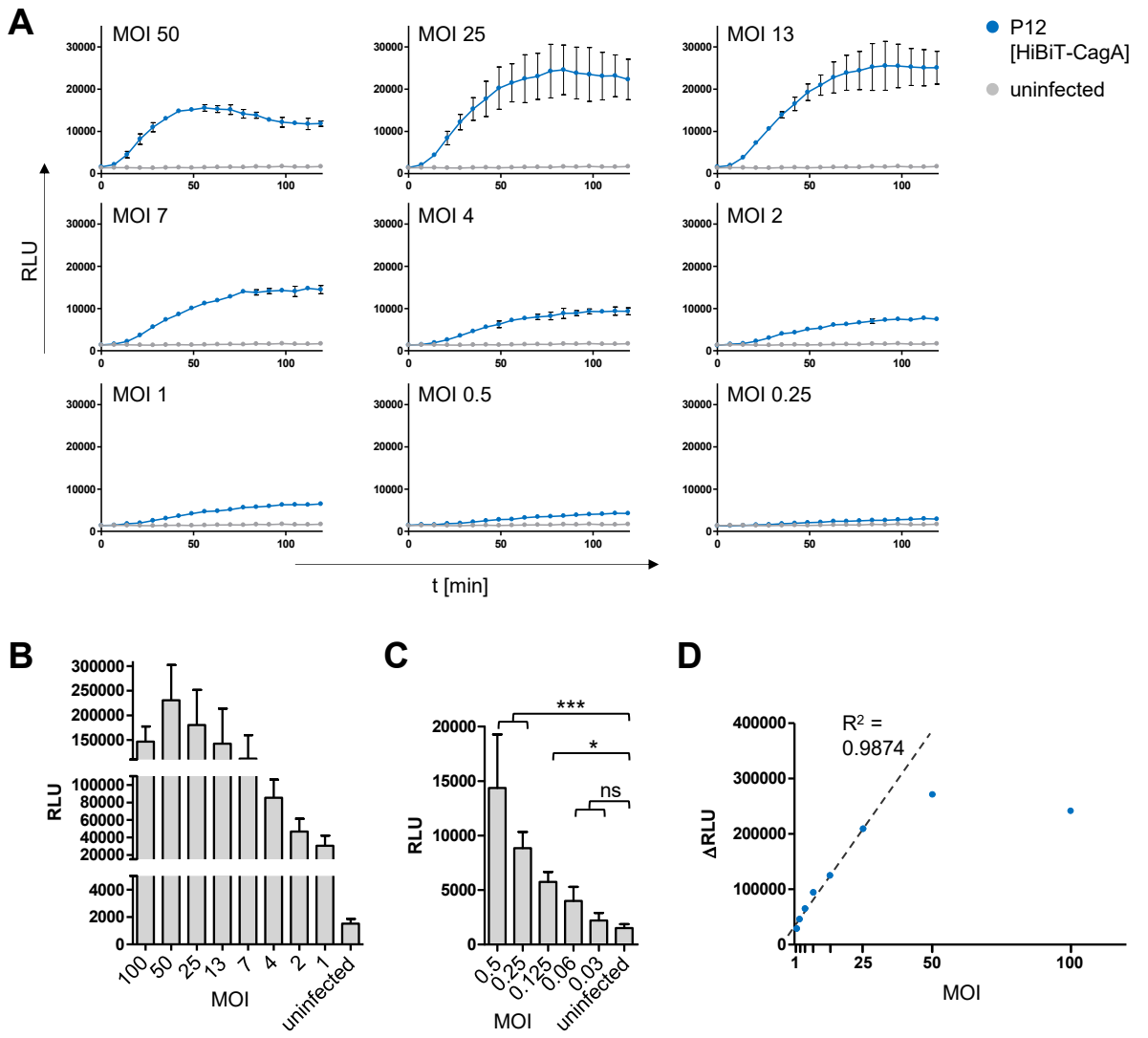

Figure 4.7 Detection limits of the split-luciferase complementation assay. (A) The real-time HiBiT-CagA translocation assay was performed as described in Figure 4.5 A using different MOIs. A representative experiment with means and standard deviations of two technical replicates is shown. (B/C) Using different MOIs, the endpoint HiBiT-CagA translocation was performed as described above. Data show means and standard deviations of three independent experiments. (Statistics: One-Way ANOVA, Dunnett post test, *p<0.05, ***p<0.001) (D) Linear regression analysis correlating the detected luminescence signal (RLU) and the amount of infecting bacteria (MOI 1-100) in the endpoint assay. Data shown are means of six independent experiments. Goodness of fit is indicated as R^2.

4.1.3 Comparison of the split-luciferase and the β-lactamase reporter assay

Since the HiBiT tag comprises just eleven amino acids, only minor changes had to be introduced to the genetic context and finally to the protein structure of CagA. Thus, synthesis, translocation, and phosphorylation of HiBiT-CagA were expected to be close to wt CagA levels. CagA phosphorylation and the induction of the hummingbird phenotype, two hallmarks of oncoprotein translocation into AGS cells, were examined for P12, P12[HiBiT-CagA] and P12[TEM-CagA] (Figure 4.8). As already described previously (Schindele *et al.,* 2016), TEM-CagA protein levels were lower than wt CagA levels and no phosphorylation of TEM-CagA was observed (Figure 4.8 A). But even though the HiBiT is a very small tag, its fusion to the N-terminus of CagA had an impact on protein levels (Figure 4.3 C and Figure 4.8 A) resulting in reduced, however clearly detectable amounts of tyrosine-phosphorylated CagA. Furthermore, the HiBiT-CagA-producing P12 was able to induce the hummingbird phenotype, as P12 but not P12[TEM-CagA] did (Figure 4.8 B).

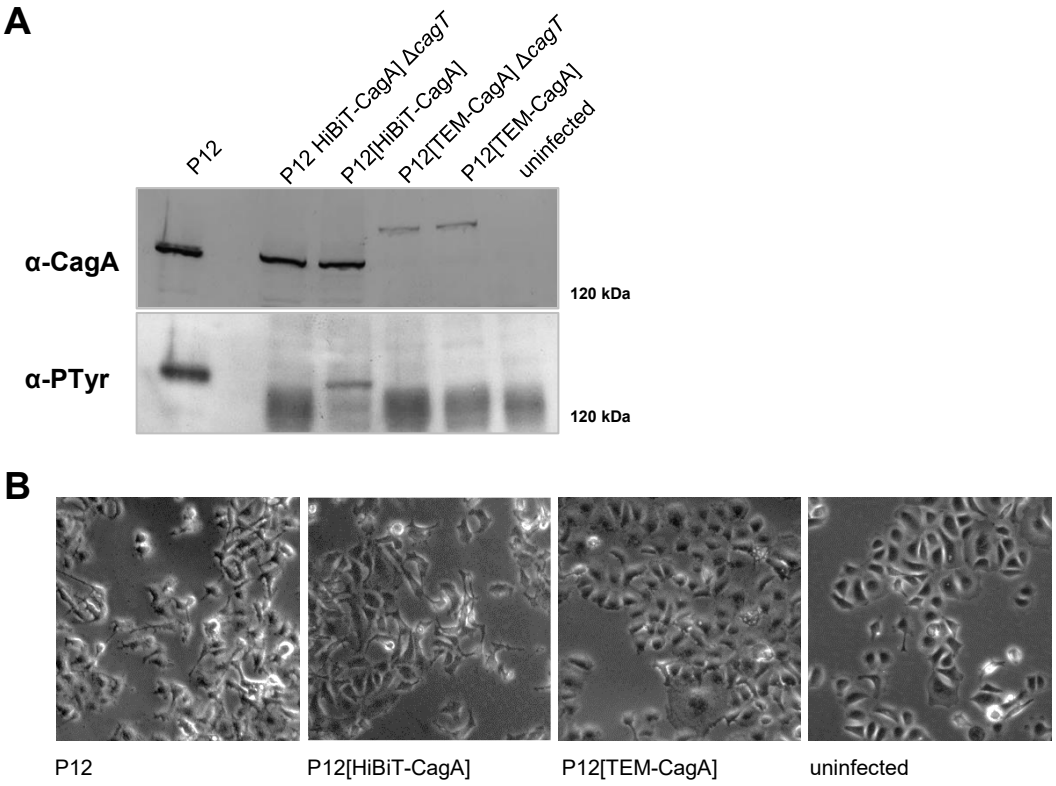

Figure 4.8 *In vitro* infection characteristics of P12, P12[HiBiT-CagA] and P12[TEM-CagA]. (A) AGS cells were infected with P12, P12[HiBiT-CagA], P12[TEM-CagA] and the corresponding translocation-deficient mutant strains (Δ*cagT*) for 4 h at an MOI of 100. Infection lysates were analyzed by CagA and phosphotyrosine-specific Western blots. (B) Induction of the hummingbird phenotype was observed after 4 h infection with P12 and P12[HiBiT-CagA] but not for cells co-incubated with P12[TEM-CagA].

4.2 Characterization of the CagT4SS activity using the HiBiT-CagA reporter assay

4.2.1 Comparison of CagA protein levels and translocation rates

CagA is one of the most abundant proteins synthesized by *H. pylori* under standard conditions *in vitro* (Jungblut *et al.,* 2000). In contrast, only a small fraction of this total CagA pool is injected into eukaryotic host cells, as observed by *in vitro* infections and subsequent immunoblotting (Jiménez-Soto and Haas, 2016).

The HiBiT-CagA endpoint assay was adapted to get further insights into translocation rates. Thus, LgBiT-producing AGS cells were infected with the P12[HiBiT-CagA] reporter strain for 2.5 h at different MOIs and HiBiT-CagA translocation was determined as described (Figure 4.9 A). Next, 50 µl RIPA buffer were added to each sample, lysing the host cells and the adherent bacteria. An aliquot of the lysate (20 µl, *i.e.* 1/5 of the sample) was mixed with an equal volume of 2x master mix containing fresh furimazine substrate and recombinant LgBiT protein, guaranteeing an excess of both components. The total amount of CagA was determined and turned out to perfectly correlate with the number of bacteria in the sample, indicating that adhesion to the host cells is not saturated at an MOI of 100 (Figure 4.9 B). Considering a dilution factor of five in case of the total HiBiT-CagA measurement, the amount of translocated CagA was determined to account for 5-10 % of the total CagA pool with a tendency to higher translocation rates if less bacteria are infecting the cells (Figure 4.9 C). Since the comparably low amount of translocated CagA in the MOI 50 and MOI 100 samples most likely resulted from substrate or LgBiT limitations (Figure 4.9 A, Figure 4.7 D), those values were excluded from further calculations (Figure 4.9 C).

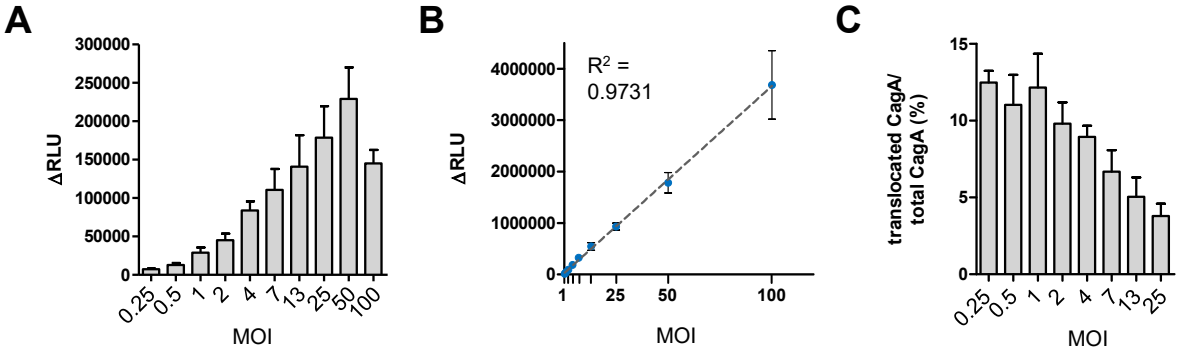

Figure 4.9 A small fraction of the total bacterial CagA is translocated into host cells *in vitro*. (A) AGS[LgBiT] were co-incubated with P12[HiBiT-CagA] for 2.5 h at the indicated MOI and CagA translocation was determined. (B) Subsequently, host cells and adherent *H. pylori* were lysed and the total amount of CagA was measured, which perfectly correlated with the number of bacteria. (C) The portion of translocated HiBiT-CagA was calculated as percentage of the total HiBiT-CagA pool. Shown are means and standard errors of the means of three independent experiments.

4.2.2 Requirement of protein unfolding for CagA translocation

For several T4SS (and T3SS) it has already been shown that the cargo proteins are transported in a completely or at least partially unfolded state (Amyot *et al.,* 2013; Trokter and Waksman, 2018; Lee and Schneewind, 2002). Using the newly developed HiBiT-CagA translocation assay, the question was addressed, if CagA is delivered folded or unfolded to the eukaryotic host cell via the CagT4SS. Hence, fusion proteins of HiBiT-CagA with ubiquitin (Ub), $Ub^{I3G,\ I13G}$ or GFP were generated. While Ub and GFP are known to fold rapidly and tightly, the $Ub^{I3G,\ I13G}$ variant is less stable, due to the amino acid exchanges in the hydrophobic core of the β-grasp fold (Johnsson and Varshavsky, 1994).

Murine Ub has a molecular weight of about 8.6 kDa and an approximate size of 20x30 Å, GFP, that forms a β-barrel, is about 26.7 kDa in mass and 24x48 Å in size (Figure 4.10 D). All three protein domains, Ub, $Ub^{I3G,\ I13G}$ and GFP, were inserted between the HiBiT tag and the N-terminus of CagA (Figure 4.10 A). To generate the respective mutants, *H. pylori* P12[pWS556] (Δ*cagA´*) was transformed with modified versions of pCL3 (Table 2.4) as explained for HiBiT-CagA (Figure 4.3 A). Murine genomic DNA was used to amplify the sequence of one Ub monomer. The PCR fragment obtained was ligated in the pGEM®-T easy vector to sort for allelic variants. For the further cloning of pCL19, the variant corresponding to the protein sequence of the UniProt entry P0CG50 was chosen. HiBiT-Ub-CagA and HiBiT-GFP-CagA were well synthesized, reaching overall protein levels of 30-40 % compared to HiBiT-CagA itself. In contrast, only very low amounts of HiBiT- $Ub^{I3G,\ I13G}$-CagA were synthesized (Figure 4.10 B**,** E). Folding of the GFP as well as equal synthesis of the fusion protein in the bacterial population was confirmed by flow cytometry analysis of the respective bacterial strain detecting GFP-dependent green fluorescence (Figure 4.10 C).

No translocation of HiBiT-GFP-CagA was detected using the HiBiT-CagA endpoint assay, but HiBiT-Ub-CagA was almost as efficiently translocated as HiBiT-CagA (Figure 4.10 E). The HiBiT-CagA variant fused to the easily unfoldable $Ub^{I3G,\ I13G}$ was translocated even stronger than HiBiT-CagA.

In summary, it was concluded, that the large and tightly folded GFP cannot pass the secretion apparatus, while the smaller Ub can either be unfolded by the CagT4SS or can be translocated in a folded conformation.

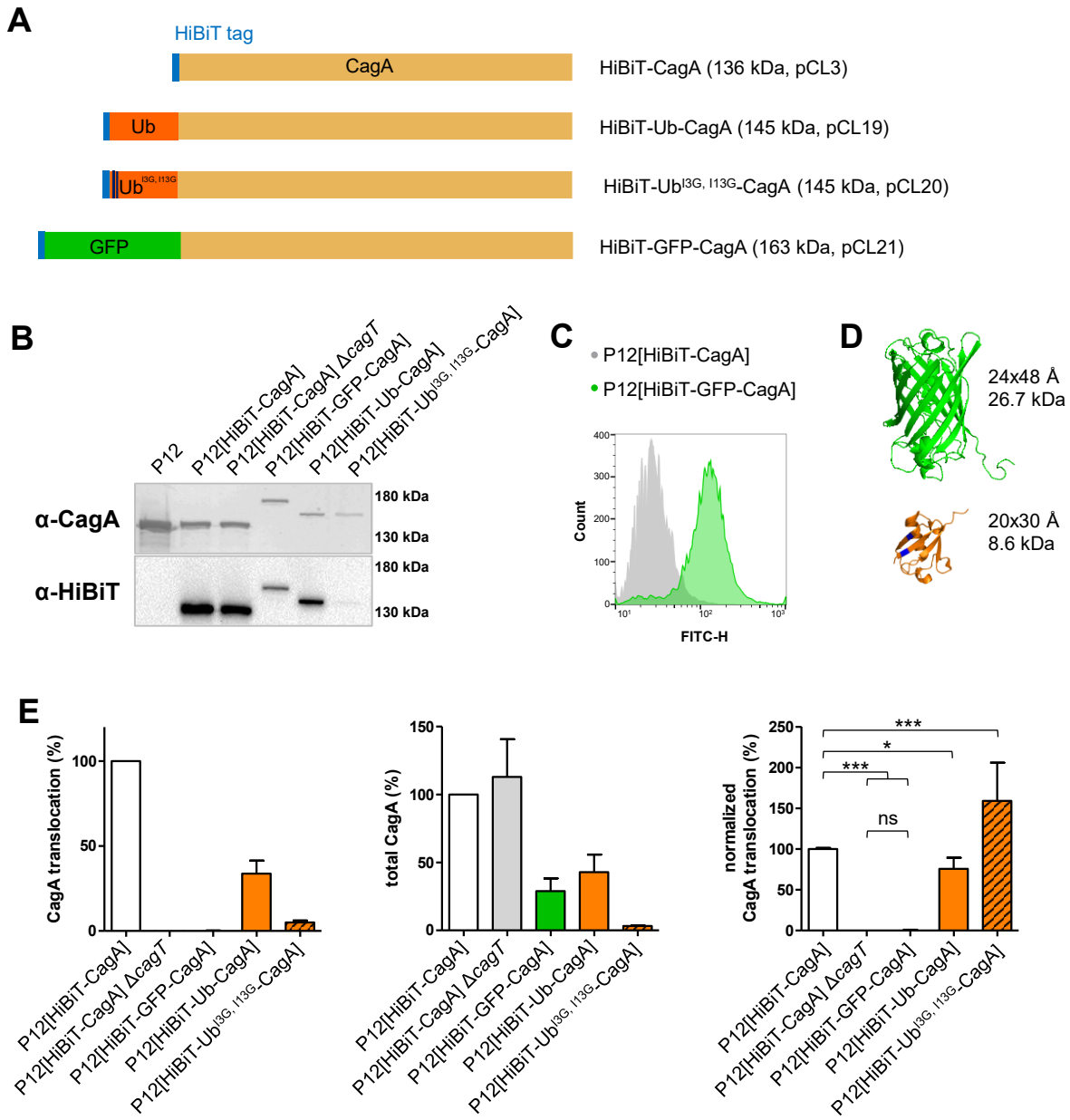

Figure 4.10 Impact of tightly folded protein domains on CagA translocation. (A) Schematic overview of tested HiBiT-CagA variants. (B) Immunoblots to confirm synthesis of HiBiT-Ub-CagA, HiBiT-Ub$^{I3G, I13G}$-CagA and HiBiT-GFP-CagA (α-CagA (AK299)/α-HiBiT). (C) Flow cytometry analysis of the HiBiT-GFP-CagA production. (D) Crystal structures of GFP (5DTX (Adam and Martins, 2016), green) and murine Ub (3WWQ (Sato and Fukai, 2015), orange), the approximate sizes were determined using PyMol. I3^{Ub} and I13^{Ub} are highlighted in blue. (E) Translocation of the different HiBiT-CagA variants was determined by HiBiT-CagA endpoint translocation assay (left) and subsequent determination of the amount of total CagA (middle). Finally, CagA translocation was normalized to the total CagA amount (right). HiBiT-CagA was set to 100 %, data shown are means and standard deviations of at least five independent experiments. (Statistics: One-Way ANOVA, Bonferroni post test, *p<0.05, ***p<0.001)

To further confirm this finding, a fusion variant of HiBiT-CagA and dihydrofolate reductase (DHFR) was generated (Figure 4.11 A). DHFR is a ubiquitous enzyme that catalyzes the reduction of dihydrofolic acid to tetrahydrofolic acid. The murine protein has an average size of 30x40 Å and a molecular mass of 21.7 kDa (Figure 4.11 B). It is in general easily unfoldable,

but gets tightly folded if bound to the inhibitor methotrexate (MTX) (Eilers and Schatz, 1986). As described above for HiBiT-Ub-CagA and HiBiT-GFP-CagA, *HiBiT-dhfr-cagA´* was introduced in P12[pWS556] using the respective modified version of pCL3 (pCL23). The murine *dhfr*-encoding sequence was amplified from plasmid pCMV6-Kan/Neo-*dhfr* using primers CL71/CL72. While the protein level of HiBiT-DHFR-CagA detected by the CagA-specific antibody AK299 via immunoblotting was comparable to the amount of HiBiT-CagA, only a faint band at the expected size of ca. 160 kDa was detectable in the HiBiT-specific blot (Figure 4.11 C). In contrast, a strong luminescence signal, comparable to HiBiT-CagA itself, was observed for HiBiT-DHFR-CagA using the HiBiT-lysate assay (data not shown). Most likely, HiBiT-DHFR-CagA got partially degraded, and small HiBiT-tagged fragments co-existed with the full-length fusion protein. Those fragments were detected at the dye front (<10 kDa) of the blot (Figure 4.11 C).

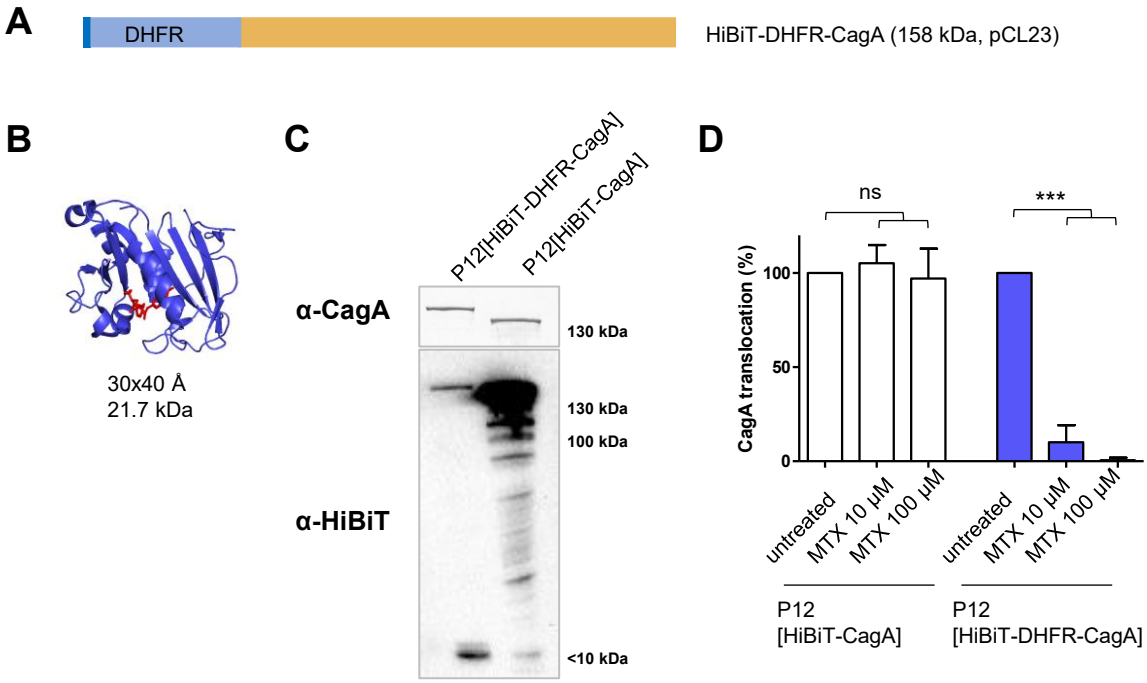

Figure 4.11 Impact of tightly folded protein domains on CagA translocation (2). (A) Scheme of HiBiT-DHFR-CagA. (B) Crystal structure of human DHFR (1U72 (Cody, 2005)), the bound inhibitor MTX is shown in red. Human and murine DHFR share 90 % sequence identity. The approximate diameters were determined using PyMol. (C) Immunoblots to confirm HiBiT-DHFR-CagA synthesis (α-CagA (AK299)/α-HiBiT). (D) Translocation of HiBiT-CagA and HiBiT-DHFR-CagA was determined by HiBiT-CagA endpoint translocation assays. Bacteria were pre-treated with the indicated concentrations of MTX for 0.5 h and infections were conducted in the presence of the inhibitor. CagA translocation was normalized to the respective untreated control, data shown are means and standard deviations of five independent experiments. (Statistics: One-Way ANOVA, Dunnett post test, ***p<0.001)

HiBiT-CagA and HiBiT-DHFR-CagA injection into AGS[LgBiT] cells was measured in the presence of different concentrations of MTX (Figure 4.11 D). Due to the above-mentioned partial degradation of HiBiT-DHFR-CagA and the resulting presence of HiBiT-tagged fragments, a normalization to the total amount of HiBiT-tagged CagA was not possible. While

the translocation of HiBiT-CagA was not affected by the drug, a concentration-dependent reduction in HiBiT-DHFR-CagA translocation was observed. To exclude that the rigid MTX-bound DHFR interferes with the interaction of HiBiT and LgBiT and causes a reduced luminescence signal that does not account for translocation inhibition, an additional CagA variant was generated carrying a C-terminal HiBiT tag and being N-terminally fused to DHFR. Thus, *dhfr-cagA´* was first introduced in P12[pWS556] using plasmid pCL24 and in a second step, the HiBiT tag was added to the C-terminus of CagA via pCL26. The detailed cloning strategy is depicted in Figure 4.12 A. While DHFR-CagA was highly synthesized as observed in CagA-specific immunoblots, the average amount of DHFR-CagA-HiBiT was only about 10 % of HiBiT-CagA (Figure 4.12 B). The translocation of DHFR-CagA-HiBiT was very weak and only marginally above the background (P12[HiBiT-CagA] Δ*cagT*). Since it was even lower than the translocation of HiBiT-DHFR-CagA it has to be concluded, that a C-terminal HiBiT tag interferes with Cag-type IV secretion itself. Nevertheless, a strong reduction in DHFR-CagA-HiBiT translocation was observed when the bacteria were pre-treated with MTX 0.5 h prior to infection, confirming the results of HiBiT-DHFR-CagA (Figure 4.12 C).

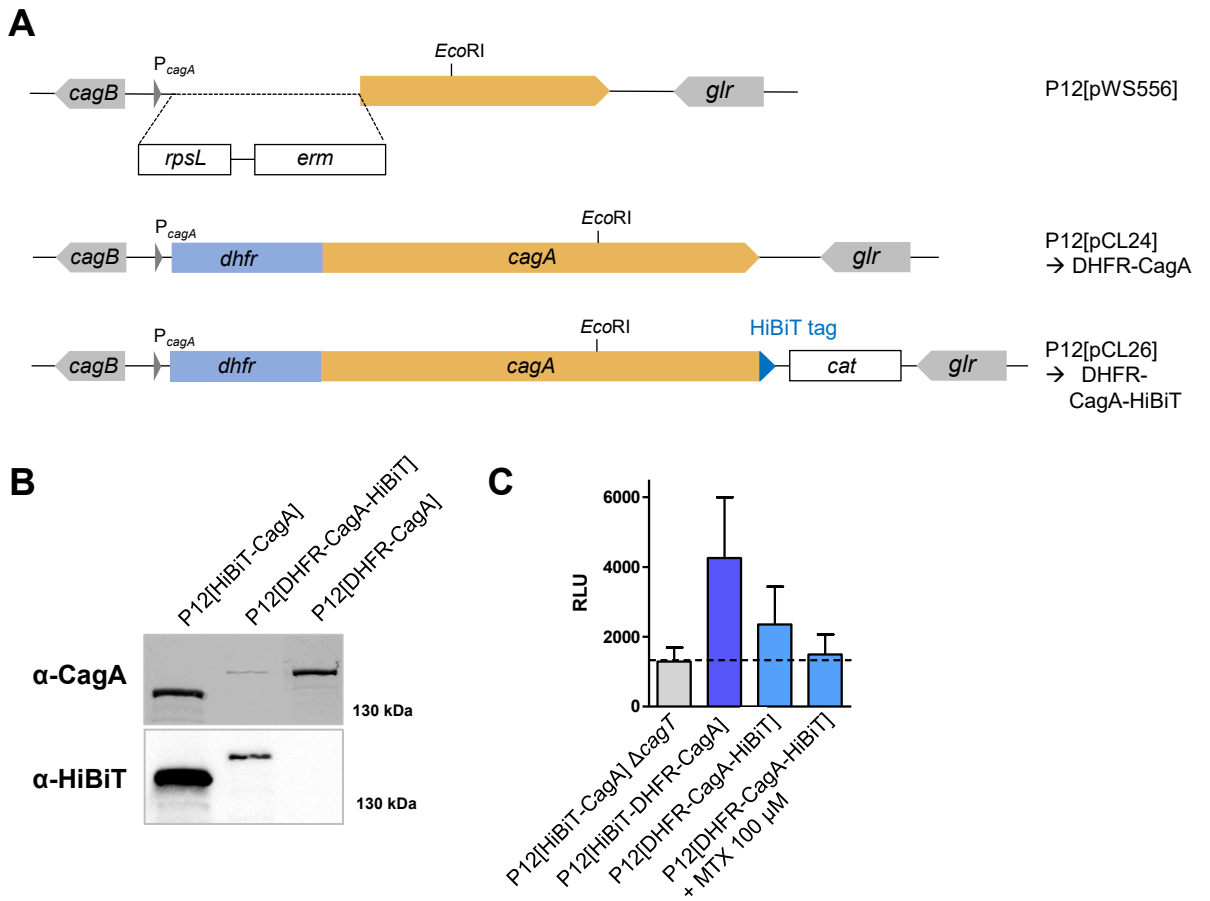

Figure 4.12 Impact of tightly folded protein domains on CagA translocation (3). (A) Schematic overview of the cloning strategy of DHFR-CagA and DHFR-CagA-HiBiT. (B) Immunoblots to confirm DHFR-CagA and DHFR-CagA-HiBiT synthesis (α-CagA (AK299)/α-HiBiT). (C) Translocation of the different CagA variants was determined as described. Means and standard deviations of absolute RLU values of five independent experiments are shown.

To endorse the results obtained with the HiBiT-CagA reporter assay, translocation of the different CagA variants was tested in an orthologous setup, *i.e.* the detection of phosphorylated and thus intracellular CagA via immunoblotting. To enhance the sensitivity, phosphorylated CagA was first immunoprecipitated and subsequently detected using the phosphotyrosine-specific antibody PY99. In parallel, CagA was detected in the input samples using AK257. (Figure 4.13) Translocation of DHFR-tagged CagA was very weak, but completely lost if bacteria were treated with 100 µM MTX. As expected from the HiBiT-CagA translocation assay results, no translocation of HiBiT-GFP-CagA was detectable. In accordance with the split-luciferase reporter assay, translocation of both HiBiT-Ub-CagA variants was observed. Interestingly, HiBiT-Ub-CagA, but not HiBiT-Ub$^{I3G, I13G}$-CagA was cleaved inside the eukaryotic cells, resulting in two bands in the CagA-specific blot, one corresponding to full-length HiBiT-Ub-CagA (145 kDa) and one to CagA only (135 kDa). The putative degradation of the HiBiT-Ub fusion inside the host cells might account for the slightly reduced translocation efficiency observed in the endpoint assay (Figure 4.10 E).

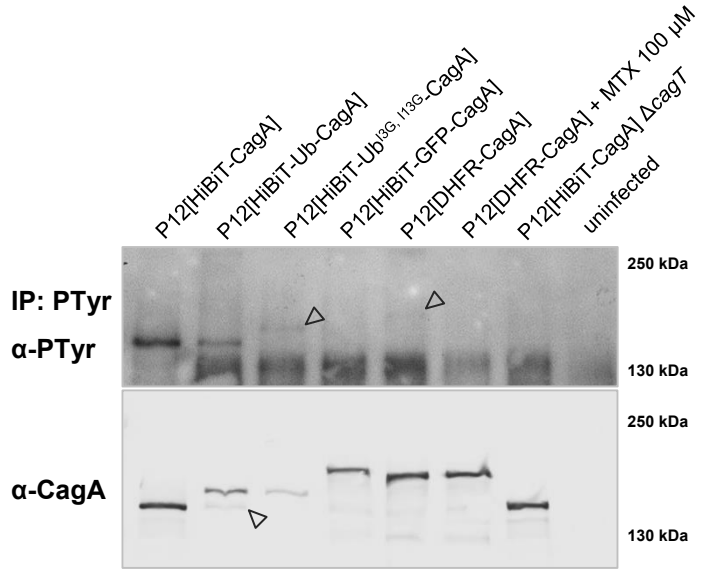

Figure 4.13 Immunoblot to detect translocation of the different CagA variants. Bacteria were pre-incubated for 2 h, and subsequently co-incubated with AGS cells for 4 h. Tyrosine-phosphorylated and thus intracellular CagA was enriched by immunoprecipitation and subsequently detected by a phosphotyrosine-specific antibody (α-PTyr, PY99). Additionally, the overall synthesis of CagA was determined (α-CagA, AK257). In the upper blot, bands of phosphorylated HiBiT-Ub$^{I3G, I13G}$-CagA and DHFR-CagA are highlighted by arrows. In the lower blot, the arrow points at the faint band of ca. 135 kDa that is caused by cleaving of HiBiT-Ub-CagA inside the host cells.

Finally, a strain simultaneously expressing DHFR-CagA and HiBiT-CagA was generated. Thus, P12[pCL24] was transformed with pCL27 to introduce *HiBiT-cagA* into the *recA* locus. The synthesis of the two CagA variants was assessed by immunoblotting (Figure 4.14 A) confirming equal protein levels. Infection of LgBiT-producing AGS cells with the respective strain revealed a strongly reduced translocation of HiBiT-CagA (ca. 1-2 % of P12[HiBiT-CagA], Figure 4.14 B), indicating that the poorly transported DHFR-CagA interfered with the

translocation process probably by blocking the CagT4SS. Consistently, pre-incubation of the reporter strain with 100 µM MTX further decreased the translocation of HiBiT-CagA.
Taken together, these observations strongly suggest that unfolding of CagA is required for the translocation via the CagT4SS.

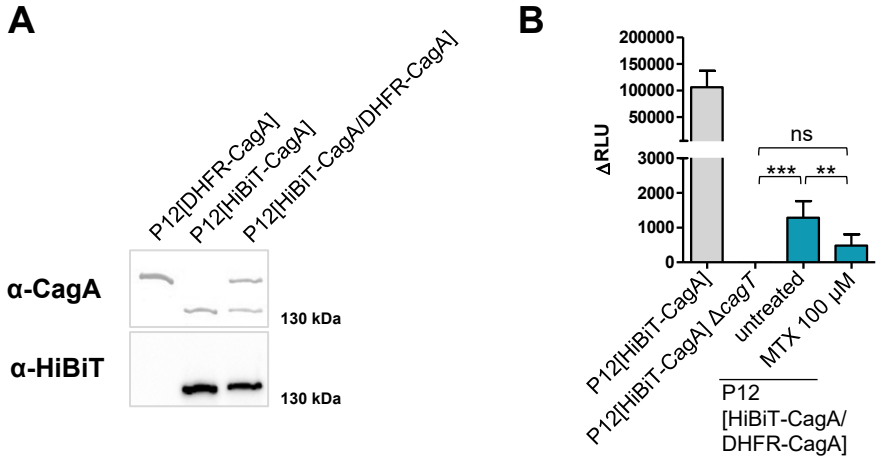

Figure 4.14 Co-production of DHFR-CagA and HiBiT-CagA results in drastically reduced translocation of HiBiT-CagA. (A) Immunoblots to confirm DHFR-CagA and HiBiT-CagA synthesis. (B) AGS[LgBiT] cells were co-incubated with the indicated strains for 2.5 h and HiBiT-CagA translocation was determined as described. Optionally, the *dhfr-cagA* and *HiBiT-cagA* encoding strain was incubated for 0.5 h with 100 µM MTX prior to the infection. Means and standard deviations of five independent experiments are shown. (Statistics: One-Way ANOVA, Bonferroni post test, **p<0.01, ***p<0.001)

4.2.3 Motility and CagA translocation

H. pylori is able to quickly move through the acidic stomach lumen and penetrate the mucus layer finally reaching its ecological niche, the stomach mucosa, due to flagella-mediated movement. Sophisticated processes coordinate the synthesis, post-translational modification and coordination of the four to six unipolar flagella that enable *H. pylori* to move. The sheathed flagella consist of two flagellin species, namely FlaA, that builds up the flagellum filament, and FlaB, that is only found on the flagellum base (Kostrzynska *et al.,* 1991; Eaton *et al.,* 1996). It is well known that motility is a crucial factor for successful colonization of experimental animals (Eaton *et al.,* 1996; Zhong *et al.,* 2016). But little is known about the impact of motility during *in vitro* infections, in fact contradictory effects of motility on adhesion to epithelial cells *in vitro* were described: Though a non-motile Δ*flaA*/Δ*flaB* double knockout mutant of *H. pylori* N6 was found as not impaired in adhesion to KatoIII cells (Clyne *et al.,* 2000), others reported a strong adhesion defect of an immotile *H. pylori* G27 Δ*flaA* mutant to AGS cells while a hypermotile mutant (Δ*hp0518*) showed increased binding (Asakura *et al.,* 2010). Other studies showed conflicting results, too (Tharmalingam *et al.,* 2014; Zhong *et al.,* 2016).

Using the TEM-CagA translocation assay and the newly developed HiBiT-CagA reporter assay, the impact of motility on adhesion and CagA translocation of *H. pylori* P12 were evaluated.

Immotile *H. pylori* P12[TEM-CagA] and [HiBiT-CagA] *flaA* deletion mutants were generated by homologous recombination (pRH121, *flaA::cat*). The respective complementation strains were obtained by reintroducing *flaA* under control of the *flaA* promotor in the *recA* locus (pCL6).

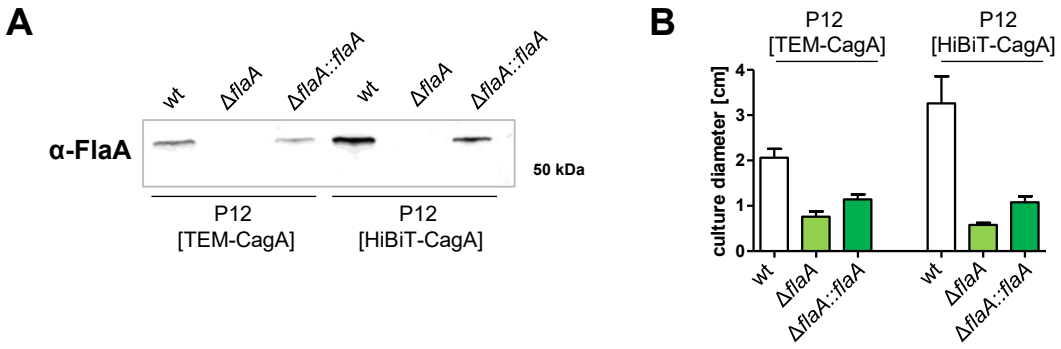

Figure 4.15 Verification of P12 Δ*flaA* mutants and the respective complemented strains. (A) FlaA-specific Western blot, FlaA has an estimated size of 53 kDa. (B) Motility was evaluated by soft agar experiments. Shown are means and standard deviations of five independent experiments.

Using Western blotting, FlaA synthesis of the knockout mutants and the respective complemented strains was tested (Figure 4.15 A). Additionally, motility was assessed by soft agar assay experiments, proving a complete loss of motility in the Δ*flaA* strains and a partial recovery in the respective complementants (Figure 4.15 B). In general, the HiBiT-CagA-producing parental strain was much more motile than the TEM-CagA-producing parental strain, which correlated with the higher amounts of FlaA detected by Western blotting.

The adhesion of the immotile P12[TEM-CagA] Δ*flaA* strain to gastric epithelial cells was reduced to more than 50 % compared to the wt parental strain (Figure 4.16 A). Accordingly, CagA translocation was significantly reduced, too (Figure 4.16 B, C). Interestingly, adhesion and CagA translocation were completely restored in the complemented strain in case of P12[TEM-CagA], or almost completely in case of the P12[HiBiT-CagA], although both strains were not as motile as the respective parental strains (Figure 4.16).

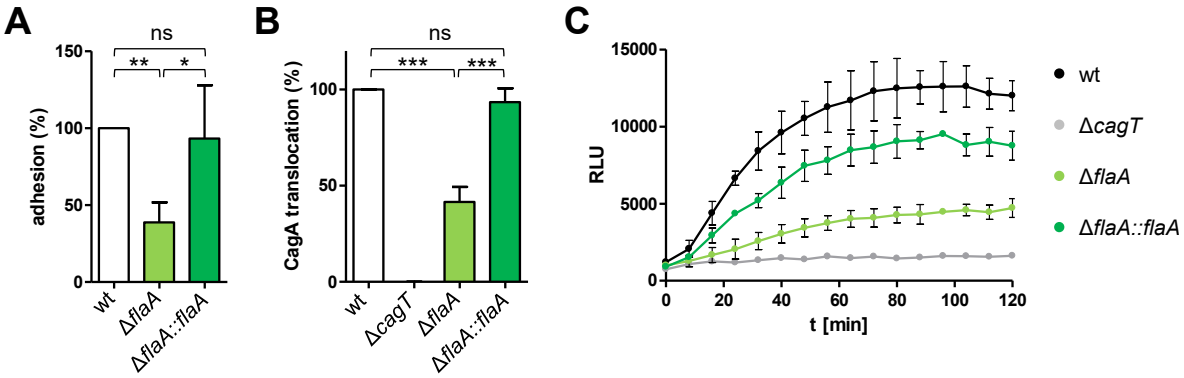

Figure 4.16 Motility has a strong impact on adhesion and CagA translocation *in vitro*. (A) Adhesion of P12[TEM-CagA] and the corresponding mutant strains to AGS cells was measured after 1 h of infection using flow cytometry. (B/C) CagA translocation was detected by the TEM-CagA reporter assay or the HiBiT-CagA real-time translocation assay. Data shown are means and standard deviations of at least three independent experiments (A, B). A representative experiment is depicted in case of the real-time assay, data shown are means and standard deviations of two technical replicates (C). (Statistics: One-Way ANOVA, Bonferroni post test, *p<0.05, **p<0.01, ***p<0.001)

Assuming that the immotile mutants need longer time to reach the epithelial cell layer at the bottom of each well and thus adhere to lower extent, which in the end results in reduced CagA translocation, it was postulated that bringing the bacteria mechanically to their target cells would compensate for the motility defect. Hence, bacteria were centrifuged (5 min, 2500xg) on the AGS layer at the start of the infection. Indeed, it could be demonstrated by both CagA translocation reporter assays, that the motility defect (Δ*flaA* mutant) was abolished in the centrifuged samples, whereas the translocation impairment of a Δ*hopQ* mutant strain was not altered (Figure 4.17). As mentioned in the introduction, HopQ is an *H. pylori* outer membrane protein that interacts with human CEACAMs on the host cells. T4SS-dependent CagA translocation strongly depends on this adhesin-receptor interaction (Königer *et al.,* 2016). Interestingly, the amount of translocated CagA of the wt TEM-CagA reporter strain and both mutants was almost doubled when bacteria were centrifuged onto the cells (Figure 4.17 A). This is in line with published data showing that *H. pylori* G27 wt and the corresponding hypermotile mutant can be “synchronized” regarding adhesion and CagA translocation by centrifugation. In this context, the authors observed an up to three-fold enhanced binding and subsequent CagA translocation by mechanically bringing the bacteria to their host cells. (Asakura *et al.,* 2010)

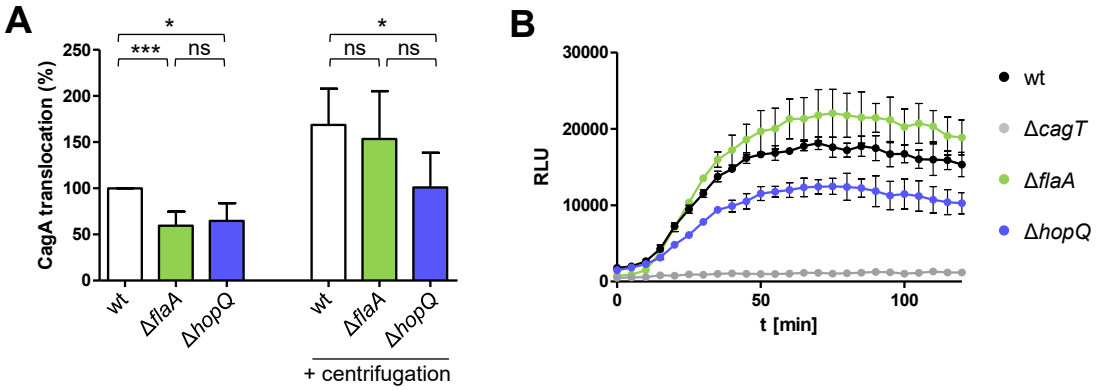

Figure 4.17 Centrifugation of the bacteria to the host cells can compensate the motility defect. (A) CagA translocation was determined by the TEM-CagA reporter assay. Cells were infected either with (right) or without (left) centrifuging the bacteria onto the AGS cell layer. (B) Same experiment as in (A) using the HiBiT-CagA real-time translocation assay. Only samples with centrifugation are depicted. Data show means and standard deviations of at least three independent experiments (A) or a representative experiment with means and standard deviations of two technical replicates (B). (Statistics: One-Way ANOVA, Bonferroni post test, *p<0.05, ***p<0.001)

So far, adhesion and CagA translocation were always analyzed in separate experimental setups. Combining flow cytometry (adhesion) and Western blotting or the TEM-CagA reporter assay (translocation) in one assay would facilitate the characterization of T4SS processes and the discrimination between mutations directly affecting CagA translocation and others acting indirectly, for example by reducing the adhesion or the amount of CagA. The endpoint HiBiT-CagA translocation assay can easily be adapted to cover both, adhesion and translocation by quantifying CagA translocation and subsequently determining the amount of total CagA as described before.

The effects of motility and HopQ-CEACAM interaction were reevaluated using this experimental setup. Firstly, HiBiT-CagA translocation was measured using the endpoint assay. As expected, a strongly reduced translocation was observed in both deletion mutants (Figure 4.18 A). Next, infection samples were lysed and the amount of total CagA, *i.e.* the CagA injected into the host cells and the CagA from the adherent bacteria, was determined (Figure 4.18 B). The data confirmed that the type IV secretion-deficient Δ*cagT* mutant produces high amounts of HiBiT-CagA and readily adheres to the host cell. Furthermore, no significant difference in total CagA levels was observed between the Δ*hopQ* mutant and the wt, indicating that the missing HopQ-CEACAM interaction does not drastically impair the adhesion to AGS cells. In contrast, only strongly reduced HiBiT-CagA levels were observed for the Δ*flaA* mutant. Indeed, in this case the amount of total CagA reflected the amount of translocated CagA. Thus, normalizing the CagA translocation to the quantity of total CagA completely abolished the CagA translocation deficiency in case of the mutant with reduced motility (and adhesion) but not in case of the T4SS-impaired mutants Δ*cagT* and Δ*hopQ* (Figure 4.18 C). To prove that the observed lower amounts of total CagA are really caused by a reduced adhesion and not

by decreased overall HiBiT-CagA production, an aliquot of the initial bacterial preculture was analyzed regarding the HiBiT-CagA levels. No differences between the tested strains were detected (Figure 4.18 D).

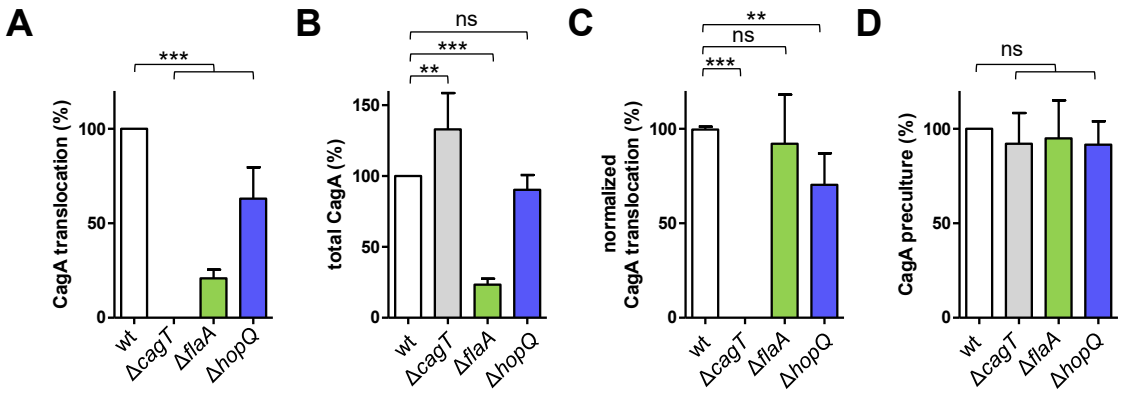

Figure 4.18 Monitoring CagA translocation and adhesion using the HiBiT-CagA endpoint reporter assay. After quantifying the translocated CagA via the HiBiT-CagA endpoint assay (A), samples containing host cells and adherent bacteria were lysed and the amount of total CagA was determined (B). Combining (A) and (B), the CagA translocation was normalized to the total CagA level (C). Additionally, an aliquot of bacteria from the initial preculture was lysed and HiBiT-CagA was measured (D). Data show means and standard deviations of at least five independent experiments. (Statistics: One-Way ANOVA, Bonferroni post test, **p<0.01, ***p<0.001)

4.2.4 Priming of CagA translocation during pre-incubation with FCS

As observed by the real-time assay, *H. pylori* is able to translocate CagA immediately after the start of infection, *i.e.* immediately after contacting the cells. This fast onset, that was detectable within the first 10-15 min after starting the real-time measurement, indicated that bacteria were already primed for CagA translocation and all components necessary for type IV secretion activity were prepared. Comparing the translocation kinetics of bacteria pre-incubated for 2 h in PBS/FCS and bacteria without preculture but directly taken from serum plates, it could be shown, that the priming occurs during the liquid preculture (Figure 4.19 A). The effect was most pronounced during the early and exponential phase of T4SS activity (0-60 min), finally resulting in an about two-fold higher overall amount of translocated CagA in the samples of pre-incubated bacteria after 2-2.5 h of infection (Figure 4.19 B). Consistently, 50 % CagA translocation was observed in samples without preculture, using the TEM-CagA translocation reporter assay (Figure 4.19 C).

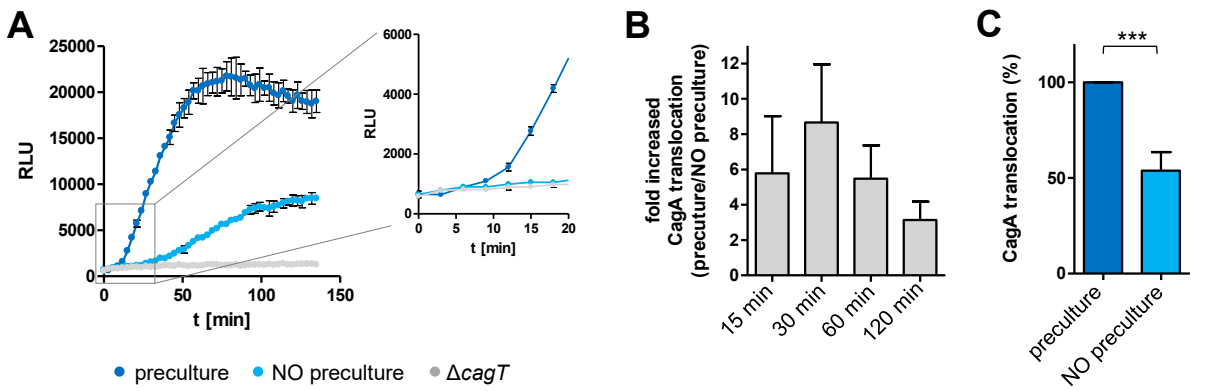

Figure 4.19 *H. pylori* is primed for CagA translocation during preculture in PBS/FCS. (A) HiBiT-CagA translocation of bacteria pre-incubated for 2 h in PBS/FCS or bacteria without preculture was monitored as described. The zoom-in visualizes the early phase of infection. Data shown are means and standard deviations of two technical replicates of a representative experiment. (B) The amount of HiBiT-CagA translocation of precultured bacteria and bacteria with no preculture was compared at different times after the start of infection. Thus, HiBiT-CagA translocation assays were performed as in (A) and HiBiT-CagA translocation was calculated as $\Delta RLU_{t=x\ -\ t=0\ min}$. For each time point, the ratio of $\Delta RLU_{preculture}/\Delta RLU_{NO\ preculture}$ was computed. Data show means and standard deviations of five independent experiments. (C) Same experiment as in (A) using the TEM-CagA translocation assay. CagA translocation was determined after 2.5 h of infection. Data show means and standard deviations of at least five independent experiments. (Statistics: Student`s t-test, ***p<0.001)

A characteristic property of *H. pylori* incubated under optimal conditions in liquid culture is the gain of motility. As described above, motility has an impact on adherence and thus on CagA translocation (4.2.3). To test, if the priming of T4SS activity during the pre-incubation is linked to the increased motility, the HiBiT-CagA translocation kinetics of the immotile Δ*flaA* mutant were analyzed. Even though the preculture effect was less pronounced compared to the parental HiBiT-CagA reporter strain or the corresponding Δ*flaA::flaA* complemented strain, a clearly higher HiBiT-CagA translocation was observed in the pre-incubated samples (Figure 4.20 A). Furthermore, as already described above, the motility defect could be restored by mechanically bringing the bacteria to their target cells, but the priming during the preculture could not be substituted by centrifugation (Figure 4.20 B).

The CagA translocation-promoting effect was not only observed for *H. pylori* P12 but for strain G27, too (Figure 4.20 C). Yet, the translocation kinetics of G27[HiBiT-CagA] was reminiscent of the ones observed for the P12 Δ*flaA* mutant. Indeed, soft agar motility assays revealed that the used G27[HiBiT-CagA] strain (as well as its parental G27 wt strain) were impaired regarding motility (Figure 4.20 D).

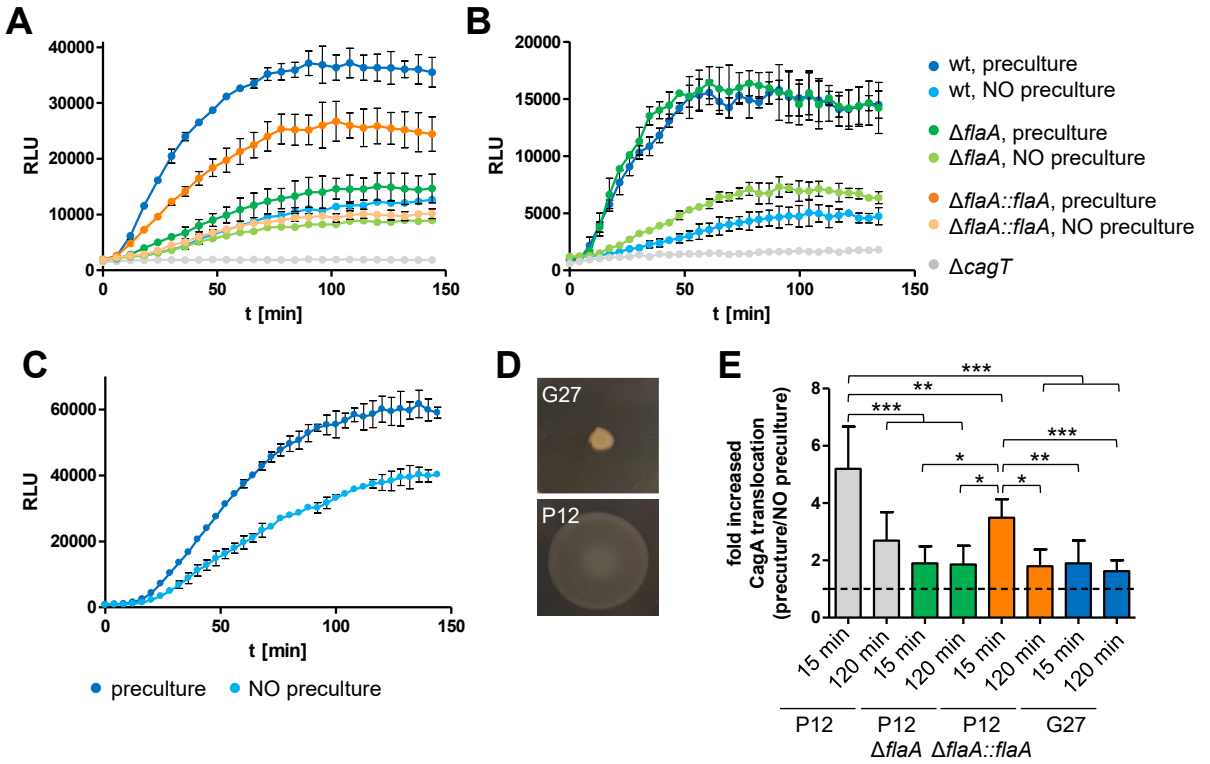

Figure 4.20 Motility and priming of CagA translocation are distinct features obtained during preculture in PBS/FCS. (A) HiBiT-CagA translocation of bacteria pre-incubated for 2 h in PBS/FCS or bacteria without preculture was monitored using the respective reporter strains (all P12). (B) Same experiment as in (A), but additionally, bacteria were mechanically brought to their target cells by centrifugation. The assay performance was in general affected by the centrifugation step, thus lower overall RLU values were detected compared to (A). (C) HiBiT-CagA translocation of a G27[HiBiT-CagA] strain. Bacteria were either pre-incubated for 2 h in PBS/FCS or not. (D) Soft agar assay to check the motility of the two reporter strains G27[HiBiT-CagA] and P12[HiBiT-CagA]. (E) HiBiT-CagA real-time translocation assays were evaluated regarding the ratio $\Delta RLU_{preculture}/\Delta RLU_{NO\ preculture}$ as described in Figure 4.19. Infection kinetics of motile and immotile strains were compared at an early time point of infection (15 min) and after 2 h. Representative experiments with means and standard deviations of technical replicates are shown in (A-D). Means and standard deviations of at least six independent assays are shown in (E). (Statistics: One-Way ANOVA, Bonferroni post test, *p<0.05, **p<0.01, ***p<0.001)

Comparing the translocation kinetics of the non-motile and the motile strains enabled to discriminate the impact of motility and T4SS priming on CagA translocation. The ability to quickly move and reach the AGS cell layer had a strong influence on type IV secretion activity during the early phases of infection, as observed by four to six times increased CagA translocation by the motile strains 15 min after starting the infection compared to the same strains without preculture. In contrast, at the same time point immotile strains precultured for 2 h in PBS/FCS translocated roughly double the amount of CagA compared to bacteria directly taken from serum plates. Thus, the strongly increased CagA translocation by bacteria precultured in PBS/FCS at the early time of infections is mainly due to the gain of motility during liquid culture. Additionally, a motility-independent, FCS-dependent priming of type IV secretion

activity occurs, that doubles the CagA translocation efficacy throughout the time of infections. (Figure 4.20 E)

To further characterize the priming of the T4SS activity during liquid culture in PBS/FCS, the translocation characteristics of a Δ*hopQ* mutant strain were analyzed. As already mentioned, the HopQ-CEACAM adhesin-receptor interaction plays a substantial role in CagA translocation. As observed for the wt P12[TEM-CagA], a strongly enhanced type IV secretion activity was detectable if the *hopQ*-deficient mutant was pre-incubated prior to infection (Figure 4.21). Thus, it can be excluded that the HopQ-CEACAM interaction is involved in the CagA translocation priming detected in the *in vitro* assays.

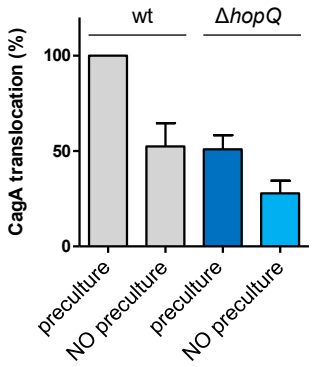

Figure 4.21 CagA translocation priming during preculture in PBS/FCS is independent of the HopQ-CEACAM interaction. The translocation reporter strains P12[TEM-CagA] wt or Δ*hopQ* were either pre-incubated for 2 h in PBS/FCS or directly taken from serum plates and used for co-incubation with AGS cells. The amount of translocated TEM-CagA was determined after 2.5 h of infection. Shown are means and standard deviations of three independent experiments.

First attempts to identify the critical, stimulating factor(s) were performed testing the CagA translocation activity in PBS supplemented with differently treated or fractionated FCS samples. Importantly, the priming during the liquid preculture was not observed for bacteria cultivated in PBS only, clearly indicating an FCS-dependent effect. While the CagA translocation-promoting factor(s) were highly heat-resistant and still active in FCS boiled for 20 min, they were susceptible to proteinase K treatment hinting towards peptides or proteins. Furthermore, FCS was subjected to size exclusion fractionations using spin columns with 100 kDa cutoff. The stimulating factors were found to be in the high molecular weight fraction. Finally, extracellular vesicles were separated from the soluble FCS components by ultracentrifugation and the CagA translocation-promoting factor(s) were only present in the non-membrane-bound soluble fraction. (Figure 4.22 A)

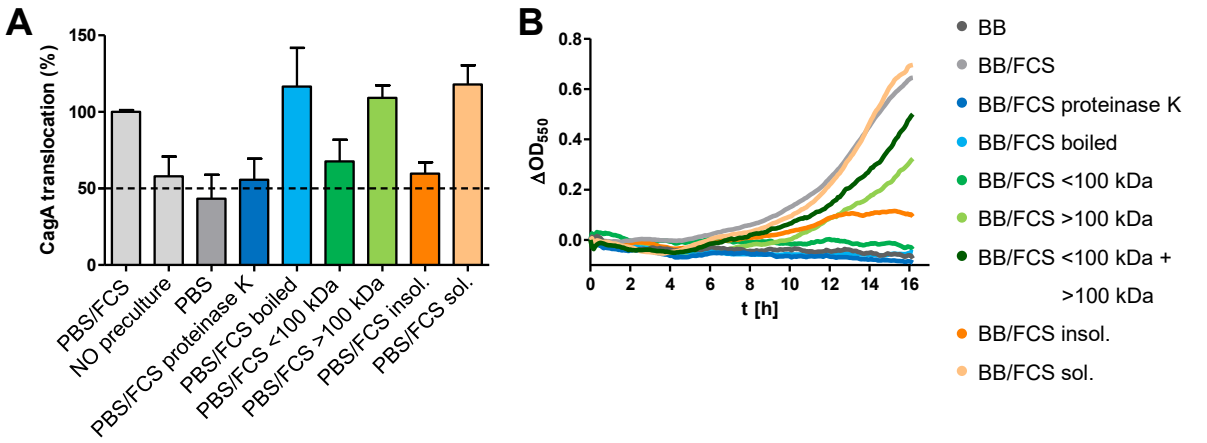

Figure 4.22 The CagA translocation priming factors in the FCS are highly heat resistant soluble proteins and distinct from the growth-promoting factors. (A) Using the TEM-CagA reporter assay, different FCS fractions were analyzed regarding their translocation priming potential. Thus, bacteria were precultured in the indicated PBS/FCS mixtures or PBS only for 2 h, subsequently AGS cells were infected with the respective samples for 2.5 h and CagA translocation was determined as described. Data show means and standard deviations of at least five independent experiments. (B) Growth of *H. pylori* P12 in BB or BB supplemented with the indicated FCS fractions was monitored over time. A representative result is shown.

Since *H. pylori* is usually cultivated on agar plates supplemented with horse serum or cholesterol, the question was addressed, whether liquid culture in PBS spiked with either heat-inactivated horse serum or heat-inactivated horse serum and vitamin mix or cholesterol could prime CagA translocation, but none of the three conditions could stimulate type IV secretion as FCS. (Figure 4.23 A)

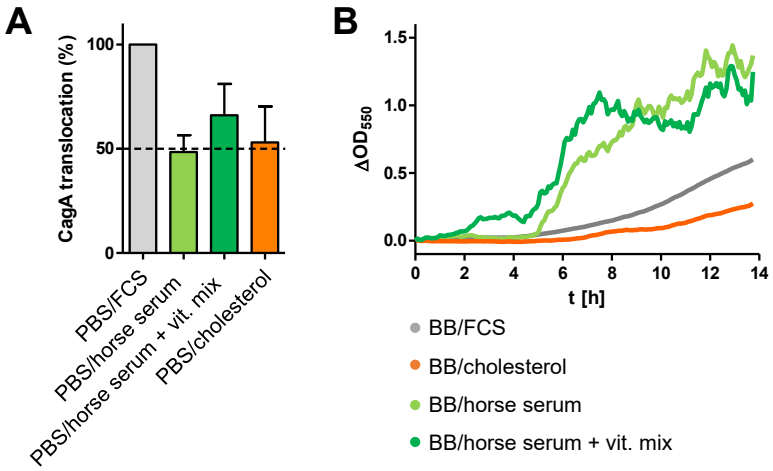

Figure 4.23 FCS but not horse serum or cholesterol stimulate CagA translocation. (A) TEM-CagA translocation of the reporter strain pre-incubated for 2 h in PBS supplemented with heat-inactivated horse serum (and vitamin mix) or cholesterol was determined after 2.5 h of infection. Data show means and standard deviations of at least five independent experiments. (B) Growth curves of *H. pylori* P12 in BB supplemented with either 10 % FCS or cholesterol (1x) or 10 % horse serum or 10 % horse serum and vitamin mix (1 %). Strong clumping of the bacteria was observed in the samples with heat-inactivated horse serum. A representative result is shown.

Interestingly, the CagA translocation priming factor(s) turned out to be distinct from growth-promoting factors as growth curve assays using BB supplemented with the above-mentioned different serum samples or cholesterol revealed. While bacteria did not grow in medium without supplements (BB, Figure 4.22 B), the addition of cholesterol was sufficient to enable at least 50 % growth rates compared to the reference condition BB/FCS (Figure 4.23 B). Notably, PBS/cholesterol was not sufficient for elevated CagA translocation. In contrast, *H. pylori* did not grow in BB supplemented with boiled FCS that was on the other hand priming type IV secretion activity. As observed for CagA translocation, the component(s) important for *H. pylori* growth were sensitive towards proteinase K digestion. (Figure 4.22 B)

While the CagA translocation-promoting factor was exclusively found in the soluble fraction after depletion of extracellular vesicles, bacteria grew in BB supplemented with the insoluble FCS fraction, even though only to minor degrees. It cannot be excluded that this was caused by some carry-over of soluble components of the FCS. (Figure 4.22)

Bacteria cultivated in BB supplemented with the >100 kDa fraction showed reduced growth compared to BB/FCS, whereas no growth was observed in BB supplemented with the <100 kDa fraction. Combining the >100 kDa fraction and the <100 kDa fraction could partially restore growth rates. This further indicates that the growth-promoting factors are distinct from the type IV secretion-activating ones, since the >100 kDa fraction alone was sufficient for full CagA translocation activity. (Figure 4.22)

Finally, the growth of *H. pylori* P12 in BB supplemented with either 10 % horse serum or 10 % horse serum and additionally 1 % vitamin mix was monitored. In both cases, bacteria were able to grow, but a strong clumping was observed. (Figure 4.23 B)

To get insights into cellular processes induced upon cultivation in PBS/FCS, RNAseq data were generated from bacteria grown on serum plates and compared to those of *H. pylori* cultivated for 2 h in PBS/FCS. 292 mRNAs were identified to be significantly differentially expressed. Almost 50 % (144) of those encoded for proteins with unknown function or putative function only. The remaining 149 mRNAs were grouped according to the COG (clusters of orthologous groups of proteins, Tatusov *et al.,* 1997) classification, considering *cag*PAI encoded genes as an additional, *H. pylori* specific sub-group. In total 16 different categories were identified (Figure 4.24), whereby genes encoding proteins involved in membrane biogenesis accounted for the largest fraction. This group includes OMPs, as well as proteins essential for the generation of the different membrane layers and LPS. Interestingly, levels of almost all OMP-encoding mRNAs were significantly decreased after 2 h in PBS/FCS. In contrast, elevated levels of mRNAs encoding proteins involved in LPS biosynthesis were detected. Energy production and conversion represented the second largest group (11 %), mRNAs classified to this category were in general downregulated in the liquid culture samples. Restriction modification systems are commonly assigned to the COG “defense mechanisms”,

yet in case of *H. pylori* they might be involved in transcription regulation (Scarlato *et al.,* 2001; Srikhanta *et al.,* 2011; Estibariz *et al.,* 2019). After 2 h incubation in PBS/FCS, mRNAs coding for proteins of the restriction-modification systems were in general upregulated.

Consistently with the gain of motility of *H. pylori* in liquid media, mRNAs categorized to “cell motility and chemotaxis” accounted for a comparably large fraction of differentially expressed genes (8 %).

Even though the 28 genes of the *cag*PAI only represent 1.8 % of all mRNAs detected in the RNAseq samples, they account for 6 % of the differentially expressed genes and thus for a significant fraction.

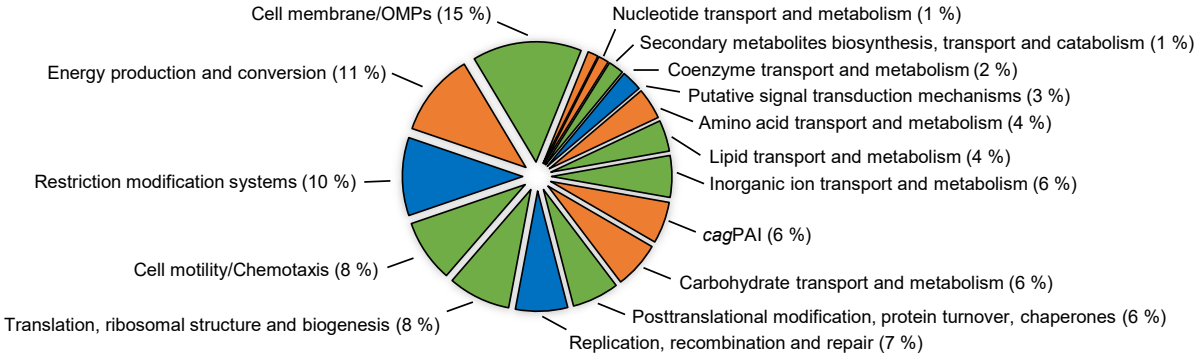

Figure 4.24 Functional classification of mRNAs that were differentially expressed between *H. pylori* incubated for 2 h in PBS/FCS and bacteria cultured on serum plates. Groups are adapted to the standard COG categories. Blue coloring of the segments indicates that most members of the group are upregulated upon liquid culture, orange codes for decreased mRNA levels, respectively. In several categories, mRNA levels were up- or downregulated, those segments are shown in green.

The 20 most strongly differentially expressed mRNAs are listed in Table 4.1.

The ten most upregulated mRNAs encoded proteins of unknown or predicted function. Some of them might be involved in signal transduction mechanisms. *Hpp12_0983*, that was clearly the most strongly upregulated gene, encodes a DUF2357 domain-containing protein (DUF = Domain of unknown function) that is yet uncharacterized. All ten upregulated genes are part of the plasticity zone 2 of *H. pylori* and might be organized within an operon (Fischer *et al.,* 2010). Notably, three of those genes lack homologs in *H. pylori* G27 (*hpp12_0994*, *hpp12_0985*, *hpp12_0987*), a strain that is primed for CagA translocation during preculturing, too. In addition, the respective mRNAs were in general only detectable at very low levels, thus the observed fold changes are based on minimal alterations and thus not reliable.

Table 4.1 List of the 20 strongest down- or upregulated mRNAs in *H. pylori* incubated for 2 h in PBS/FCS compared to bacteria cultured on serum plates.

	fold change (PBS/FCS vs. plate)		**COG**
hpp12_0452	0.18	Uncharacterized protein	**S**
pfr	0.18	Ferritin	**P**
hpp12_0449	0.20	Uncharacterized protein	**S**
napA	0.23	Neutrophil-activating protein A	**-**
horE	0.25	Outer membrane protein HorE	**M**
cagζ	0.26	Cagζ	***cag*PAI**
hpp12_0874	0.26	Uncharacterized protein	**S**
hpp12_0708	0.27	Acetone carboxylase gamma subunit	**Q**
hpp12_1554	0.27	Alkyl hydroperoxide reductase C	**V**
hpp12_1032	0.28	Carboxy-S-adenosyl-L-methionine synthase	**-**
hpp12_0994	7.85	Uncharacterized protein	**S**
terY	7.88	Phage/colicin/tellurite resistance cluster protein	**V**
hpp12_0991	8.00	Serine/threonine phosphatase 2C-like protein	**R/T**
hpp12_0984	8.43	Uncharacterized protein	**S**
hpp12_0990	10.40	Serine/threonine kinase C-like protein	**R/T**
hpp12_0989	11.15	Serine/threonine kinase C-like protein	**R/T**
hpp12_0985	12.98	Uncharacterized protein	**S**
hpp12_0987	13.52	Uncharacterized protein	**S**
hpp12_0988	16.64	Uncharacterized protein	**S**
hpp12_0983	45.52	Uncharacterized protein	**S**

M = Membrane biogenesis/OMPs; P = Inorganic ion transport and metabolism; Q = Secondary metabolites biosynthesis, transport and catabolism; R = General function predicted only; S = unknown function; T = Signal transduction mechanisms; V = defense mechanisms

The mRNA level of Cagζ, a *cag*PAI encoded protein with so far unknown function, was strongly reduced in the PBS/FCS samples.

To assess the effect of FCS on Cagζ protein levels, a marker-free N-terminal HiBiT-tagged Cagζ variant was generated. Thus, *cagζ* was replaced by an *rpsL-erm* cassette using plasmid pCL7 and subsequently *HiBiT-cagζ* was reintroduced by plasmid pCL12. The synthesis of

HiBiT-Cagζ was proven via HiBiT-specific immunoblotting (Figure 4.25 A). Additionally, relative protein levels were quantified using the HiBiT-lysate assay (Figure 4.25 B).

Due to the marker-free cloning strategy, conclusions on the effect of external stimuli on protein levels of HiBiT-Cagζ could be drawn. Comparing bacteria incubated for 2 h in PBS/FCS at 37 °C and at 0 °C, respectively, a twofold increase in luminescence signal intensity was measured (Figure 4.25 C), *i.e.* an induction of HiBiT-Cagζ synthesis during the preculture, that is in contrast to the reduced mRNA level observed. While the priming of CagA translocation was only detected if the bacteria were pre-incubated in PBS/FCS, but not if they were cultured in PBS supplemented with horse serum, HiBiT-Cagζ production was comparably stimulated under both conditions (Figure 4.25 C).

To finally test the impact of Cagζ on CagA translocation priming, a P12[HiBiT-CagA] Δ*cagζ* strain was generated using plasmid pCL7. No alterations in translocation dynamics were observed in a real-time HiBiT-CagA translocation assay (Figure 4.25 D).

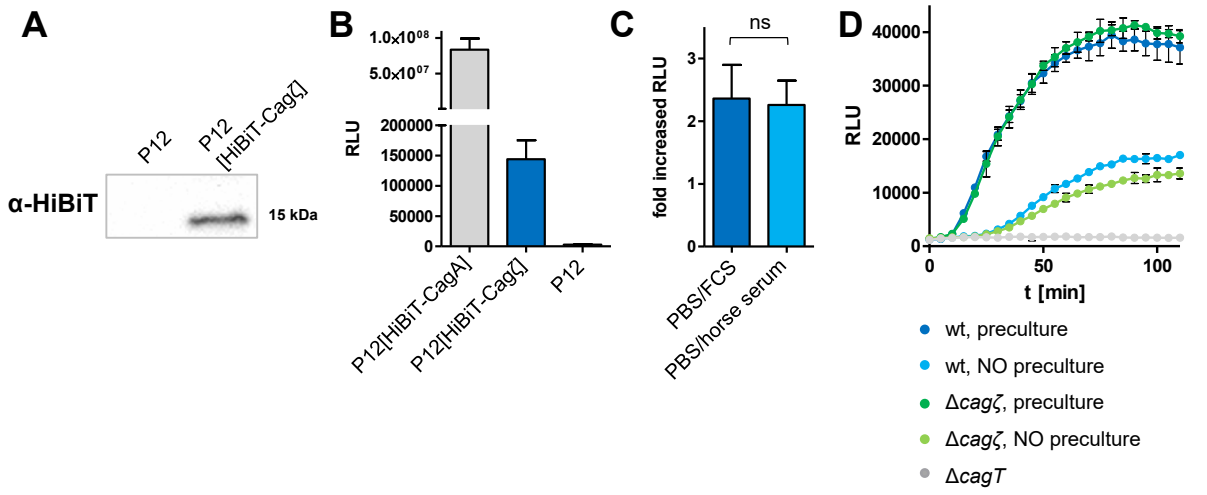

Figure 4.25 Cagζ protein levels are increased upon liquid culture in medium supplemented with serum, but have no impact on CagA translocation dynamics. (A) Immunoblot to confirm HiBiT-Cagζ synthesis (expected size 14 kDa). (B) The amount of the HiBiT-tagged protein variants was measured using the HiBiT-lysate assay. Therefor bacteria were harvested from serum plates adjusted to an equal OD_{550} of 1 and lysed in RIPA buffer. *H. pylori* P12 wt lysates were used to detect background luminescence. Data show means and standard deviations of at least five independent experiments. (C) P12[HiBiT-Cagζ] was incubated for 2 h in the indicated media at 10 % CO_2, 37 °C or on ice. The amount of HiBiT-Cagζ in each sample was measured and the fold increased protein amount was calculated ($RLU_{37\,°C}/RLU_{0\,°C}$). Shown are means and standard deviations of at least three independent experiments. (Statistics: Student`s t-test) (D) AGS[LgBiT] cells were co-incubated with the respective HiBiT-CagA-producing strains that were either pre-incubated in PBS/FCS for 2 h or not. HiBiT-CagA translocation was monitored as described above. A representative result is shown.

Taken together, these data indicate, that upon cultivation in liquid medium containing FCS, a plethora of cellular processes is induced. After 2 h of incubation, initial regulatory effects on transcript levels might already have translated in an altered protein composition. Nevertheless,

the RNAseq data generated in the present work strongly support, that the pre-incubation in PBS/FCS has a huge impact on motility-related and *cag*PAI-encoded genes.

The assembly of the type IV secretion apparatus and the translocation process is considered to be highly energy consuming. As a measure of the energy status of the bacterial cells, the ATP content of *H. pylori* grown on serum plates or incubated for different time frames in PBS/FCS was quantified. Already within the first 30 min of liquid culture, a significant increase in the ATP level was detectable (Figure 4.26 A). After 2 h of pre-incubation, the ATP content was still elevated, thus at an early time point, the preculture in PBS/FCS might provide the energy for synthesis of T4SS components and their assembly and later on the ATP essential for CagA translocation.

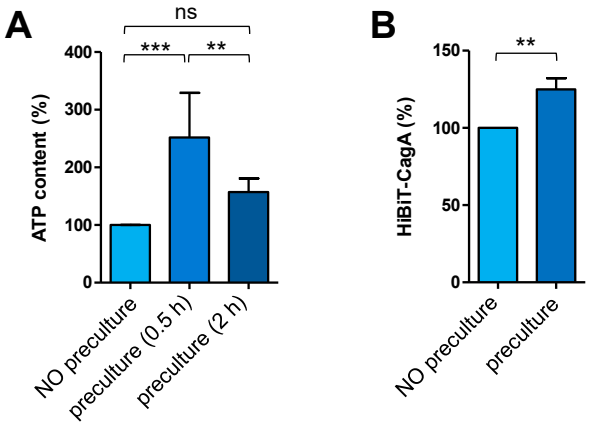

Figure 4.26 Bacteria cultured in PBS/FCS produce more ATP and contain higher amounts of CagA than bacteria grown on serum plates. (A) The cellular ATP content of *H. pylori* P12 harvested from serum plates or incubated for the indicated time in PBS/FCS was determined using the ATP Bioluminescence Assay Kit CLS II. The ATP content of bacteria harvested from serum plates was set to 100 %. Data shown are means and standard deviations of six independent experiments. (Statistics: One-Way ANOVA, Bonferroni post test, **p<0.01, ***p<0.001) (B) To assess the amount of newly synthesized CagA, P12[HiBiT-CagA] was diluted to an OD_{550} of 0.1 in PBS/FCS and incubated for 2 h at 37 °C, 10 % CO_2. Subsequently the amount of HiBiT-CagA was quantified using the HiBiT-lysate assay. In addition, the amount of HiBiT-CagA of bacteria incubated for 2 h at 37 °C, 10 % CO_2 on serum plates was determined and used as reference and for normalization. Data shown are means and standard deviations of five independent experiments. (Statistics: Student`s t-test, **p<0.01)

Recently, it was postulated, that only newly synthesized CagA is in a translocation-competent status (Schindele *et al.,* 2016). To assess if CagA synthesis is induced during preculturing, the amount of HiBiT-CagA of bacteria harvested from serum plates was quantified and compared to the HiBiT-CagA levels of bacteria incubated for 2 h in PBS/FCS. Indeed, a moderately induced synthesis of CagA was detectable, possibly providing the translocation-competent CagA fraction and thus accelerating the onset of the secretion process (Figure 4.26 B).

4.2.5 Characterization of the *cag*PAI encoded genes *cagε*, *cagQ/R* and *cagB*

Even though the CagT4SS is evolutionarily related to other T4SS, only a few Cag proteins have clear sequence similarity to the prototypical secretion apparatus proteins of *A. tumefaciens*. Many genes that are essential for full functionality are unique for the CagT4SS. (Fischer, 2011) Furthermore, the *cag*PAI contains several open reading frames with yet unknown function, amongst them, four predicted genes, namely *cagε*, *cagQ*, *cagR*, and *cagB* that were further investigated in the present work

Independent studies identified transcription start sites (TSS) upstream of *cagQ* and *cagB* (Sharma *et al.,* 2010; Spohn *et al.,* 1997, Figure 4.27). *Cagε* is presumably transcribed together with *cagζ* (Ta *et al.,* 2012).

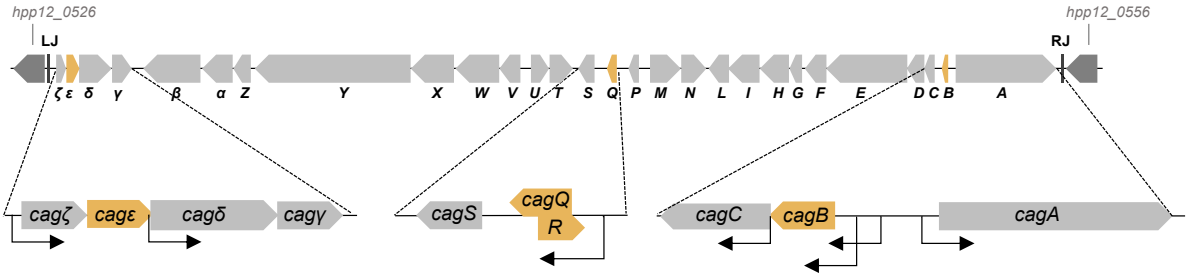

Figure 4.27 Scheme of the four hypothetical open reading frames and the corresponding TSS. A graphical illustration of the genetic organization of the *cag*PAI of *H. pylori* P12 was adapted from Fischer, 2011, the four genes of interest are highlighted. In *H. pylori* strain 26695, a TSS (shown as black arrow) upstream of *cagζ* was identified by Ta *et al.,* 2012. It is hypothesized that genes *cagζ* to *cagγ* build an operon, but additionally a second TSS was found upstream of *cagδ*. *CagQ* and *cagR* partially overlap and are antisense to each other. The TSSs upstream of *cagQ* and *cagC* were determined from dRNA-seq data using strain 26695 (Sharma *et al.,* 2010). Two promotors upstream of *cagB* were identified in *H. pylori* strain NCTC11638 by primer extension analysis (Spohn *et al.,* 1997), the more distant one was further confirmed by dRNA-seq data using strain 26695 (Sharma *et al.,* 2010).

Transcripts of *cagQ* are found *in vitro* and *in vivo* (strain J166, Boonjakuakul *et al.,* 2005). RNAseq data generated within the present work could confirm the transcription of *cagQ* in *H. pylori* P12. Furthermore, transcripts of *cagε* and *cagB* were detected. No mRNA specific for *cagR* was observed under the tested conditions. (Figure 4.28)

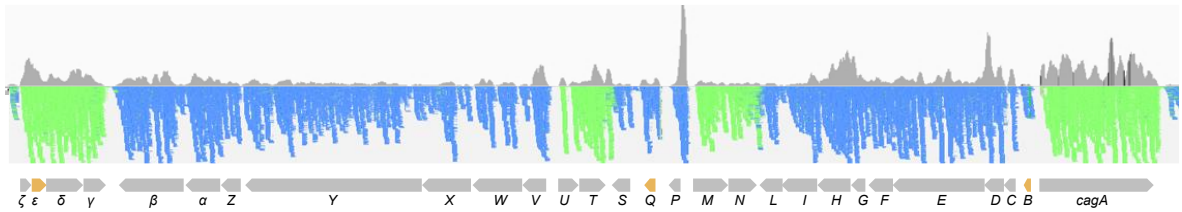

Figure 4.28 RNAseq profile of the *cag*PAI region of *H. pylori* P12. Total RNA of bacteria grown on serum plates under standard conditions was isolated and sequenced as described above. The upper panel shows the overall sequence coverage mapped on the P12 genome. In the lower panel the single 150 bp reads are depicted and color coded according to the respective parental genomic DNA strand (blue: (-) green: (+)). *Cagε*, *cagQ* and *cagB* are highlighted in yellow. Data were visualized using IGV 2.8.12.

Previously, it was hypothesized, that these four hypothetical proteins might be further effector proteins of the CagT4SS (Fischer, 2011). Thus, in the present work, the HiBiT-LgBiT split-luciferase system was adapted to firstly examine if these four putative open reading frames are translated into proteins and next, to test for potential translocation into eukaryotic host cells.

As described for HiBiT-CagA, the eleven amino acid HiBiT tag was inserted at the N-terminus of each protein using the *rpsL-erm* counterselection system, resulting in marker-free gene variants under the control of the intrinsic promotor and genetic environment. Plasmids used for this purpose are listed in Table 2.4. Neither via immunoblotting, nor via the HiBiT-lysate assay, HiBiT-tagged Cagε or CagR were detectable (Figure 4.29 A). As no mRNA of *cagR* was detectable in the RNAseq data of *H. pylori* P12 (Figure 4.28), it has to be concluded, that (under the tested conditions), *cagR* is not expressed, indeed it might not be a coding sequence. In case of HiBiT-Cagε, it cannot be excluded, that the N-terminal tag interfered with protein synthesis. Furthermore, even though the split-luciferase-based assay is highly sensitive, protein levels might have been below the detection limit. The synthesis of HiBiT-tagged CagB and CagQ could be demonstrated for the first time using the HiBiT-LgBiT system (Figure 4.29 A). HiBiT-CagQ was only weakly produced and thus only detectable via the HiBiT-lysate assay but not in a HiBiT-specific immunoblot. In contrast, HiBiT-CagB levels were sufficient to be visualized by Western blot (Figure 4.29 B). No translocation of HiBiT-CagB or HiBiT-CagQ into AGS[LgBiT] cells was detected in standard infections (2.5 h, data not shown).

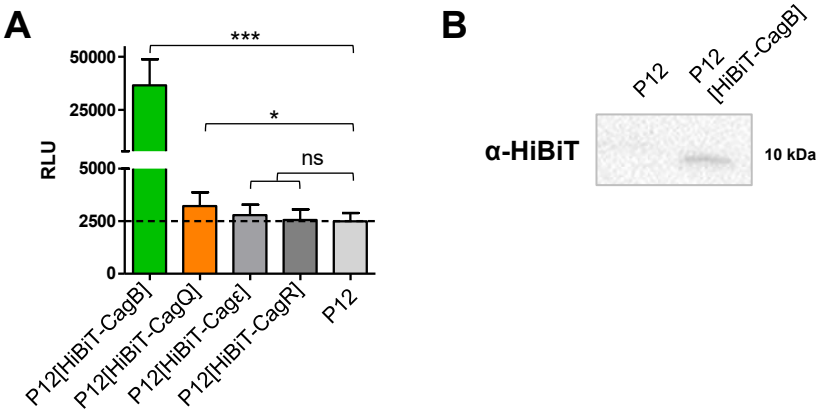

Figure 4.29 CagB and CagQ are synthesized by *H. pylori* P12. (A) The amount of the HiBiT-tagged protein variants was measured using the HiBiT-lysate assay. To do so, bacteria were harvested from serum plates adjusted to an equal OD_{550} of 1 and lysed in RIPA buffer. *H. pylori* P12 wt lysates were used to detect background luminescence. Data show means and standard deviations of at least five independent experiments. (Statistics: Student`s t-test *p<0.05, ***p<0.001). (B) Western blot to confirm HiBiT-CagB synthesis. HiBiT-CagB has an expected molecular weight of 10 kDa.

Next, the impact of CagQ and CagB on CagA translocation dynamics was analyzed. Thus, P12[HiBiT-CagA] Δ*cagQ* and Δ*cagB* mutants were generated and HiBiT-CagA translocation was monitored. Deletion of *cagQ* had no impact on CagT4SS activity, but CagA translocation

rates were reduced to 50-70 % in the Δ*cagB* mutant (Figure 4.30 A, C). The reduction was also observed in *H. pylori* G27[HiBiT-CagA] (Figure 4.30 B).

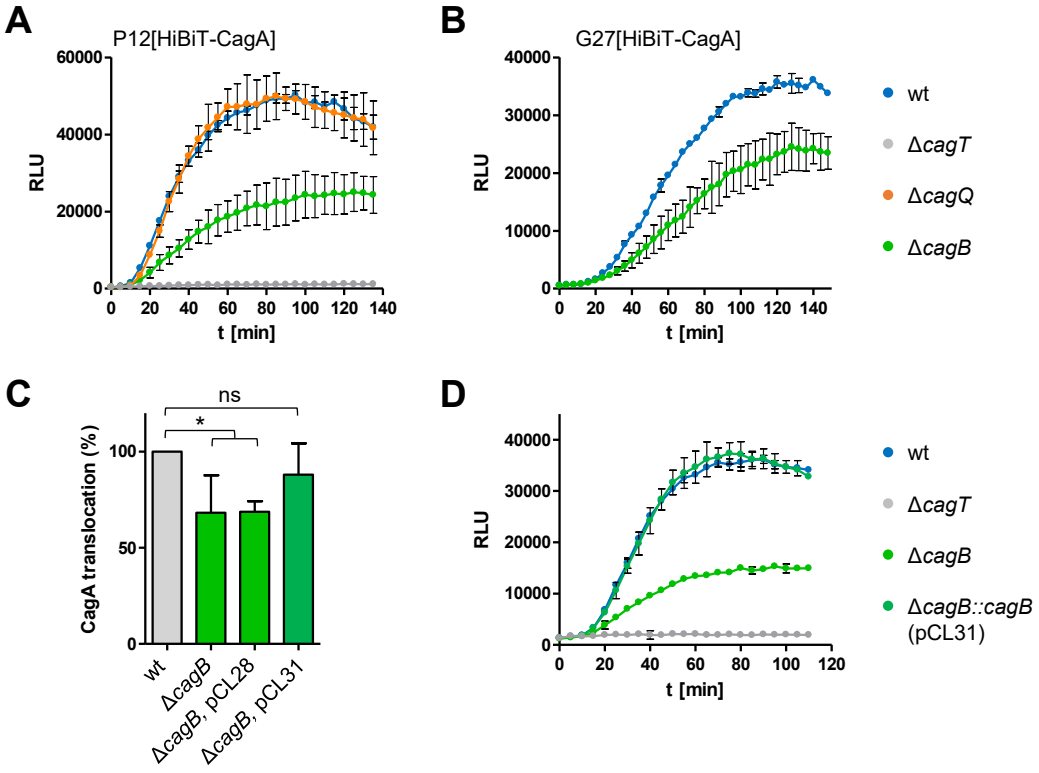

Figure 4.30 CagB has a moderate impact on CagA translocation. (A) AGS[LgBiT] cells were co-incubated with the respective mutants of P12[HiBiT-CagA], and HiBiT-CagA translocation was monitored in real time as described above. (B) Same experiment as in (A) performed with strain G27[HiBiT-CagA] and the corresponding Δ*cagB* mutant. (C/D) HiBiT-CagA translocation of the indicated strains (all P12) was measured using the live assay. To statistically analyze the results, the amount of translocated HiBiT-CagA was quantified as $\Delta RLU_{t=60\ min\ -\ t=0\ min}$ and normalized to P12[HiBiT-CagA] (= wt). Data shown are means and standard deviations of at least three independent experiments. (Statistics: One-Way ANOVA, Dunnett post test, *p<0.05)

Complementation of Δ*cagB* in the *recA* locus of *H. pylori* P12 under the control of the *cagA* promotor was not successful (Figure 4.30 C, pCL28). Since the TSS and the promotor region of *cagB* is not exactly known (see Figure 4.27), and a second, alternative start codon was suggested (Spohn *et al.,* 1997), in a second attempt, *cagB* and its corresponding upstream region (position 585151-585577 in P12), were reintroduced in the *recA* locus (pCL31), resulting in a complete recovery of HiBiT-CagA translocation (Figure 4.30 C, D).

To further characterize CagB, the subcellular localization of HiBiT-CagB was determined. Thus, bacteria were lysed via ultrasonication and subsequently, the insoluble membrane fraction was separated from the soluble components via ultracentrifugation. The amount of HiBiT-tagged target protein in the respective fractions was calculated as percentage of the total HiBiT-tagged protein amount in the lysed sample prior to ultracentrifugation (see 3.5.3). The major part of HiBiT-CagB was found in the insoluble fraction, indicating that the protein is membrane-bound (Figure 4.31 A). In contrast, HiBiT-tagged CtkA that was analyzed as control

for lysis and fractionation was as expected exclusively found in the soluble fraction. Thus, a contamination of the insoluble membrane fraction with intact bacteria and thus soluble proteins was excluded. CtkA (cell translocating kinase A, *jhp940*) is a serine/threonine-protein kinase and a putative effector protein of *H. pylori* J99. In a previous study, CtkA was shown to induce proinflammatory signaling in macrophages (Kim *et al.,* 2010). Since CtkA can be detected in the supernatant of *H. pylori in vitro*, it was assumed, that the kinase is a soluble protein (Tenguria *et al.,* 2014).

As a further quality control, aliquots of the two fractions and the lysate prior to ultracentrifugation were subjected to SDS-PAGE and subsequent Western blotting. As expected, the OMP HopQ was only detectable in the whole lysate and in the insoluble fraction (Figure 4.31 B).

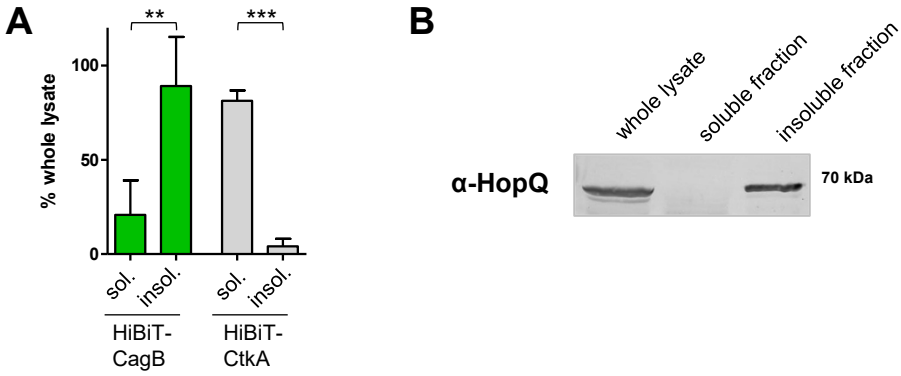

Figure 4.31 CagB is a membrane-bound protein. (Data generated and kindly provided by S. Niedermaier.) (A) Bacterial lysates were fractionated by ultracentrifugation and the amount of HiBiT-tagged proteins in the respective fractions was detected via the split-luciferase assay (sol. = soluble fraction, supernatant after ultracentrifugation, insol. = insoluble fraction, pellet after ultracentrifugation). In addition to HiBiT-CagB, the localization of HiBiT-CtkA was determined. While HiBiT-CagB was mainly found in the insoluble (membrane) fraction, HiBiT-CtkA was almost exclusively found in the soluble part. Data shown are means and standard deviations of five independent experiments. (Statistics: Student`s t-test **p<0.01, ***p<0.001). (B) To further prove a clear separation of the two fractions, an aliquot of each sample was tested for the localization of HopQ via Western blotting. Only samples, where HopQ was exclusively found in the initial lysate and the insoluble fraction were used for the statistics shown in A. A representative blot is shown.

In summary, using the HiBiT-LgBiT split-luciferase system, the existence of CagQ and CagB as proteins was shown. CagB was found to be membrane-bound and an up to 50 % reduction in CagA translocation was observed in a Δ*cagB* mutant strain. Further work has to be done to characterize the function of CagB more precisely.

4.3 Inhibitors of T4SS-dependent CagA translocation

The resistance rates of *H. pylori* towards the commonly used antibiotics are rapidly increasing worldwide (Savoldi *et al.,* 2018). Already in 2017, clarithromycin-resistant strains were listed on the priority list for research and development of novel antibiotics by the WHO. At the same time, the importance of species-specific targets and inhibitors that do not impair the commensal microbiota is gaining attention. Pathoblockers, *i.e.* inhibitors that only affect a virulence factor of the pathogen but not its viability, are in the focus of current research. Species specificity, minor side effects and reduced resistance development are the benefits of a virulence factor-targeting treatment. In case of *H. pylori*, T4SS-dependent translocation of the oncoprotein CagA is a promising target of a pathoblocker.

Recently, several compound libraries were screened for CagA translocation inhibition using the TEM-CagA reporter assay (Schindele, 2017). The most promising candidates were the anti-cancer drug cisplatin and small molecule inhibitors targeting the eukaryotic respiratory chain. In the present work, those compounds were further characterized.

4.3.1 Cisplatin: Inhibitor of type IV secretion and *H. pylori* growth

4.3.1.1 Identification of cisplatin as inhibitor of CagA translocation

The inhibitory potential of cisplatin on CagA translocation was analyzed using the TEM-CagA reporter assay. A strong, concentration-dependent inhibition was observed with a half-maximal inhibitory concentration (IC_{50}) of about 5 µM (Figure 4.32 A). On the same time, apparently no adverse effect on *H. pylori* growth was detected in a broth microdilution assay (Figure 4.32 B).

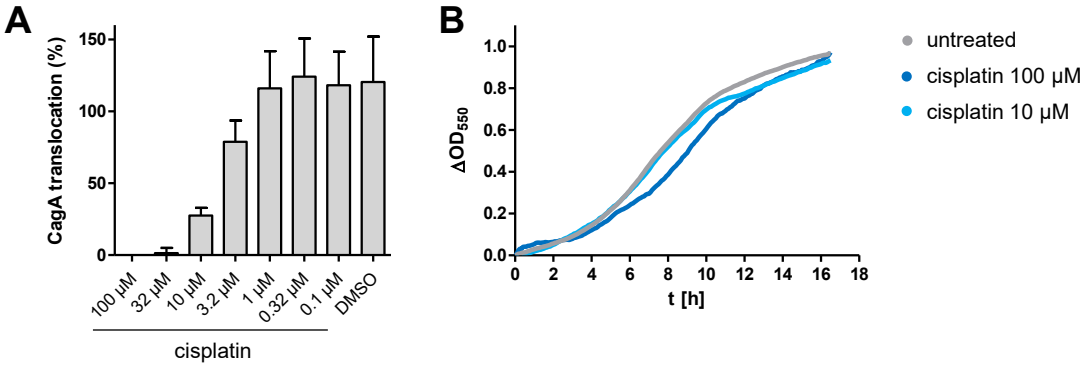

Figure 4.32 Cisplatin strongly inhibits CagA translocation, but apparently does not interfere with *H. pylori* growth. (A) To analyze the effect of cisplatin on T4SS activity, the TEM-CagA reporter strain was pre-incubated for 0.5 h with the indicated concentrations of cisplatin or DMSO in PBS/FCS. Cells were infected with the pre-treated bacteria in the presence of the compound and CagA translocation was measured. Data shown are means and standard deviations of five independent experiments. (B) *H. pylori* viability in the presence of cisplatin was assessed using broth microdilution assay. Growth curves were performed in BB/FCS. A representative experiment is shown.

Next, the impact on other infection-related processes was tested, namely bacterial adhesion, a prerequisite for CagA translocation, and IL-8 secretion by the host cells, that is known to be induced by *H. pylori*. Adhesion of a GFP-producing *H. pylori* strain to AGS cells was significantly reduced when bacteria were pre-treated for 0.5 h with cisplatin, but the impact on adherence was clearly less pronounced than on CagA translocation ($IC_{50} \approx 20$ µM, Figure 4.33 A). Furthermore, while the strong inhibitory effect on CagA translocation was even observed when bacteria were not pre-incubated with the compound, but cisplatin was added during an ongoing infection (*i.e.* 30 min after start of infection), the drug had no impact on already established adherence (Figure 4.33 B, C).

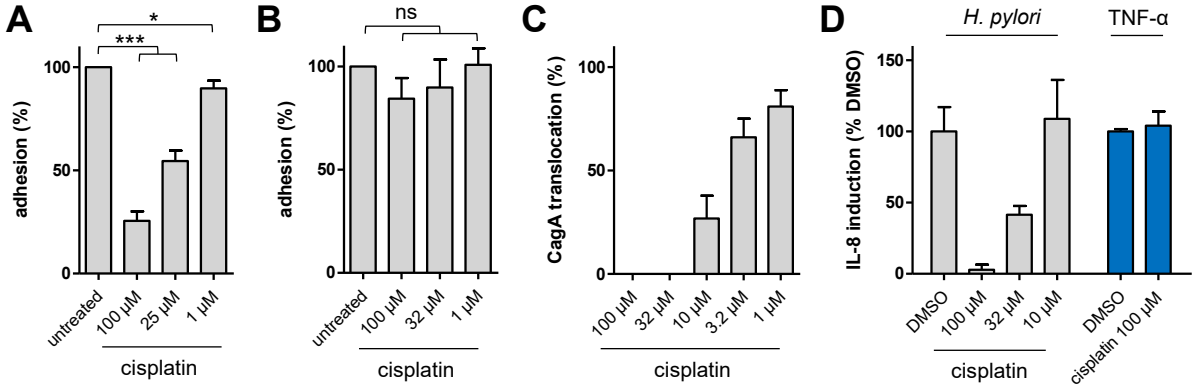

Figure 4.33 Effect of cisplatin on adherence and IL-8 secretion induction. (A) Adhesion of GFP-producing *H. pylori* P12 to AGS cells was analyzed by flow cytometry. Bacteria were pre-treated with the indicated concentrations of cisplatin 30 min prior to infection. (B) Same experiment as in (A) but cisplatin was added 30 min after the start of infection. (C) CagA translocation was determined as in Figure 4.32, but cisplatin was added 30 min after the start of infection. (D) AGS cells were either co-incubated with *H. pylori* P12 in the presence of the indicated concentrations of cisplatin or treated with 20 ng/ml TNF-α in the presence or absence of cisplatin. After 4 h, IL-8 secretion into the culture medium was measured by sandwich-ELISA. Concentrations were normalized to the DMSO-treated control. Shown are means and standard deviations of at least three independent experiments. Data in (B) and (C) were generated by F. Schindele. (Statistics: One-Way ANOVA, Dunnett post test, *p<0.05, ***p<0.001)

IL-8 secretion by gastric epithelial cells infected with *H. pylori* is induced by CagT4SS-dependent signaling. While a functional T4SS system is required, CagA itself only plays a minor role in IL-8 induction. Recently, ADP-heptose, a metabolite of LPS biosynthesis, was found to be an important effector in CagT4SS-dependent proinflammatory signaling (Gall *et al.,* 2017; Stein *et al.,* 2017; Zimmermann *et al.,* 2017; Pfannkuch *et al.,* 2019). AGS cells infected with bacteria pre-treated with cisplatin secreted considerably less IL-8 into the culture supernatant than the respective DMSO control (Figure 4.33 D). In contrast, the presence of cisplatin had no impact on IL-8 secretion induced by the proinflammatory cytokine TNF-α, indicating that the inhibitory effect of cisplatin on the IL-8 response was due to inhibition of the bacteria. Taken together, the data suggested that type IV secretion activity is highly sensitive to cisplatin treatment, while bacterial adhesion was only impaired to a minor degree.

4.3.1.2 Effect of other platinum complexes on CagA translocation and growth

The antimicrobial action of platin was first described in 1965 by Rosenberg *et al.* discovering that cell division of *E. coli* is impaired by electrolysis products from platin electrodes. Four years later, the same group published an anti-tumorigenic effect of cisplatin and other platinum complexes (Rosenberg *et al.,* 1969).

It was shown that the strong anti-tumor activity of this planar platin complex is due to the formation of intrastrand DNA adducts and cross-linking of purine bases, finally inducing apoptotic signaling (Fichtinger-Schepman *et al.,* 1985; Rocha *et al.,* 2018). Importantly, the antimicrobial and anti-cancer activity is restricted to platin complexes dissolved in aqueous solvents, since an efficient DNA cross-linking requires an exchange of at least one chloride ligand by a water molecule (= aquation) (Davies *et al.,* 2000). In contrast, cisplatin stocks dissolved in DMSO have almost no cytotoxic effect. The nucleophilic sulfur of DMSO coordinates with the central platinum ion and replaces the chloride ligand. Since DMSO is a poor leaving group, the newly formed complex is no longer able to interact with N-7 of the purine bases (Annibale *et al.,* 1983; Hall *et al.,* 2014).

The cisplatin stocks tested for T4SS inhibition in the present study were prepared in DMSO. Mass-spectrometry experiments confirmed the replacement of one chloride ligand by DMSO and a further exchange after diluting the DMSO stock in water, in the end resulting in a monoammine-monochloro-*bis*-DMSO complex (Lettl *et al.,* 2020, Figure 4.34). Thus, it is most likely that the CagA translocation inhibition is caused by a DMSO-containing complex, and this in turn means that the mode of action is most likely independent of DNA interactions.

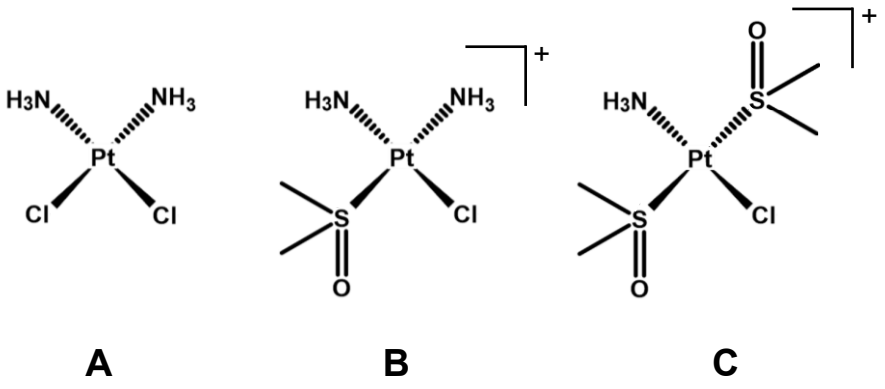

Figure 4.34 Cisplatin in DMSO-containing solutions is rather instable and ligand exchange reactions can be observed by mass-spectrometry. (A) *cis*-diamminedichloridoplatinum(II) (= cisplatin); (B/C) Upon solution of cisplatin in DMSO, sequential ligand exchange reactions occur, finally resulting in a monoammine-monochloro-*bis*-DMSO complex. Adapted from Lettl *et al.,* 2020.

To further evaluate if type IV secretion inhibition is connected to DNA interaction, several platin complexes with variable properties regarding cytotoxicity and DNA-binding were tested. Notably, all stocks were prepared in DMSO, but due to the steric shielding by the more complex

N-heterocyclic carbene (NHC) (benzimidazol-2-ylidene or imidazol-2-ylidene) ligands, no ligand exchange reactions are expected, rendering the complexes stable.

First, dichloridoplatinum(II) complexes with an NHC ligand and a DMSO ligand were analyzed regarding their T4SS inhibitory potential and their effect on *H. pylori* growth (Figure 4.35). The benzimidazol-2-ylidene- or imidazol-2-ylidene-containing compounds showed a concentration-dependent reduction in CagA translocation, while growth was not or only slightly influenced. No correlation with the size and lipophilicity of the NHC ligand was observed, but T4SS inhibition was in general weaker than in case of cisplatin.

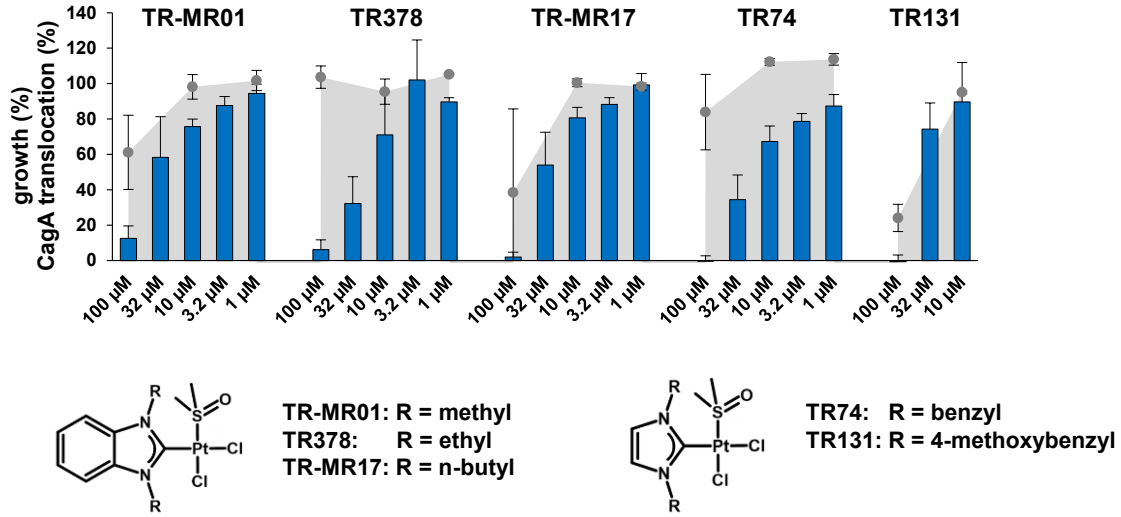

Figure 4.35 NHC- and DMSO-containing dichloridoplatinum(II) complexes. *H. pylori* was pre-treated with the different compounds at the indicated concentrations for 0.5 h in PBS/FCS and CagA translocation was measured using the TEM-CagA translocation assay (blue bars). In parallel, broth microdilution assays were performed to evaluate the impact on *H. pylori* growth (grey dots). Shown are means and standard deviations of at least two independent experiments with technical duplicates.

Next, complexes where the DMSO ligand was substituted by triphenylphosphane (PPh_3) were tested. Those compounds are in general slightly more cytotoxic and combine DNA coordination and to some extent DNA aggregation (Muenzner *et al.,* 2015; Rehm *et al.,* 2016; Rehm *et al.,* 2018).

Regarding the type IV secretion, those larger and more lipophilic complexes showed no specific inhibition: either no impact on CagA translocation was detected, or growth was affected to the same extent as T4SS activity (Figure 4.36). This indicates, that DMSO cannot functionally be substituted by PPh_3 in case of type IV secretion inhibition. Comparing the two benzimidazol-2-ylidene complexes, TR395 was slightly more toxic for *H. pylori* than TR-DW13. This is in accordance with the cytotoxic effect on cancer cell lines, which can be explained by a lower uptake rate due to the high lipophilicity of TR-DW13 (Rehm *et al.,* 2018).

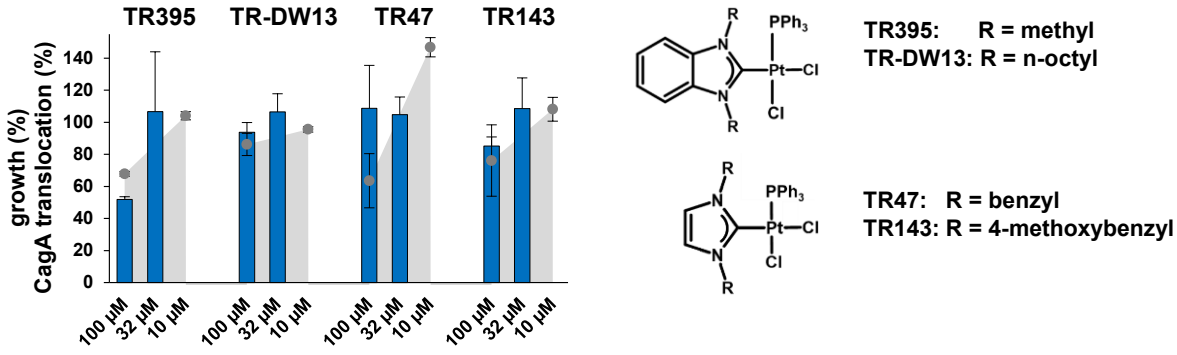

Figure 4.36 NHC- and PPh_3-containing dichloridoplatinum(II) complexes. CagA translocation and *H. pylori* growth were analyzed as described in Figure 4.35.

While cisplatin, dichlorido-NHC-Pt-DMSO and dichlorido-NHC-Pt-PPh_3 complexes coordinatively bind to DNA, cationic monochlorido-NHC-Pt-bis-PPh_3 complexes mainly interact with negatively charged DNA via noncovalent interactions exclusively inducing DNA aggregation (Muenzner *et al.,* 2015; Rehm *et al.,* 2016). Those compounds have IC_{50} values in the low micromolar or even nanomolar range and are active against tumor cell lines that already developed cisplatin resistance (Rehm *et al.,* 2018). Due to the high cytotoxicity of those compounds, CagA translocation to AGS cells was not measurable. The tested complexes had a strong antimicrobial effect on *H. pylori*, too (Figure 4.37).

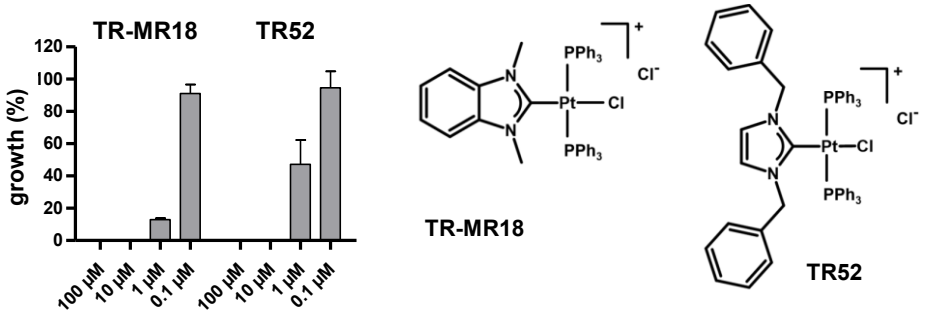

Figure 4.37 Bis-PPh_3-containing NHC-platinum(II) complexes. Compounds had a strong antimicrobial effect on *H. pylori* as observed by broth microdilution assay. Shown are means and standard deviations of at least two independent experiments in technical duplicates.

Next, three different groups of platinum(II) complexes were tested, containing two NHC ligands instead of DMSO: while compounds bearing two imidazol-2-ylidene substituents in *cis* were extremely cytotoxic and strongly inhibited *H. pylori* growth (Figure 4.38), those complexes with two benzimidazol-2-ylidene groups in *cis* had no effect on type IV secretion and viability (TR429/TR400) or affected growth and CagA translocation to the same extent (TR407) (Figure 4.39). This correlates well with the anti-tumorigenic activity: TR429 and TR400 are not cytotoxic, but the n-butyl substituted complex is (Rehm *et al.,* 2019).

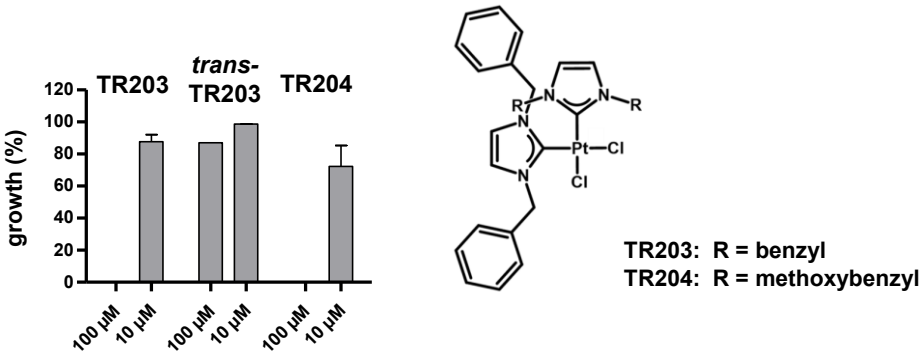

Figure 4.38 Platinum(II) complexes bearing two imidazol-2-ylidene substituents. *Cis*-NHC platinum compounds had a strong antimicrobial effect on *H. pylori* as tested by broth microdilution assay, while the *trans* complex was inactive. Shown are means and standard deviations of at least two independent experiments in technical duplicates.

The corresponding *trans*-NHC-Pt complexes of TR203 and TR407, that are both not able to bind to DNA (Muenzner *et al.,* 2015; Rehm *et al.,* 2019) had no impact on *H. pylori* growth (Figure 4.38, Figure 4.39).

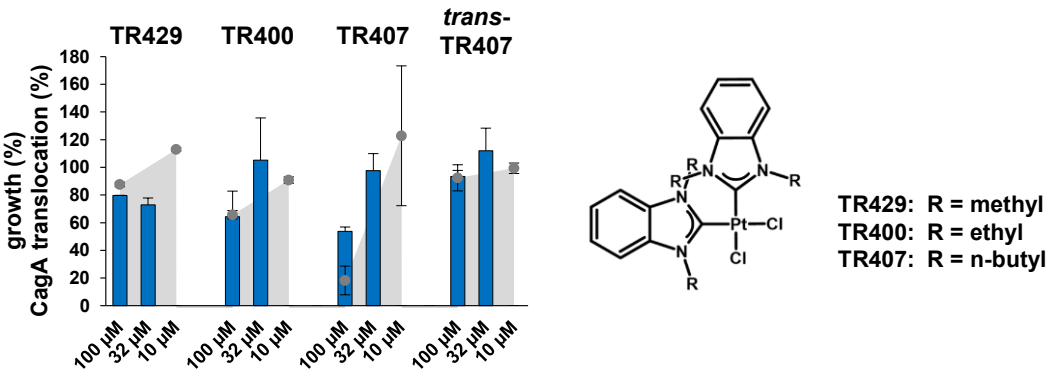

Figure 4.39 Platinum(II) complexes bearing two benzimidazol-2-ylidene substituents. CagA translocation and *H. pylori* growth were analyzed as described in Figure 4.35.

As third group, mixed *cis*-NHC complexes were analyzed, combining an imidazol-2-ylidene and a benzimidazol-2-ylidene ligand. Interestingly, those complexes were most similar to cisplatin, sharing a stronger inhibitory impact on CagA translocation than on bacterial growth (Figure 4.40).

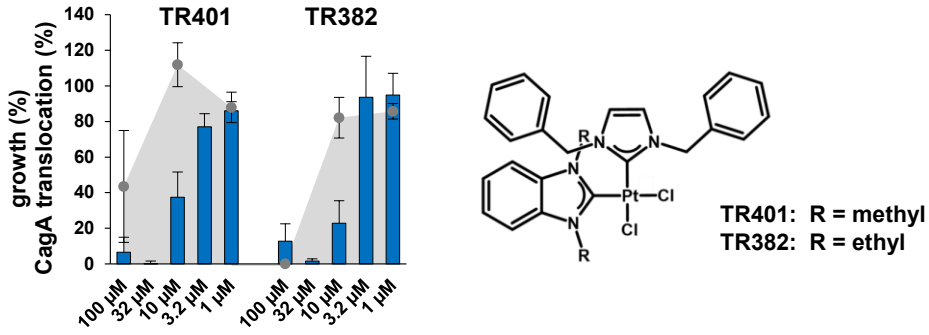

Figure 4.40 Platinum(II) complexes with mixed NHC ligands. CagA translocation and *H. pylori* growth were analyzed as described in Figure 4.35.

In addition, an octahedral tetrachloridoplatinum(IV) complex (TR425) was tested, which is known to have a slightly stronger anti-tumorigenic effect compared to its analogous platinum(II) complex TR400 (Rehm *et al.,* 2019). Platinum(IV) complexes in general are biologically more inert due to reduced DNA-binding properties and additional DNA metalation-independent modes of action are likely (Rehm *et al.,* 2019). As the analogous platinum(II) complex TR400, TR425 had no influence on *H. pylori* growth, but CagA translocation was strongly impaired (Figure 4.41).

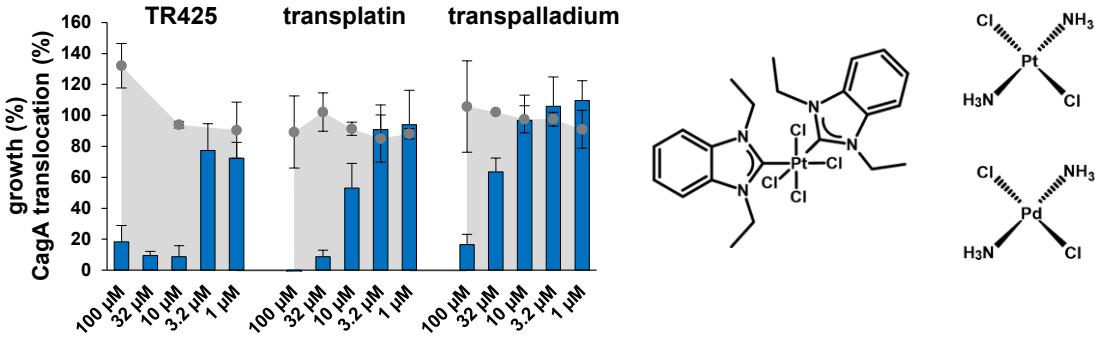

Figure 4.41 Inhibitory effects of an octahedral platinum(IV) complex, transplatin and transpalladium. All three compounds strongly reduced CagA translocation (blue bars) without affecting *H. pylori* growth (grey dots). Data were obtained as described in Figure 4.35.

Finally, transplatin (*trans*-dichloridodiammineplatinum(II)) and transpalladium were analyzed regarding T4SS and *H. pylori* growth inhibition. Both compounds only reduced CagA translocation, though they were less potent than cisplatin ($IC_{50,\ transplatin} \approx 10$ µM, $IC_{50,\ transpalladium} > 32$ µM, Figure 4.41).

Taken together, these data further underlined a DNA interaction-independent mode of T4SS interference, fitting well with the very fast inhibitory action described above.

4.3.1.3 Impact of complex media on the inhibitory potential of cisplatin

Recently, it was shown that the inhibitory effect of cisplatin on type IV secretion and *H. pylori* growth is strongly solvent-dependent: Cisplatin from stocks prepared in DMF, had three characteristics distinct from cisplatin dissolved in DMSO. (1) No ligand exchanges were observed for cisplatin in DMF. (2) Cisplatin in DMF had only minor impact on CagA translocation. And (3) cisplatin in DMF was highly toxic for *H. pylori*. (Lettl *et al.,* 2020)

Based on this, and since further ligand substitutions were observed when cisplatin dissolved in DMSO was further diluted in aqueous solutions (see Figure 4.34), it was hypothesized, that different culture media might additionally influence the activity of cisplatin. While CagA translocation via the TEM-CagA reporter assay is recorded in phosphate buffer based medium (PBS/FCS), growth of *H. pylori* can only be assessed in complex media (BB/FCS). Therefore, CagA translocation inhibition of bacteria treated with cisplatin in PBS/FCS and BB/FCS as well as in different mixtures of PBS/FCS with BB was compared. Interestingly, the inhibitory potential decreased with increasing amounts of BB resulting in almost complete abrogation of inhibition in pure BB/FCS (Figure 4.42 A). The same effect was observed for BB only and BHI, which is another complex growth medium. It was also detectable for a platinum complex without DMSO ligand as well as for the platinum(IV) complex (Figure 4.42 B). Interestingly, when bacterial viability was checked after 2 h incubation with 100 µM cisplatin in PBS/FCS or in BB/FCS in the presence of AGS cells, only *H. pylori* treated in the complex medium were able to grow, clearly indicating a toxic effect of cisplatin in PBS/FCS (Figure 4.42 C).

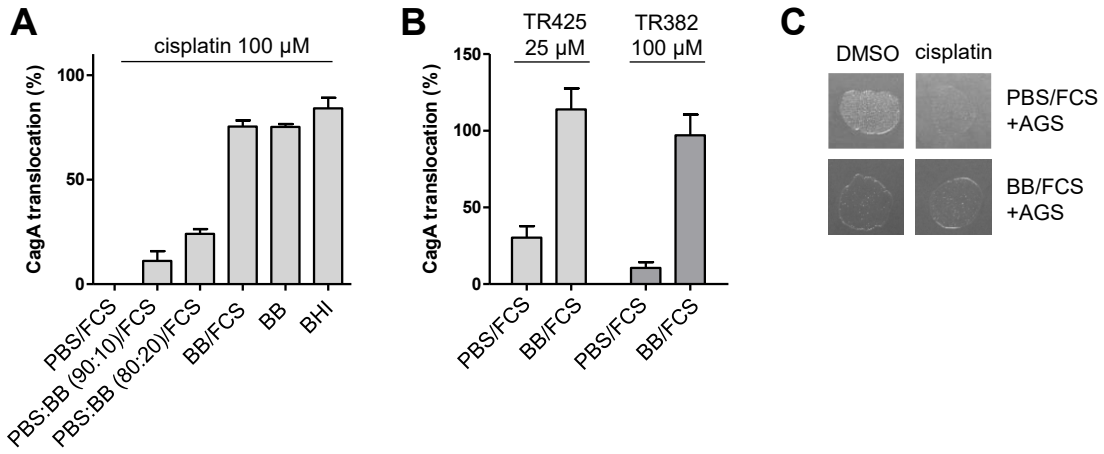

Figure 4.42 The inhibitory potential of cisplatin is reduced in complex media. (A) The TEM-CagA reporter strain was pre-incubated with 100 µM cisplatin in PBS/FCS, BB/FCS or mixtures of both media as well as in BB or in BHI and subsequently, CagA translocation was analyzed. (B) Not only cisplatin but also other platinum(II) and platinum(IV) complexes showed reduced CagA translocation inhibition in BB/FCS compared to PBS/FCS at the indicated concentrations as observed by the TEM-CagA reporter assay. (C) *H. pylori* P12 was treated with either 100 µM cisplatin or DMSO in PBS/FCS or BB/FCS in the presence of AGS cells and aliquots were spotted on serum plates to assess bacterial viability. Quantitative data show means and standard deviations from at least three independent experiments.

For many years, it has been known, that besides its interaction with nucleic acids, cisplatin can bind to sulfur-containing amino acids, too. In fact, this interaction is independent of an aquation of the drug, since the high reactivity of the sulfur-containing nucleophiles enables a direct replacement of the chloride ligand forming stable platinum-sulfur complexes (Mezencev, 2015).

To analyze whether the inhibitory effect of cisplatin on *H. pylori* T4SS activity is altered in the presence of thiol-containing reagents, the drug was mixed with different concentrations of cysteine, methionine, or alanine. Indeed, a dose-dependent reduction of the inhibitory potential was observed in case of cysteine and less pronounced also in case of methionine but not with alanine (Figure 4.43). Hence, those data strongly suggest an inactivation of cisplatin in complex media that is probably based on thiol-containing ingredients and hint further towards a DNA coordination independent but protein interaction-based mode of T4SS inhibition by cisplatin.

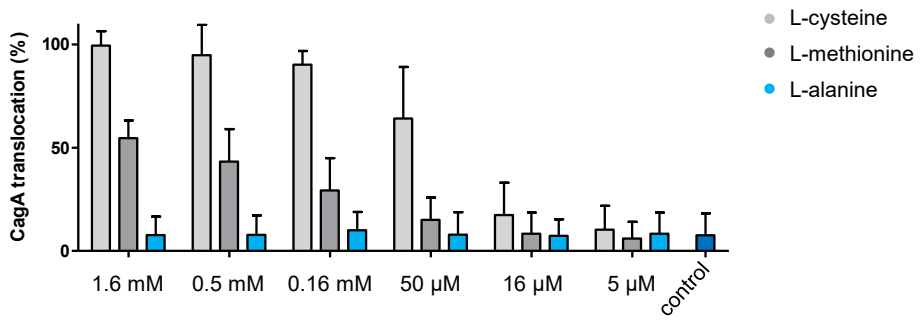

Figure 4.43 The addition of thiol-containing amino acids inactivates the inhibitory potential of cisplatin. The TEM-CagA reporter strain was incubated with mixtures of 32 µM cisplatin and the indicated amino acids at the respective concentrations, and CagA translocation was measured. Data show means and standard deviations of five independent experiments.

4.3.2 Respiratory chain inhibitors: New anti-*H. pylori* compounds with strong impact on CagA translocation

In the previous study mentioned above (Schindele, 2017) several respiratory chain inhibitors from various sources were identified to interfere with the T4SS activity. Follow-up studies could further show a strong inhibitory effect on *H. pylori* growth. Notably, this inhibition was highly species-specific: even at very high concentrations the growth of other tested bacteria was not affected.

4.3.2.1 Eukaryotic complex I inhibitors: Highly potent and species-specific anti-*H. pylori* compounds

To get further insights into the mode of action, the effects of four reference inhibitors, known to interfere with different targets of the eukaryotic cellular respiration, were evaluated (Table 4.2, Schindele, 2017). Only the complex I inhibitor rotenone and the complex III inhibitor

antimycin A selectively affected the growth of *H. pylori* but not of the other tested bacteria. Cruentaren A that targets the F_0F_1-ATPase was highly potent regarding T4SS and growth inhibition, but the effect on growth was not species-specific. This was also the case for CCCP, an ionophore.

In parallel, it was shown, that the inhibitory effect of the four reference compounds on type IV secretion activity was due to interference with a bacterial target and not due to an inhibition of processes in the eukaryotic host cells (Schindele, 2017).

Based on these data, it was hypothesized, that eukaryotic respiratory chain complex I and III inhibitors are highly potent and specific inhibitors of *H. pylori* growth with a strong impact on T4SS-dependent CagA translocation.

Table 4.2 Reference inhibitors of the eukaryotic respiratory chain (data taken from Schindele, 2017)

	Target	**CagA translocation***	***H. pylori* growth**		**Effects on growth****		
		IC_{50} [µM]	**MIC [µM]**	**IC_{50} [µM]**	***E. coli***	***S. aureus***	***C. jejuni***
Rotenone	complex I	0.45	0.50	0.08	no	no	no
Antimycin A	complex III	6.10	8.00	2.90	no	no	no
Cruentaren A	F_0F_1-ATPase	0.14	0.03	0.01	no	weak	yes
CCCP	protonophore	3.80	2.00	0.67	yes	yes	yes

* CagA translocation was determined using the TEM-CagA reporter assay. Bacteria were pre-treated with the respective compounds in PBS/FCS for 30 min and subsequently co-incubated with AGS cells in the presence of the compounds for 2.5 h. ** 50 µM rotenone/antimycin A; 4 µM cruentaren A; 10 µM CCCP

To assess this hypothesis, a set of commercially available respiratory chain inhibitors that are commonly used as fungicides, insecticides or acaricides was tested for *H. pylori* growth inhibition (Table 4.3). Except in case of pyridaben, all compounds targeting the eukaryotic complex I were highly active against *H. pylori* with MIC and IC_{50} values mostly in the low nanomolar range and without effects on other bacteria tested. In contrast, complex III inhibitors were less potent, as already observed for antimycin A, and less species-specific.

Table 4.3 Set of respiratory chain complex I and III inhibitors (MIC and IC_{50} values were determined by broth microdilution assay. Data show means of at least three independent experiments.)
(classification based on FRAC Code List 2021; IRAC MoA Classification; Degli Esposti, 1998)

	***H. pylori* growth**		**Effects on growth (100 µM)**		
	MIC [µM]	**IC_{50} [µM]**	***E. coli***	***S. aureus***	***C. jejuni***
Complex I inhibitors					
Pyridaben	>10	5.73	no	no	no
Tolfenpyrad	1.2	0.554	no	no	no
Diflumetorim (**#14**)	0.15	0.018	no	no	no
Tebufenpyrad	0.6	0.122	no	no	no
Fenpyroximate (**#16**)	0.075	0.013	no	no	no
Fenazaquin (**#17**)	0.15	0.022	no	no	no
Piericidin A	0.25	0.039	no	no	no data
Complex III inhibitors (Data generated by F. Schindele)					
Trifloxystrobin	37.5	6.57	no	no	weak
Dimoxystrobin	75	14.92	no	no	weak
Fluacrypyrim	75	13.90	no	no	no
Picoxystrobin	37.5	10.33	no	no	weak
Kresoxim-methyl	75	13.27	no	no	no
Cyazofamid	75	16.92	weak	yes	yes
Azoxystrobin	37.5	9.74	no	no	weak

4.3.2.2 Target identification

To get first insights into the mode of action of *H. pylori* growth inhibition, several experiments were performed monitoring the impact of the compounds on the bacterial energy metabolism. Therefore, *H. pylori* was treated with the three most potent complex I inhibitors, namely diflumetorim (#14), fenpyroximate (#16) and fenazaquin (#17) (Figure 4.44), and the impact on bacterial membrane potential, O_2 consumption and ATP content was evaluated.

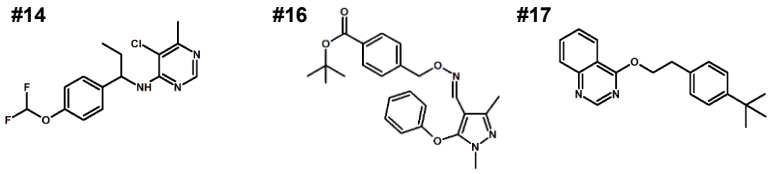

Figure 4.44 Chemical structures of the three most potent novel anti-*H. pylori* compounds. The eukaryotic complex I inhibitors diflumetorim (#14, left), fenpyroximate (#16, middle) and fenazaquin (#17, right) are highly potent and specific inhibitors of *H. pylori* growth.

For all three compounds a destruction of the membrane potential was observed by staining the treated bacteria with a membrane potential-sensitive dye ($DiOC_2(3)$) and subsequent flow cytometry (Figure 4.45 A). Furthermore, the O_2 consumption was blocked in bacteria pre-treated for 10 min with the respective compounds (Figure 4.45 B) and the ATP content was drastically reduced in a concentration-dependent manner in *H. pylori* incubated for 5 min with the inhibitors (Figure 4.45 C).

Taken together, these data strongly suggest, that the compounds, that are known to target the eukaryotic respiratory chain complex I, inhibit *H. pylori* respiration, too.

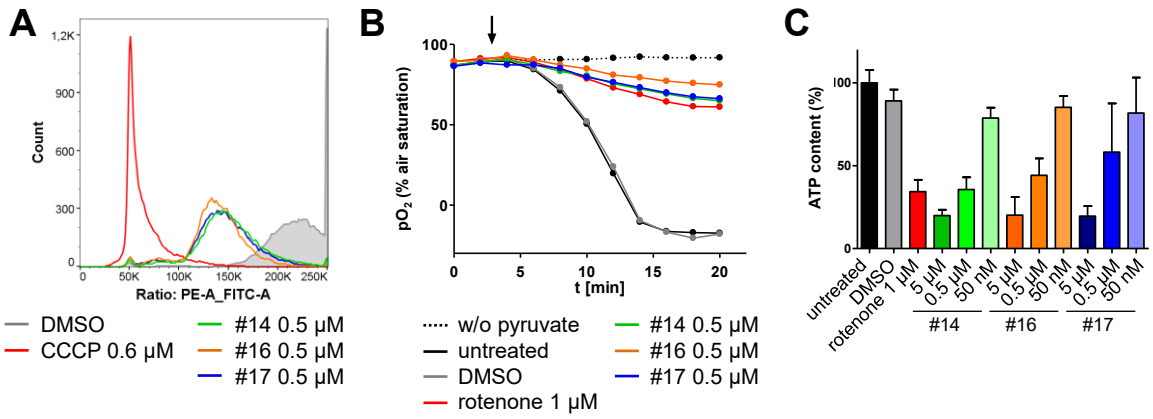

Figure 4.45 Effects on membrane potential, O_2 consumption and ATP content hint towards respiratory chain inhibition. (A) *H. pylori* was incubated for 3 h with the respective compounds at the indicated concentrations and membrane potential was determined using $DiOC_2(3)$. The unspecific H^+ ionophore CCCP was taken as control. (B) O_2 consumption was measured using OxoPlates. Bacteria were pre-incubated in nutrient-free buffer with the compounds of interest or rotenone for 10 min. Measurement was started, 7 mM of pyruvate was injected (arrow), and O_2 consumption was monitored over time. (C) *H. pylori* was treated for 5 min with the small molecule inhibitors and ATP contents were determined using the ATP Bioluminescence Assay Kit CLS II. As in (B) the complex I inhibitor rotenone was taken as a control. (A/B) A representative experiment is shown. (C) Data shown are means and standard deviations of five independent experiments.

To obtain further evidence for the exact target within the bacterial respiratory chain, isotopologue profiling was performed. This method enables the analysis of metabolic pathways in living organisms. Due to its high sensitivity, isotopologue profiling can be used to monitor and compare the impact of inhibitors and antibiotics on the bacterial metabolism. Briefly, bacteria cultivated overnight in BB/FCS supplemented with [U-$^{13}C_6$]D-glucose, were treated for

5 min with the novel anti-*H. pylori* compounds or different reference inhibitors. Pellets were harvested and inactivated and ^{13}C enrichment and isotopologue distribution in key metabolites were detected by GC/MS.

In general, significant levels of ^{13}C incorporation (*i.e.* >1 %) were detected in lactate and glycerol as well as in the tricarboxylic acid (TCA) cycle intermediates succinate and fumarate. Amongst the proteinogenic amino acids, tyrosine, aspartate, and glutamate showed a high labeling. In terms of their ^{13}C-excess and isotopologue composition, the latter ones can be used as approximations for oxaloacetate and α-ketoglutarate, respectively (Eisenreich *et al.,* 2006). Finally, a strong labeling was observed in all tested fatty acids. (Figure 4.46 A)

When the bacteria were treated with the reference inhibitors rotenone, antimycin A or CCCP, alterations in the ^{13}C-excess were observed for the TCA cycle-related metabolites lactate and tyrosine. The three compounds showed distinct patterns allowing the discrimination between complex I and complex III inhibition as well as the unspecific disruption of the H^+ gradient by the ionophore CCCP (Figure 4.46 B). While rotenone and antimycin A caused a strong decrease in tyrosine ^{13}C-excess and an increase in lactate ^{13}C-surplus, the ionophore CCCP had no impact on tyrosine ^{13}C-levels and was the only inhibitor decreasing ^{13}C-excess of lactate. Furthermore, the effect of the complex III inhibitor antimycin A on the TCA intermediates aspartate, succinate and glutamate differed from the pattern of the complex I-targeting compound rotenone allowing for a clear discrimination.

As indicated in Figure 4.46 C, an interference with the activity of complex I by rotenone or complex III by antimycin A is directly linked to the operability of the TCA cycle: Inhibition of the Nuo complex impeded the oxidation of the reducing equivalent NADPH, hence interfering with multiple steps of the TCA cycle, and enforcing an increased lactate production. Similarly, antimycin A that was previously shown to interfere with the succinate-cytochrome *c* reductase of *H. pylori* (Chen *et al.,* 1999), *i.e*. the interplay between complex II and III, caused decreased TCA cycle activity and increased lactate generation. In addition, antimycin A treatment resulted in an accumulation of succinate and aspartate, probably due to the dependency of the reversibly acting quinol:fumarate reductase (complex II, enzyme (5)) and the unidirectional malate:quinone oxidoreductase (enzyme (6)) on the supply of quinone provided by the complex III. Finally, the synthesis of tyrosine via the shikimate pathway is dependent on ATP, whose levels were drastically reduced upon treatment with the three inhibitors (Figure 4.45 C).

Next, the isotopologue profiling fingerprints of the reference inhibitors were compared with those of #14, #16 and #17. The ^{13}C-excess patterns were comparable with the metabolic signature of rotenone but showed clear differences to the antimycin A- or CCCP-treated samples, further indicating that the compounds act on the complex I of the respiratory chain of *H. pylori* (Figure 4.46 B).

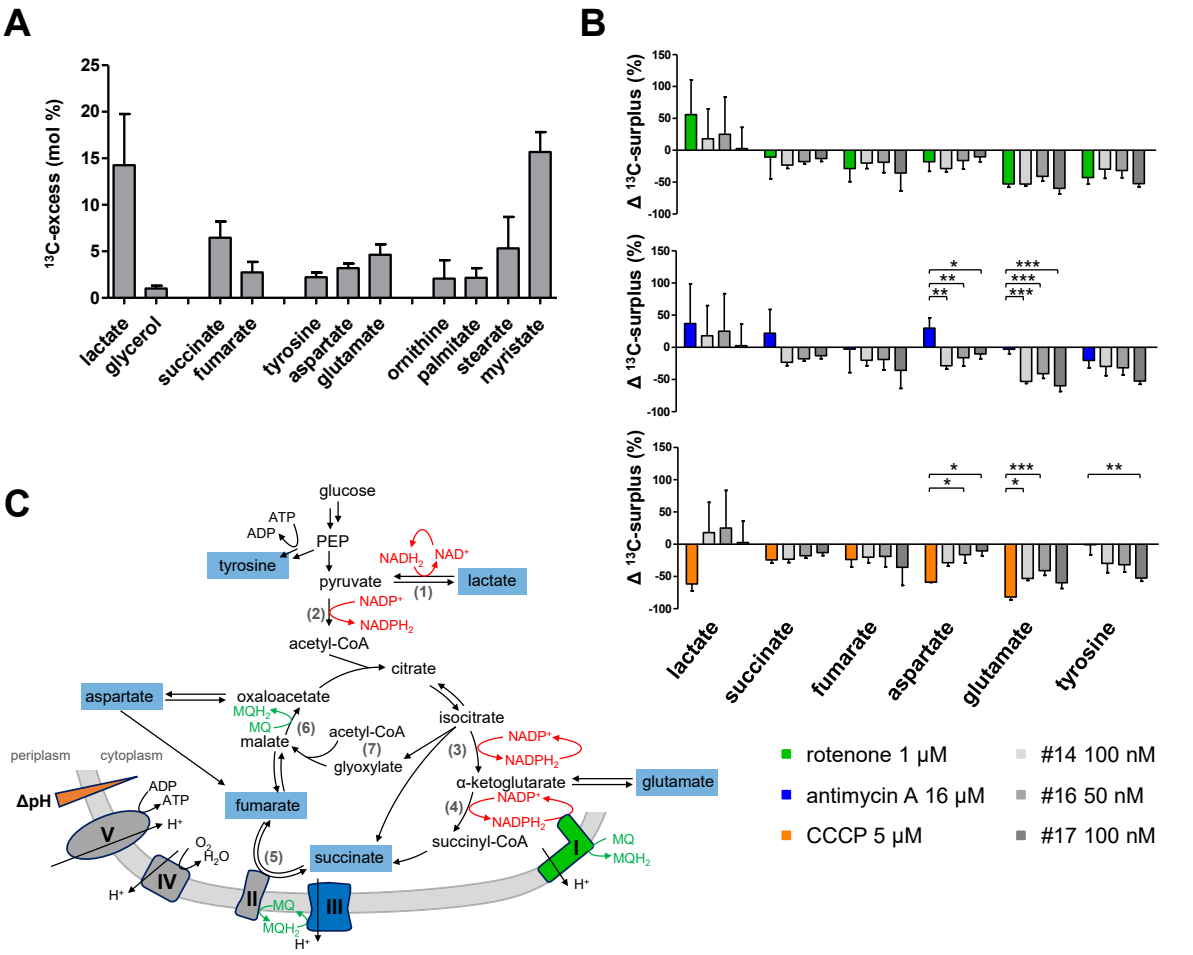

Figure 4.46 Isotopologue profiling of hit molecules reveals a similar metabolic signature as a complex I inhibitor. (A) Characteristic metabolic signature of *H. pylori* labeled overnight with [U-$^{13}C_6$]D-glucose. Depicted are only metabolites with ^{13}C-excess values higher than 1 %. Shown are means and standard deviations of at least five independent experiments. (B) Comparison of the metabolic signature of the reference inhibitors and the new respiratory chain inhibitors that are most likely to act as complex I inhibitors like rotenone. Data shown are means and standard deviations of at least two independent experiments. (Statistics: One-Way ANOVA, Bonferroni post test, *p<0.05, **p<0.01, ***p<0.001, only significant differences are indicated) (C) Simplified scheme of the TCA cycle of *H. pylori* and the link to the respiratory chain (complexes I-V). Key metabolites analyzed by isotopologue profiling are highlighted in blue boxes. Complex I (green) is the target of rotenone, complex III (blue) is inhibited by antimycin A, the ionophore CCCP disrupts the proton gradient (ΔpH, orange) and thus collapses the proton motive force (PMF). While the lactate dehydrogenase (enzyme 1) of *H. pylori* was shown to transfer electrons to NAD$^+$ (Iwatani *et al.,* 2014), other enzymes involved in the TCA cycle use NADP$^+$ as major electron acceptor: (2) pyruvate:flavodoxin oxidoreductase (Hughes *et al.,* 1998), (3) isocitrate dehydrogenase (Huang *et al.,* 2009), (4) α-ketoglutarate:ferredoxin oxidoreductase (Hughes *et al.,* 1998). Furthermore, the complex I of *H. pylori* most likely relies on $NADPH_2$ as electron donor (Finel, 1998; Chen *et al.,* 1999). A classical complex II, *i.e.* a succinate dehydrogenase is absent in *H. pylori*, instead a reversibly acting quinol:fumarate reductase complex might be active (enzyme 5, Lancaster and Simon, 2002). Additionally, *H. pylori* was shown to possess a unidirectional malate:quinone oxidoreductase (enzyme 6), rather than an NAD-dependent, reversible malate dehydrogenase (Kather *et al.,* 2000). Finally, we provided evidence for an active glyoxylate bypass (7) in *H. pylori* P12 (Steiner *et al.,* 2021). (PEP: phosphoenolpyruvate, MQ: menaquinone, MQH_2: menaquinol)

A commonly used tool to identify the target of antibiotic compounds is the characterization of resistant mutants or mutants with reduced sensitivity. To prove the interference with the complex I of *H. pylori* and further narrow down the target to the protein level, bacteria with reduced sensitivity were selected. Thus, *H. pylori* P12 was grown on serum plates containing sublethal concentrations of #14, #16 or #17. After several selection rounds, mutants with reduced sensitivity were obtained (for MIC values see Table 4.4). Transformation of wt *H. pylori* P12 with genomic DNA isolated from the mutant strains resulted in the same phenotype, suggesting that a mutation of the target rather than an upregulation of efflux pumps was causative for resistance. Next, the bacterial complex I-encoding *nuo* operon was amplified in 1.5 kb fragments by PCR using ten primer sets covering the complete operon (CL3-CL22). Interestingly, transformation of a wt *H. pylori* P12 with the *nuoD*-spanning PCR product from the variant with reduced sensitivity was sufficient to confer resistance towards #16. Sequencing of the *nuoD* gene revealed a single, causative point mutation: $V133M^{NuoD}$. In the same way, two mutants in the *nuoB* gene (T27N and T27A) were found to be less sensitive to #14 and #17. Subsequent sequencing of the spontaneous mutant resistant to #16 revealed that the strain acquired two mutations, the causative mutation $V133M^{NuoD}$ and in addition $T27A^{NuoB}$. Interestingly, the point mutation in $T27A^{NuoB}$ has already been described to conduct resistance of *H. pylori* to benzimidazole derivatives (Mills *et al.,* 2004). In the same study, NuoD and NuoB were shown to be essential proteins in *H. pylori*.

Notably, all variants were only obtained after numerous selection rounds, hinting towards an increased selection pressure due to high fitness costs. Indeed, severe growth defects were observed for the $T27N^{NuoB}$ and $V133M^{NuoD}$ mutants but not for the $T27A^{NuoB}$ strain. Growth was most strongly affected in case of $T27N^{NuoB}$ (Figure 4.47 A).

All mutant strains were tested for cross-resistance to #16 and #14 or #17, respectively (Figure 4.47 B). While the $T27N^{NuoB}$ and $T27A^{NuoB}$ variants were less sensitive to #16, too, the $V133M^{NuoD}$ mutation was specific for #16 resistance, indicating different binding modes to complex I. Furthermore, a reduced sensitivity of the $T27N^{NuoB}$ and $V133M^{NuoD}$/$T27A^{NuoB}$ strains was observed for the complex I inhibitor rotenone, while no mutant was resistant to the complex III inhibitor antimycin A.

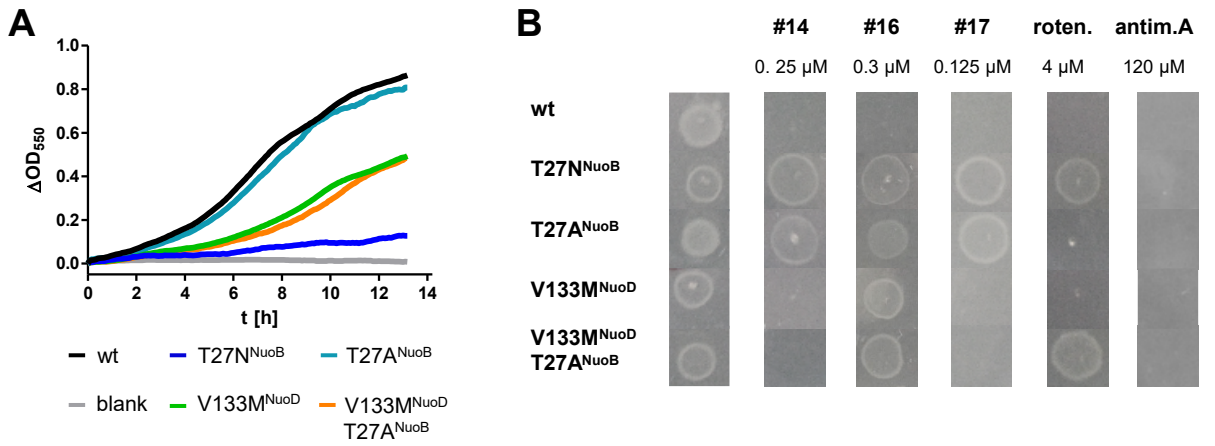

Figure 4.47 A single amino acid exchange in NuoB or NuoD is sufficient for reduced sensitivity, but is associated with severe growth defects. (A) T27N^{NuoB} and V133M^{NuoD} variants show only strongly reduced growth compared to wt *H. pylori* P12 and the T27A^{NuoB} mutant. A representative experiment is shown. (B) T27N^{NuoB}, T27A^{NuoB} and V133M^{NuoD} mutants show distinct cross-resistance to the different substances and rotenone (roten.) but not to the complex III inhibitor antimycin A (antim.A). All compounds were tested at MIC$_{wt}$, notably, these might differ from values determined by the broth microdilution assay probably due to lower local concentration. Shown are representative results of at least three independent experiments.

To further characterize this resistance pattern, the MIC values of the respective mutants for the different compounds were determined (Table 4.4): While the T27A^{NuoB} mutant strain was only marginally less sensitive to #14, #16 and #17, the MIC values of the T27N^{NuoB} mutant for #14 and# 17 were 16 times higher than for P12 wt. V133M^{NuoD} and V133M^{NuoD}/T27A^{NuoB} strains tolerated even more than 32 times higher concentrations of #16 than the wt, but at the same time both strains were more susceptible to #14 and #17.

Table 4.4 MIC values of *H. pylori* P12 wt and the different Nuo mutants. Data were obtained by spotting the respective strains on serum plates supplemented with the indicated compounds (see Figure 4.47 B). All inhibitors were tested in two-fold dilutions starting at 0.5xMIC$_{wt}$. MIC values were determined from at least three independent experiments.

	#14	**#16**	**#17**	**rotenone**
wt	0.25 µM	0.3 µM	0.125 µM	4 µM
T27N^{NuoB}	16xMIC$_{wt}$	4xMIC$_{wt}$	16xMIC$_{wt}$	2xMIC$_{wt}$
T27A^{NuoB}	2xMIC$_{wt}$	4xMIC$_{wt}$	2xMIC$_{wt}$	1xMIC$_{wt}$
V133M^{NuoD}	<MIC$_{wt}$	>32xMIC$_{wt}$	<MIC$_{wt}$	1xMIC$_{wt}$
V133M^{NuoD}/T27A^{NuoB}	<MIC$_{wt}$	>32xMIC$_{wt}$	<MIC$_{wt}$	2xMIC$_{wt}$

The V133M^{NuoD} mutant strain was chosen to further characterize the reduced sensitivity to #16 in additional experimental setups. First, the O_2 consumption of #16-treated wt and mutant strains was analyzed. While the V133M^{NuoD} variant in general showed a decreased respiration

compared to wt P12, #16 treatment could not further reduce O_2 consumption in the mutant: in both cases, O_2 consumption was reduced to about 30 % of the untreated wt. In contrast, respiration was completely blocked in the #16-treated wt bacteria (ca. 8 % O_2 consumption). (Figure 4.48 A).

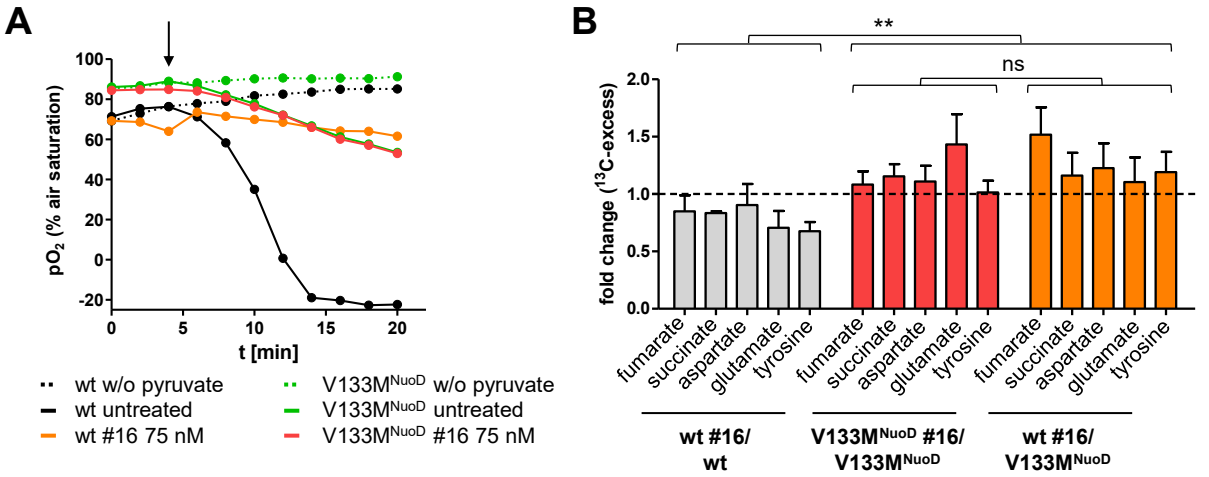

Figure 4.48 The acitvity of the respiratory chain complex I of the V133M^{NuoD} mutant strain is not affected by #16. (A) O_2 consumption was reduced in *H. pylori* wt treated with 75 nM #16 but not in the V133M^{NuoD} mutant. A lower overall metabolic activity of the V133M^{NuoD} mutant was observed. The arrow indicates the injection of 7 mM pyruvate. A representative experiment is shown. (B) *H. pylori* wt or V133M^{NuoD} mutant were treated with 50 nM #16 for 5 min and key metabolites were analysed by isotopologue profiling. ^{13}C-excess values were compared by calculating the fold change between the respective #16 treated samples and the indicated untreated control. Data shown are means and standard errors of the means of at least three independent experiments. (Statistics: One-Way ANOVA, Bonferroni post test, **p<0.01)

Furthermore, in isotopologue profiling experiments, the ^{13}C incorporation signature of the V133M^{NuoD} mutant strain was not changed when incubated with the complex I inhibitor, as indicated by a fold change of 1.0 of the analyzed metabolites (V133M^{NuoD} #16/V133M^{NuoD}, Figure 4.48 B).

Indeed, the overall ^{13}C-excess in TCA intermediates and tyrosine of the mutant strain was highly similar to the one of the #16-treated wt strain, hinting towards a shift in the metabolism caused by lower overall respiratory activity.

The *nuo* operon is highly conserved amongst bacteria encoding in general the 13-14 subunits of the NADH:ubiquinone oxidoreductase (EC. 1.6.5.3, Figure 4.49 A, B). In eukaryotes, the ubiquitous multiprotein complex is formed by over 40 subunits and encoded by the mitochondrial DNA. (Degli Esposti, 2015)

Orthologs of the *H. pylori* NuoB and NuoD can for example be found in *E. coli* (NuoB, NuoCD), *Thermus thermophilus* (Nqo6, Nqo4) or *Yarrowia lipolytica* (NUKM, NUCM). For those organisms, both proteins are known to be involved in quinone binding (Table 4.5) and partially, structures are available. In marked contrast to other prokaryotic species or eukaryotes, *H. pylori* most likely utilizes exclusively menaquinone-6 and not ubiquinone as initial electron acceptor (Marcelli *et al.,* 1996). In the following, the term “quinone” is used to cover both.

Table 4.5 Core subunits of the NADH:quinone oxidoreductase in different species (* Degli Esposti, 2015)

H. pylori	***E. coli***	***T. thermophilus***	***H. sapiens***	**SwissProt code**	**Function (*)**
nuoA	*nuoA*	*nqo7*	*nd3*	NU3M	proton pumping
nuoB	***nuoB***	***nqo6***	***ndufs7***	**NUKM**	**quinone binding**
nuoC	***nuoCD*** (fused)	*nqo5*	*ndufs3*	NUGM	quinone binding
nuoD		***nqo4***	***ndufs2***	**NUCM**	**quinone binding**
(*)	*nuoE*	*nqo2*	*ndufv2*	NUHM	NADH binding
(*)	*nuoF*	*nqo1*	*ndufv2*	NUBM	NADH binding
nuoG	*nuoG*	*nqo3*	*ndufs1*	NUAM	NADH binding
nuoH	*nuoH*	*nqo8*	*nd1*	NU1M	quinone binding
nuoI	*nuoI*	*nqo9*	*ndufs8*	NUIM	quinone binding
nuoJ	*nuoJ*	*nqo10*	*nd6*	NU6M	proton pumping
nuoK	*nuoK*	*nqo11*	*nd4l*	NU4LM	proton pumping
nuoL	*nuoL*	*nqo12*	*nd5*	NU5M	proton pumping
nuoM	*nuoM*	*nqo13*	*nd4*	NU4M	proton pumping
nuoN	*nuoN*	*nqo14*	*nd2*	NU2M	proton pumping

(*) *NuoE* and *nuoF* are not encoded in the genome of *H. pylori* (Finel, 1998). The respective annotations corresponding to HPP12_1230 and HPP12_1231 in the P12 genome, respectively, show no sequence similarity to the proteins of other species.

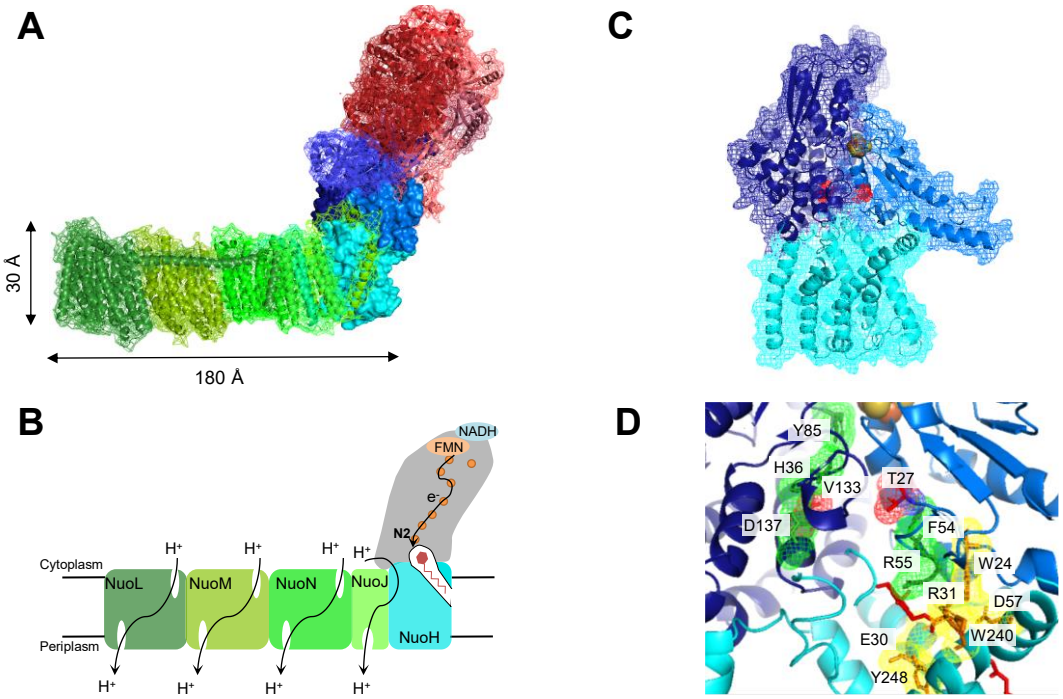

Figure 4.49 The prokaryotic complex I. (A) Crystal structure of the complex I from *T. thermophilus* (PDB 4HEA (Baradaran *et al.,* 2013)). Subunits are colored according to their function (red: NADH binding, blue: quinone binding, green: proton pumping). Nqo4/6/8, the orthologs of NuoB/D/H, are shown as surface. (B) Illustration of the electron transfer and proton pumping. Two electrons are transferred from NADH to flavin mononucleotide (FMN) and subsequently the electrons are passed one by one to a chain of seven iron-sulfur clusters (orange circles) finally passing from cluster N2 to quinone (Baradaran *et al.,* 2013). The negatively charged quinone then induces conformational changes in the transmembrane subunits resulting in the translocation of protons into the periplasm. Per two electrons four protons are pumped. Quinone (red) enters its binding cavity via NuoH (Adapted from Berrisford *et al.,* 2016). (C) Model of the NuoB (marine, B6JNA1), NuoD (dark blue, B6JNA3) and NuoH (cyan, B6JNA7) subcomplex of *H. pylori* (template: PDB 6RFR (Parey *et al.,* 2019)). $T27^{NuoB}$ and $V133^{NuoD}$ are shown in red, the iron-sulfur cluster N2 is depicted in yellow and orange. (D) $T27^{NuoB}$ and $V133^{NuoD}$ (shown as red mesh) are part of the residues involved in quinone binding and located at the interface of NuoB (marine) and NuoD (dark blue). Further residues of the main quinone-binding pocket are depicted as green mesh. There is a second quinone-binding site (selected residues shown as yellow mesh), which is discussed to be a resting position and involves NuoH (cyan). An electron cryo-microscopy structure of ubiquinone (red) at this position was resolved for *Y. lipolytica* (PDB 6RFR) and was modelled in the *H. pylori* protein complex. The iron-sulfur cluster N2 (yellow and orange balls) is depicted as orientation guide.

A comparison of sequence similarity and identity of NuoB and NuoD was calculated using Emboss Needle pairwise sequence alignment (default setting, Madeira *et al.,* 2019) and is depicted in Table 4.6. NuoB and NuoD of *C. jejuni*, an ε-proteobacterium closely related to *H. pylori*, showed the highest sequence similarity and identity to the respective proteins in *H. pylori*, while the NuoB and NuoD orthologs of the other analyzed organisms had an overall sequence identity below 50 %.

Table 4.6 Sequence similarity of NuoB (B6JNA1) and NuoD (B6JNA3) in different organisms (All sequences were compared with *H. pylori* P12.)

NuoB	**Uniprot-ID**	**Identity (%)**	**Similarity (%)**
C. jejuni	A0A1S2U3S4	75.4	85.6
E. coli	P0AFC7	35.6	49.8
H. sapiens	O75251-1	41.7	55.1
T. thermophilus	Q56218	52.5	69.4
Y. lipolytica	Q9UUT7	42.7	53.5
NuoD	**Uniprot-ID**	**Identity (%)**	**Similarity (%)**
C. jejuni	A0A1E7NKA7	60.1	76.3
E. coli	P33599	25.1	37.9
H. sapiens	O75306-1	36.9	51.9
T. thermophilus	Q56220	40.8	58.3
Y. lipolytica	Q9UUU1	38.6	55.8

In contrast, the residues, known to be involved in quinone binding, were highly conserved (Table 4.7). Only in case of *E. coli* NuoB >50 % of residues differed from the *H. pylori* sequence.

Table 4.7 Residues involved in quinone binding (Parey *et al.,* 2019; Degli Esposti, 2015) *T. thermophilus* and *H. pylori* numbering is depicted. Sequence identity was calculated as percentage of *H. pylori* P12. T27^{NuoB} and V133^{NuoD} (*H. pylori* numbering) are highlighted. Completely conserved residues are shown in italic.
UniProt-IDs as in Table 4.6.

NuoB									**Identity (%)**
T. thermophilus	**T40**	*C46*	A47	I48	*M50*	M51	F68	*R69*	100
C. jejuni	**S**	*C*	A	I	*M*	M	F	*R*	87.5
E. coli	**N**	*C*	Y	V	*M*	V	L	*R*	37.5
H. sapiens	**T**	*C*	A	V	*M*	M	F	*R*	87.5
Y. lipolytica	**T**	*C*	A	V	*M*	M	F	*R*	87.5
H. pylori	**T27**	*C33*	A34	I35	*M37*	M38	F54	*R54*	

NuoD												**Identity (%)**
T. thermophilus	S36	*H38*	*Y87*	**T135**	L138	*D139*	L143	F146	R350	D401	*V403*	63.6
C. jejuni	S	*H*	*Y*	**T**	L	*D*	M	F	K	N	*V*	90.9
E. coli	S	*H*	*Y*	**T**	Q	*D*	M	V	K	D	*V*	63.6
H. sapiens	A	*H*	*Y*	**T**	L	*D*	M	F	K	D	*V*	72.7
Y. lipolytica	A	*H*	*Y*	**S**	M	*D*	L	F	K	D	*V*	54.5
H. pylori	S34	*H36*	*Y85*	**V133**	L136	*D137*	M141	F144	K350	N401	*V403*	

Based on sequence similarity and resolution of the available structures, *Y. lipolytica* complex I (6RFR (Parey *et al.,* 2019)) was chosen for computer-based modelling visualizing the protein-protein interface of NuoB and NuoD (UniProt entries B6JNA3, B6JNA1). Thereby, it could be confirmed that T27^{NuoB} and V133^{NuoD} are directly located at the protein-protein interface and probably within the main quinone-binding pocket (Degli Esposti, 2015, Figure 4.49 C, D).
While complex I inhibitors in general display a wide diversity regarding their chemical structures, all usually interfere with the quinone entry and/or binding in the quinone-reaction chamber (Murai and Miyoshi, 2016). In principle, two binding modes of the inhibitors are conceivable, both completely blocking the complex I activity by competitively interfering with quinone binding. The two binding sites were first proposed in 1994 (Friedrich *et al.,* 1994). The first binding position, the main quinone-binding site, is built by NuoB and NuoD and comprises the protein-protein interface mentioned above (Table 4.7, Figure 4.49 D). Quinone itself is thought to stay only for a minimal time frame in this position and once there, it gets rapidly reduced. Residues, essential for quinone binding, like T27^{NuoB} are highly conserved amongst

species. The second binding position represents a resting position for quinone and is located at the interface of NuoB, NuoD and NuoH. In 2019 the electron cryo-microscopy structure of the *Yarrowia* complex I with ubiquinone captured in the second binding position was solved, confirming this second binding spot. In this position, the head of the ubiquinone is 26.7 Å away from the iron-sulfur cluster N2. (Parey *et al.,* 2019)
Selected residues of this binding site are listed in Table 4.8.

Table 4.8 Residues involved in quinone binding at the second binding site (Parey *et al.,* 2019; Degli Esposti, 2015; Warnau *et al.,* 2018). *T. thermophilus* and *H. pylori* numbering is depicted, sequence identity was calculated as percentage of *H. pylori* P12. Completely conserved residues are shown in italic. UniProt-IDs of NuoB homologs as in Table 4.6

NuoB								**Identity (%)**
T. thermophilus	*W37*	V67	*R69*					66.7
C. jejuni	*W*	I	*R*					100
E. coli	*W*	V	*R*					66.7
H. sapiens	*W*	V	*R*					66.7
Y. lipolytica	*W*	I	*R*					100
H. pylori	*W24*	I53	*R55*					
NuoH							**UniProt-ID**	**Identity (%)**
T. thermophilus	*E35*	*R36*	*D62*	W241	*Y249*	*R294*	Q60019	100
C. jejuni	*E*	*R*	*D*	W	*Y*	*R*	A0A1E7NKG8	100
E. coli	*E*	*R*	*D*	F	*Y*	*R*	P0AFD4	83.3
H. sapiens	*E*	*R*	*D*	F	*Y*	*R*	P03886	83.3
Y. lipolytica	*E*	*R*	*D*	F	*Y*	*R*	Q9B6E8	83.3
H. pylori	*E30*	*R31*	*D57*	W240	*Y248*	*R293*	B6JNA7	

Using molecular docking algorithms, the most likely binding positions of #17 in the NuoB/NuoD and NuoH subcomplex were calculated. Those *in silico* data gave additional insights regarding the binding to the two different sites and further underlined the importance of $T27^{NuoB}$, since #17 was almost exclusively found at the second binding site and the pathway towards $T27^{NuoB}$ (Figure 4.50 A). Since $T27^{NuoB}$ is directly located at the entry of the binding pocket (Figure 4.50 B), it could be reasoned, that the $T27N^{NuoB}$ mutant has a narrowed entry into the pocket preventing the binding of the small molecule inhibitors.

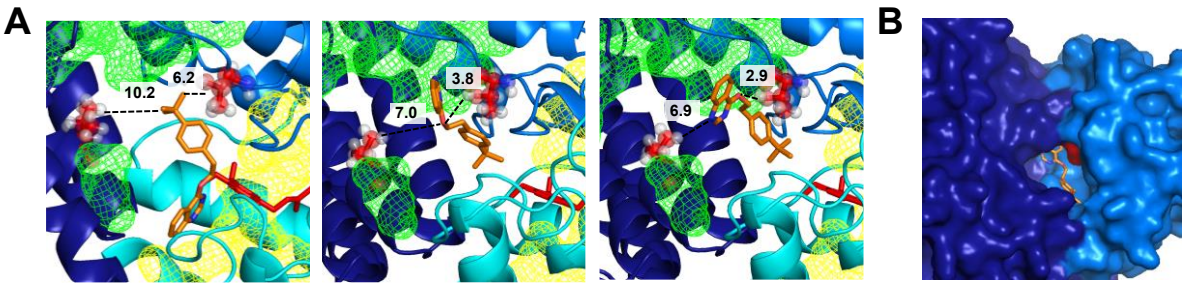

Figure 4.50 Predicted binding of #17 in the quinone pocket underscoring the importance of $T27^{NuoB}$. (A) Exemplary poses of an induced fit docking of #17 (orange) in the NuoB (marine)/NuoD (dark blue)/NuoH (cyan) interface of *H. pylori* (template: 6RFR). $T27^{NuoB}$ and $V133^{NuoD}$ are highlighted as balls and sticks. The main quinone-binding site is depicted as green mesh, the second one as yellow mesh. As explained in Figure 4.49, ubiquinone (red) was modelled in the complex. Distances were measured using PyMol and are displayed in Å. (B) Plan view of the entry of the quinone channel built by NuoB (marine) and NuoD (dark blue). The pose of #17 (orange) is the same as the right one in (A). $T27^{NuoB}$ (red) is directly located at the entry.

4.3.2.3 Structure-activity relationship

To further confirm the proposed target and to optimize the potency of the compounds a structure-activity relationship (SAR) screening was performed. Over 100 small molecule compounds were screened for anti-*H. pylori* activity. Amongst them, 19 shared the pyrimidine moiety of #14, 17 were analogous to #16 and 65 were closely related to #17. In a first screening approach, all compounds were tested at a concentration of 25 µg/ml and 2.5 µg/ml. All active molecules (*i.e.* MIC < 2.5 µg/ml) were further evaluated regarding MIC and IC_{50} values. In case of #16 no compounds with improved inhibitory potential were obtained, probably due to the small number of molecules tested (Figure 4.51 B). Three analogs were found to have lower MIC values than #14 and ten lower than #17 (Figure 4.51 A, C). The most potent compounds belonged to the group of #17 analogs and had MIC and IC_{50} values in the sub-nanomolar range, but some of them also inhibited the growth of *C. jejuni* at very high concentrations (1000x$MIC_{H.\ pylori}$, data not shown).

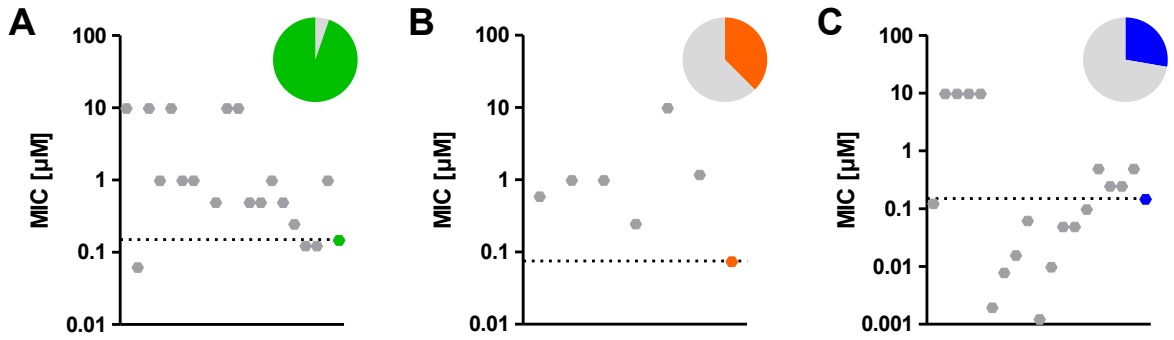

Figure 4.51 Follow-up screening of structurally related small molecule inhibitors. MIC values were determined by broth microdilution assays. Compounds were initially tested in 1:10 dilution steps (10 µM, 1 µM, 0.1 µM), if the MIC was lower than 1 µM, further tests were performed using 1:1 dilutions. The respective original compounds are highlighted: #14 (A, green), #16 (B, orange) and #17 (C, blue). The coloured part of the pie charts indicates the portion of compounds with MIC values lower than 2.5 µg/ml, which are shown as individual dots (#14: 18/19, #16: 6/17, #17: 18/65).

For #14 and #17 distinct structural characteristics could be identified, that improved or decreased the anti-*H. pylori* activity. (For better understanding, the subdivision of the two molecules is depicted in Figure 4.52.)

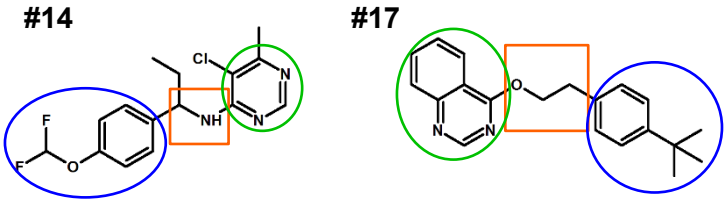

Figure 4.52 Subdivision of #14 and #17 for SAR description. The pyrimidine (#14) and quinazoline moieties (#17) are highlighted in green. The linker region is framed in orange and the substituent R in blue.

Overall, the linker region between the pyrimidine (#14) or quinazoline moiety (#17) and the substituent R turned out to be critical. Beside the length (see Appendix, Figure 6.1 A, Figure 6.2 A), the flexibility of this linker strongly influenced the inhibitory potential (Figure 6.2 B). Furthermore, in case of #17, derivatives with nitrogen at position 4 instead of oxygen in general had lower MIC values (Figure 6.2 B). For #14, an additional methyl group in the linker always increased the inhibitory potential, *i.e.* for example a phenylethyl instead of a phenylmethyl substituent (Figure 6.1 B). Regarding the quinazoline head of #17, it was observed, that other moieties like thieno[2,3-*d*]pyrimidine but especially 3-methyl[1,2]oxazolo[5,4-*d*]pyrimidine strongly reduced the anti-*H. pylori* activity (Figure 6.2 C). In contrast, the fluorination of the head group drastically increased the inhibitory potential (Figure 6.2 D). A huge potential for compound optimization was found for the substituent R. While in case of #14, MIC and IC_{50} values were slightly improved by chlorination (Figure 6.1 C), MIC and IC_{50} in the sub-nanomolar range were obtained for #17-related structures with complex, fluorine-containing substituents (Figure 6.2 E).

Combining the observation, that the length and flexibility of the linker are crucial, and the insights obtained by *in silico* modeling, six #17 derivatives were tested regarding their inhibitory effect on T27^{NuoB} mutants. Those compounds on the one hand differed regarding the length of the linker (ACA#1 vs. ACA#2/#4), postulating, that a substance with longer linker region could still bind the T27N^{NuoB} variant. On the other hand, molecules were tested with expanded linker region and an additional methyl group, rendering the quinazoline head/linker connection bulkier (ACA#3/#5/#6).

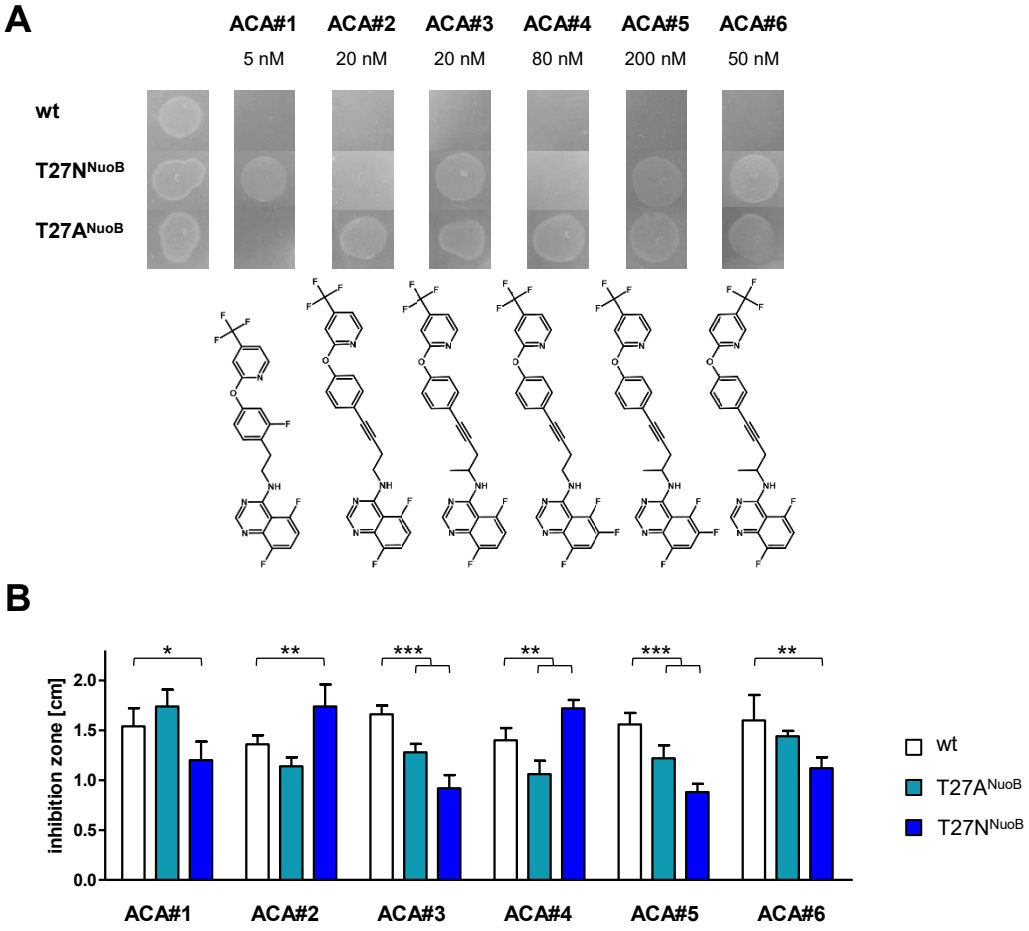

Figure 4.53 NuoB mutants display distinct cross-resistance patterns to analogs of #17 with modified linker region. (A) Resistance of the different strains was tested as in Figure 4.47. A representative result of at least three independent experiments is shown. The structures of the respective inhibitors are depicted. The different MIC values of *H. pylori* wt resulted from the varying purities of the stock solution. (B) The susceptibility of the two NuoB mutants and P12 wt was assessed by disk diffusion tests. ACA#1, #3, #4 and #6 were tested at 10 µM, ACA#2 at 2 µM and ACA#5 at 20 µM, respectively. The diameters of the zone of inhibition were determined from five independent experiments, shown are means and standard deviations. (Statistics: One-Way ANOVA, Dunnett post test, *p<0.05, **p<0.01, ***p< 0.001, only significant differences are indicated)

All compounds were tested for their inhibitory effects on *H. pylori* P12 wt, the T27N^{NuoB}, and the T27A^{NuoB} mutant strain, respectively. In line with the prediction, the T27N^{NuoB} but not the T27A^{NuoB} variant was susceptible to compounds with extended linker region but still resistant to those derivatives with the additional methyl group (Figure 4.53 A). To evaluate the resistance

pattern quantitatively, the zones of inhibition of the respective small molecules were determined (Figure 4.53 B). As already observed for #14 and #17, the T27A^{NuoB} mutant was in general only slightly less sensitive than the wt strain, and the resistance did not correlate with composition of the linker region of the particular compound. Hence, while the resistance of the T27N^{NuoB} strain can be rationalized by an altered architecture at the entry of the pocket, the reduced sensitivity due to the T27A^{NuoB} mutation might be caused by a slightly reduced binding affinity of the inhibitors to the NuoB/NuoD interface.

4.3.2.4 Susceptibility of CagT4SS activity for complex I inhibition

The finding, that several complex I inhibitors from various sources were identified via their interference with the T4SS activity by screening with the TEM-CagA translocation assay (Schindele, 2017), led to the theory that type IV secretion-dependent CagA translocation is especially sensitive to compounds targeting the respiratory chain.

Indeed, already after a short exposure time (30 min prior to infection), #14, #16 and #17 strongly inhibited CagA translocation in a concentration-dependent manner as observed by the TEM-CagA reporter assay (Figure 4.54 A).

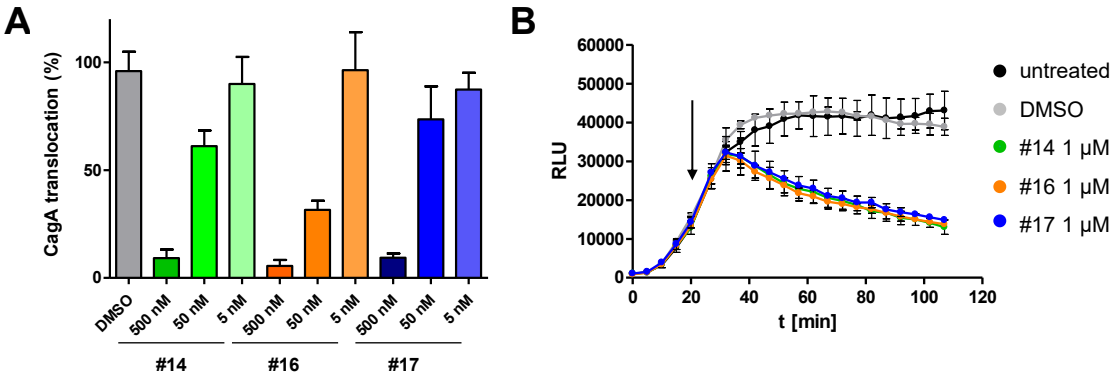

Figure 4.54 The novel anti-*H. pylori* compounds strongly inhibit CagA translocation. (A) The TEM-CagA-producing reporter strain was pre-treated with the indicated compounds at the respective concentrations for 30 min. TEM-CagA translocation was quantified after 2.5 h of infection in the presence of the inhibitors and normalized to the untreated control. Data show means and standard deviations of five independent experiments. (B) AGS[LgBiT] cells were infected with the HiBiT-CagA reporter strain, and the real-time translocation assay was started as described. After 25 min (cycle 5, arrow), the measurement was paused, compounds were added to the indicated concentrations and the measurement was continued. A representative result with means and standard error or the means of technical replicates is shown.

Using the newly developed HiBiT-CagA translocation reporter assay, the kinetics of the inhibition were further investigated. Thus, LgBiT-producing AGS cells were infected with the reporter strain and HiBiT-CagA translocation was monitored in real time. After 20-30 min of infection, the measurement was shortly paused to add the respective compounds and measurement was continued. All three small molecule inhibitors blocked HiBiT-CagA

translocation within 10 min after addition (Figure 4.54 B) as observed by decreasing RLU values, that resembled the course of decay of active luciferases described in Figure 4.6.

Next, the same experimental setup was performed with other antibiotics and inhibitors. To ensure comparability between the experiments, all compounds were analyzed at 10xMIC concentrations.

As observed for #14, #16 and #17, the two respiratory chain inhibitors rotenone and antimycin A blocked HiBiT-CagA translocation almost immediately after being added. Apparently, antimycin A had even more severe effects on the secretion process, but since the decrease in luminescence signal was stronger than expected for a stop of HiBiT-CagA translocation followed by a slow decay of the active luciferases, it has to be concluded, that the complex III inhibitor has additional effects on the host cells. In contrast, the protein synthesis blocker erythromycin could not stop HiBiT-CagA translocation when added during an ongoing infection (Figure 4.55 A).

In parallel, the HiBiT-CagA reporter strain was pre-treated for 30 min with the respective compounds and translocation was monitored (Figure 4.55 B). No HiBiT-CagA translocation was detected in the samples pre-treated with rotenone or antimycin A, while an about 50 % reduction was observed in the erythromycin pre-treated samples. This was further confirmed by Western blotting: After 4 h co-incubation of *H. pylori* P12 with AGS cells in the presence of the respective compounds, CagA translocation was determined by phosphotyrosine and CagA-specific immunoblotting (Figure 4.55 C). No translocated and thus phosphorylated CagA was observed in the respiratory chain inhibitor-treated samples, while erythromycin treatment only resulted in a diminished CagA phosphorylation. Additionally, the overall amount of CagA was clearly reduced in the erythromycin-treated sample. This was not the case for the other inhibitors. Time-to-kill kinetics experiments showed, that at the respective concentration of 10xMIC, erythromycin that is known to act bactericidal against *H. pylori* (Goodwin *et al.,* 1986) caused a ≥3 $\log_{10}$ cfu/ml reduction in colony count from the initial inoculum within 1-2 h of exposure. In contrast, after 1 h of treatment with the respiratory chain inhibitors #14, #16 and #17 no decrease in viable bacteria count was observed. At the tested concentration, all three compounds arrested bacterial growth like the bacteriostatic antibiotic chloramphenicol and caused a 1 $\log_{10}$ cfu/ml reduction within 8 h of treatment. (Figure 4.55 D) Notably, no viable bacteria were observed after 24 h exposure (data not shown). Thus, the reduced CagA translocation in case of erythromycin exposure is most likely due to bacterial killing within the time of pre-treatment and infection, while the novel anti-*H. pylori* compounds directly affect type IV secretion-dependent CagA translocation.

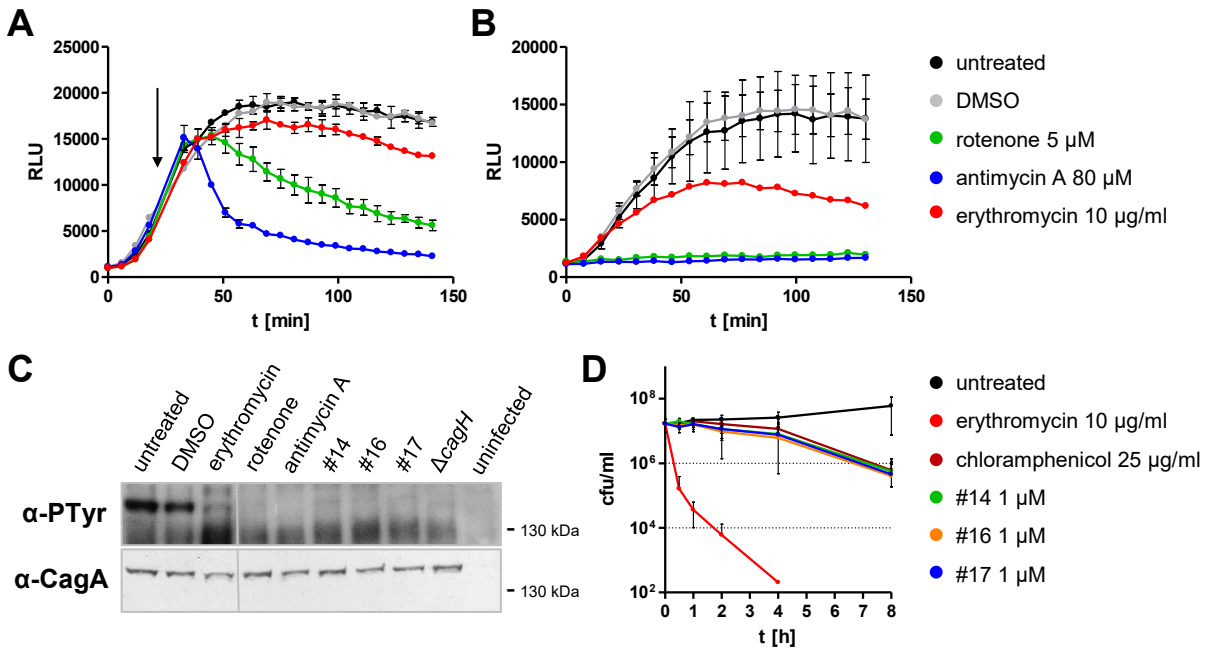

Figure 4.55 Respiratory chain inhibitors but not erythromycin directly interfere with CagA translocation. (A) AGS[LgBiT] cells were infected with P12[HiBiT-CagA] and the real-time translocation assay was started as described. After 25 min (cycle 5, arrow), the measurement was paused, compounds were added to the indicated concentrations and the measurement was continued. (B) Same experiment as in (A) but bacteria were pre-treated with the respective compounds at the indicated concentrations 30 min prior to infection. (C) Bacteria were co-incubated with AGS cells in the presence of the different inhibitors for 4 h and subsequently, translocated and thus phosphorylated CagA was detected by phosphotyrosine- and CagA-specific immunoblotting. As a control, cells were infected with a translocation-deficient P12 Δ*cagH* mutant. All compounds were tested at 10xMIC concentrations. (D) Killing kinetics of the three respiratory chain inhibitors and the two protein biosynthesis inhibitors erythromycin and chloramphenicol. 1 and 3 $\log_{10}$ cfu/ml reduction in colony count are indicated by dashed lines. (A/B) A representative result with means and standard error or the means of technical replicates is shown. (D) Data shown are means and standard deviations of at least three independent experiments.

To confirm that the complex I inhibitors target T4SS activity by interfering with cellular respiration only, a V133M^{NuoD} mutant of the P12[HiBiT-CagA] reporter strain was generated and HiBiT-CagA translocation was monitored in the presence of different concentrations of #16 (Figure 4.56). Overall, the V133M^{NuoD} mutant showed lower CagA translocation capacities than the wt strain, probably due to the lower metabolic activity and reduced fitness described above. Compared to the wt reporter strain, HiBiT-CagA translocation of the V133M^{NuoD} mutant was considerably less impaired by #16 treatment. Thus, the interference with the respiratory chain complex I activity was causative for the inhibition of CagT4SS activity.

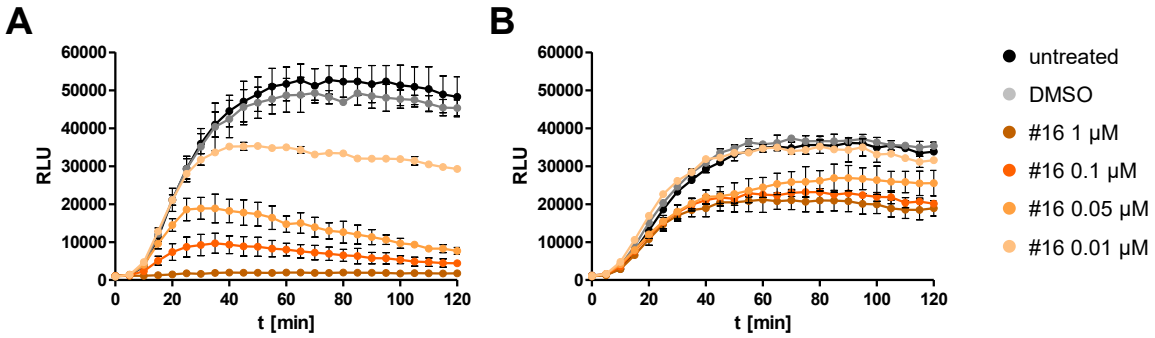

Figure 4.56 CagA translocation of a V133M^{NuoD} mutant is considerably less impaired by #16. P12[HiBiT-CagA] (A) and P12[HiBiT-CagA] V133M^{NuoD} (B) were pretreated for 0.5 h with #16 at the indicated concentrations, and subsequently HiBiT-CagA translocation was monitored in real-time using the split-luciferase-based assay as described above. A representative result with means and standard deviations of technical replicates is shown.

For other bacterial secretion systems, the dependence on the membrane potential and the resulting PMF is well known (Wilharm *et al.,* 2004). Thus, the impact of the three complex I inhibitors and CCCP on the bacterial membrane potential was quantified in a time-dependent manner (Figure 4.57). Briefly, *H. pylori* P12 was treated with the respective compounds (10xMIC) for the indicated period of time in PBS/FCS and afterwards stained for 30 min with the membrane potential-sensitive dye $DiOC_2(3)$, as described above. While CCCP immediately destroyed the membrane potential, #14, #16 and #17 in general had a clearly lower overall impact and the effect was highly time-dependent: whereas an about 50 % reduction was observed after 3 h treatment with 10xMIC concentrations, the membrane potential was only slightly impaired, when the inhibitors were added just prior to the $DiOC_2(3)$ staining (0 h).

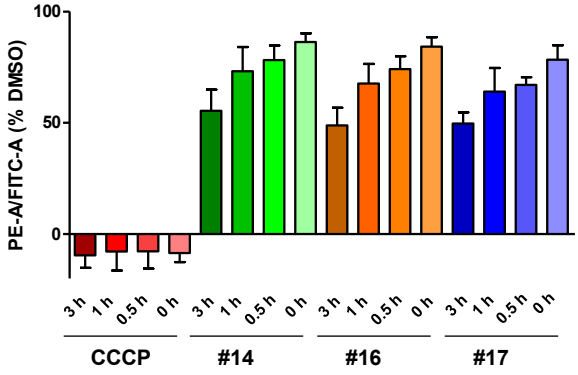

Figure 4.57 Short time exposure to the complex I inhibitors does not destroy the bacterial membrane potential. Bacteria were treated for different durations with the indicated compounds at 10xMIC concentrations (CCCP 20 µM, #14/16/17 1 µM) and membrane potential was measured using the membrane potential-sensitive dye $DiOC_2(3)$. Data were normalized to the DMSO-treated control, shown are means and standard deviations at least three independent experiments.

4.3.2.5 Species specificity

As already mentioned above, the three new small molecule inhibitors targeting *H. pylori* growth by interfering with the quinone binding to complex I, had no impact on the growth of other bacteria tested. Even the closely related *C. jejuni* was not affected when compounds were added at concentrations considerably higher than needed for *H. pylori* growth inhibition. (Figure 4.58 A-D)

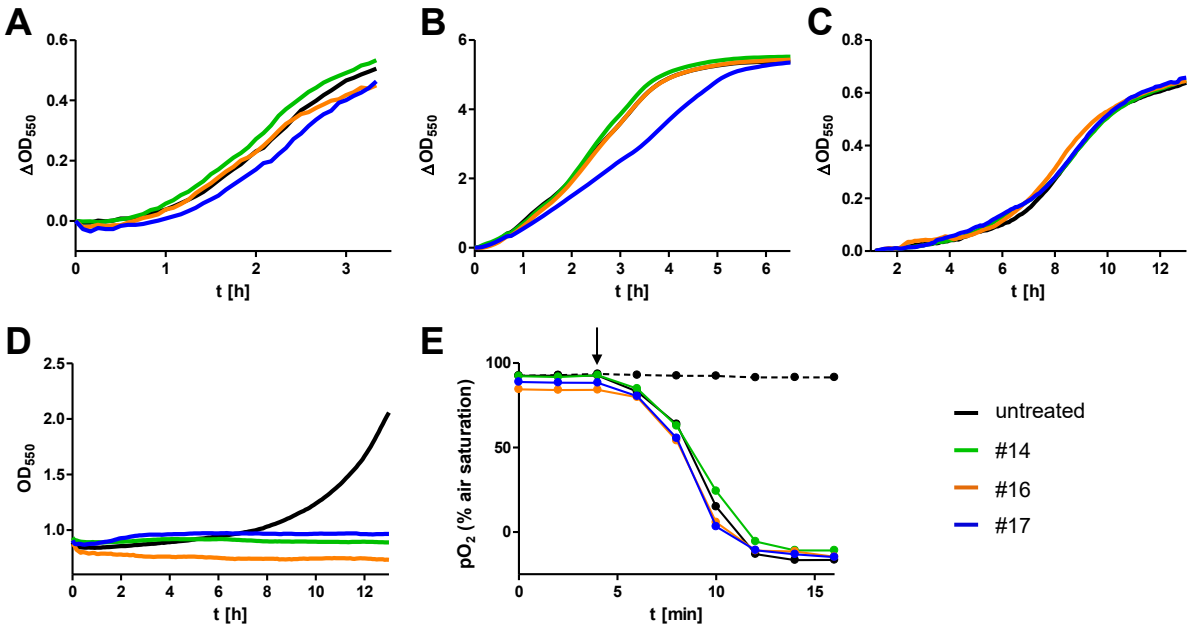

Figure 4.58 *E. coli*, *S. aureus* and *C. jejuni* are not affected by the complex I inhibitors of *H. pylori*. Bacterial growth of an exemplary gram-negative (*E. coli,* A) and an exemplary gram-positive species (*S. aureus,* B) was not or only minimally inhibited by the new small molecule inhibitors even at concentrations of 100xMIC$_{H.\ pylori}$. Furthermore, *C. jejuni* that is closely related to *H. pylori* tolerated high doses of the compounds (C). (D) *H. pylori* was not growing in the presence of the inhibitors. (E) O_2 consumption of *E. coli* is not altered by high doses of #14, #16 or #17. The arrow indicates the addition of 7 mM pyruvate, the control sample without pyruvate is shown as a dashed line. (A-D compound concentration: 15 µM, E: 100 µM. Representative experiments are shown.)

Due to its easy handling and the availability of knockout mutants, *E. coli* was chosen to elucidate the reason for species specificity of the complex I inhibitors.

To exclude that *E. coli*, a facultative anaerobic bacterium, can grow in the presence of complex I inhibitors due to its independency of aerobic respiration, O_2 consumption of #14-, #16- or #17-treated bacteria was monitored (Figure 4.58 E). No alterations in the O_2 consumption were observed.

One hypothesis, why *E. coli* (and other bacteria) are especially resistant to complex I inhibitors is the presence of an additional NADH dehydrogenase (Ndh2) that can compensate for NADH:ubiquinone oxidoreductase inhibition. While the Ndh1, *i.e.* the *nuo* encoded complex I, is a huge multi-protein complex, that shuttles electrons from NADH to quinones in the respiratory chain and couples the redox reaction to proton translocation, Ndh2 is a single-subunit enzyme of 47 kDa that transfers electrons from NADH to the respiratory chain, but is

not involved in proton translocation (Kaila and Wikström, 2021). *Ndh2* is absent in *H. pylori* (and *C. jejuni*), but expressed, for example, by *E. coli* and *Helicobacter hepaticus* (Smith *et al.,* 2000; Suerbaum *et al.,* 2003).

While the deletion of either Ndh1 or Ndh2 has no adverse effect on *E. coli* growth, double mutants have severe growth defects (Calhoun and Gennis, 1993). Thus, it was analyzed if an *ndh2* knockout mutant would be susceptible to the complex I inhibitors. The respective *ndh2* knockout was generated in *E. coli* TOP10 according to the protocol established by Datsenko and Wanner in 2000 (Figure 4.59 A). The successful gene deletion was confirmed by PCR (Figure 4.59 B).

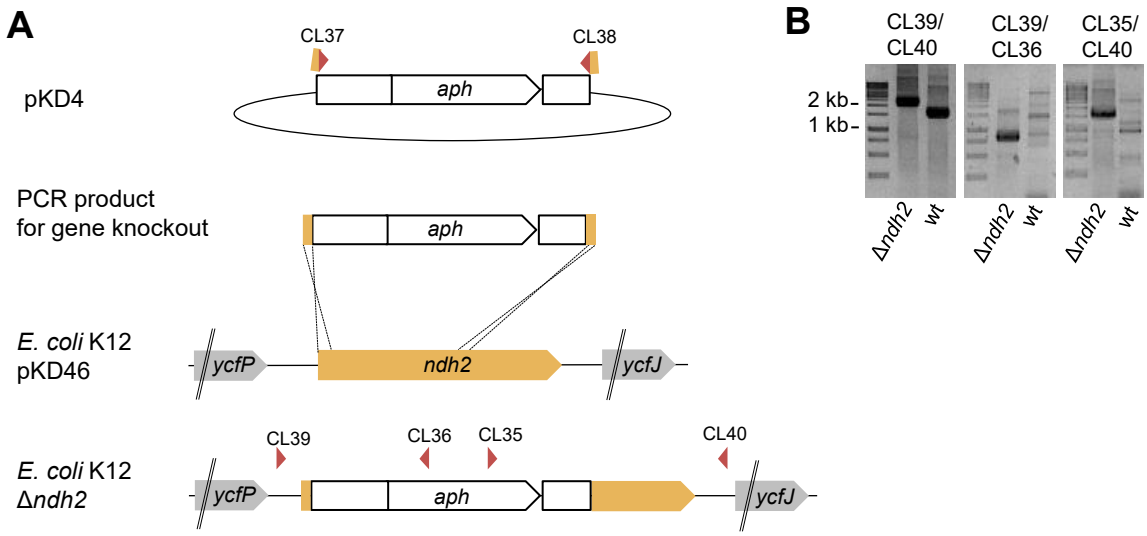

Figure 4.59 One-step inactivation of *ndh2* in *E. coli* using linear PCR products. (A) The DNA fragment used for targeted gene-replacement was generated by PCR using primers with 40-nt extensions that are homologous to *ndh2* and a resistance cassette encoding template plasmid (pKD4). Chemically competent *E. coli* K12 carrying the pKD46 plasmid (λ Red system) were transformed with the PCR product and knockouts obtained by recombination were selected via kanamycin resistance. (B) The gene deletion was confirmed by PCR. The expected amplicon size of the PCR using primer CL39 and CL40 is 2.4 kb (Δ*ndh2*) and 1.7 kb (wt), respectively. Additionally, PCRs were performed with primers binding within the resistance cassette. The corresponding amplicon sizes for the Δ*ndh2* strain are 0.8 kb (CL39/CL36) or 1.6 kb (CL35/CL40). As expected, no specific bands were observed in the wt samples using these primer sets.

As observed for the wt strain, the growth of the *E. coli* Δ*ndh2* strain was not affected by #14, #16 or #17, indicating that the presence of a second NADH dehydrogenase is not causative for resistance (Figure 4.60 B).

Another reason for the species specificity could be effective concentration differences of the compounds at their target site. Membrane permeability of the inhibitor and efflux pumps are key factors for the bioavailability. In *E. coli*, TolC (Tolerance colicin E1), that forms outer membrane channels is an essential part of several efflux systems like AcrAB-TolC, HlyDB-TolC, EmrAB-TolC and MacAB-TolC (Neuberger *et al.,* 2018). In *H. pylori* three efflux pumps of the resistance-nodulation-cell division family are described so far: HefABC, HefDEF

(= CznABC), HefGHI (= CzcAB-CrdB), with HefABC being most similar to multridrug efflux pumps. For every system, a TolC homolog was found: HefA, HefD, HefG (Marques *et al.,* 2020).

E. coli Δ*tolC* knockout strains are known to be hypersensitive to many antibiotics (Sulavik *et al.,* 2001; Nishino *et al.,* 2003; Cristóbal *et al.,* 2006) and are frequently used as controls in mass-spectrometry-based approaches to measure intracellular compound concentrations (Zhou *et al.,* 2015).

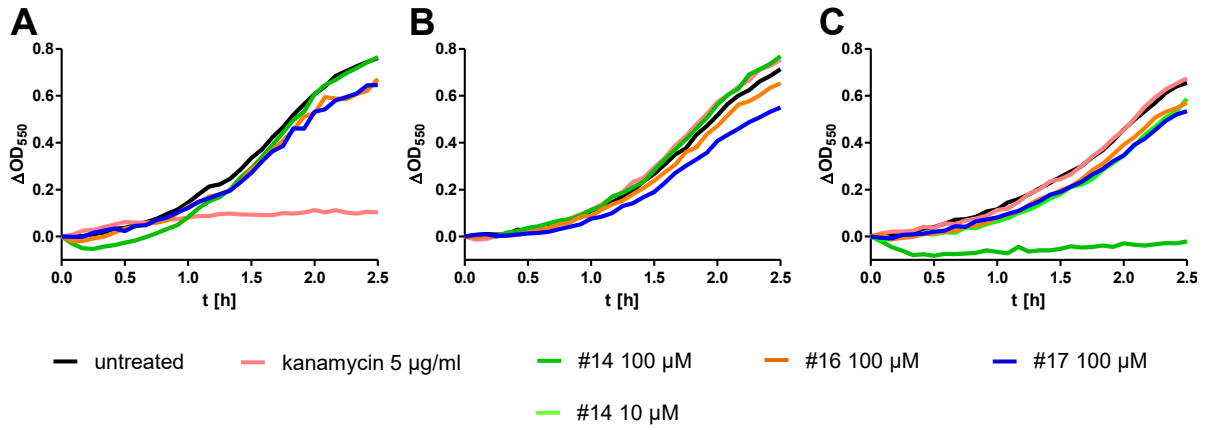

Figure 4.60 Growth of *E. coli* Δ*ndh2* and Δ*tolC* mutants in the presence of high doses of the inhibitors. The growth of the wt strain (A) and the Δ*ndh2* mutant (B) was not affected by 100 µM of the respective inhibitors. Furthermore, the Δ*tolC* mutant (C) tolerated high doses (100 µM) of #16 and #17. Even though the mutant was not growing at a concentration of 100 µM of #14, it was still considerably less sensitive than *H. pylori* and fully grew at a concentration of 10 µM. As expected, both mutants were resistant to kanamycin (*ndh2::aph, tolC::aph*). Representative growth curves are shown.

An *E. coli* K12 Δ*tolC* mutant (JW5503-1) and the corresponding wt strain (BW25113) from the Keio collection were tested for sensitivity towards #14, #16 or #17 treatment (Figure 4.60 A, C). While both strains grew well in the presence of #16 and #17, high concentrations of #14 strongly impaired the growth of the Δ*tolC* mutant. Nevertheless, the inhibitory potential was much weaker than in case of *H. pylori*. These data indicate that the architecture of the binding pocket at the NuoB/NuoD interface is the reason for the species specificity. To further confirm this hypothesis, the growth of the Δ*tolC* and the Δ*ndh2* mutant was analyzed in the presence of the #17 derivatives with extended linker region. As the *H. pylori* T27N^{NuoB} mutant, *E. coli* possesses an asparagine residue at the entry of the quinone-binding site (see Table 4.7). While neither the *E. coli* wt nor the Δ*ndh2* mutant were inhibited by the different compounds, the Δ*tolC* mutant showed strongly reduced growth rates in the presence of ACA#2 and ACA#4 (Figure 4.61). Notably, this was only observed at very high concentrations (100 µM) of the respective substances.

Taken together, the inhibitors seem to have only a very low affinity to the complex I of other bacteria like *E. coli*. Thus, the compounds have no impact on the fitness of those species, except at exceedingly high concentrations in combination with drug efflux pump deficiency.

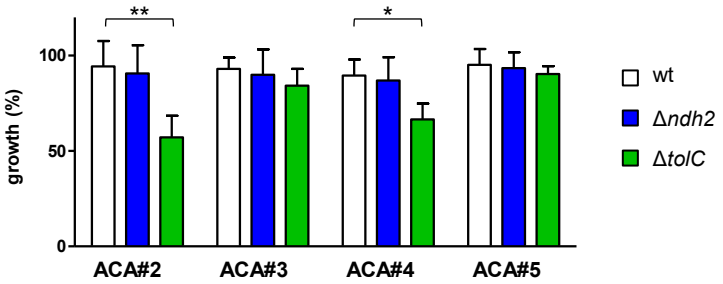

Figure 4.61 Growth of *E. coli* Δ*ndh2* and Δ*tolC* mutants treated with #17 derivatives with extended linker region. Bacteria were grown in the presence of the respective compounds at a concentration of 100 µM. Percental growth was calculated compared to the untreated control. Data shown are means and standard deviations from five independent experiments. (Statistics: One-Way ANOVA, Dunnett post test, *p<0.05, **p<0.01, only significant differences are indicated)

4.3.2.6 Emergence of spontaneous resistance

A major problem in *H. pylori* treatment is the rising prevalence of antibiotic resistance. Thus, the *in vitro* emergence of spontaneous mutations leading to reduced sensitivity towards a drug is an important figure in the development of novel antibiotics. To evaluate the prevalence of $V133M^{NuoD}$ and $T27N^{NuoB}$ mutations, the frequency of #16 or #17 resistant clones was determined representatively. Using the experimental setup described in the methods section (3.1.6), no resistant colonies were obtained in case of #17 using 4xMIC concentrations (4 µM). Thus, experiments were repeated at lower concentrations (1.25 µM), but still no spontaneous emergence of resistance was observed. Considering a total cfu of at least 10^9 bacteria/ml in the final culture, the occurrence of the $T27N^{NuoB}$ mutation was estimated to be very unlikely, probably due to the high fitness costs. On the other hand, the median frequency of #16 resistant colonies was $5.5x10^{-8}$, which was significantly lower than for rifampicin and lower than for metronidazole ($1.2x10^{-7}$), a nitroimidazole antibiotic commonly used in *H. pylori* eradication therapies (Figure 4.62).

In contrast to #16 resistance, which is at high concentrations most likely only due to a single point mutation ($V133M^{NuoD}$), several resistance mechanisms are described for metronidazole, with *rdxA* inactivation being the predominant (Wang *et al.,* 2001). This might explain the high variance in the metronidazole samples ($1.6x10^{-6}$ - $7.2x10^{-9}$). Rifampicin, that was taken as a reference, can be used as an estimation for overall mutation frequency, since single point mutations in the *rpoB* gene are sufficient for resistance (Wang *et al.,* 2001). The median mutation frequency for rifampicin resistance in case of *H. pylori* P12 was $6.1x10^{-7}$, which is in line with data published for other *H. pylori* strains ($3x10^{-5}$ to $4x10^{-8}$, Björkholm *et al.,* 2001).

Since single point mutations are sufficient to confer resistance to the complex I inhibitors, the low frequency of resistant colonies is most likely due to the high fitness cost described above.

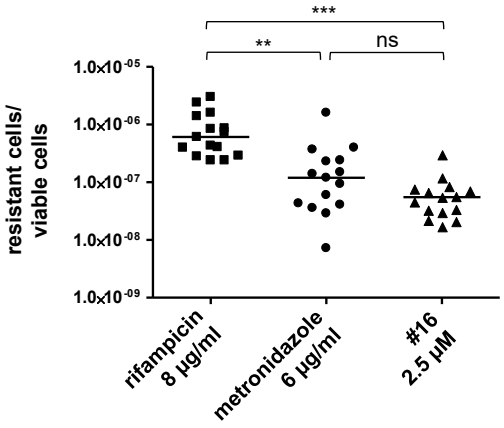

Figure 4.62 Emergence of spontaneous resistance. *H. pylori* P12 was grown for 48-72 h under standard conditions and then plated on serum plates supplemented with the indicated antibiotics. All compounds were tested at 4xMIC concentrations. Since the respective substances were directly added to the hot agar prior to solidification, values differ from those obtained by broth microdilution assay or from experiments with compounds spread on the solidified, chilled agar. (Statistics: One-Way ANOVA, Bonferroni post test, **p<0.01, ***p<0.001)

4.3.2.7 Evaluation of cytotoxicity in mammalian cells

Rotenone, the active component of the *Derris spec.* root extract was used for a long time as insecticide and piscicide (Lümmen, 1998; Ling, 2003). Meanwhile, it is well known, that insect and fish mitochondria are especially sensitive to respiratory chain inhibition, while plants, fungi and mammals can tolerate high doses of those compounds (Degli Esposti, 1998).

To access the cytotoxicity of the novel anti-*H. pylori* compounds, murine L929 fibroblasts, that are commonly used to evaluate cytotoxic effects *in vitro,* were treated with the small molecule inhibitors. Using the WST-1 assay, the impact of #14, #16 and #17 on cellular proliferation and fitness was measured. Even at the highest tested concentration (16 µM), that is about 100xMIC of *H. pylori*, the viability was only reduced to less than 50 %. Additionally, the O_2 consumption of L929 fibroblasts after short exposure (10 min) to the respective compounds was monitored. Even though respiration was blocked at high doses (10 µM), no adverse effect on O_2 consumption was observed applying 1 µM of #14 or 17. Only #16 strongly inhibited respiration at a concentration of 1 µM. Taken together it could be proven that *H. pylori* is much more susceptible to the novel compounds, than mammalian cells.

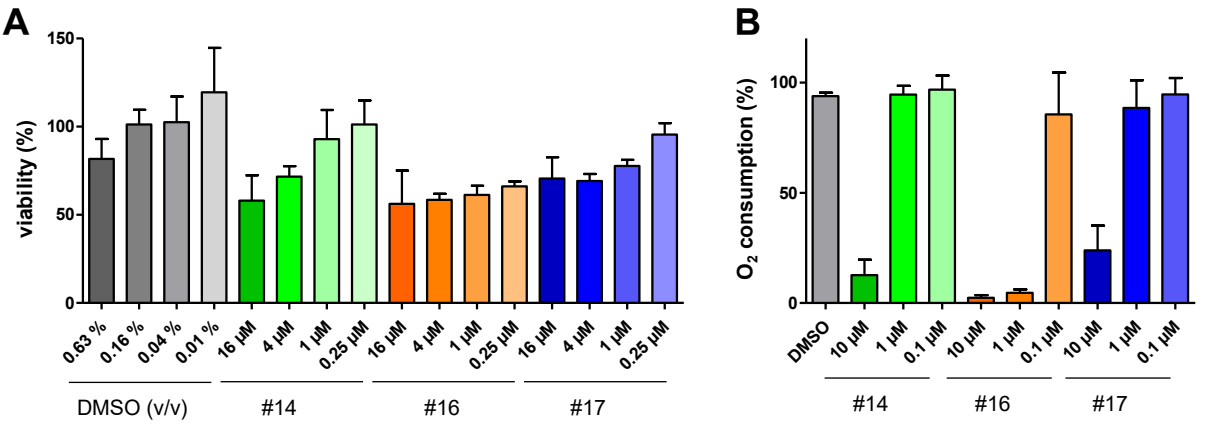

Figure 4.63 *In vitro* cytotoxicity against mammalian cells. (A) Murine L929 fibroblasts were incubated with the different compounds or DMSO at the indicated concentrations for 3 days and viability was measured using the WST-1 assay. (B) O_2 consumption of murine fibroblast after 10 min exposure to the respective compound concentrations was determined via OxoPlates. Data show means and standard deviations of at least three independent experiments.

4.3.2.8 Impact on growth of members of the human gut microbiome

As described above, no inhibitory effect of the compounds on the growth of three bacterial species, namely *E. coli*, *S. aureus*, and *C. jejuni* was observed. To further evaluate the impact on the fitness of the commensal gut microbiota, the growth of nine different human relevant species was tested in the presence of high concentrations (100 µM) of the compounds. Neither the facultative anaerobic species *E. coli* Nissle, *Enterococcus faecalis* and *L. reuteri*, nor the tested obligate anaerobic bacteria were susceptible to the novel-*H. pylori* compounds (Figure 4.64). Only the growth of the two members of the phyla Bacteroidetes was slightly reduced in the presence of #14.

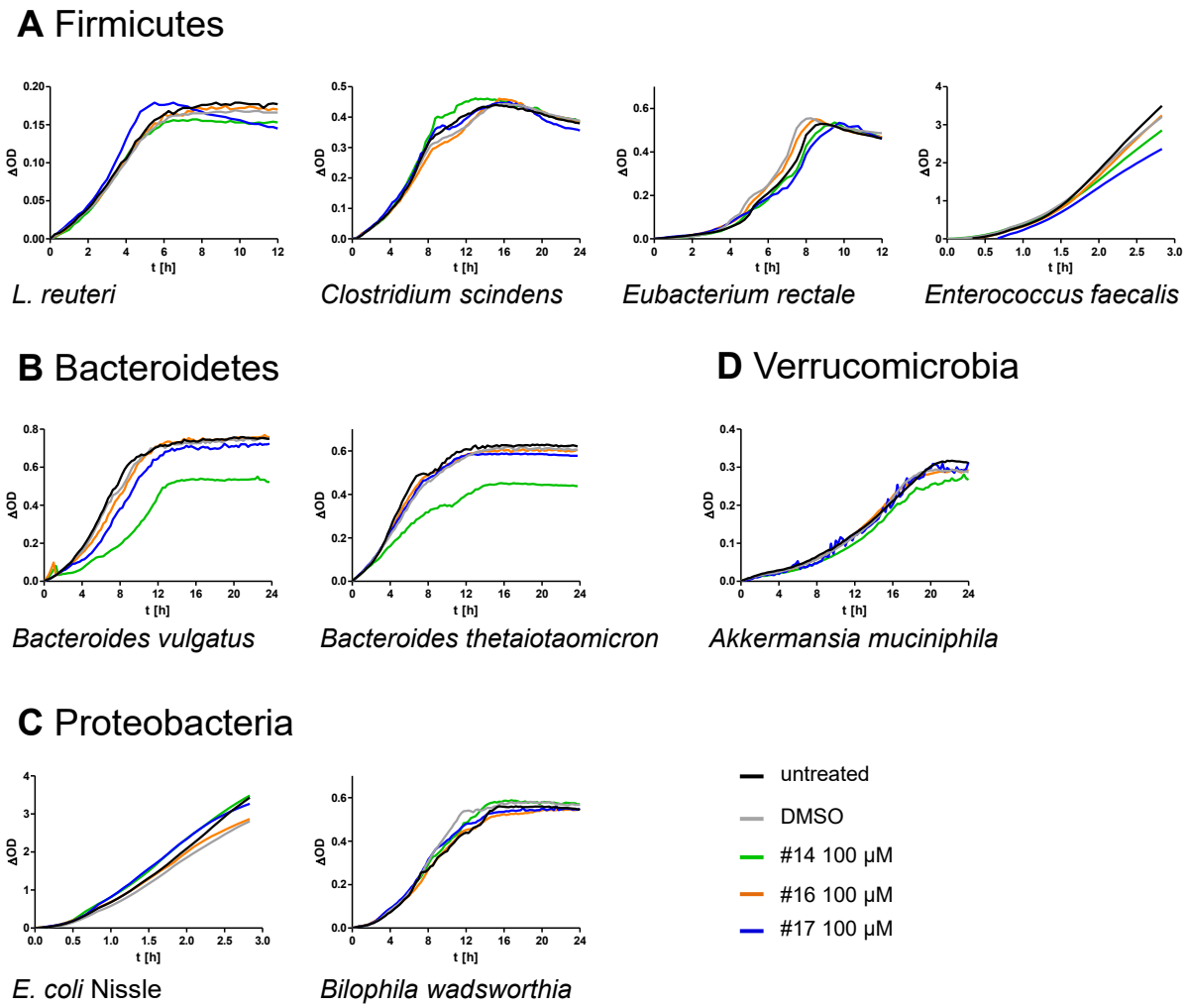

Figure 4.64 Members of the healthy human gut microbiome are not affected by high concentrations of the novel anti-*H. pylori* compounds. Selected species from the predominant human gut microbiome phyla Firmicutes (A), Bacteroidetes (B) and Proteobacteria (C) as well as a representative bacterium from the phylum Verrucomicrobia (D) were grown in the presence of 100 µM of the respective compounds or DMSO. A representative result is shown. Data were kindly provided by Prof. Bärbel Stecher and Diana Ring.

5 Discussion

The human pathogen *H. pylori* is the most important infectious cause of malignant tumors accounting for over 800,000 new cases of gastric cancer per year, and thus for thousands of cancer-related deaths (De Martel *et al.,* 2020). Even though treatment regimens are still available, the rapid emergence of antibiotic resistance and the lack of a prophylactic vaccination necessitate research and development of new, innovative anti-*H. pylori* drugs. Species-specific pathogen blockers and pathoblockers, *i.e*. compounds targeting virulence factors of the bacterium instead of killing it, are two promising strategies to discover new inhibitors with minor side effects and a reduced emergence of resistant strains.

CagA is a major virulence factor of *H. pylori*. Once injected into the eukaryotic host, it hijacks cellular processes, hence promoting the development of gastric cancer and other severe diseases. The inhibition of type IV secretion-dependent translocation of CagA is a reasonable approach to develop new pathoblocker-based therapeutic strategies. Even though in the recent years huge progress was achieved elucidating the structure of the CagT4SS and characterizing the oncoprotein CagA, deeper knowledge on the translocation process is needed to successfully identify and specify CagT4SS inhibitors.

In order to characterize CagT4SS activity more precisely, in the present study, a novel split-luciferase-based CagA translocation reporter assay was developed and implemented. Furthermore, several recently identified small molecule inhibitors that have a strong impact on type IV secretion activity were further investigated and their subcellular targets were characterized.

5.1 Elucidating CagA translocation – Development of a split-luciferase reporter assay

High sensitivity and reproducibility, low background signal, high versatility, and easy handling are major advantages of luminescence-based reporter systems. Thus, they are broadly applied tools to monitor for example gene expression, analyze protein-protein interactions and investigate protein synthesis, localization, and trafficking. (England *et al.,* 2016)

The NanoLuc split-luciferase complementation assay is based on an engineered, optimized version of the luciferase of the deep-sea shrimp *Oplophorus gracilirostris* (Hall *et al.,* 2012). The two fragments of the luciferase, called LgBiT (“large bioluminescence tag”) and HiBiT (“high affinity bioluminescence tag”), interact with high affinity and together form a functional enzyme that oxidizes the substrate furimazine in an ATP-independent manner and thus generates stable glow-type luminescence. While the small HiBiT tag is usually fused to the protein of interest, recombinant LgBiT can for example be provided together with the assay master mix to monitor protein levels of the tagged target. Alternatively, LgBiT is synthesized in a certain cellular sub-compartment or host cell type to detect delivery of the HiBiT-tagged cargo protein to a specific site. Recently this system was successfully implemented to monitor Sec-

dependent protein secretion in bacteria and mitochondrial protein import in yeast (Pereira *et al.,* 2019). Furthermore, the NanoLuc split-luciferase complementation assay was engineered to characterize type III secretion activity in *Salmonella* in a quantitative and time-resolved manner (Westerhausen *et al.,* 2020).

In the present work, the system was adapted to monitor the T4SS-dependent translocation of CagA into AGS cells, a human gastric adenocarcinoma cell line widely used to investigate *H. pylori* infections *in vitro.*

Previous studies revealed, that certain N-terminally tagged variants of CagA are well synthesized and translocated (Hohlfeld *et al.,* 2006; Murata-Kamiya *et al.,* 2010; Schindele *et al.,* 2016). Thus, to generate the split-luciferase reporter strain, the eleven amino acid HiBiT tag was inserted at the N-terminus of CagA. *In vitro* infections and subsequent phosphotyrosine-specific immunoblots proved that the small N-terminal HiBiT tag is well tolerated and has only negligible effects on synthesis and translocation rates.

To monitor HiBiT-CagA delivery via its interaction with the LgBiT fragment of the luciferase, AGS cells were stably transfected with a plasmid encoding LgBiT as a fusion protein with the self-labeling HaloTag under the control of a strong CMV promotor. Staining for the LgBiT-HaloTag protein with chloroalkane linker-containing dyes revealed a homogenous synthesis of the recombinant protein in the eukaryotic cells and enabled the selection and subsequent expansion of a single cell clone-derived LgBiT-producing reporter cell line.

Co-incubation of AGS[LgBiT] cells with P12[HiBiT-CagA] for 2.5 h under standard infection conditions and subsequent addition of the furimazine substrate resulted in a strong luminescence signal that could be recorded in a plate reader. In contrast, no light emission was observed in uninfected samples or cells co-incubated with a CagT4SS-deficient P12[HiBiT-CagA] Δ*cagT* mutant. Thus, the detectable increase in luminescence in the P12[HiBiT-CagA] samples is a measure for translocated HiBiT-CagA and type IV secretion activity. Thereby, the enhanced signal stability (>10 min) of the glow-type luminescence emitted by the NanoLuc luciferase enabled the robust measurement of up to 96 samples and ensured the easy handling.

Endpoint infections performed with different amounts of bacteria demonstrated the high sensitivity of the novel reporter assay: in the endpoint system, HiBiT-CagA translocation was even detectable if statistically only every eighth host cell was infected by one bacterium (MOI 0.125). Hence, the new split-luciferase-based assay was even more sensitive than the recently developed β-lactamase-based reporter system. Furthermore, a linear correlation between the count of infecting bacteria and the detected HiBiT-CagA translocation was observed over a wide range of MOIs (MOI 1-25), underlining the versatility and robustness of the assay. At higher bacterial loads, no further increase in the amount of injected HiBiT-CagA was detectable, most likely due to limited availability of LgBiT protein provided by the host cells.

The exceptionally low detection limit of the HiBiT-CagA endpoint assay provided the possibility to analyze translocation of poorly synthesized CagA variants as well as variants with low translocation rates or mutants with strongly impaired type IV secretion activity.
Optionally, the amount of total CagA, *i.e*. the translocated HiBiT-CagA and the HiBiT-CagA of adherent bacteria could easily be quantified immediately after measuring CagA translocation. In contrast to previous attempts to distinguish between injected and total CagA pools via Western blotting (Jiménez-Soto and Haas, 2016), the new assay needed minimal efforts and provided fast and reliable data. HiBiT-CagA variants with different synthesis levels could be compared easily, combining the results from the HiBiT-CagA translocation assay and the total HiBiT-CagA quantification. In case of *H. pylori* mutants that produce equal amounts of HiBiT-CagA, total HiBiT-CagA was shown to provide a measure for adherence. Thus, the new split-luciferase-based reporter system could be applied to distinguish between mutations directly affecting CagT4SS activity, *e.g*. deletion of *cagT* or *hopQ*, and mutations that only have an indirect impact on CagA translocation *e.g*. due to reduced bacterial motility (Δ*flaA* mutant). Hence, the novel HiBiT-CagA translocation assay can not only be used as an orthologous reporter system to the recently developed β-lactamase-based assay, but provides substantial additional information and a wide range of further applications.
Using the split-luciferase-based assay, CagT4SS activity could be monitored for the first time *in vitro* in real time using a continuous and fully automated measuring setup. Visualizing CagA translocation dynamics revealed an immediate onset of type IV secretion activity within less than 15 min after the start of infection, detectable due to the high sensitivity and time resolution of the assay. During the first hour of co-incubation, a linear increase in luminescence was recorded, finally passing to a stationary phase with constantly high luminescence values. In case of split-luciferase-based reporter systems, light emission directly and only correlates with the count of active luciferase complexes, and no signal accumulation occurs (Westerhausen *et al.,* 2020). Hence, the initial linear increase in luminescence signal intensity was caused by a high HiBiT-CagA translocation rate exceeding the parallel decay of HiBiT-LgBiT complexes (see also Figure 4.6), while during the later phase of infection, type IV secretion activity declined: newly injected HiBiT-CagA and decay of active luciferases balanced out each other resulting in a stationary phase. Those particular kinetics of CagA translocation were detected for different MOIs as well as for different *H. pylori* P12 mutants and different strains (P12; G27), thus it can be excluded that the saturation was an artefact caused by limitations of available substrate or LgBiT. The observed translocation dynamics are in accordance with previously published data based on the TEM-CagA reporter system (Schindele *et al.,* 2016), but the new assay provided a better time resolution. Furthermore, the fully automated, continuous real-time measurement reduces handling times and labor input, and facilitates the simultaneous analysis of many samples. Only due to the high resolution of the split-luciferase-based assay, minimal

alterations in translocation kinetics could be detected and characterized, *e.g*. CagT4SS activity in non-motile bacteria or bacteria without preculture (see Figure 4.20).

Finally, since luminescence-based assays lack, as already mentioned, any signal accumulation, the HiBiT-CagA reporter assay was suitable to compare and quantify the amount of translocated CagA in relation to the totally available CagA pool and could further be used to monitor the impact of several small molecule inhibitors on an ongoing infection process.

Taken together, the novel split-luciferase-based reporter assay is versatile, robust and reliable and thus a very useful tool to get new insights into T4SS-dependent CagA translocation. It overcomes limitations of the so far used standard techniques, *i.e*. immunoblots detecting phosphorylated CagA and the recently developed β-lactamase-dependent TEM-CagA reporter system: It is a phosphorylation-independent method to detect the transport of the oncoprotein, that is considerably less work intensive and time consuming but more sensitive than Western blotting. At the same time, the comparably small eleven amino acid HiBiT tag hardly influenced CagA protein synthesis and translocation, while the 29 kDa TEM-1 tag resulted in strongly reduced CagA protein levels, hence rendering it impossible to induce hallmarks of *in vitro H. pylori* infections. Furthermore, the HiBiT-CagA translocation could additionally be implemented as continuous real-time reporter assay. While the HiBiT-CagA translocation assay necessitates the usage of genetically modified LgBiT-producing host cells, the TEM-CagA reporter assay can virtually be performed with any kind of eukaryotic cells, *i.e*. primary cells, too. Nevertheless, in cells with low cytosolic portion, *e.g*. macrophages, loading with the CCF4-AM dye is not possible and thus the TEM-CagA reporter system is not applicable (Behrens *et al.,* 2020).

So far, the HiBiT-CagA reporter assay was not evaluated for high-throughput applications. Due to the sensitivity and robustness in combination with minimal handling times, assay steps and durations, basic requirements are certainly provided. The stable-glow type luminescence generated by the NanoLuc luciferase is an essential prerequisite, enabling the measurement of many samples. Furthermore, as the assay was already proven to be applicable in a 96-well microtiter format, a further down-scaling is feasible. Since no washing steps are required, an “addition only” protocol could be implemented facilitating the automated handling. Thus, the assay fulfills substantial criteria to be implemented in high-throughput screening assays (Inglese *et al.,* 2007). Compound-dependent assay interference that causes screening artefacts is a major problem in any high-throughput screening. Notably, β-lactamase- and luciferase-based assays are known to be prone to distinct compound effects (Inglese *et al.,* 2007): fluorescence-dependent systems are highly susceptible to compound fluorescence and absorbance, luminescence-based assays on the other hand are mainly inhibited by compound aggregation or light absorbance due to impurities. In addition, inhibition or activation of the respective reporter enzyme (biological interference) might account for false-positive or

-negative results. Specific inhibition of reporter luciferases by low molecular weight compounds is frequently observed, but the NanoLuc enzyme was already shown to be comparably robust to such inhibitors (Ho *et al.,* 2013). In general, luciferase inhibitors are not amongst the “pan assay interference compounds”, *i.e*. they would not affect a β-lactamase-based system (Auld *et al.,* 2018). Thus, the HiBiT-CagA translocation assay could be applied as an orthologous method to complement a high-throughput screening with the TEM-CagA reporter assay.

5.2 Fast onset, fast saturation – Insights into the early and late phase of *in vitro* CagA translocation

The observed real-time HiBiT-CagA translocation kinetics indicated a fast onset of oncoprotein injection within less than 10 min after the beginning of the bacteria-host cell co-incubation. Thus, the *in vitro* culture conditions are likely to prime *H. pylori* for type IV secretion activity. The ability to actively move to the AGS cell layer was observed to be a prerequisite for the onset of translocation, but could easily be substituted by mechanically bringing the bacteria to their target cells via centrifugation. Once bound to the cells, *H. pylori* precultured for 2 h in FCS-containing media immediately started to translocate the effector protein, which was not observed for bacteria without pre-incubation. In any case, the kinetics of CagA translocation were characterized by an initial burst of effector delivery followed by a stationary phase. In case of bacteria without preculture in PBS/FCS, *i.e*. without CagT4SS priming, those distinct kinetics were observed, too, albeit with some delay. Interestingly, similar courses of effector protein delivery are already described for enteropathogenic *E. coli* or *Salmonella enterica* serovar *typhimurium* T3SS (Mills *et al.,* 2008; Westerhausen *et al.,* 2020) and the immediate onset of T3SS activity after the docking to the host cells was monitored by time-lapse microscopy for *Shigella flexneri* and *S. typhimurium* (Enninga *et al.,* 2005; Schlumberger *et al.,* 2005). In the latter cases a rapid exhaustion of the bacterial effector protein pool was observed. For *S. typhimurium* real-time imaging of the secretion process revealed, that the bacterial pool of SipA, a key effector protein of the T3SS, is rapidly exhausted within 100-600 s, clearly indicating a limited amount of cargo proteins (Schlumberger *et al.,* 2005). Furthermore, it was shown that under *in vitro* conditions only a minor fraction (26 %) of the total *S. typhimurium* population expresses *sipA*, while flow cytometry experiments performed within the present work indicated that (GFP-)CagA is constitutively produced by all bacteria of an *H. pylori* culture (see Figure 4.10 C). Additionally, in marked contrast to other pathogens, *H. pylori* synthesized high levels of its single known effector protein CagA *in vitro* independently of bacterial densitiy during preculture and infection, as observed by measuring total HiBiT-CagA amounts. Still, only a minor fraction of the total oncoprotein pool was translocated into eukaryotic host cells. This is not only distinct from the above-mentioned T3SS-dependent processes, but also from other T4SS like the Dot/Icm system of *L. pneumophila*, the causative agents of Legionnaires’

disease, that injects over 300 different effectors via an expanded T4SS, but was shown to produce several of these cargo proteins only to a low abundance (Schroeder, 2017).

While *in vitro* infections and competition experiments had already indicated that only a minor portion of the total available CagA is injected (Jiménez-Soto and Haas, 2016; Schindele *et al.,* 2016), it is so far unclear, whether the bacteria themselves or the host cells are regulating the CagA translocation rate. It seems plausible that too strong delivery of the oncoprotein is toxic for the host cells and a tight regulation might be advantageous for the pathogens. Such autoinhibitory mechanisms are for example assumed in case of the T3SS-dependent translocation of several effector proteins in enteropathogenic *E. coli* (Mills *et al.,* 2008). On the other hand, real-time HiBiT-CagA translocation assays performed with different MOIs or translocation-impaired mutants always resulted in a stationary phase of translocation about 60-80 min after the start of infection. Thus, even if only low amounts of HiBiT-CagA were translocated (*e.g.* MOI 4), translocation rates got reduced, indicating that other factors than the amount of injected, intracellular CagA regulate the translocation efficiency. This is in line with previously published data, showing that a 60 min pre-infection with a *cag*PAI-negative strain significantly reduces the translocation rate of a second infecting *cag*PAI-positive strain (Zeitler *et al.,* 2017). It could further be excluded, that competition for adhesion is a limiting factor for CagA translocation, since the amount of total HiBiT-CagA detected in the infection mixture perfectly correlated with the number of bacteria used for infection. This supported previous findings, that pre-incubation of AGS cells with one *H. pylori* strain has no impact on the adhesion of a second strain, even at comparably high overall MOIs (Jiménez-Soto *et al.,* 2013). Despite these observations, the question remains if the *in vitro* data reflect the *in vivo* situation. So far, no methods are established to quantify CagA synthesis and translocation in animal models. But quantitative real-time reverse transcriptase PCR data from *in vivo* experiments in rhesus macaques and from gastric biopsies indicated that *cagA* is one of the most abundantly expressed virulence genes *in vivo*, too (Boonjakuakul *et al.,* 2005; Avilés-Jiménez *et al.,* 2012). The fast initial onset of CagA translocation observed in the real-time split-luciferase reporter assay and the time delay upon infection with bacteria that were not precultured in FCS-containing media prompted the question of the necessary stimuli and the mechanisms of priming. Despite the fact that the gain of motility accounted for the largest portion of the increased translocation at an early time of infection, bacteria primed for T4SS activity translocated approximately double the amount of CagA than bacteria directly taken from serum plates independently of their motility. Receptor-adhesin interactions that confer tight adhesion, but might also be directly involved in the secretion process are supposed to facilitate oncoprotein delivery. But HopQ-CEACAM interaction that was previously shown to substantially impact CagA translocation (Königer *et al.,* 2016) could be excluded to be responsible for the faster onset, since the T4SS priming was detected in a Δ*hopQ* mutant as well.

Analysis of the transcriptome by RNAseq indicated, that liquid culture in medium supplemented with FCS drastically alters the gene expression of the bacteria. Even though the analysis of the most strongly up- or downregulated mRNAs could not decipher the CagA translocation priming phenomenon, the manual categorization of the single hits using an expanded COG classification considering the *cag*PAI as an additional, *H. pylori* specific category highlighted the strong impact of culture conditions on cellular processes involved in adhesion, motility and T4SS activity.

Strikingly, a short incubation (30 min) of the bacteria drastically changed the energy status of the cells as measurements of the relative ATP levels indicated. ATP powers not only mRNA and protein synthesis in general, but might also be essential for the assembly of the type IV secretion apparatus. Even though the three cytosolic ATPases Cagα, Cagβ and CagE are not involved in the formation of the periplasmic cylinder and the outer membrane complex, they might build up the energy center for the recruitment of cytoplasmic Cag subunits and the final assembly of the IMC (Hu *et al.,* 2019). Furthermore, the trafficking ATPase Cagα is essential for CagA translocation itself and thus represents an additional candidate for ATP consumption and energy requirement during type IV secretion (Savvides *et al.,* 2003).

The high requirement of energy for a functioning T4SS is further supported by the observation, that inhibitors of the respiratory chain that immediately affect the ATP pool of the bacteria had a direct, negative impact on CagA translocation (see sections 4.3.2.4 and 5.6).

Finally, a reason for the comparably low fraction of translocated CagA as well as the priming of the translocation could be, that only newly synthesized proteins are in a translocation-competent conformation. Previous experiments monitoring the translocation of TEM-CagA in the presence of protein biosynthesis inhibitors indicated that only newly produced CagA is translocated (Schindele *et al.,* 2016). Thus, the slight increase in CagA production during the 2 h preculture detectable by the HiBiT-lysate assay might be decisive for the immediate start of translocation after docking to the host cells.

First attempts to identify the stimulating factors in the FCS indicated, that they are not required for the growth and thus the viability of the bacteria. Hence, targeting CagA translocation priming might be a promising new approach for developing a pathoblocker.

Several fractionation methods and serum treatments could already narrow down the spectrum of potential factors. Further work is necessary to combine the different separation strategies (size exclusion, heating and ultracentrifugation) to further down-scale the relevant FCS fraction and finally analyze a reasonable sample by mass spectrometry.

In parallel, P12[HiBiT-CagA] knockout mutants of selected transcription factors acting as hubs for mRNA expression might be investigated. Furthermore, the impact of quorum sensing factors like LuxS and the autoinducer-2 (AI-2), that were recently shown to impact CagA synthesis and translocation (Wen *et al.,* 2021), might be analyzed in this context.

5.3 Transport across three membranes – Requirement of protein unfolding for CagA translocation

Nearly 20 years ago, the translocation route of the T-DNA through the prototypical VirB/D4 secretions system of *A. tumefaciens* was deciphered (Cascales and Christie, 2004b): the secretion process is initiated by the recognition of the cargo DNA by the cytoplasmic coupling protein VirD4, subsequently transferred to the inner membrane ATPases and finally introduced into the translocation channel to pass the inner membrane, the periplasm and the outer membrane. So far, the transport of the T-DNA is the only solved route, while it is not fully understood, how other cargo is translocated in a T4SS-dependent manner.

It is in general assumed that the transport occurs in an unfolded state directly from the cytoplasm across the outer membrane in a one-step process. To achieve this, the T4SS substrates might initially interact with a type IV coupling protein as observed for the T-DNA transfer. (Christie *et al.,* 2014)

But hitherto, experimental evidence is lacking and the variety of cargo molecules and the diversity of T4SS architectures imply the possibility of different translocation mechanisms and routes. Indeed, contradicting an exclusively one-step process, periplasmic intermediates of at least some T4SS substrates were shown in case of the *Brucella* VirB system (Del Giudice *et al.,* 2016). Similarly, periplasmic intermediates were postulated to be essential for the translocation of some effector proteins of the archetypical *A. tumefaciens* VirB/D4 system (Pantoja *et al.,* 2002).

A further example for a two-step translocation process is the secretion of the pertussis toxin (Ptx) of *Bordetella pertussis*: the different subunits of the Ptx are channeled into the periplasm via the Sec system, after multimerization, the completely folded 105 kDa holotoxin is secreted into the extracellular space via a T4SS (Locht *et al.,* 2011).

While the transport across the outer membrane in a folded state is rather common and for example found in type II secretion systems or the chaperone-usher pathway (Filloux, 2004; Geibel *et al.,* 2013), the inner membrane transport is considered to be dependent on protein unfolding or the chaperone-mediated maintenance in an unfolded state. An exception is the Tat secretion system that transports folded proteins across the inner membrane (Frain *et al.,* 2019).

In case of *H. pylori*, it is suggested that CagA – as most T4SS substrates – is probably translocated in a one-step process from the cytoplasm to the bacterial surface and the host cell, which in turn is supposed to require unfolding prior to the transport.

To examine the role of protein unfolding on the Cag type IV secretion process, in the present work variants of HiBiT-CagA and different tightly folding protein domains were generated, and their translocation was measured.

As already shown for other T4SS (Trokter and Waksman, 2018), the rigid β-barrel fold of GFP completely impeded transport, while a fusion with the smaller Ub was almost as efficiently

translocated as HiBiT-CagA. The latter observation is in marked contrast to other T4SS or T3SS systems that cannot translocate Ub-tagged cargo proteins (Trokter and Waksman, 2018; Lee and Schneewind, 2002; Radics *et al.,* 2014). Even the expanded Icm/Dot T4BSS of *L. pneumophila* was incapable to transfer fusions of Ub and the respective substrates (Amyot *et al.,* 2013). As already observed in other secretion systems (Amyot *et al.,* 2013; Trokter and Waksman, 2018), a fusion with the destabilized $Ub^{I3G,\ I13G}$ variant was translocated with a slightly increased efficiency as compared to HiBiT-CagA. Interestingly, HiBiT-Ub-CagA but not the easily unfoldable $Ub^{I3G,\ I13G}$ variant was readily cleaved inside the eukaryotic host cells, indicating a recognition of Ub by cellular deubiquitinases and thus a proper folding of Ub in the fusion protein.

A reason for the different transport capacities might be the unique architecture of the CagT4SS and its comparably large dimensions. In case of the *Y. enterolitica* T3SS, rejection of substrates fused to the rigid folded Ub or DHFR could be rationalized by the incompatibility with the lumen of the type III needle (20 Å diameter) (Lee and Schneewind, 2002). Structural analyses of the *L. pneumophila* complex indicated a comparably wide inner diameter (ca. 60 Å) of the central channel in the periplasm and the outer membrane, but an only 30 Å comprising pore through the inner membrane that might be the bottleneck for substrate transport (Chetrit *et al.,* 2018). So far, the exact inner diameter of the CagT4SS apparatus and its narrowest part are not known. The opening of the OMCC at the bacterial cell surface that is built by the VirB10 homolog CagY was calculated to have an inner diameter of 35 Å (Chung 2019) and is so far the smallest diameter assigned for the CagT4SS. However, it remains unclear, how rigid the system is *in vivo*.

Taken together, protein unfolding is most likely required for transport via the CagT4SS. Hence, the inability to translocate GFP resulted from the general resistance of GFP to get unfolded that was already observed in other systems (Akeda and Galán, 2005). According to this, the unfolding of Ub would require less energy, or the comparably small fusion protein can be maintained in an unfolded state insight the bacteria, thus enabling the translocation of HiBiT-Ub-CagA.

The observation, that the TEM-1 β-lactamase, that has a similar size as GFP, is well translocated together with CagA (Schindele *et al.,* 2016) additionally indicated that rigid folding and not the size of the fusion partner limits the translocation via the CagT4SS. This could further be confirmed by investigating the transport of CagA fused to DHFR. As described for other systems (Amyot *et al.,* 2013; Lee and Schneewind, 2002), this fusion protein *per se* was only poorly translocated, but translocation was completely blocked when the bacteria were treated with the active-site ligand MTX, that irreversibly binds to the folded DHFR arresting it in a fully folded conformation (Eilers and Schatz, 1986).

Due to the presence of a C-terminal signaling sequence as well as the incapability of the N-terminal D1 domain to fold autonomously, it was previously postulated, that CagA is channeled

into the secretion system with the C-terminus first (Woon *et al.,* 2013). The present data further underline this hypothesis, since the N-terminal fusion partners GFP and DHFR could clearly fold prior to the translocation process. Thus, CagA is not co-translationally translocated, but might be carried by its chaperone CagF to the IMC ATPases and the secretion system. This would be similar to the type III secretion process, where it is already described, that the substrates are initially bound in a partially unfolded conformation by their respective chaperones and subsequently carried to the ATPase complex for complete unfolding and translocation (Akeda and Galán, 2005). But in marked contrast, translocation via the *Y. enterocolitica* Ysc T3SS, for example, strictly requires the permanent maintenance of the cargo protein in an unfolded state, as reasoned from the inability of folate analogs to block the secretion of DHFR fusion proteins (Feldman *et al.,* 2002).

The finding that the co-expression of DHFR-CagA and HiBiT-CagA resulted in drastically reduced HiBiT-CagA translocation rates compared to a strain only producing HiBiT-CagA could be explained by a blocking of the secretion channel by the poorly unfoldable DHFR-fusion or by a competition for binding to the chaperone CagF or other resources required prior to the secretion initiation. The observation that the addition of the inhibitor MTX and the resulting tight folding could further reduce the transfer of HiBiT-CagA more strongly supports the first possibility, assuming that CagF successfully passes the DHFR-CagA fusion protein to the ATPase center followed by an introduction with the C-terminus first into the secretion channel. DHFR would then act as a plug preventing successful translocation, while at the same time the partly transferred protein could not easily be released from the secretion channel. A similar phenomenon was already observed for the *Y. enterocolitica* Ysc system (Feldman *et al.,* 2002): The injectisome was jammed by a fusion protein of the full-length effector YopE (*Yersinia* outer protein E) with DHFR but not by DHFR fused to shorter versions of YopE. Thus, it was postulated, that the secretion machinery can reject proteins, if they are not deeply engaged into the secretion channel.

Taken together, these data further support that CagA is directly transported from the cytoplasm through the T4SS and that transfer requires prior unfolding. However, it remains unclear how the oncoprotein is delivered across the membrane of the host cell and if CagA is directly injected or initially brought to the bacterial surface and subsequently translocated. Surface-exposed CagA was already detected in previous studies (Kwok *et al.,* 2007; Jiménez-Soto *et al.,* 2009; Murata-Kamiya *et al.,* 2010), but delivery of CagA into the host cell was not observed after co-incubation of AGS cells with bacterial lysates (Schindele *et al.,* 2016).

It is in general assumed, that the direct contact between donor and recipient is strictly required for T4SS-dependent translocation with the exception of the above-mentioned Ptx that once secreted into the extracellular space binds to host cell receptors and thus mediates its endocytosis (Christie *et al.,* 2014; Locht *et al.,* 2011). While T3SS were shown to build

membrane pores to translocate their respective substrates (Costa *et al.,* 2015), it remains unclear how the effectors of T4SS cross the host cell membrane.

A current hypothesis suggests, that the internalization of CagA is mediated via the interaction of PS in the host cell membrane with basic patches in the D3 domain of CagA (Murata-Kamiya *et al.,* 2010), but the exact mechanisms remain unclear. Further work is needed to characterize the role of surface-exposed CagA and address the question of the transport across the third and final membrane.

5.4 *Cag*PAI components with unknown function – Analysis of *cagε*, *cagQ/R* and *cagB*

Almost two thirds of the *cag*PAI open reading frames encode for genes that lack any homologs in the prototypical VirB/D4 T4SS. Most of them were shown to be either involved in the apparatus assembly or in the translocation of the effector protein CagA, however, the function of some genes is still unknown. To get new insights, in the present work RNAseq data and the HiBiT-LgBiT split luciferase complementation system were combined to analyze the expression and synthesis of four so far uncharacterized *cag*PAI genes. The data strongly suggest that *cagε*, *cagQ* and *cagB* but not *cagR* are constitutively transcribed in strain P12 under standard culture conditions. Previous studies could show that *cagζ* and *cagε* are organized as an operon that might also include *cagδ* and *cagγ*. Cagδ is an essential component of the OMCC and Cagγ is the VirB1-homologous enzyme involved in peptidoglycan hydrolysis, but the function of Cagζ and Cagε remains unknown (Fischer, 2011). Recently Cagζ synthesis by *H. pylori* strain NCTC11637 was proven via immunoblot (Wang *et al.,* 2016), but conflicting data exist regarding the relevance of Cagζ for CagT4SS functionality (Fischer *et al.,* 2001; Wang *et al.,* 2016). Using the HiBiT-LgBiT system, no translation of *cagε* was detectable in strain P12 under the tested conditions. Systematic mutagenesis experiments indicated that Cagε is dispensable for CagA translocation and IL-8 induction (Fischer *et al.,* 2001), but an epidemiological study in East Asia revealed a putative correlation between allelic variants of *cagε* and certain EPIYA motifs (Schmidt *et al.,* 2010). Furthermore, in some Japanese *H. pylori* strains, Cagε and Cagδ were expressed as one fusion protein which did not impact the CagA translocation capacity (Azuma *et al.,* 2004). Further work is needed to characterize the expression and function of *cagε*.

Early work on the *cag*PAI annotated the two open reading frames *cagQ* and *cagR* as putative genes located antisense to each other (Censini *et al.,* 1996). The data obtained in the present work and previous characterizations of TSS (see Figure 4.27) suggest, that *cagQ,* but not *cagR*, is protein encoding. Conflicting data exist regarding the impact of CagQ on the CagT4SS: while systematic mutagenesis experiments in strain 26695 indicated that CagQ is not involved in the type IV secretion activity *in vitro* (Fischer *et al.,* 2001), others reported a negative impact on CagA levels and postulated an effect on CagT4SS activity (Yao *et al.,* 2018). In the present work, HiBiT-CagQ levels were only marginal and a deletion of *cagQ* in

strain P12 did not affect CagA translocation. The low protein levels measured are intriguing, since the *cagQ* promotor was already shown to be one of the strongest promotors of the *cag*PAI in strain G27 (Vannini *et al.,* 2014). To get further insights into the biological relevance of CagQ, interaction partners and differential synthesis could be analyzed *in vitro* using the HiBiT-tagged protein. Furthermore, CagQ production could be examined in other *H. pylori* strains.

Despite the prediction of two TSS upstream of *cagB* (Spohn *et al.,* 1997), and intensive studies on the promotor activity under different environmental conditions (Vannini *et al.,* 2014), so far nothing is known about this gene. Recently, *cagB* mRNA was shown to be upregulated upon biofilm formation, but functional data are not available (Hathroubi *et al.,* 2020).

Using the split-luciferase-based complementation assay, the production of CagB could be shown for the first time. The overall synthesis level was rather low, but fitted well with the weak expression detected via RNAseq. This is in line with the observation that the promotor of this monocistronic operon is comparably weak (Vannini *et al.,* 2014). Subcellular fractionation experiments indicated that the major part of HiBiT-CagB is membrane associated even though previous predictions categorized CagB as a soluble, cytoplasmic protein (Fischer, 2011). A possible explanation could be that the protein is strongly interacting with some inner membrane-associated components and hence mainly co-precipitates with the insoluble fraction.

So far, CagB was assumed to be non-essential for T4SS assembly and the translocation of CagA. However, due to the high sensitivity of the HiBiT-CagA reporter assay, it could be shown that Δ*cagB* mutant strains of *H. pylori* P12 and G27 have an impaired secretion activity. In the respective strains, HiBiT-CagA translocation was reduced to about 50-80 % of the wt levels. This phenotype could be complemented by reintroducing *cagB* and its upstream region in the *recA* locus (pCL31), but was not restored by *cagB* under the control of the *cagA* promotor (pCL28). Two different reasons are possible: (1) CagB protein levels must be tightly regulated for full functionality, which is not given by the strong *cagA* promotor, or (2) the coding sequence of CagB is not correctly annotated in the P12 genome and the open reading frame introduced by pCL28 is not functional. Indeed, two different translational start codons were mentioned before (Spohn *et al.,* 1997) and additional experiments are needed to distinguish between them.

To further characterize CagB and its function within the CagT4SS, interaction studies as well as analyses of protein levels under different environmental conditions are feasible. The above-mentioned study on the activity of the *cagB* promotor already indicated, that growth phase of the bacteria and pH of the medium could have a strong impact (Vannini *et al.,* 2014).

5.5 Drug repositioning – Targeting the CagT4SS with the anti-cancer drug cisplatin

Research and development of novel therapeutics is prone to high failure rates and associated with immense costs and risks. Drug repositioning is the strategy to identify new applications for already approved or investigational drugs and is now frequently used to reduce development times, costs and risks (Ashburn and Thor, 2004; Pushpakom *et al.,* 2019).

The Library of Pharmacologically Active Compounds (LOPAC^{1280} library, Sigma-Aldrich) comprises a collection of inhibitors mainly targeting neurotransmission, but also a wide range of other cell signaling pathways covering all major drug target classes (LOPAC1280 – Library of Pharmacologically Active Compounds | Sigma-Aldrich, 2021). A screening of this compound collection with the TEM-CagA reporter assay identified the anti-cancer drug cisplatin as a potential inhibitor of the *H. pylori* CagT4SS. In tumor therapy the DNA crosslinking properties of cisplatin are used to arrest cancer cell growth and to induce apoptosis. Furthermore, in different bacterial species growth-arresting properties of cisplatin were observed and the effects were likely to depend on cisplatin-induced DNA damage (Rosenberg *et al.,* 1965; Chowdhury *et al.,* 2016; Yuan *et al.,* 2018).

In contrast, the data obtained in the present work clearly indicated that the inhibition of the type IV secretion in *H. pylori* is not dependent on the interaction of cisplatin with genomic DNA:

The binding of the planar platinum complex with the purine bases of DNA strictly requires a prior aquation of the drug, which is not possible when cisplatin is dissolved in DMSO instead of aqueous solution (Davies *et al.,* 2000; Hall *et al.,* 2014). Furthermore, the rapid inhibition of the CagT4SS activity that was already observed after 30 min of compound exposure or even when cisplatin was added during an ongoing infection argued against an involvement of DNA interaction. DNA crosslinking by cisplatin was already shown to induce morphological changes of bacteria by causing cell division defects (Johnstone *et al.,* 2014), but cannot explain the immediate interference with CagA translocation, especially since *H. pylori* is not dividing in the minimal medium (PBS/FCS) used for co-incubation with AGS cells.

In addition, the testing of several stable platinum complexes with different DNA-binding capacities further supported the hypothesis since DNA interaction capability and T4SS inhibition did not correlate. The biologically inert platinum(IV) complex TR425, for example, was highly active in terms of CagA translocation, but was previously shown to have only a very low affinity to DNA (Rehm *et al.,* 2019). On the other hand, those compounds that bear a PPh_3 ligand (*e.g.* TR47, TR-DW13) were not able to specifically block T4SS activity, even though they are known to strongly interact with nucleic acids (Muenzner *et al.,* 2015; Rehm *et al.,* 2018). Additionally, substances were tested that act independently of ligand exchange reaction and covalent binding: platinum complexes that carry two PPh_3 exert their cytotoxic effect by non-covalent interaction with the negatively charged DNA causing aggregation rather than DNA-cross linking. All respective compounds had a strong antibacterial effect on *H. pylori*, in line with the already published cytotoxicity (Muenzner *et al.,* 2015; Rehm *et al.,* 2018). Finally

transplatin, the stereoisomer of cisplatin, that forms altered platinum-DNA adducts and is hence less cytotoxic for cancer cells (Rosenberg, 1985; Abu-Surrah and Kettunen, 2006) showed the same T4SS inhibition characteristics as cisplatin albeit with minimally reduced potency. An interference with CagA translocation but not with the bacterial growth was furthermore observed for transpalladium, that has a similar coordination chemistry as transplatin, but is prone to fast hydrolysis which might account for the comparably weak inhibitory activity (Abu-Surrah and Kettunen, 2006). Assuming that the impact on the CagT4SS is not dependent on DNA interaction, the lower inhibitory potential of transplatin could be explained by slower binding to proteins which was already described previously (Peleg-Shulman *et al.,* 2002).

Protein adducts are a major reason for severe side effects of cisplatin treatments, but also account for the resistance of cancer cells to the drug (Messori and Merlino, 2016). It is, for example, well known that cisplatin is highly bound by proteins of the blood plasma (De Conti *et al.,* 1973), furthermore, cisplatin reacts with copper trafficking proteins to enter the target cells and mutations of such transporters are associated with resistance towards the drug (Boal and Rosenzweig, 2009; Wang and Lippard, 2005). A further mechanism of cisplatin inactivation is the increased production of glutathione: since thiol-platinum(II) complexes are more stable than the respective amine complexes (Appleton, 1997), glutathione can sequester the drug and thereby prevent the DNA interaction (Wang and Lippard, 2005). In general, sulfur-containing molecules or amino acids like cysteine and methionine can react with cisplatin without prior aquation (Wexselblatt *et al.,* 2012), while this step is essential and rate-limiting for the interaction with DNA, *e.g*. the N7 atom of guanine (Davies *et al.,* 2000; Kozelka, 2009). Thus, cisplatin dissolved in DMSO can readily form protein but not DNA adducts and might be causative for the inhibitory effect on the type IV secretion activity in *H. pylori*. The observation that the addition of cysteine or methionine but not alanine was sufficient to cause an inactivation of cisplatin further supported this mode of action. An interference of cisplatin with cysteine-rich proteins of pathogenic bacteria was previously described: Inteins, that are self-splicing elements for example found in *Mycobacterium tuberculosis* were shown to form cisplatin adducts via cysteine residues essential for the functionality of the proteins (Zhang *et al.,* 2011; Chan *et al.,* 2016). Furthermore, the co-administration of cisplatin dissolved in DMSO protected mice from the lethal effects of *Bacillus anthracis* lethal toxin (Moayeri *et al.,* 2006). Notably, these experiments were performed with purified proteins and thus completely independent of cisplatin-DNA interaction.

Assuming that the observed inhibitory effect on CagA translocation is based on cisplatin protein interactions, virtually any cysteine- or methionine-containing protein could be targeted by the drug. Such unspecific binding might explain the impact on bacterial viability that was observed in the minimal medium PBS/FCS, but is unlikely to account for the rapid interference with the CagT4SS activity, especially since CagA translocation but not adherence to the host

cells was inhibited if the drug was added during an ongoing infection. Furthermore, a direct effect on the secretion process is feasible, since it is known that cysteine residues and the formation of disulfide bonds are important for full functionality of the CagT4SS which is indicated by the observation that a mutant strain lacking the disulfide bond oxidoreductase gene *hp0231* is defective for CagA translocation (Zhong *et al.,* 2016). Moreover, disulfide bonds were shown to be involved in the structural stability of the VirB10 homolog CagY, that is essential for CagT4SS functionality (Delahay *et al.,* 2008). Finally, disulfide bonds are essential for the interaction of the adhesin HopQ with CEACAMs and thus crucial for CagA translocation (Hamway *et al.,* 2020). However, since cisplatin could inhibit CagT4SS activity in a Δ*hopQ* mutant strain (Lettl *et al.,* 2020), the interference with the HopQ-CEACAM interaction was excluded to account for the observed effects.

Finally, NuoB and NuoD, two proteins of the respiratory chain complex I, contain cysteine and methionine residues in their substrate-binding interface (see Table 4.7). Indeed, adverse effects of cisplatin on the mitrochondrial respiration due to the interference with complex I-IV activity were already described previoulsy (Kruidering *et al.,* 1997). In case of *H. pylori*, an inhibition of the energy providing respiratory chain drastically impacts the delivery of the oncoprotein as shown in section 4.3.2.4. However, in contrast to the highly specific complex I inhibitors #14, #16 and #17, binding of cisplatin to the Nuo complex proteins is most likely only one out of many interactions.

Taken together, cisplatin dissolved in DMSO probably deploys the interference with the CagT4SS via reacting with cysteine- or methionine-containing proteins, but the exact target remains unknown. While it is clearly bactericidal in minimal medium, cisplatin as well as other highly active NHC-platinum complexes were readily inactivated in complex media, hence, further work is needed to evaluate the feasibility to develop derivatives that specifically target CagA translocation and are sufficiently stable under *in vivo* conditions.

5.6 Pathogen blockers with pathoblocker activity – Inhibitors of the respiratory chain complex I

In the present work, inhibitors of the eukaryotic respiratory chain complex I were shown to specifically impede the growth of *H. pylori* with IC_{50} and MIC values in the nanomolar range. Intriguingly, those compounds could block type IV secretion activity within minutes, pointing towards a direct interference with the translocation process.

Using various experimental setups, the subcellular target of three novel inhibitors was investigated. General approaches monitoring oxygen consumption, membrane potential and ATP content of the bacteria hinted towards interference with cellular respiration. The ^{13}C-surplus profiles obtained by isotopologue profiling analyses resembled the reference inhibitor rotenone, indicating, that the compounds act on the respiratory chain complex I. Finally, mutants in two proteins of the respiratory chain complex I were identified to be less sensitive

towards #14, #16 and #17. Notably, those amino acid exchanges that conferred high resistance were connected to severe growth defects. However, several observations supported that the NuoB/NuoD interface is the direct target site of the inhibitors and argued against an unspecific drug tolerance due to metabolic adaption: First, the mutants were only cross-resistant to the reference complex I inhibitor rotenone but not to the complex III-targeting drug antimycin A. Second, mutants were only obtained after several passages on serum plates with sub-lethal concentrations of the respective compounds, *i.e*. under experimental conditions mimicking classical evolution. Recently, such laboratory setups were shown to favor the emergence of mutations in the direct target genes and not indirect resistance mechanisms due to alterations in metabolic pathways (Lopatkin *et al.,* 2021). In contrast, the authors established a method to induce a "metabolic evolution" by altering culture conditions to decrease the overall metabolic activity and by exposing the bacteria for short time periods to high antibiotic concentrations followed by incubations without selection pressure. Indeed, this approach resulted in a significant redistribution of resistance mechanisms. But since in the present work a classical evolution approach was conducted, the mutations in genes of the respiratory chain are most likely directly linked to altered compound-binding to the target. This was further supported and rationalized by *in silico* modelling followed by directed testing of compound analogs (ACA#1-6). As predicted, derivatives of #17 with extended linker region were active against the T27N^{NuoB} mutant, the strain with the most pronounced resistance against various compounds.

In the following, the proposed binding to the NuoB/NuoD interfaced is discussed with particular focus on species-specificity including recently published experimental data on the binding of the inhibitors rotenone and piericidin A, two compounds that were active against *H. pylori*, too. In 2020, cryo-electron microscopy structures of the mitochondrial NADH:ubiquinone oxidoreductase bound to these inhibitors were solved to a resolution of less than 2.5 Å or 3 Å, respectively (Kampjut and Sazanov, 2020; Bridges *et al.,* 2020). Rotenone was co-purified with ovine complex I and identified at two different sites of the quinone-binding pocket as well as at a third unrelated position in ND4 (= NuoM) that is involved in proton pumping (Kampjut and Sazanov, 2020). Within the quinone pocket built by NDUFS2/49kDa (= NuoD), NDUFS7/PSST (= NuoB) and ND1 (= NuoH), rotenone was found at the first and second quinone-binding site, in the former one clearly mimicking the conformation of ubiquinone during reduction by the iron-sulfur cluster N2. This was rather unexpected, since until then, the bulky rotenone was considered to bind only outside or at the entry of the pocket, but further supports the observation, that the T27A^{NuoB}/V133M^{NuoD} mutant in *H. pylori* has reduced sensitivity to the compound. V133^{NuoD} is deep inside the binding pocket, directly adjacent to two conserved residues (H36^{NuoD}, Y85^{NuoD} = H59^{49kDa}/Y108^{49kDa} in the ovine protein, see Figure 4.49 D) that are likely to build hydrogen bonds with rotenone. A replacement with the comparably bulkier methionine might interfere and thus destabilize the binding. A similar mode of action might be

assumed in case of #16. Furthermore, the published data suggest that rotenone is interacting with T49^{PSST} (= T27^{NuoB}) via a hydrogen bond. Thus, the T27A^{NuoB} and T27N^{NuoB} variants in *H. pylori* might on the one hand confer resistance due to a lower binding affinity (T27A^{NuoB}) and on the other hand due to sterically blocking the entry of the channel (T27N^{NuoB}). Those two different modes of action might also explain the varying degrees of resistance (see MIC values, Table 4.4).

In the second study, the binding of piericidin A to the NuoB/D/H subunits of the murine heart mitochondria was characterized (Bridges *et al.,* 2020). Structural data indicated, that two piericidin A molecules can bind simultaneously to the quinone-binding pocket covering the full length of the channel. Again, the authors observed a possible interaction with T156^{49kDa} (residue corresponding to V133^{NuoD} in *H. pylori*). Interestingly, in *Y. lipolytica*, this particular residue was already previously described to be decisive for the susceptibility towards rotenone but not to 2-decyl-4-quinazolinylamine (DQA) that is closely related to #17. Compared to the wt (S192^{NUCM} (residue corresponding to V133^{NuoD} in *H. pylori*)) a S192T^{NUCM} mutant was highly more sensitive to rotenone but not to DQA (Angerer *et al.,* 2012). Interestingly, different studies observed reduced NADH:ubiquinone oxidoreductase activity in such S192^{NUCM} mutants (Tocilescu *et al.,* 2007; Angerer *et al.,* 2012), in line with the reduced respiratory activity detected in the *H. pylori* V133M^{NuoD} mutant, indicating a minimal tolerance of structural changes in the perfectly arranged quinone-binding pocket.

As an additional example for resistance caused by a single amino acid exchange *Streptomyces mobaraensis* should be mentioned. The gram-positive bacterium is the original source of piericidin A, and resistant to its own toxin due to an amino acid exchange in NuoD (Y108W^{NuoD}, residue corresponding to Y85^{NuoD} in *H. pylori*) (Degli Esposti, 2015).

Thus, even though the residues in the quinone-binding pocket are highly conserved between different species (see Table 4.7 and Table 4.8), minimal differences are sufficient to confer resistance and can thus explain the specific inhibition of *H. pylori*.

In addition, already soon after its discovery, *H. pylori* was found to be in general more susceptible to antibiotics compared, for example, to the closely related *C. jejuni* (Goodwin *et al.,* 1986). A reason could be that the bacterium possesses highly active, unspecific uptake systems or less efficient drug efflux pumps. In contrast, *E. coli* can easily avoid high intracellular concentrations of the herein tested compounds, as indicated by the higher susceptibility observed in the efflux deficient Δ*tolC* mutant.

Furthermore, *H. pylori* might be especially sensitive to interference with cellular respiration, since in contrast to other bacteria, the respiratory chain of *H. pylori* is comparably simple. Indeed, the overall arrangement rather resembles that of the mitochondria than the branched version observed in most aerobic or microaerobic bacteria (Kelly *et al.,* 2001).

In line with this, others already reported a highly potent and specific inhibition of *H. pylori* by complex I inhibitors (Iwahi *et al.,* 1991; Nagata *et al.,* 2001; Mills *et al.,* 2004; Mugengana *et al.,* 2021).

Importantly, in contrast to other bacteria, that rely on different NADH deydrogenases, namely combinations of the NADH:ubiquinone oxidoreductase (Ndh1 = complex I), the alternative type II NADH:ubiquinone oxidoreductase (Ndh2) and the Na^+-translocating NADH:ubiquinone oxidoreductase (Kaila and Wikström, 2021), the *nuo* encoded complex I is the only initial electron acceptor of the respiratory chain in *H. pylori*. Similarly, mammalian cellular respiration is entirely based on the NADH:ubiquinone oxidoreductase, but in marked contrast to the eukaryotic system the complex I of *H. pylori* most likely uses exclusively menaquinone instead of ubiquinone as electron acceptor (Marcelli *et al.,* 1996). In bacteria, ubiquinone is typically used for aerobic respiration, while menaquinone is part of anaerobic respiration processes (Sharma *et al.,* 2012; Unden and Bongaerts, 1997). The two coenzymes differ in the structure of the head group, hence, the quinone-binding pocket of *H. pylori* should be particularly adapted to menaquinone, rendering the architecture of the pocket species-specific and thus a good target for selective inhibitors.

Finally, based on the simple composition of the respiratory chain, *H. pylori* should hypothetically be sensitive to inhibitors of other complexes, too. However, the bacteria tolerated high doses of complex III inhibitors (see Table 4.3). Antimycin A-cytochrome b interaction was extensively studied in the model organism *Saccharomyces cerevisiae* (Ding *et al.,* 2006; Rotsaert *et al.,* 2008). The low potency of antimycin A against *H. pylori* can be rationalized by sequence comparison with the cytochrome b of *S. cerevisiae* (HPP12_1545 vs. P00163): Despite a low overall sequence similarity (<31%), several residues known to be involved in antimycin A interaction are conserved (*e.g.* $K228^{P00163}$/$K256^{HPP12\_1545}$, $D229^{P00163}$/$D257^{HPP12\_1545}$). But strikingly, *H. pylori* cytochrome b carries phenylalanine instead of leucine at position 221 (= residue 198 in yeast), which was previously reported to confer resistance to antimycin A and other complex III inhibitors like ilicicolin H and funiculosin (Ding *et al.,* 2006).

In summary, while *H. pylori* seems to be intrinsically less susceptible to complex III inhibitors, complex I inhibitors are strong and specific antibiotics against the bacterium. The particular architecture of the NuoB/NuoD interface in combination with poor drug efflux and the dependency on a single initial electron acceptor render *H. pylori* highly sensitive.

In addition to the new approach to develop species-specific anti-*H. pylori* compounds, the complex I inhibitors turned out to strongly interfere with CagT4SS activity. This gave further insights into the CagA translocation process and might offer the possibility to design pathoblockers. The observation that the addition of #14, #16 and #17 or rotenone during an ongoing infection resulted in a decrease in absolute RLU values in less than 10 min, as observed via the real-time translocation assay, clearly pointed towards a direct interference with CagA translocation. In contrast, the protein biosynthesis inhibitor erythromycin, that was

previously shown to hinder CagA delivery of pre-treated bacteria (Schindele *et al.,* 2016), could not block an ongoing secretion process. This indicates, that after establishing cell contact and starting type IV secretion, the system is not strictly and permanently dependent on *de novo* protein biosynthesis. Similar observations were previously reported for the Dot/Icm system of *L. pneumophila* (Charpentier *et al.,* 2009).

Previously, the complex I inhibitor piericidin A was found to block the Ysc T3SS needle assembly in *Y. pseudotuberculosis*, but the effect shown to be independent of the complex I inhibition (Duncan *et al.,* 2014; Morgan *et al.,* 2017). In contrast, experiments monitoring CagA-translocation of a V133M^{NuoD} mutant in the presence of the novel anti-*H. pylori* compound #16 clearly indicated, that T4SS inhibition is directly and only caused by interference with the respiratory chain complex I activity in *H. pylori*.

Since the respiratory chain complex I is involved in the translocation of protons across the inner membrane, it is relevant to maintain the PMF which in turn is linked to the cellular ATP content. The immediate interference of the small molecule inhibitors with the CagA translocation process might thus be directly caused by the destruction of the PMF or by the resulting depletion of intracellular ATP.

For T3SS that are evolutionary related to flagella (Denise *et al.,* 2020), the dependency on the PMF is well known (Wilharm *et al.,* 2004). Furthermore, the PMF is the driving force of the Tat secretion system, where either the electric potential (Δψ) or the proton gradient (ΔpH), the two components of the PMF, is sufficient (Frain *et al.,* 2019). In contrast, the Sec pathway depends on PMF and ATP hydrolysis (Collinson, 2019). For type II secretion systems and T4SS, it is still unclear, whether the cargo transport is driven by ATP hydrolysis or PMF. Especially the discrimination between requirements for secretion apparatus assembly and for effector translocation hamper a clear answer. Nevertheless, experimental evidence exists, that the archetypical delivery of the T-DNA by the VirB/D4 secretion system is driven by ATP hydrolysis and not by the PMF (Cascales and Christie, 2004a). In this case, the cytosolic ATPases VirB11 and VirD4 sense the energy status of the cell in form of ATP and thereby induce a conformational change in the membrane-spanning VirB10 subunits, which in turn is a prerequisite for T-DNA transfer. The authors suggest two possible scenarios: the conformational change of VirB10 is (1) a late state of apparatus assembly that establishes the connection between the inner and the outer membrane complex or (2) opens the channel for the passage of the substrate.

Combining the observations, that in the present study the small molecule inhibitors immediately and drastically interfered with CagA translocation (Figure 4.54) and to the same extent resulted in cellular ATP depletion (Figure 4.45 C), but had only minor impacts on the membrane potential (Figure 4.57), hints towards a dependency on ATP hydrolysis. This is in line with already published data regarding the Dot/Icm system of *L. pneumophila* (Charpentier *et al.,* 2009) and is supported by the finding that inhibitors of the ATPase and VirB11 ortholog

Cagα can interfere with CagA translocation (Hilleringmann *et al.,* 2006). Even though this observation cannot discriminate between apparatus assembly and CagA translocation.

Taken together, the novel anti-*H. pylori* compounds are highly potent and species-specific. They furthermore strongly interfere with a major virulence principle of the bacteria, the delivery of the oncoprotein CagA, in *in vitro* infections of gastric epithelial cells. Emergence of resistance was rarely observed, probably due to the high fitness costs of the respective mutants. While strictly anaerobic bacteria were in general resistant to the inhibitors, since they lack the respective target, all tested aerobic species were resistant as well. Thus, the new compounds are unlikely to disturb the healthy gut microbiome, preventing typical adverse side effects of broad-spectrum antibiotic treatments.

In vitro cytotoxicity experiments indicated a considerably lower susceptibility of mammalian cells to the tested inhibitors, compared to the concentrations required for *H. pylori* growth inhibition. It is worth to mention, that respiratory chain complex I inhibitors are already in use or under investigation as drugs in humans. Recently, an inhibitor of the NADH:ubiquinone oxidoreductase was shown to be highly active against cancer cells and first *in vitro* data indicated an otherwise low cytotoxicity (Molina *et al.,* 2018). Furthermore, metformin that is commonly used to treat type II diabetes and that is under investigation to be applied as anti-cancer medication, is a biguanide inhibitor that amongst others interferes with the respiratory chain complex I. Interestingly biguanides are used in anti-malaria therapy as well, targeting the pathogenic parasites. While metformin accumulates in the mammalian mitochondria and hence targets the human organism, anti-malaria drugs like proguanil and cycloguanil are excluded from the mammalian mitochondria and are hence selectively toxic for the parasites. (Bridges *et al.,* 2014)

The small molecule inhibitors identified and characterized in the present work already fulfill basic requirements, like species specificity and high potency. But further chemical design certainly offers the possibility to lower the risk of the emergence of resistance. Furthermore, in follow-up studies, pharmacological properties of the compounds have to be analyzed and improved to select for derivatives with suitable profiles to be tested *in vivo* for their *H. pylori* eradication potential.

5.7 Summary and outlook

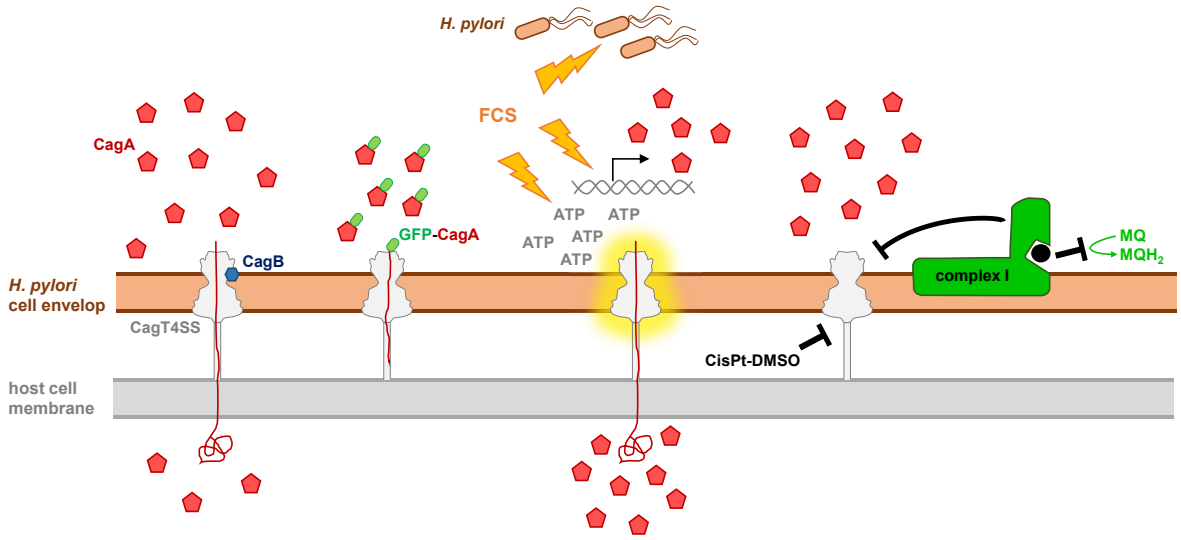

Figure 5.1 Graphical summary. In the present work novel insights into the CagA translocation process were obtained and several small molecule inhibitors targeting CagT4SS activity were characterized. It was shown that beside a fast onset of CagT4SS activity immediately after the start infection, only a minor amount of the total available CagA (red pentagons/red line) is translocated via the CagT4SS (grey silhouette). CagB (blue hexagon) was identified as a further *cag*PAI encoded protein involved in the translocation process. Various experiments indicated that unfolding of effector proteins is a prerequisite for the transport via the CagT4SS. *E.g.* fusion of CagA with tightly folded GFP (green oval) prevented translocation. It was further observed, that preincubation of the bacteria in media supplemented with FCS (yellow flashes) resulted in increased motility (depicted as *H. pylori* with flagella), as well as in CagA translocation priming (yellow shining CagT4SS) likely due to elevated energy levels (indicated as “ATP”) and induced protein biosynthesis of the effector CagA. Upon dissolving in DMSO, the anti-cancer drug cisplatin (CisPt-DMSO) was shown to directly interfere with T4SS function in a protein-interaction based mode of action. Finally, the quinone binding pocket of the respiratory chain complex I (green silhouette) was identified as the subcellular target of three novel small molecule inhibitors (representative black circle). Interference with bacterial respiration and the consequential immediate depletion of ATP was found to directly impact CagA translocation.

The split-luciferase-based CagA translocation assay developed in the present work is the first method to monitor CagA translocation *in vitro* in real time. The novel reporter system is highly sensitive and robust with a wide range of applications, complementing the recently developed β-lactamase-dependent CagA translocation assay. Using this system, novel insights into the secretion process were obtained that pave the way for the development of inhibitors targeting the CagT4SS. A graphical summary is given in Figure 5.1.

Besides the intriguing observation, that the bacteria only inject a minor amount of their available CagA pool, the fast onset of the CagA translocation process indicated a priming of CagT4SS activity during the *in vitro* preculture that was strictly dependent on yet unknown factors in the FCS. Notably, those factors were shown to be dispensable for bacterial viability. First experiments indicated that the availability of newly synthesized translocation-competent CagA might be decisive for the observed priming, but the exact mechanisms remain to be

further investigated. Certainly, interference with the CagT4SS priming should be considered as a promising strategy to develop pathoblockers.

In addition, the dependency of the CagA translocation process on a continuous energy supply was observed: inhibitors that interfered with bacterial ATP levels immediately blocked the oncoprotein delivery. A possible explanation could be that protein unfolding, that was shown to be strictly required for CagA translocation, is highly energy consuming.

Combining CagA translocation quantification and measurement of the total bacterial CagA, the HiBiT-CagA reporter assay was adapted to discriminate between different modes to interfere with the translocation process: while the deletion of the apparatus component CagT or the adhesin HopQ directly affected the secretion process, the loss of motility was only indirectly associated with reduced CagA translocation. In future studies, this assay setup can be easily applied to investigate the mode of action of inhibitors.

Finally, the so far uncharacterized *cag*PAI encoded CagB was identified to be involved in the CagA translocation process. Further work is needed to clarify its function within the CagT4SS.

In addition to the basic research on type IV secretion activity and CagA translocation, several small molecule inhibitors were investigated: cisplatin and three eukaryotic respiratory chain inhibitors that all inhibit *H. pylori* growth were shown to directly interfere with the translocation of CagA. While the exact mode of action of cisplatin remained unclear, the NuoB/NuoD interface was identified as the subcellular target of #14, #16 and #17. Extensive characterization of those three compounds was conducted, including the investigation of resistance mechanisms, first SAR studies and *in vitro* cytotoxicity evaluation. In the next steps, the pharmacological applicability should be investigated via *in vitro* pharmacokinetic experiments and ADME-tox studies.

6 Appendix

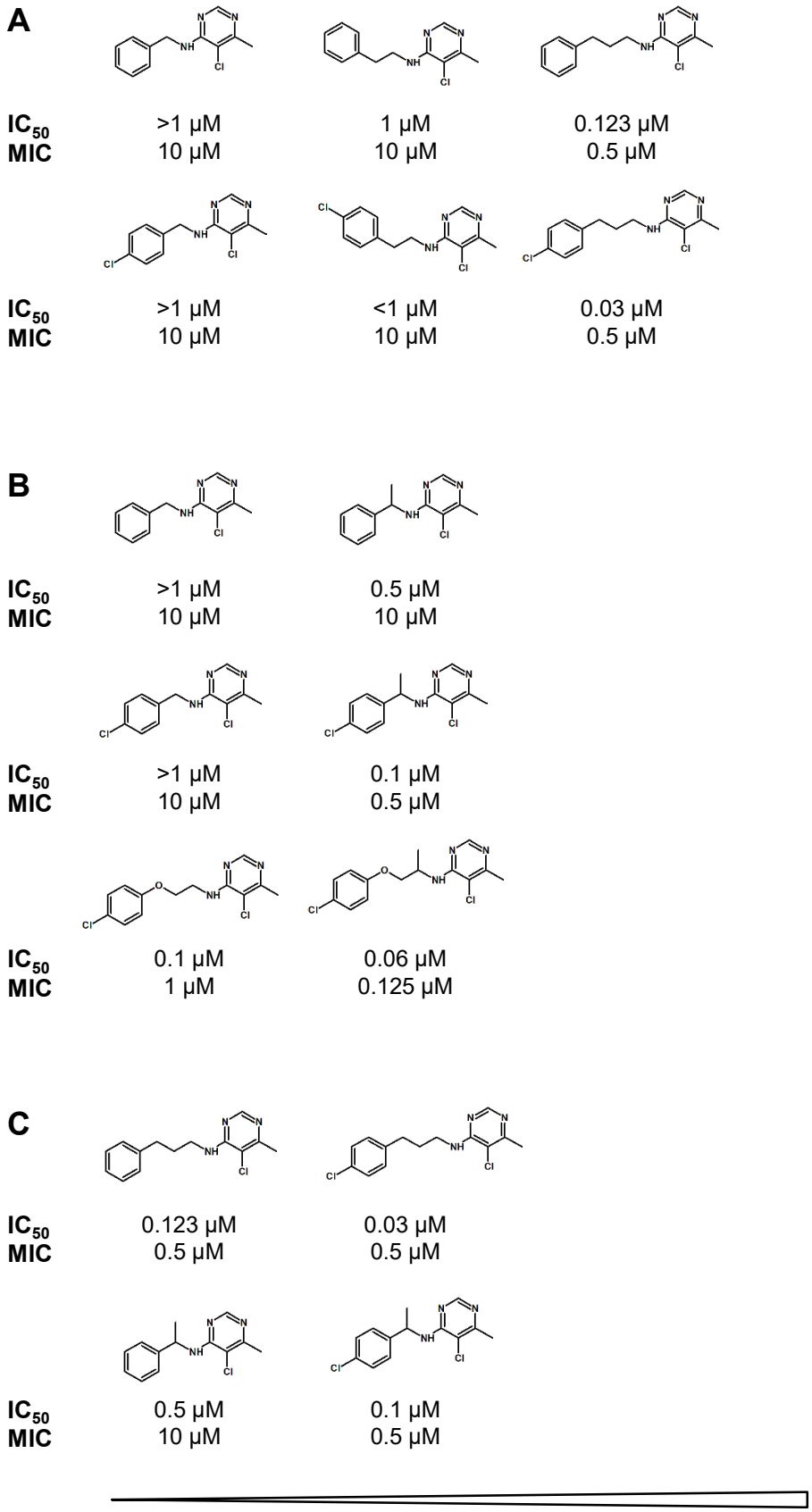

Figure 6.1 SAR – #14

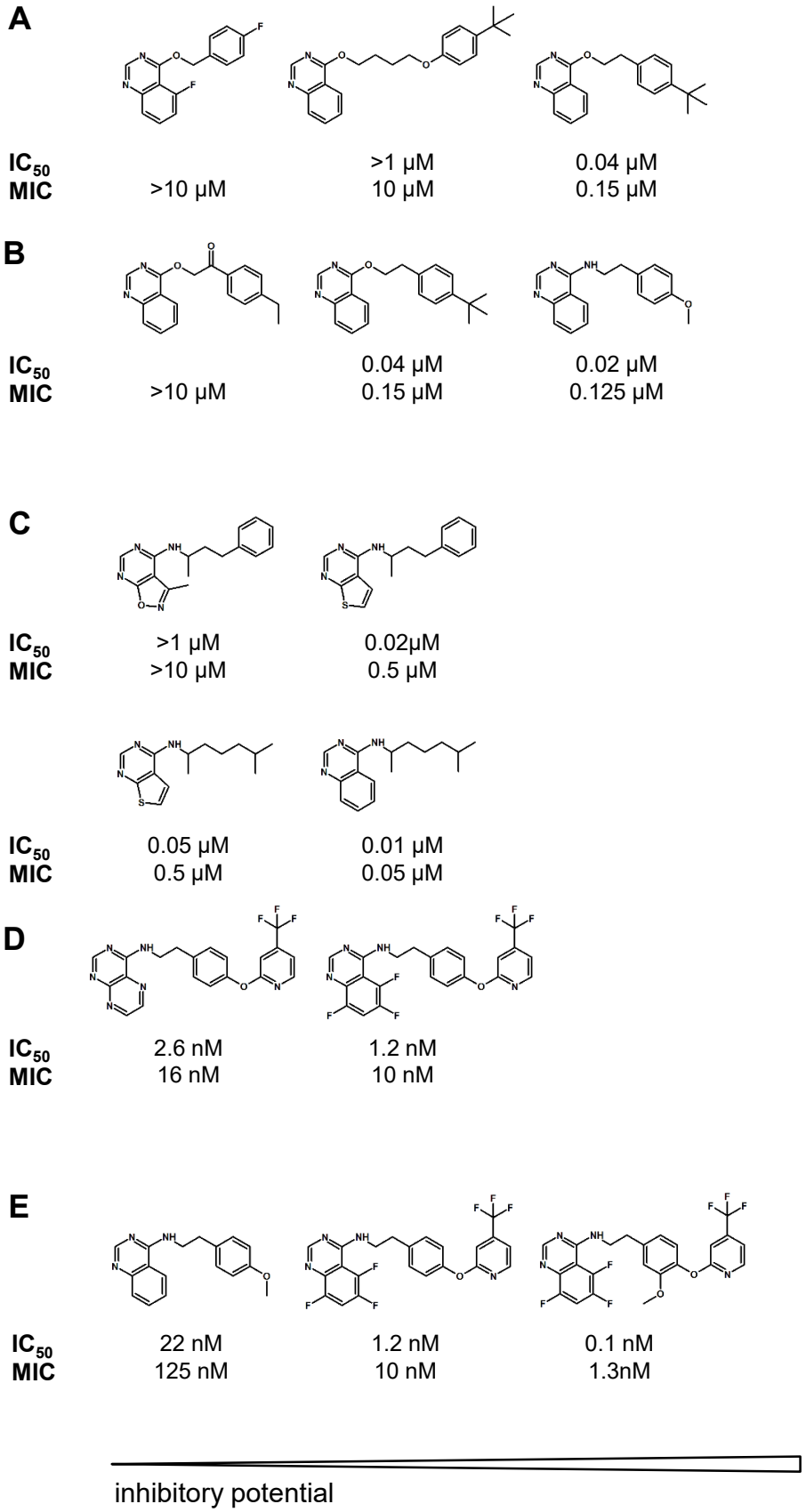

Figure 6.2 SAR – #17

7 List of abbreviations

#14	Diflumetorim
#16	Fenpyroximate
#17	Fenazaquin
A	Absorbance at the indicated wavelength
AlpA/B	Adherence-associated lipoproteins A and B
Amp^R	Ampicillin resistance
AP	Alkaline phosphatase
APS	Ammonium peroxide sulfate
ASPP2	Apoptosis stimulating protein of p53 2
ATP	Adenosine triphosphate
BabA	Blood group antigen-binding adhesin A
BB	Brucella broth
BB/FCS	Brucella broth/10 % FCS
BCIP	5-Bromo-4-chloro-3-indolyl phosphate
BHI	Brain heart infusion
bp	Base pair
C	Cytoplasmic
c-Abl	Abelson murine leukemia viral oncogene homolog 1
cag/Cag	Cytotoxin-associated gene
CagA	Cytotoxin-associated gene A
*cag*PAI	*cag* pathogenicity island
CBS	C-terminal binding sequence
CCCP	Carbonyl cyanide m-chlorophenyl hydrazine
CEACAM	Carcinoembryonic antigen-related cell adhesion molecule
cfu	Colony-forming unit
CM	CagA-multimerization motif
Cm^R	Chloramphenicol resistance
CMV	Cytomegalovirus
COG	Clusters of orthologous groups of proteins
CRPIA	Conserved repeat responsible for phosphorylation-independent activity
CSK	C-terminal Src kinase
CtkA	Cell translocating kinase A
DAPI	4′,6-Diamidino-2-phenylindole dihydrochloride
DC	Dendritic cell
DHFR	Dihydrofolate reductase
$DiOC_2(3)$)	3,3-Diethyloxacarbocyanine iodide
DMEM	Dulbecco´s Modified Eagle medium
DMF	Dimethylformamide
DMSO	Dimethyl sulfoxide
DNA	Deoxyribonucleic acid
dNTP	Deoxyribonucleotide triphosphate
dNTP	Deoxynucleotide triphosphate
Dot/Icm	Defect in organelle trafficking and intracellular multiplication
D-PBS	Dulbecco’s PBS without calcium and magnesium

DQA	2-Decyl-4-quinazolinylamine
DUF	Domain of unknown function
EDTA	Ethylenediaminetetraacetic acid
ELISA	Enzyme-linked immunosorbent assay
EPIYA	Glutamic acid-proline-isoleucine-tyrosine-alanine (amino acid sequence)
Erm^R	Erythromycin resistance
FACS	Fluorescence activated cell sorting
FAK	focal adhesion kinase
FCS	Fetal calf serum
FMN	Flavin mononucleotide
g	Relative centrifugal force
GC/MS	Gas chromatography/mass spectrometry
GFP	Green fluorescent protein
GGT	γ-Glutamyl transpeptidase
HiBiT	High affinity bioluminescence tag
HopQ	*Helicobacter* outer membrane protein Q
HtrA	High-temperature requirement A
I	Fluorescence intensity at the indicated wavelength
IC50	Half maximal inhibitory concentration
IgV	Variable domain of immunoglobulins
IL-8/10	Interleukin-8
IM	Inner membrane
IMC	Inner membrane complex
IP	Immunoprecipitation
Kan^R	Kanamycin resistance
kb	Kilo base
kDa	Kilodalton
LB	Lennox-L broth
Le^b	Lewis b
LgBiT	Large bioluminescence tag
LJ	Left junction
LPS	Lipopolysaccharide
MALT	Mucosa-associated lymphoid tissue
MARK	Microtubule affinity regulating kinase (= PAR-1)
MIC	Minimal inhibitory concentration
MOI	Multiplicity of infection
MOPS	3-(*N*-morpholino)propanesulfonic acid
MQ	Menaquinone
MQH_2	Menaquinol
MTX	Methotrexate
NA	Not annotated
NAD(P)	Nicotinamide adenine dinucleotide (phosphate)
NBS	N-terminal binding sequence
NBT	Nitro blue tetrazolium
Ndh1	NADH:ubiquinone oxidoreductase (complex I)

Ndh2	Alternative NADH-ubiquinone oxidoreductase
NE	Not essential
NHC	N-heterocyclic carbene
NO	Nitric oxide
ns	Not significant
nt	Nucleotide
OD_{550}	Optical density at 550 nm
OipA	Outer inflammatory protein A
OM	Outer membrane
OMCC	Outer membrane core complex
OMP	Outer membrane protein
Opti-MEM	Improved Minimal Essential Medium
PAMP	Pathogen-associated molecular pattern
PAR-1	Polarity regulating serine/threonine kinase partitioning defective-1
PBP	Penicillin-binding protein
PBS	Phosphate-buffered saline
PBS*	D-PBS supplemented with the protease and phosphatase inhibitors
PBS/FCS	D-PBS/10 % FCS
PCR	Polymerase chain reaction
PEP	Phosphoenolpyruvate
PMF	Proton motive force
PMSF	Phenylmethylsulfonyl fluoride
pO_2	Partial oxygen pressure
POX	Horse radish peroxidase
PP	Periplasmic
PPh_3	Triphenylphosphane
PPI	Proton-pump inhibitor
PPXY	Prolin-prolin-X-tyrosin sequence
PR	Periplasmic ring
PS	Phosphatidylserine
Ptx	Pertussis toxin
pTyr	Phosphorylated tyrosine
PVDF	Polyvinylidene difluoride
RIPA	Radioimmunoprecipitation buffer
RJ	Right junction
RLU	Relative light unit
RNA	Ribonucleic acid (r: ribosomal, m: messenger)
ROS	Reactive oxygen species
rpm	Revolutions per minute
RPMI	Roswell Park Memorial Institute medium
RT	Room temperature
RUNX2	Runt-related transcription factor 2
S	Surface-exposed or supernatant
SA	Secretion apparatus components
SabA	Sialic acid-binding protein A

SC	Supportive components
SDS	Sodium dodecyl sulfate
SDS-PAGE	Sodium dodecyl sulfate-polyacrylamide gel electrophoresis
Sec pathway	General secretory pathway
SH2-domain	Src homology 2 domain
SHP	SH2-domain-containing phosphatase
SHP-2	Src homology region 2 domain-containing phosphatase-2
SipA	Salmonella invasion protein A
SOD	superoxide dismutase
spp.	*Species pluralis*
src	Sarcoma
Str^R	Streptomycin resistance
T3SS	Type III secretion system
T4SS	Type IV secretion system
TAE	Tris-acetate-EDTA
Tat pathway	Twin-arginine translocation pathway
TBS(-T)	Tris-buffered saline (with Tween)
TCA	Tricarboxylic acid
T-DNA	Transfer-DNA
TEM/TEM-1	*E. coli* β-lactamase
TEMED	Tetramethylethylenediamine
TF	Translocation factors
Tfs3/4	Type IV secretion system 3 and 4
TLR	Toll-like receptor
TMR	Tetramethylrhodamine
TNF-α	Tumor necrosis factor α
TolC	Tolerance colicin E1
TSS	Transcription start site
Ub	Ubiquitin
v/v	Volume to volume ratio
VacA	Vacuolating toxin
Vir	Virulence
w/v	Weight to volume ratio
WHO	World health organization
wt	Wild-type
WW motif	Tryptohan-tryptophan motif
YopE	*Yersinia* outer protein E

8 List of figures

9 List of tables

References

Abu-Surrah AS, Kettunen M (2006): Platinum group antitumor chemistry: design and development of new anticancer drugs complementary to cisplatin. *Current medicinal chemistry* 13 (11):1337–1357.

Adam V, Martins A (2016): Crystal structure of rsEGFP2 in the fluorescent on-state.

Akeda Y, Galán JE (2005): Chaperone release and unfolding of substrates in type III secretion. *Nature* 437 (7060):911–915.

Alkim H, Koksal AR, Boga S, Sen I, Alkim C (2017): Role of Bismuth in the Eradication of Helicobacter pylori. *American journal of therapeutics* 24 (6):e751-e757.

Amyot WM, deJesus D, Isberg RR (2013): Poison domains block transit of translocated substrates via the Legionella pneumophila Icm/Dot system. *Infection and immunity* 81 (9):3239–3252.

Andersen-Nissen E, Smith KD, Strobe KL, Barrett SLR, Cookson BT, Logan SM, Aderem A (2005): Evasion of Toll-like receptor 5 by flagellated bacteria. *Proceedings of the National Academy of Sciences of the United States of America* 102 (26):9247–9252.

Ando T, Peek RM, Pride D, Levine SM, Takata T, Lee Y-C *et al.* (2002): Polymorphisms of Helicobacter pylori HP0638 reflect geographic origin and correlate with cagA status. *Journal of Clinical Microbiology* 40 (1):239–246.

Angerer H, Nasiri HR, Niedergesäß V, Kerscher S, Schwalbe H, Brandt U (2012): Tracing the tail of ubiquinone in mitochondrial complex I. *Biochimica et biophysica acta* 1817 (10):1776–1784.

Annibale G, Cattalini L, Canovese L, Michelon G, Marangoni G, Tobe ML (1983): Reactivity of sulfoxides toward the tetrachloroplatinate(II) anion. *Inorg. Chem.* 22 (6):975–978.

Appleton TG (1997): Donor atom preferences in complexes of platinum and palladium with amino acids and related molecules. *Coordination Chemistry Reviews* 166:313–359.

Aras RA, Kang J, Tschumi AI, Harasaki Y, Blaser MJ (2003): Extensive repetitive DNA facilitates prokaryotic genome plasticity. *Proceedings of the National Academy of Sciences of the United States of America* 100 (23):13579–13584.

Arslan N, Yılmaz Ö, Demiray-Gürbüz E (2017): Importance of antimicrobial susceptibility testing for the management of eradication in Helicobacter pylori infection. *World journal of gastroenterology* 23 (16):2854–2869.

Arya T, Oudouhou F, Casu B, Bessette B, Sygusch J, Baron C (2019): Fragment-based screening identifies inhibitors of ATPase activity and of hexamer formation of Cagα from the Helicobacter pylori type IV secretion system. *Sci Rep* 9 (1):6474.

Arzanlou M, Chai WC, Venter H (2017): Intrinsic, adaptive and acquired antimicrobial resistance in Gram-negative bacteria. *Essays in biochemistry* 61 (1):49–59.

Asakura H, Churin Y, Bauer B, Boettcher JP, Bartfeld S, Hashii N *et al.* (2010): Helicobacter pylori HP0518 affects flagellin glycosylation to alter bacterial motility. *Molecular microbiology* 78 (5):1130–1144.

Ashburn TT, Thor KB (2004): Drug repositioning: identifying and developing new uses for existing drugs. *Nat Rev Drug Discov* 3 (8):673–683.

Atherton JC (2006): The pathogenesis of Helicobacter pylori-induced gastro-duodenal diseases. *Annual review of pathology* 1:63–96.

Auld DS, Narahari J, Ho P, Casalena D, Nguyen V, Cirbaite E *et al.* (2018): Characterization and Use of TurboLuc Luciferase as a Reporter for High-Throughput Assays. *Biochemistry* 57 (31):4700–4706.

Avilés-Jiménez F, Reyes-Leon A, Nieto-Patlán E, Hansen LM, Burgueño J, Ramos IP *et al.* (2012): In vivo expression of Helicobacter pylori virulence genes in patients with gastritis, ulcer, and gastric cancer. *Infection and immunity* 80 (2):594–601.

Aziz RK, Khalifa MM, Sharaf RR (2015): Contaminated water as a source of Helicobacter pylori infection: A review. *Journal of Advanced Research* 6 (4):539–547.

Azuma T, Yamakawa A, Yamazaki S, Ohtani M, Ito Y, Muramatsu A *et al.* (2004): Distinct diversity of the cag pathogenicity island among Helicobacter pylori strains in Japan. *Journal of Clinical Microbiology* 42 (6):2508–2517.

Baba T, Ara T, Hasegawa M, Takai Y, Okumura Y, Baba M *et al.* (2006): Construction of Escherichia coli K-12 in-frame, single-gene knockout mutants: the Keio collection. *Molecular systems biology* 2:2006.0008.

Backert S, Tegtmeyer N, Selbach M (2010): The versatility of Helicobacter pylori CagA effector protein functions: The master key hypothesis. *Helicobacter* 15 (3):163–176.

Bagnoli F, Buti L, Tompkins L, Covacci A, Amieva MR (2005): Helicobacter pylori CagA induces a transition from polarized to invasive phenotypes in MDCK cells. *Proceedings of the National Academy of Sciences of the United States of America* 102 (45):16339–16344.

Baradaran R, Berrisford JM, Minhas GS, Sazanov LA (2013): Crystal structure of the entire respiratory complex I. *Nature* 494 (7438):443–448.

Bauer B, Pang E, Holland C, Kessler M, Bartfeld S, Meyer TF (2012): The Helicobacter pylori virulence effector CagA abrogates human β-defensin 3 expression via inactivation of EGFR signaling. *Cell Host & Microbe* 11 (6):576–586.

Behrens IK (2020): The role of human CEACAMs for the interaction of Helicobacter pylori with neutrophils. Ludwig-Maximilians-Universität München.

Behrens IK, Busch B, Ishikawa-Ankerhold H, Palamides P, Shively JE, Stanners C *et al.* (2020): The HopQ-CEACAM Interaction Controls CagA Translocation, Phosphorylation, and Phagocytosis of Helicobacter pylori in Neutrophils. *mBio* 11 (1).

Belogolova E, Bauer B, Pompaiah M, Asakura H, Brinkman V, Ertl C *et al.* (2013): Helicobacter pylori outer membrane protein HopQ identified as a novel T4SS-associated virulence factor. *Cellular Microbiology* 15 (11):1896–1912.

Bergé C, Waksman G, Terradot L (2017): Structural and Molecular Biology of Type IV Secretion Systems. *Current topics in microbiology and immunology* 413:31–60.

Berrisford JM, Baradaran R, Sazanov LA (2016): Structure of bacterial respiratory complex I. *Biochimica et biophysica acta* 1857 (7):892–901.

Björkholm B, Sjölund M, Falk PG, Berg OG, Engstrand L, Andersson DI (2001): Mutation frequency and biological cost of antibiotic resistance in Helicobacter pylori. *Proceedings of the National Academy of Sciences of the United States of America* 98 (25):14607–14612.

Blaser MJ, Perez-Perez GI, Kleanthous H, Cover TL, Peek RM, Chyou PH *et al.* (1995): Infection with Helicobacter pylori strains possessing cagA is associated with an increased risk of developing adenocarcinoma of the stomach. *Cancer Res* 55 (10):2111–2115.

Boal AK, Rosenzweig AC (2009): Crystal structures of cisplatin bound to a human copper chaperone. *Journal of the American Chemical Society* 131 (40):14196–14197.

Bonis M, Ecobichon C, Guadagnini S, Prévost M-C, Boneca IG (2010): A M23B family metallopeptidase of Helicobacter pylori required for cell shape, pole formation and virulence. *Molecular microbiology* 78 (4):809–819.

Bonsor DA, Sundberg EJ (2019): Roles of Adhesion to Epithelial Cells in Gastric Colonization by Helicobacter pylori. *Advances in experimental medicine and biology* 1149:57–75.

Bonsor DA, Zhao Q, Schmidinger B, Weiss E, Wang J, Deredge D *et al.* (2018): The Helicobacter pylori adhesin protein HopQ exploits the dimer interface of human CEACAMs to facilitate translocation of the oncoprotein CagA. *The EMBO Journal* 37 (13).

Boonjakuakul JK, Canfield DR, Solnick JV (2005): Comparison of Helicobacter pylori virulence gene expression in vitro and in the Rhesus macaque. *Infection and immunity* 73 (8):4895–4904.

Bray F, Ferlay J, Soerjomataram I, Siegel RL, Torre LA, Jemal A (2018): Global cancer statistics 2018: GLOBOCAN estimates of incidence and mortality worldwide for 36 cancers in 185 countries. *CA: A Cancer Journal for Clinicians* 68 (6):394–424.

Bridges HR, Fedor JG, Blaza JN, Di Luca A, Jussupow A, Jarman OD *et al.* (2020): Structure of inhibitor-bound mammalian complex I. *Nat Commun* 11 (1):5261.

Bridges HR, Jones AJY, Pollak MN, Hirst J (2014): Effects of metformin and other biguanides on oxidative phosphorylation in mitochondria. *Biochem J* 462 (3):475–487.

Bugaytsova JA, Björnham O, Chernov YA, Gideonsson P, Henriksson S, Mendez M *et al.* (2017): Helicobacter pylori Adapts to Chronic Infection and Gastric Disease via pH-Responsive BabA-Mediated Adherence. *Cell Host & Microbe* 21 (3):376–389.

Busch B, Weimer R, Woischke C, Fischer W, Haas R (2015): Helicobacter pylori interferes with leukocyte migration via the outer membrane protein HopQ and via CagA translocation. *International journal of medical microbiology : IJMM* 305 (3):355–364.

Buti L, Spooner E, van der Veen AG, Rappuoli R, Covacci A, Ploegh HL (2011): Helicobacter pylori cytotoxin-associated gene A (CagA) subverts the apoptosis-stimulating protein of p53 (ASPP2) tumor suppressor pathway of the host. *PNAS* 108 (22):9238–9243.

Calhoun MW, Gennis RB (1993): Demonstration of separate genetic loci encoding distinct membrane-bound respiratory NADH dehydrogenases in Escherichia coli. *Journal of bacteriology* 175 (10):3013–3019.

Cao P, Cover TL (2002): Two different families of hopQ alleles in Helicobacter pylori. *Journal of Clinical Microbiology* 40 (12):4504–4511.

Cascales E, Christie PJ (2004a): Agrobacterium VirB10, an ATP energy sensor required for type IV secretion. *Proceedings of the National Academy of Sciences of the United States of America* 101 (49):17228–17233.

Cascales E, Christie PJ (2004b): Definition of a bacterial type IV secretion pathway for a DNA substrate. *Science (New York, N.Y.)* 304 (5674):1170–1173.

Casu B, Smart J, Hancock MA, Smith M, Sygusch J, Baron C (2016): Structural Analysis and Inhibition of TraE from the pKM101 Type IV Secretion System. *The Journal of biological chemistry* 291 (45):23817–23829.

Celli JP, Turner BS, Afdhal NH, Keates S, Ghiran I, Kelly CP *et al.* (2009): Helicobacter pylori moves through mucus by reducing mucin viscoelasticity. *Proceedings of the National Academy of Sciences of the United States of America* 106 (34):14321–14326.

Censini S, Lange C, Xiang Z, Crabtree JE, Ghiara P, Borodovsky M *et al.* (1996): cag, a pathogenicity island of Helicobacter pylori, encodes type I-specific and disease-associated virulence factors. *Proceedings of the National Academy of Sciences of the United States of America* 93 (25):14648–14653.

Centers for Disease Control and Prevention (1999): Achievements in Public Health, 1900-1999: Control of Infectious Diseases. Morbidity and Mortality Weekly Report (48(29):621-629). https://www.cdc.gov/mmwr/preview/mmwrhtml/mm4829a1.htm, (accessed 11/28/2020).

Chan H, Pearson CS, Green CM, Li Z, Zhang J, Belfort G *et al.* (2016): Exploring Intein Inhibition by Platinum Compounds as an Antimicrobial Strategy. *J. Biol. Chem.* 291 (43):22661–22670.

Chandran V, Fronzes R, Duquerroy S, Cronin N, Navaza J, Waksman G (2009): Structure of the outer membrane complex of a type IV secretion system. *Nature* 462 (7276):1011–1015.

Chang WL, Yeh YC, Sheu BS (2018): The impacts of H. pylori virulence factors on the development of gastroduodenal diseases. *Journal of Biomedical Science* 25 (1):68.

Charpentier X, Gabay JE, Reyes M, Zhu JW, Weiss A, Shuman HA (2009): Chemical genetics reveals bacterial and host cell functions critical for type IV effector translocation by Legionella pneumophila. *PLOS Pathogens* 5 (7):e1000501.

Chen M, Andersen LP, Zhai L, Kharazmi A (1999): Characterization of the respiratory chain of Helicobacter pylori. *FEMS Immunol Med Microbiol* 24 (2):169–174.

Chetrit D, Hu B, Christie PJ, Roy CR, Liu J (2018): A unique cytoplasmic ATPase complex defines the Legionella pneumophila type IV secretion channel. *Nat Microbiol* 3 (6):678–686.

Chevalier C, Thiberge JM, Ferrero RL, Labigne A (1999): Essential role of Helicobacter pylori gamma-glutamyltranspeptidase for the colonization of the gastric mucosa of mice. *Molecular microbiology* 31 (5):1359–1372.

Chowdhury N, Wood TL, Martínez-Vázquez M, García-Contreras R, Wood TK (2016): DNA-crosslinker cisplatin eradicates bacterial persister cells. *Biotechnology and bioengineering* 113 (9):1984–1992.

Christie PJ, Whitaker N, González-Rivera C (2014): Mechanism and structure of the bacterial type IV secretion systems. *Biochimica et biophysica acta* 1843 (8):1578–1591.

Chung JM, Sheedlo MJ, Campbell AM, Sawhney N, Frick-Cheng AE, Lacy DB *et al.* (2019): Structure of the Helicobacter pylori Cag type IV secretion system. *eLife* 8.

Churin Y, Al-Ghoul L, Kepp O, Meyer TF, Birchmeier W, Naumann M (2003): Helicobacter pylori CagA protein targets the c-Met receptor and enhances the motogenic response. *J Cell Biol* 161 (2):249–255.

Clyne M, Ocroinin T, Suerbaum S, Josenhans C, Drumm B (2000): Adherence of isogenic flagellum-negative mutants of Helicobacter pylori and Helicobacter mustelae to human and ferret gastric epithelial cells. *Infection and immunity* 68 (7):4335–4339.

Cody V (2005): Understanding the Role of Leu22 Variants in Methotrexate Resistance: Comparison of Wild-type and Leu22Arg Variant Mouse and Human Dihydrfolate Reductase Ternary Crystal Complexes with Methotrexate and NADPH.

Collinson I (2019): The Dynamic ATP-Driven Mechanism of Bacterial Protein Translocation and the Critical Role of Phospholipids. *Front. Microbiol.* 10:1217.

Costa TRD, Felisberto-Rodrigues C, Meir A, Prevost MS, Redzej A, Trokter M, Waksman G (2015): Secretion systems in Gram-negative bacteria: structural and mechanistic insights. *Nat Rev Microbiol* 13 (6):343–359.

Covacci A, Censini S, Bugnoli M, Petracca R, Burroni D, Macchia G *et al.* (1993): Molecular characterization of the 128-kDa immunodominant antigen of Helicobacter pylori associated with cytotoxicity and duodenal ulcer. *Proceedings of the National Academy of Sciences of the United States of America* 90 (12):5791–5795.

Cover TL, Lacy DB, Ohi MD (2020): The Helicobacter pylori Cag Type IV Secretion System. *Trends in microbiology* 28 (8):682–695.

Cristóbal RE de, Vincent PA, Salomón RA (2006): Multidrug resistance pump AcrAB-TolC is required for high-level, Tet(A)-mediated tetracycline resistance in Escherichia coli. *J Antimicrob Chemother* 58 (1):31–36.

Cullen TW, Giles DK, Wolf LN, Ecobichon C, Boneca IG, Trent MS (2011): Helicobacter pylori versus the host: remodeling of the bacterial outer membrane is required for survival in the gastric mucosa. *PLOS Pathogens* 7 (12):e1002454.

Dailidiene D, Dailide G, Kersulyte D, Berg DE (2006): Contraselectable streptomycin susceptibility determinant for genetic manipulation and analysis of Helicobacter pylori. *Applied and environmental microbiology* 72 (9):5908–5914.

Datsenko KA, Wanner BL (2000): One-step inactivation of chromosomal genes in Escherichia coli K-12 using PCR products. *Proceedings of the National Academy of Sciences of the United States of America* 97 (12):6640–6645.

Davies GR, Banatvala N, Collins CE, Sheaff MT, Abdi Y, Clements L, Rampton DS (1994): Relationship between infective load of Helicobacter pylori and reactive oxygen metabolite production in antral mucosa. *Scandinavian Journal of Gastroenterology* 29 (5):419–424.

Davies MS, Berners-Price SJ, Hambley TW (2000): Slowing of cisplatin aquation in the presence of DNA but not in the presence of phosphate: improved understanding of sequence selectivity and the roles of monoaquated and diaquated species in the binding of cisplatin to DNA. *Inorg. Chem.* 39 (25):5603–5613.

De Conti RC, Toftness BR, Lange RC, Creasey WA (1973): Clinical and pharmacological studies with cis-diamminedichloroplatinum (II). *Cancer Res* 33 (6):1310–1315.

De Jonge R, Durrani Z, Rijpkema SG, Kuipers EJ, Van Vliet AHM, Kusters JG (2004): Role of the Helicobacter pylori outer-membrane proteins AlpA and AlpB in colonization of the guinea pig stomach. *Journal of Medical Microbiology* 53 (Pt 5):375–379.

De Martel C, Georges D, Bray F, Ferlay J, Clifford GM (2020): Global burden of cancer attributable to infections in 2018: a worldwide incidence analysis. *The Lancet. Global health* 8 (2):e180-e190.

Degli Esposti M (1998): Inhibitors of NADH–ubiquinone reductase: an overview. *Biochimica et Biophysica Acta (BBA) - Bioenergetics* 1364 (2):222–235.

Degli Esposti M (2015): Genome Analysis of Structure-Function Relationships in Respiratory Complex I, an Ancient Bioenergetic Enzyme. *Genome Biology and Evolution* 8 (1):126–147.

Del Giudice MG, Döhmer PH, Spera JM, Laporte FT, Marchesini MI, Czibener C, Ugalde JE (2016): VirJ Is a Brucella Virulence Factor Involved in the Secretion of Type IV Secreted Substrates. *J. Biol. Chem.* 291 (23):12383–12393.

Delahay RM, Balkwill GD, Bunting KA, Edwards W, Atherton JC, Searle MS (2008): The highly repetitive region of the Helicobacter pylori CagY protein comprises tandem arrays of an alpha-helical repeat module. *Journal of molecular biology* 377 (3):956–971.

Denise R, Abby SS, Rocha EPC (2020): The Evolution of Protein Secretion Systems by Co-option and Tinkering of Cellular Machineries. *Trends in microbiology* 28 (5):372–386.

Dickey SW, Cheung GYC, Otto M (2017): Different drugs for bad bugs: antivirulence strategies in the age of antibiotic resistance. *Nature reviews. Drug discovery* 16 (7):457–471.

Ding MG, Di Rago JP, Trumpower BL (2006): Investigating the Qn site of the cytochrome bc1 complex in Saccharomyces cerevisiae with mutants resistant to ilicicolin H, a novel Qn site inhibitor. *The Journal of biological chemistry* 281 (47):36036–36043.

Dinos GP (2017): The macrolide antibiotic renaissance. *British journal of pharmacology* 174 (18):2967–2983.

Dixon AS, Schwinn MK, Hall MP, Zimmerman K, Otto P, Lubben TH *et al.* (2016): NanoLuc Complementation Reporter Optimized for Accurate Measurement of Protein Interactions in Cells. *ACS chemical biology* 11 (2):400–408.

Dixon MF (2001): Chapter 38: Pathology of Gastritis and Peptic Ulceration. In: Harry L. T. Mobley, George L. Mendz und Stuart L. Hazell (Hg.): Helicobacter pylori. Physiology and Genetics. Washington, DC: ASM Press.

Dodds DR (2017): Antibiotic resistance: A current epilogue. *Biochemical Pharmacology* 134:139–146.

Dooley CP, Cohen H, Fitzgibbons PL, Bauer M, Appleman MD, Perez-Perez GI, Blaser MJ (1989): Prevalence of Helicobacter pylori infection and histologic gastritis in asymptomatic persons. *The New England journal of medicine* 321 (23):1562–1566.

Duncan MC, Wong WR, Dupzyk AJ, Bray WM, Linington RG, Auerbuch V (2014): An NF-κB-based high-throughput screen identifies piericidins as inhibitors of the Yersinia pseudotuberculosis type III secretion system. *Antimicrobial agents and chemotherapy* 58 (2):1118–1126.

Durie CL, Sheedlo MJ, Chung JM, Byrne BG, Su M, Knight T *et al.* (2020): Structural analysis of the Legionella pneumophila Dot/Icm Type IV Secretion System Core Complex. *bioRxiv*:2020.08.28.271460.

Eaton KA, Krakowka S (1994): Effect of gastric pH on urease-dependent colonization of gnotobiotic piglets by Helicobacter pylori. *Infection and immunity* 62 (9):3604–3607.

Eaton KA, Suerbaum S, Josenhans C, Krakowka S (1996): Colonization of gnotobiotic piglets by Helicobacter pylori deficient in two flagellin genes. *Infection and immunity* 64 (7):2445–2448.

Eberl C, Ring D, Münch PC, Beutler M, Basic M, Slack EC *et al.* (2019): Reproducible Colonization of Germ-Free Mice With the Oligo-Mouse-Microbiota in Different Animal Facilities. *Front. Microbiol.* 10:2999.

Eilers M, Schatz G (1986): Binding of a specific ligand inhibits import of a purified precursor protein into mitochondria. *Nature* 322 (6076):228–232.

Eisenreich W, Slaghuis J, Laupitz R, Bussemer J, Stritzker J, Schwarz C *et al.* (2006): 13C isotopologue perturbation studies of Listeria monocytogenes carbon metabolism and its modulation by the virulence regulator PrfA. *Proceedings of the National Academy of Sciences of the United States of America* 103 (7):2040–2045.

England CG, Ehlerding EB, Cai W (2016): NanoLuc: A Small Luciferase Is Brightening Up the Field of Bioluminescence. *Bioconjugate chemistry* 27 (5):1175–1187.

Enninga J, Mounier J, Sansonetti P, van Tran Nhieu G (2005): Secretion of type III effectors into host cells in real time. *Nat Methods* 2 (12):959–965.

Estibariz I, Overmann A, Ailloud F, Krebes J, Josenhans C, Suerbaum S (2019): The core genome m5C methyltransferase JHP1050 (M.Hpy99III) plays an important role in orchestrating gene expression in Helicobacter pylori. *Nucleic acids research* 47 (5):2336–2348.

Fallone CA, Chiba N, van Zanten SV, Fischbach L, Gisbert JP, Hunt RH *et al.* (2016): The Toronto Consensus for the Treatment of Helicobacter pylori Infection in Adults. *Gastroenterology* 151 (1):51-69.e14.

Feldman MF, Müller S, Wüest E, Cornelis GR (2002): SycE allows secretion of YopE-DHFR hybrids by the Yersinia enterocolitica type III Ysc system. *Molecular microbiology* 46 (4):1183–1197.

Fichtinger-Schepman AM, van der Veer JL, Hartog JH den, Lohman PH, Reedijk J (1985): Adducts of the antitumor drug cis-diamminedichloroplatinum(II) with DNA: formation, identification, and quantitation. *Biochemistry* 24 (3):707–713.

Filloux A (2004): The underlying mechanisms of type II protein secretion. *Biochimica et biophysica acta* 1694 (1-3):163–179.

Finel M (1998): Does NADH play a central role in energy metabolism in Helicobacter pylori? *Trends in Biochemical Sciences* 23 (11):412–414.

Fischer W (2011): Assembly and molecular mode of action of the Helicobacter pylori Cag type IV secretion apparatus. *The FEBS journal* 278 (8):1203–1212.

Fischer W, Püls J, Buhrdorf R, Gebert B, Odenbreit S, Haas R (2001): Systematic mutagenesis of the Helicobacter pylori cag pathogenicity island: essential genes for CagA translocation in host cells and induction of interleukin-8. *Molecular microbiology* 42 (5):1337–1348.

Fischer W, Tegtmeyer N, Stingl K, Backert S (2020): Four Chromosomal Type IV Secretion Systems in Helicobacter pylori: Composition, Structure and Function. *Front. Microbiol.* 11:1592.

Fischer W, Windhager L, Rohrer S, Zeiller M, Karnholz A, Hoffmann R *et al.* (2010): Strain-specific genes of Helicobacter pylori: genome evolution driven by a novel type IV secretion system and genomic island transfer. *Nucleic acids research* 38 (18):6089–6101.

Fleming A (1929): On the antibacterial action of cultures of a penicillium, with special reference to their use in the isolation of B. influenzae. *The British Journal of Experimental Pathology* 10:226–236.

Fleming A (1945): Penicillin. Nobel Lecture, December 11, 1945. https://www.nobelprize.org/uploads/2018/06/fleming-lecture.pdf, (accessed 12/12/2020).

Frain KM, van Dijl JM, Robinson C (2019): The Twin-Arginine Pathway for Protein Secretion. *EcoSal Plus* 8 (2).

French GL (2006): Bactericidal agents in the treatment of MRSA infections--the potential role of daptomycin. *The Journal of antimicrobial chemotherapy* 58 (6):1107–1117.

Frick-Cheng AE, Pyburn TM, Voss BJ, McDonald WH, Ohi MD, Cover TL (2016): Molecular and Structural Analysis of the Helicobacter pylori cag Type IV Secretion System Core Complex. *mBio* 7 (1):e02001-15.

Friedrich T, Van Heek P, Leif H, Ohnishi T, Forche E, Kunze B *et al.* (1994): Two binding sites of inhibitors in NADH: ubiquinone oxidoreductase (complex I). Relationship of one site with the ubiquinone-binding site of bacterial glucose:ubiquinone oxidoreductase. *European journal of biochemistry* 219 (1-2):691–698.

Fujimoto S, Olaniyi Ojo O, Arnqvist A, WU JY, Odenbreit S, Haas R *et al.* (2007): Helicobacter pylori BabA expression, gastric mucosal injury, and clinical outcome. *Clinical gastroenterology and hepatology : the official clinical practice journal of the American Gastroenterological Association* 5 (1):49–58.

Fungicide Resistance Action Committee (FRAC): FRAC Code List 2021. Fungal control agents sorted by cross resistance pattern and mode of action (including coding for FRAC Groupson product labels). https://www.frac.info/docs/default-source/publications/frac-code-list/frac-code-list-2021--final.pdf?sfvrsn=f7ec499a_2, (accessed 5/31/2021).

Gall A, Gaudet RG, Gray-Owen SD, Salama NR (2017): TIFA Signaling in Gastric Epithelial Cells Initiates the cag Type 4 Secretion System-Dependent Innate Immune Response to Helicobacter pylori Infection. *mBio* 8 (4).

Gebert B, Fischer W, Weiss E, Hoffmann R, Haas R (2003): Helicobacter pylori vacuolating cytotoxin inhibits T lymphocyte activation. *Science (New York, N.Y.)* 301 (5636):1099–1102.

Geibel S, Procko E, Hultgren SJ, Baker D, Waksman G (2013): Structural and energetic basis of folded-protein transport by the FimD usher. *Nature* 496 (7444):243–246.

Genta RM, Hamner H, Graham DY (1993): Gastric lymphoid follicles in Helicobacter pylori infection: Frequency, distribution, and response to triple therapy. *Human Pathology* 24 (6):577–583.

Gobert AP, McGee DJ, Akhtar M, Mendz GL, Newton JC, Cheng Y *et al.* (2001): Helicobacter pylori arginase inhibits nitric oxide production by eukaryotic cells: a strategy for bacterial survival. *Proceedings of the National Academy of Sciences of the United States of America* 98 (24):13844–13849.

Goodwin CS, Blake P, Blincow E (1986): The minimum inhibitory and bactericidal concentrations of antibiotics and anti-ulcer agents against Campylobacter pyloridis. *Journal of Antimicrobial Chemotherapy* 17 (3):309–314.

Haas R, Meyer TF, van Putten JP (1993): Aflagellated mutants of Helicobacter pylori generated by genetic transformation of naturally competent strains using transposon shuttle mutagenesis. *Molecular microbiology* 8 (4):753–760.

Hall MD, Telma KA, Chang K-E, Lee TD, Madigan JP, Lloyd JR *et al.* (2014): Say no to DMSO: dimethylsulfoxide inactivates cisplatin, carboplatin, and other platinum complexes. *Cancer research* 74 (14):3913–3922.

Hall MP, Unch J, Binkowski BF, Valley MP, Butler BL, Wood MG *et al.* (2012): Engineered luciferase reporter from a deep sea shrimp utilizing a novel imidazopyrazinone substrate. *ACS chemical biology* 7 (11):1848–1857.

Hamway Y, Taxauer K, Moonens K, Neumeyer V, Fischer W, Schmitt V *et al.* (2020): Cysteine Residues in Helicobacter pylori Adhesin HopQ are Required for CEACAM-HopQ Interaction and Subsequent CagA Translocation. *Microorganisms* 8 (4).

Hanahan D (1983): Studies on transformation of Escherichia coli with plasmids. *Journal of molecular biology* 166 (4):557–580.

Harrer A, Boehm M, Backert S, Tegtmeyer N (2017): Overexpression of serine protease HtrA enhances disruption of adherens junctions, paracellular transmigration and type IV secretion of CagA by Helicobacter pylori. *Gut pathogens* 9:40.

Hatakeyama M (2017): Structure and function of Helicobacter pylori CagA, the first-identified bacterial protein involved in human cancer. *Proc. Jpn. Acad., Ser. B* 93 (4):196–219.

Hathroubi S, Hu S, Ottemann KM (2020): Genetic requirements and transcriptomics of Helicobacter pylori biofilm formation on abiotic and biotic surfaces. *npj Biofilms Microbiomes* 6 (1):56.

Hayashi T, Senda M, Morohashi H, Higashi H, Horio M, Kashiba Y *et al.* (2012): Tertiary structure-function analysis reveals the pathogenic signaling potentiation mechanism of Helicobacter pylori oncogenic effector CagA. *Cell Host & Microbe* 12 (1):20–33.

Hazell SL, Lee A, Brady L, Hennessy W (1986): Campylobacter pyloridis and gastritis: association with intercellular spaces and adaptation to an environment of mucus as important factors in colonization of the gastric epithelium. *The Journal of infectious diseases* 153 (4):658–663.

Higashi H, Tsutsumi R, Fujita A, Yamazaki S, Asaka M, Azuma T, Hatakeyama M (2002): Biological activity of the Helicobacter pylori virulence factor CagA is determined by variation in the tyrosine phosphorylation sites. *Proceedings of the National Academy of Sciences of the United States of America* 99 (22):14428–14433.

Higashi H, Yokoyama K, Fujii Y, Ren S, Yuasa H, Saadat I *et al.* (2005): EPIYA motif is a membrane-targeting signal of Helicobacter pylori virulence factor CagA in mammalian cells. *The Journal of biological chemistry* 280 (24):23130–23137.

Hilleringmann M, Pansegrau W, Doyle M, Kaufman S, MacKichan ML, Gianfaldoni C *et al.* (2006): Inhibitors of Helicobacter pylori ATPase Cagalpha block CagA transport and cag virulence. *Microbiology* 152 (Pt 10):2919–2930.

Ho P, Yue K, Pandey P, Breault L, Harbinski F, McBride AJ *et al.* (2013): Reporter enzyme inhibitor study to aid assembly of orthogonal reporter gene assays. *ACS chemical biology* 8 (5):1009–1017.

Hofreuter D, Odenbreit S, Henke G, Haas R (1998): Natural competence for DNA transformation in Helicobacter pylori: identification and genetic characterization of the comB locus. *Molecular microbiology* 28 (5):1027–1038.

Hohlfeld S, Pattis I, Püls J, Plano GV, Haas R, Fischer W (2006): A C-terminal translocation signal is necessary, but not sufficient for type IV secretion of the Helicobacter pylori CagA protein. *Molecular microbiology* 59 (5):1624–1637.

Holcombe C (1992): Helicobacter pylori: the African enigma. *Gut* 33 (4):429–431.

Hooi JKY, Lai WY, Ng WK, Suen MMY, Underwood FE, Tanyingoh D *et al.* (2017): Global Prevalence of Helicobacter pylori Infection: Systematic Review and Meta-Analysis. *Gastroenterology* 153 (2):420–429.

Hoy B, Löwer M, Weydig C, Carra G, Tegtmeyer N, Geppert T *et al.* (2010): Helicobacter pylori HtrA is a new secreted virulence factor that cleaves E-cadherin to disrupt intercellular adhesion. *EMBO reports* 11 (10):798–804.

Hu B, Khara P, Song L, Lin AS, Frick-Cheng AE, Harvey ML *et al.* (2019): In Situ Molecular Architecture of the Helicobacter pylori Cag Type IV Secretion System. *mBio* 10 (3).

Huang D, Liu J, Shen G (2009): Cloning, expression, and enzymatic characterization of isocitrate dehydrogenase from Helicobacter pylori. *Protein J* 28 (9-10):443–447.

Hughes NJ, Clayton CL, Chalk PA, Kelly DJ (1998): Helicobacter pylori porCDAB and oorDABC genes encode distinct pyruvate:flavodoxin and 2-oxoglutarate:acceptor oxidoreductases which mediate electron transport to NADP. *Journal of bacteriology* 180 (5):1119–1128.

IARC Working Group on the Evaluation of Carcinogenic Risks to Humans (1994): INFECTION WITH HELICOBACTER PYLORI. In: Humans, IARC Working Group on the Evaluation of Carcinogenic Risks to (Hg.): Schistosomes, Liver Flukes and Helicobacter pylori: International Agency for Research on Cancer.

Inglese J, Johnson RL, Simeonov A, Xia M, Zheng W, Austin CP, Auld DS (2007): High-throughput screening assays for the identification of chemical probes. *Nat Chem Biol* 3 (8):466–479.

Insecticide Resistance Action Committee (IRAC) (2020): IRAC MoA Classification. https://irac-online.org/documents/moa-classification/, (accessed 5/31/2021).

Ishijima N, Suzuki M, Ashida H, Ichikawa Y, Kanegae Y, Saito I *et al.* (2011): BabA-mediated adherence is a potentiator of the Helicobacter pylori type IV secretion system activity. *The Journal of biological chemistry* 286 (28):25256–25264.

Iwahi T, Satoh H, Nakao M, Iwasaki T, Yamazaki T, Kubo K *et al.* (1991): Lansoprazole, a novel benzimidazole proton pump inhibitor, and its related compounds have selective activity against Helicobacter pylori. *Antimicrobial agents and chemotherapy* 35 (3):490–496.

Iwatani S, Nagashima H, Reddy R, Shiota S, Graham DY, Yamaoka Y (2014): Identification of the genes that contribute to lactate utilization in Helicobacter pylori. *PLOS ONE* 9 (7):e103506.

Javaheri A, Kruse T, Moonens K, Mejías-Luque R, Debraekeleer A, Asche CI *et al.* (2016): Helicobacter pylori adhesin HopQ engages in a virulence-enhancing interaction with human CEACAMs. *Nat Microbiol* 2:16189.

Jiménez-Soto LF, Clausen S, Sprenger A, Ertl C, Haas R (2013): Dynamics of the Cag-type IV secretion system of Helicobacter pylori as studied by bacterial co-infections. *Cellular Microbiology* 15 (11):1924–1937.

Jiménez-Soto LF, Haas R (2016): The CagA toxin of Helicobacter pylori: abundant production but relatively low amount translocated. *Sci Rep* 6:23227.

Jiménez-Soto LF, Kutter S, Sewald X, Ertl C, Weiss E, Kapp U *et al.* (2009): Helicobacter pylori type IV secretion apparatus exploits beta1 integrin in a novel RGD-independent manner. *PLOS Pathogens* 5 (12):e1000684.

John GT, Klimant I, Wittmann C, Heinzle E (2003): Integrated optical sensing of dissolved oxygen in microtiter plates: a novel tool for microbial cultivation. *Biotechnology and bioengineering* 81 (7):829–836.

Johnsson N, Varshavsky A (1994): Ubiquitin-assisted dissection of protein transport across membranes. *The EMBO Journal* 13 (11):2686–2698.

Johnstone TC, Alexander SM, Lin W, Lippard SJ (2014): Effects of monofunctional platinum agents on bacterial growth: a retrospective study. *Journal of the American Chemical Society* 136 (1):116–118.

Jungblut PR, Bumann D, Haas G, Zimny-Arndt U, Holland P, Lamer S *et al.* (2000): Comparative proteome analysis of Helicobacter pylori. *Molecular microbiology* 36 (3):710–725.

Kaebisch R, Mejías-Luque R, Prinz C, Gerhard M (2014): Helicobacter pylori cytotoxin-associated gene A impairs human dendritic cell maturation and function through IL-10-mediated activation of STAT3. *The Journal of Immunology* 192 (1):316–323.

Kaila VRI, Wikström M (2021): Architecture of bacterial respiratory chains. *Nat Rev Microbiol*:1–12.

Kampjut D, Sazanov LA (2020): The coupling mechanism of mammalian respiratory complex I. *Science* 370 (6516).

Kaplan-Türköz B, Jiménez-Soto LF, Dian C, Ertl C, Remaut H, Louche A *et al.* (2012): Structural insights into Helicobacter pylori oncoprotein CagA interaction with β1 integrin. *PNAS* 109 (36):14640–14645.

Kather B, Stingl K, van der Rest ME, Altendorf K, Molenaar D (2000): Another unusual type of citric acid cycle enzyme in Helicobacter pylori: the malate:quinone oxidoreductase. *Journal of bacteriology* 182 (11):3204–3209.

Kayali S, Manfredi M, Gaiani F, Bianchi L, Bizzarri B, Leandro G *et al.* (2018): Helicobacter pylori, transmission routes and recurrence of infection: state of the art. *Acta bio-medica : Atenei Parmensis* 89 (8-S):72–76.

Kelly DJ, Hughes NJ, Poole RK (2001): Chapter 10: Microaerobic Physiology: Aerobic Respiration, Anaerobic Respiration, and Carbon Dioxide Metabolism. In: Harry L. T. Mobley, George L. Mendz und Stuart L. Hazell (Hg.): Helicobacter pylori. Physiology and Genetics. Washington, DC: ASM Press.

Kim DJ, Park K-S, Kim J-H, Yang S-H, Yoon JY, Han B-G *et al.* (2010): Helicobacter pylori proinflammatory protein up-regulates NF-kappaB as a cell-translocating Ser/Thr kinase. *Proceedings of the National Academy of Sciences of the United States of America* 107 (50):21418–21423.

Königer V, Holsten L, Harrison U, Busch B, Loell E, Zhao Q *et al.* (2016): Helicobacter pylori exploits human CEACAMs via HopQ for adherence and translocation of CagA. *Nat Microbiol* 2:16188.

Kostrzynska M, Betts JD, Austin JW, Trust TJ (1991): Identification, characterization, and spatial localization of two flagellin species in Helicobacter pylori flagella. *Journal of bacteriology* 173 (3):937–946.

Kozelka J (2009): Molecular origin of the sequence-dependent kinetics of reactions between cisplatin derivatives and DNA. *Inorganica Chimica Acta* 362 (3):651–668.

Kruidering M, Van de Water B, De Heer E, Mulder GJ, Nagelkerke JF (1997): Cisplatin-induced nephrotoxicity in porcine proximal tubular cells: mitochondrial dysfunction by inhibition of complexes I to IV of the respiratory chain. *J Pharmacol Exp Ther* 280 (2):638–649.

Kutter S, Buhrdorf R, Haas J, Schneider-Brachert W, Haas R, Fischer W (2008): Protein subassemblies of the Helicobacter pylori Cag type IV secretion system revealed by localization and interaction studies. *Journal of bacteriology* 190 (6):2161–2171.

Kwok T, Zabler D, Urman S, Rohde M, Hartig R, Wessler S *et al.* (2007): Helicobacter exploits integrin for type IV secretion and kinase activation. *Nature* 449 (7164):862–866.

Lambert JR, Midolo P (1997): The actions of bismuth in the treatment of Helicobacter pylori infection. *Alimentary pharmacology & therapeutics* 11 Suppl 1:27–33.

Lancaster CD, Simon J (2002): Succinate:quinone oxidoreductases from ϵ-proteobacteria11Dedicated to Achim Kröger on the occasion of his 65th birthday. *Biochimica et Biophysica Acta (BBA) - Bioenergetics* 1553 (1-2):84–101.

Lee VT, Schneewind O (2002): Yop fusions to tightly folded protein domains and their effects on Yersinia enterocolitica type III secretion. *Journal of bacteriology* 184 (13):3740–3745.

Lettl C, Schindele F, Testolin G, Bär A, Rehm T, Brönstrup M *et al.* (2020): Inhibition of Type IV Secretion Activity and Growth of Helicobacter pylori by Cisplatin and Other Platinum Complexes. *Front. Cell. Infect. Microbiol.* 10:788.

Li YG, Christie PJ (2018): The Agrobacterium VirB/VirD4 T4SS: Mechanism and Architecture Defined Through In Vivo Mutagenesis and Chimeric Systems. *Current topics in microbiology and immunology* 418:233–260.

Ling N (2003): Rotenone. A review of its toxicity and use for fisheries management. Wellington, N.Z: Department of Conservation (Science for conservation, 211).

Linz B, Windsor HM, McGraw JJ, Hansen LM, Gajewski JP, Tomsho LP *et al.* (2014): A mutation burst during the acute phase of Helicobacter pylori infection in humans and rhesus macaques. *Nat Commun* 5 (1):4165.

Locht C, Coutte L, Mielcarek N (2011): The ins and outs of pertussis toxin. *The FEBS journal* 278 (23):4668–4682.

LOPAC1280 – Library of Pharmacologically Active Compounds | Sigma-Aldrich (2021). https://www.sigmaaldrich.com/life-science/cell-biology/bioactive-small-molecules/lopac1280-navigator.html, zuletzt aktualisiert am 3/20/2021, (accessed 3/22/2021).

Lopatkin AJ, Bening SC, Manson AL, Stokes JM, Kohanski MA, Badran AH *et al.* (2021): Clinically relevant mutations in core metabolic genes confer antibiotic resistance. *Science* 371 (6531).

Los GV, Encell LP, McDougall MG, Hartzell DD, Karassina N, Zimprich C *et al.* (2008): HaloTag: a novel protein labeling technology for cell imaging and protein analysis. *ACS chemical biology* 3 (6):373–382.

Low HH, Gubellini F, Rivera-Calzada A, Braun N, Connery S, Dujeancourt A *et al.* (2014): Structure of a type IV secretion system. *Nature* 508 (7497):550–553.

Lu HS, Saito Y, Umeda M, Murata-Kamiya N, Zhang HM, Higashi H, Hatakeyama M (2008): Structural and functional diversity in the PAR1b/MARK2-binding region of Helicobacter pylori CagA. *Cancer Science* 99 (10):2004–2011.

Lümmen P (1998): Complex I inhibitors as insecticides and acaricides. Dedicated to the memory of Dr. Gerhard Salbeck. *Biochimica et Biophysica Acta (BBA) - Bioenergetics* 1364 (2):287–296.

Madeira F, Park YM, Lee J, Buso N, Gur T, Madhusoodanan N *et al.* (2019): The EMBL-EBI search and sequence analysis tools APIs in 2019. *Nucleic acids research* 47 (W1):W636-W641.

Mahdavi J, Sondén B, Hurtig M, Olfat FO, Forsberg L, Roche N *et al.* (2002): Helicobacter pylori SabA adhesin in persistent infection and chronic inflammation. *Science (New York, N.Y.)* 297 (5581):573–578.

Malfertheiner P, Megraud F, O'Morain CA, Gisbert JP, Kuipers EJ, Axon AT *et al.* (2017): Management of Helicobacter pylori infection-the Maastricht V/Florence Consensus Report. *Gut* 66 (1):6–30.

Mamishi S, Eshaghi H, Mahmoudi S, Bahador A, Hosseinpour Sadeghi R, Najafi M *et al.* (2016): Intrafamilial transmission of Helicobacter pylori: genotyping of faecal samples. *British journal of biomedical science* 73 (1):38–43.

Marcelli SW, Chang HT, Chapman T, Chalk PA, Miles RJ, Poole RK (1996): The respiratory chain of Helicobacter pylori: identification of cytochromes and the effects of oxygen on cytochrome and menaquinone levels. *FEMS microbiology letters* 138 (1):59–64.

Marques AT, Vítor JMB, Santos A, Oleastro M, Vale FF (2020): Trends in Helicobacter pylori resistance to clarithromycin: from phenotypic to genomic approaches. *Microbial genomics* 6 (3).

Marshall B, Warren J (1984): Unidentified curved bacilli in the stomach of patients with gastritis and peptic ulceration. *Lancet (London, England)* 323 (8390):1311–1315.

Marshall BJ, McGechie DB, Rogers PA, Glancy RJ (1985): Pyloric Campylobacter infection and gastroduodenal disease. *The Medical journal of Australia* 142 (8):439–444.

Masetti M, Falchi F, Gioia D, Recanatini M, Ciurli S, Musiani F (2020): Targeting the Protein Tunnels of the Urease Accessory Complex: A Theoretical Investigation. *Molecules* 25 (12):2911.

McClain MS, Beckett AC, Cover TL (2017): Helicobacter pylori Vacuolating Toxin and Gastric Cancer. *Toxins* 9 (10).

Ménard R, Schoenhofen IC, Tao L, Aubry A, Bouchard P, Reid CW *et al.* (2014): Small-molecule inhibitors of the pseudaminic acid biosynthetic pathway: targeting motility as a key bacterial virulence factor. *Antimicrobial agents and chemotherapy* 58 (12):7430–7440.

Messori L, Merlino A (2016): Cisplatin binding to proteins: A structural perspective. *Coordination Chemistry Reviews* 315:67–89.

Mezencev R (2015): Interactions of cisplatin with non-DNA targets and their influence on anticancer activity and drug toxicity: the complex world of the platinum complex. *Current cancer drug targets* 14 (9):794–816.

Mills E, Baruch K, Charpentier X, Kobi S, Rosenshine I (2008): Real-time analysis of effector translocation by the type III secretion system of enteropathogenic Escherichia coli. *Cell Host & Microbe* 3 (2):104–113.

Mills SD, Yang W, MacCormack K (2004): Molecular characterization of benzimidazole resistance in Helicobacter pylori. *Antimicrobial agents and chemotherapy* 48 (7):2524–2530.

Miwa H, Go MF, Sato N (2002): H. pylori and gastric cancer: the Asian enigma. *The American journal of gastroenterology* 97 (5):1106–1112.

Moayeri M, Wiggins JF, Lindeman RE, Leppla SH (2006): Cisplatin inhibition of anthrax lethal toxin. *Antimicrobial agents and chemotherapy* 50 (8):2658–2665.

Mohi MG, Neel BG (2007): The role of Shp2 (PTPN11) in cancer. *Current opinion in genetics & development* 17 (1):23–30.

Molina JR, Sun Y, Protopopova M, Gera S, Bandi M, Bristow C *et al.* (2018): An inhibitor of oxidative phosphorylation exploits cancer vulnerability. *Nat Med* 24 (7):1036–1046.

Montecucco C, Rappuoli R (2001): Living dangerously: how Helicobacter pylori survives in the human stomach. *Nat Rev Mol Cell Biol* 2 (6):457–466.

Moodley Y, Linz B, Bond RP, Nieuwoudt M, Soodyall H, Schlebusch CM *et al.* (2012): Age of the association between Helicobacter pylori and man. *PLOS Pathogens* 8 (5):e1002693.

Morgan JM, Duncan MC, Johnson KS, Diepold A, Lam H, Dupzyk AJ *et al.* (2017): Piericidin A1 Blocks Yersinia Ysc Type III Secretion System Needle Assembly. *mSphere* 2 (1).

Mori M, Suzuki H, Suzuki M, Kai A, Miura S, Ishii H (1997): Catalase and superoxide dismutase secreted from Helicobacter pylori. *Helicobacter* 2 (2):100–105.

Mueller D, Tegtmeyer N, Brandt S, Yamaoka Y, De Poire E, Sgouras D *et al.* (2012): c-Src and c-Abl kinases control hierarchic phosphorylation and function of the CagA effector protein in Western and East Asian Helicobacter pylori strains. *The Journal of Clinical Investigation* 122 (4):1553–1566.

Muenzner JK, Rehm T, Biersack B, Casini A, De Graaf IAM, Worawutputtapong P *et al.* (2015): Adjusting the DNA Interaction and Anticancer Activity of Pt(II) N-Heterocyclic Carbene Complexes by Steric Shielding of the Trans Leaving Group. *Journal of medicinal chemistry* 58 (15):6283–6292.

Mugengana AK, Vita NA, Brown Gandt A, Moran K, Agyapong G, Sharma LK *et al.* (2021): The Discovery and Development of Thienopyrimidines as Inhibitors of Helicobacter pylori That Act through Inhibition of the Respiratory Complex I. *ACS infectious diseases*.

Murai M, Miyoshi H (2016): Current topics on inhibitors of respiratory complex I. *Biochimica et biophysica acta* 1857 (7):884–891.

Murata-Kamiya N, Kikuchi K, Hayashi T, Higashi H, Hatakeyama M (2010): Helicobacter pylori exploits host membrane phosphatidylserine for delivery, localization, and pathophysiological action of the CagA oncoprotein. *Cell Host & Microbe* 7 (5):399–411.

Nagata K, Sone N, Tamura T (2001): Inhibitory activities of lansoprazole against respiration in Helicobacter pylori. *Antimicrobial agents and chemotherapy* 45 (5):1522–1527.

Nesić D, Miller MC, Quinkert ZT, Stein M, Chait BT, Stebbins CE (2010): Helicobacter pylori CagA inhibits PAR1-MARK family kinases by mimicking host substrates. *Nat Struct Mol Biol* 17 (1):130–132.

Neuberger A, Du D, Luisi BF (2018): Structure and mechanism of bacterial tripartite efflux pumps. *Research in Microbiology* 169 (7-8):401–413.

Nishino K, Yamada J, Hirakawa H, Hirata T, Yamaguchi A (2003): Roles of TolC-dependent multidrug transporters of Escherichia coli in resistance to beta-lactams. *Antimicrobial agents and chemotherapy* 47 (9):3030–3033.

Novo D, Perlmutter NG, Hunt RH, Shapiro HM (1999): Accurate flow cytometric membrane potential measurement in bacteria using diethyloxacarbocyanine and a ratiometric technique. *Cytometry* 35 (1):55–63.

Odenbreit S, Gebert B, Püls J, Fischer W, Haas R (2001): Interaction of Helicobacter pylori with professional phagocytes: role of the cag pathogenicity island and translocation, phosphorylation and processing of CagA. *Cellular Microbiology* 3 (1):21–31.

Odenbreit S, Püls J, Sedlmaier B, Gerland E, Fischer W, Haas R (2000): Translocation of Helicobacter pylori CagA into gastric epithelial cells by type IV secretion. *Science* 287 (5457):1497–1500.

Osaki T, Konno M, Yonezawa H, Hojo F, Zaman C, Takahashi M *et al.* (2015): Analysis of intra-familial transmission of Helicobacter pylori in Japanese families. *Journal of Medical Microbiology* 64 (Pt 1):67–73.

Pallen MJ, Wren BW (1997): The HtrA family of serine proteases. *Molecular microbiology* 26 (2):209–221.

Pantoja M, Chen L, Chen Y, Nester EW (2002): Agrobacterium type IV secretion is a two-step process in which export substrates associate with the virulence protein VirJ in the periplasm. *Molecular microbiology* 45 (5):1325–1335.

Parey K, Haapanen O, Sharma V, Köfeler H, Züllig T, Prinz S *et al.* (2019): High-resolution cryo-EM structures of respiratory complex I: Mechanism, assembly, and disease. *Science Advances* 5 (12):eaax9484.

Parkin DM (2006): The global health burden of infection-associated cancers in the year 2002. *International journal of cancer* 118 (12):3030–3044.

Parsonnet J, Hansen S, Rodriguez L, Gelb AB, Warnke RA, Jellum E *et al.* (1994): Helicobacter pylori infection and gastric lymphoma. *The New England journal of medicine* 330 (18):1267–1271.

Paschos A, Hartigh A den, Smith MA, Atluri VL, Sivanesan D, Tsolis RM, Baron C (2011): An in vivo high-throughput screening approach targeting the type IV secretion system component VirB8 identified inhibitors of Brucella abortus 2308 proliferation. *Infection and immunity* 79 (3):1033–1043.

Pattis I, Weiss E, Laugks R, Haas R, Fischer W (2007): The Helicobacter pylori CagF protein is a type IV secretion chaperone-like molecule that binds close to the C-terminal secretion signal of the CagA effector protein. *Microbiology* 153 (Pt 9):2896–2909.

Peleg-Shulman T, Najajreh Y, Gibson D (2002): Interactions of cisplatin and transplatin with proteins. Comparison of binding kinetics, binding sites and reactivity of the Pt-protein adducts of cisplatin and transplatin towards biological nucleophiles. *Journal of inorganic biochemistry* 91 (1):306–311.

Pendergrass HA, May AE (2019): Natural Product Type III Secretion System Inhibitors. *Antibiotics* 8 (4).

Pereira GC, Allen WJ, Watkins DW, Buddrus L, Noone D, Liu X *et al.* (2019): A High-Resolution Luminescent Assay for Rapid and Continuous Monitoring of Protein Translocation across Biological Membranes. *Journal of molecular biology* 431 (8):1689–1699.

Perna AM, Rodrigues T, Schmidt TP, Böhm M, Stutz K, Reker D *et al.* (2015): Fragment-Based De Novo Design Reveals a Small-Molecule Inhibitor of Helicobacter Pylori HtrA. *Angewandte Chemie (International ed. in English)* 54 (35):10244–10248.

Pfannkuch L, Hurwitz R, Traulsen J, Sigulla J, Poeschke M, Matzner L *et al.* (2019): ADP heptose, a novel pathogen-associated molecular pattern identified in Helicobacter pylori. *FASEB journal : official publication of the Federation of American Societies for Experimental Biology* 33 (8):9087–9099.

Pham KT, Weiss E, Jiménez Soto LF, Breithaupt U, Haas R, Fischer W (2012): CagI is an essential component of the Helicobacter pylori Cag type IV secretion system and forms a complex with CagL. *PLOS ONE* 7 (4):e35341.

Püls J, Fischer W, Haas R (2002): Activation of Helicobacter pylori CagA by tyrosine phosphorylation is essential for dephosphorylation of host cell proteins in gastric epithelial cells. *Molecular microbiology* 43 (4):961–969.

Pushpakom S, Iorio F, Eyers PA, Escott KJ, Hopper S, Wells A *et al.* (2019): Drug repurposing: progress, challenges and recommendations. *Nat Rev Drug Discov* 18 (1):41–58.

Radics J, Königsmaier L, Marlovits TC (2014): Structure of a pathogenic type 3 secretion system in action. *Nat Struct Mol Biol* 21 (1):82–87.

Rai N, Muthukumaran R, Amutha R (2018): Identification of inhibitor against H. pylori HtrA protease using structure-based virtual screening and molecular dynamics simulations approaches. *Microbial pathogenesis* 118:365–377.

Redzej A, Ukleja M, Connery S, Trokter M, Felisberto-Rodrigues C, Cryar A *et al.* (2017): Structure of a VirD4 coupling protein bound to a VirB type IV secretion machinery. *The EMBO Journal* 36 (20):3080–3095.

Rehm T, Rothemund M, Bär A, Dietel T, Kempe R, Kostrhunova H *et al.* (2018): N,N-Dialkylbenzimidazol-2-ylidene platinum complexes - effects of alkyl residues and ancillary cis-ligands on anticancer activity. *Dalton transactions (Cambridge, England : 2003)* 47 (48):17367–17381.

Rehm T, Rothemund M, Dietel T, Kempe R, Schobert R (2019): Synthesis, structures and cytotoxic effects in vitro of cis- and trans-PtIVCl4(NHC)2 complexes and their PtII precursors. *Dalton transactions (Cambridge, England : 2003)* 48 (43):16358–16365.

Rehm T, Rothemund M, Muenzner JK, Noor A, Kempe R, Schobert R (2016): Novel cis-(NHC)1(NHC)2(L)Clplatinum(ii) complexes - synthesis, structures, and anticancer activities. *Dalton transactions (Cambridge, England : 2003)* 45 (39):15390–15398.

Ren S, Higashi H, Lu H, Azuma T, Hatakeyama M (2006): Structural basis and functional consequence of Helicobacter pylori CagA multimerization in cells. *The Journal of biological chemistry* 281 (43):32344–32352.

Rimbara E, Noguchi N, Kawai T, Sasatsu M (2008): Mutations in penicillin-binding proteins 1, 2 and 3 are responsible for amoxicillin resistance in Helicobacter pylori. *The Journal of antimicrobial chemotherapy* 61 (5):995–998.

Rocha CRR, Silva MM, Quinet A, Cabral-Neto JB, Menck CFM (2018): DNA repair pathways and cisplatin resistance: an intimate relationship. *Clinics (Sao Paulo, Brazil)* 73 (suppl 1):e478s.

Rosenberg B (1985): Charles F. Kettring prize. Fundamental studies with cisplatin. *Cancer* 55 (10):2303–2316.

Rosenberg B, Van Camp L, Krigas T (1965): Inhibition of cell division in Escherichia coli by electrolysis products from a platinum electrode. *Nature* 205:698–699.

Rosenberg B, Van Camp L, Trosko JE, Mansour VH (1969): Platinum compounds: a new class of potent antitumour agents. *Nature* 222 (5191):385–386.

Rotsaert FAJ, Ding MG, Trumpower BL (2008): Differential efficacy of inhibition of mitochondrial and bacterial cytochrome bc1 complexes by center N inhibitors antimycin, ilicicolin H and funiculosin. *Biochimica et biophysica acta* 1777 (2):211–219.

Saadat I, Higashi H, Obuse C, Umeda M, Murata-Kamiya N, Saito Y *et al.* (2007): Helicobacter pylori CagA targets PAR1/MARK kinase to disrupt epithelial cell polarity. *Nature* 447 (7142):330–333.

Salama NR, Hartung ML, Müller A (2013): Life in the human stomach: persistence strategies of the bacterial pathogen Helicobacter pylori. *Nat Rev Microbiol* 11 (6):385–399.

Salaün L, Linz B, Suerbaum S, Saunders NJ (2004): The diversity within an expanded and redefined repertoire of phase-variable genes in Helicobacter pylori. *Microbiology (Reading, England)* 150 (Pt 4):817–830.

Sato Y, Fukai S (2015): Crystal structure of FAAP20 UBZ domain in complex with Lys63-linked diubiquitin.

Savoldi A, Carrara E, Graham DY, Conti M, Tacconelli E (2018): Prevalence of Antibiotic Resistance in Helicobacter pylori: A Systematic Review and Meta-analysis in World Health Organization Regions. *Gastroenterology* 155 (5):1372-1382.e17.

Savvides SN, Yeo HJ, Beck MR, Blaesing F, Lurz R, Lanka E *et al.* (2003): VirB11 ATPases are dynamic hexameric assemblies: new insights into bacterial type IV secretion. *The EMBO Journal* 22 (9):1969–1980.

Sayer JR, Walldén K, Pesnot T, Campbell F, Gane PJ, Simone M *et al.* (2014): 2- and 3-substituted imidazo1,2-apyrazines as inhibitors of bacterial type IV secretion. *Bioorganic & Medicinal Chemistry* 22 (22):6459–6470.

Scarlato V, Delany I, Spohn G, Beier D (2001): Regulation of transcription in Helicobacter pylori: simple systems or complex circuits? *International Journal of Medical Microbiology* 291 (2):107–117.

Schindele F (2017): Development and application of a novel Cag type IV secretion reporter assay in Helicobacter pylori. Ludwig-Maximilians-Universität München.

Schindele F, Weiss E, Haas R, Fischer W (2016): Quantitative analysis of CagA type IV secretion by Helicobacter pylori reveals substrate recognition and translocation requirements. *Molecular microbiology* 100 (1):188–203.

Schlumberger MC, Müller AJ, Ehrbar K, Winnen B, Duss I, Stecher B, Hardt WD (2005): Real-time imaging of type III secretion: Salmonella SipA injection into host cells. *Proceedings of the National Academy of Sciences of the United States of America* 102 (35):12548–12553.

Schmees C, Prinz C, Treptau T, Rad R, Hengst L, Voland P *et al.* (2007): Inhibition of T-cell proliferation by Helicobacter pylori gamma-glutamyl transpeptidase. *Gastroenterology* 132 (5):1820–1833.

Schmidt HMA, Andres S, Nilsson C, Kovach Z, Kaakoush NO, Engstrand L *et al.* (2010): The cag PAI is intact and functional but HP0521 varies significantly in Helicobacter pylori isolates from Malaysia and Singapore. *Eur J Clin Microbiol Infect Dis* 29 (4):439–451.

Schreiber S, Bücker R, Groll C, Azevedo-Vethacke M, Garten D, Scheid P *et al.* (2005): Rapid loss of motility of Helicobacter pylori in the gastric lumen in vivo. *Infection and immunity* 73 (3):1584–1589.

Schroeder GN (2017): The Toolbox for Uncovering the Functions of Legionella Dot/Icm Type IVb Secretion System Effectors: Current State and Future Directions. *Front. Cell. Infect. Microbiol.* 7:528.

Schwinn MK, Machleidt T, Zimmerman K, Eggers CT, Dixon AS, Hurst R *et al.* (2018): CRISPR-Mediated Tagging of Endogenous Proteins with a Luminescent Peptide. *ACS chemical biology* 13 (2):467–474.

Segal ED, Cha J, Lo J, Falkow S, Tompkins LS (1999): Altered states: involvement of phosphorylated CagA in the induction of host cellular growth changes by Helicobacter pylori. *Proceedings of the National Academy of Sciences of the United States of America* 96 (25):14559–14564.

Selbach M, Moese S, Hauck CR, Meyer TF, Backert S (2002): Src is the kinase of the Helicobacter pylori CagA protein in vitro and in vivo. *The Journal of biological chemistry* 277 (9):6775–6778.

Senkovich OA, Yin J, Ekshyyan V, Conant C, Traylor J, Adegboyega P *et al.* (2011): Helicobacter pylori AlpA and AlpB bind host laminin and influence gastric inflammation in gerbils. *Infection and immunity* 79 (8):3106–3116.

Seyler RW, Olson JW, Maier RJ (2001): Superoxide dismutase-deficient mutants of Helicobacter pylori are hypersensitive to oxidative stress and defective in host colonization. *Infection and immunity* 69 (6):4034–4040.

Sgro GG, Costa TRD, Cenens W, Souza DP, Cassago A, Coutinho de Oliveira L *et al.* (2018): Cryo-EM structure of the bacteria-killing type IV secretion system core complex from Xanthomonas citri. *Nat Microbiol* 3 (12):1429–1440.

Shaffer CL, Good JAD, Kumar S, Krishnan KS, Gaddy JA, Loh JT *et al.* (2016): Peptidomimetic Small Molecules Disrupt Type IV Secretion System Activity in Diverse Bacterial Pathogens. *mBio* 7 (2):e00221-16.

Sharma CM, Hoffmann S, Darfeuille F, Reignier J, Findeiss S, Sittka A *et al.* (2010): The primary transcriptome of the major human pathogen Helicobacter pylori. *Nature* 464 (7286):250–255.

Sharma P, Teixeira de Mattos MJ, Hellingwerf KJ, Bekker M (2012): On the function of the various quinone species in Escherichia coli. *The FEBS journal* 279 (18):3364–3373.

Sheedlo MJ, Chung JM, Sawhney N, Durie CL, Cover TL, Ohi MD, Lacy DB (2020): Cryo-EM reveals species-specific components within the Helicobacter pylori Cag type IV secretion system core complex. *eLife Sciences Publications, Ltd*, 9/2/2020. https://elifesciences.org/articles/59495, (accessed 12/30/2020).

Smith MA, Coinçon M, Paschos A, Jolicoeur B, Lavallée P, Sygusch J, Baron C (2012): Identification of the binding site of Brucella VirB8 interaction inhibitors. *Chemistry & Biology* 19 (8):1041–1048.

Smith MA, Finel M, Korolik V, Mendz GL (2000): Characteristics of the aerobic respiratory chains of the microaerophiles Campylobacter jejuni and Helicobacter pylori. *Archives of microbiology* 174 (1-2):1–10.

Spohn G, Beier D, Rappuoli R, Scarlato V (1997): Transcriptional analysis of the divergent cagAB genes encoded by the pathogenicity island of Helicobacter pylori. *Molecular microbiology* 26 (2):361–372.

Spohn G, Scarlato V (2001): Chapter 21: Motility, Chemotaxis, and Flagella. In: Harry L. T. Mobley, George L. Mendz und Stuart L. Hazell (Hg.): Helicobacter pylori. Physiology and Genetics. Washington, DC: ASM Press.

Srikhanta YN, Gorrell RJ, Steen JA, Gawthorne JA, Kwok T, Grimmond SM *et al.* (2011): Phasevarion mediated epigenetic gene regulation in Helicobacter pylori. *PLOS ONE* 6 (12):e27569.

Stein SC, Faber E, Bats SH, Murillo T, Speidel Y, Coombs N, Josenhans C (2017): Helicobacter pylori modulates host cell responses by CagT4SS-dependent translocation of an intermediate metabolite of LPS inner core heptose biosynthesis. *PLoS pathogens* 13 (7):e1006514.

Steiner TM, Lettl C, Schindele F, Goebel W, Haas R, Fischer W, Eisenreich W (2021): Substrate usage determines carbon flux via the citrate cycle in Helicobacter pylori. *Molecular microbiology*.

Stolte M, Bayerdörffer E, Morgner A, Alpen B, Wündisch T, Thiede C, Neubauer A (2002): Helicobacter and gastric MALT lymphoma. *Gut* 50 Suppl 3 (suppl 3):III19-24.

Strauch KL, Beckwith J (1988): An Escherichia coli mutation preventing degradation of abnormal periplasmic proteins. *Proceedings of the National Academy of Sciences of the United States of America* 85 (5):1576–1580.

Suerbaum S, Josenhans C (2007): Helicobacter pylori evolution and phenotypic diversification in a changing host. *Nature reviews. Microbiology* 5 (6):441–452.

Suerbaum S, Josenhans C, Sterzenbach T, Drescher B, Brandt P, Bell M *et al.* (2003): The complete genome sequence of the carcinogenic bacterium Helicobacter hepaticus. *Proceedings of the National Academy of Sciences of the United States of America* 100 (13):7901–7906.

Suerbaum S, Michetti P (2002): Helicobacter pylori infection. *The New England journal of medicine* 347 (15):1175–1186.

Sulavik MC, Houseweart C, Cramer C, Jiwani N, Murgolo N, Greene J *et al.* (2001): Antibiotic susceptibility profiles of Escherichia coli strains lacking multidrug efflux pump genes. *Antimicrobial agents and chemotherapy* 45 (4):1126–1136.

Sutton P, Boag JM (2019): Status of vaccine research and development for Helicobacter pylori. *Vaccine* 37 (50):7295–7299.

Sutton P, Chionh YT (2013): Why can't we make an effective vaccine against Helicobacter pylori? *Expert review of vaccines* 12 (4):433–441.

Suzuki M, Mimuro H, Kiga K, Fukumatsu M, Ishijima N, Morikawa H *et al.* (2009): Helicobacter pylori CagA phosphorylation-independent function in epithelial proliferation and inflammation. *Cell Host & Microbe* 5 (1):23–34.

Ta LH, Hansen LM, Sause WE, Shiva O, Millstein A, Ottemann KM *et al.* (2012): Conserved transcriptional unit organization of the cag pathogenicity island among Helicobacter pylori strains. *Frontiers in cellular and infection microbiology* 2:46.

Tacconelli E, Carrara E, Savoldi A, Harbarth S, Mendelson M, Monnet DL *et al.* (2018): Discovery, research, and development of new antibiotics: the WHO priority list of antibiotic-resistant bacteria and tuberculosis. *The Lancet Infectious Diseases* 18 (3):318–327.

Tanaka H, Yoshida M, Nishiumi S, Ohnishi N, Kobayashi K, Yamamoto K *et al.* (2010): The CagA protein of Helicobacter pylori suppresses the functions of dendritic cell in mice. *Archives of biochemistry and biophysics* 498 (1):35–42.

Tarsia C, Danielli A, Florini F, Cinelli P, Ciurli S, Zambelli B (2018): Targeting Helicobacter pylori urease activity and maturation: In-cell high-throughput approach for drug discovery. *Biochimica et biophysica acta. General subjects* 1862 (10):2245–2253.

Tatusov RL, Koonin EV, Lipman DJ (1997): A genomic perspective on protein families. *Science (New York, N.Y.)* 278 (5338):631–637.

Taylor-Robinson D, Bébéar C (1997): Antibiotic susceptibilities of mycoplasmas and treatment of mycoplasmal infections. *The Journal of antimicrobial chemotherapy* 40 (5):622–630.

Tegtmeyer N, Moodley Y, Yamaoka Y, Pernitzsch SR, Schmidt V, Traverso FR *et al.* (2016): Characterisation of worldwide Helicobacter pylori strains reveals genetic conservation and essentiality of serine protease HtrA. *Molecular microbiology* 99 (5):925–944.

Tenguria S, Ansari SA, Khan N, Ranjan A, Devi S, Tegtmeyer N *et al.* (2014): Helicobacter pylori cell translocating kinase (CtkA/JHP0940) is pro-apoptotic in mouse macrophages and acts as auto-phosphorylating tyrosine kinase. *International journal of medical microbiology : IJMM* 304 (8):1066–1076.

Terry K, Williams SM, Connolly L, Ottemann KM (2005): Chemotaxis plays multiple roles during Helicobacter pylori animal infection. *Infection and immunity* 73 (2):803–811.

Tharmalingam N, Kim SH, Park M, Woo HJ, Kim HW, Yang JY *et al.* (2014): Inhibitory effect of piperine on Helicobacter pylori growth and adhesion to gastric adenocarcinoma cells. *Infectious Agents and Cancer* 9 (1):43.

Tocilescu MA, Fendel U, Zwicker K, Kerscher S, Brandt U (2007): Exploring the ubiquinone binding cavity of respiratory complex I. *The Journal of biological chemistry* 282 (40):29514–29520.

Trokter M, Waksman G (2018): Translocation through the Conjugative Type IV Secretion System Requires Unfolding of Its Protein Substrate. *Journal of bacteriology* 200 (6).

Tsang YH, Lamb A, Romero-Gallo J, Huang B, Ito K, Peek RM *et al.* (2010): Helicobacter pylori CagA targets gastric tumor suppressor RUNX3 for proteasome-mediated degradation. *Oncogene* 29 (41):5643–5650.

Tseng Y, Wu D, Chang C, Kuo C, Yang Y, Jan C *et al.* (2009): Amoxicillin resistance with beta-lactamase production in Helicobacter pylori. *European journal of clinical investigation* 39 (9):807–812.

Tsutsumi R, Higashi H, Higuchi M, Okada M, Hatakeyama M (2003): Attenuation of Helicobacter pylori CagA x SHP-2 signaling by interaction between CagA and C-terminal Src kinase. *The Journal of biological chemistry* 278 (6):3664–3670.

Tummuru MK, Cover TL, Blaser MJ (1993): Cloning and expression of a high-molecular-mass major antigen of Helicobacter pylori: evidence of linkage to cytotoxin production. *Infection and immunity* 61 (5):1799–1809.

Unden G, Bongaerts J (1997): Alternative respiratory pathways of Escherichia coli: energetics and transcriptional regulation in response to electron acceptors. *Biochimica et Biophysica Acta (BBA) - Bioenergetics* 1320 (3):217–234.

Van Duijkeren E, Schink AK, Roberts MC, Wang Y, Schwarz S (2018): Mechanisms of Bacterial Resistance to Antimicrobial Agents. In: Stefan Schwarz, Lina Maria Cavaco, Jianzhong Shen und Frank M. Aarestrup (Hg.): Antimicrobial resistance in bacteria from livestock and companion animals. Washington, DC: ASM Press:51–82.

Vannini A, Roncarati D, Spinsanti M, Scarlato V, Danielli A (2014): In depth analysis of the Helicobacter pylori cag pathogenicity island transcriptional responses. *PloS one* 9 (6):e98416.

Varga MG, Shaffer CL, Sierra JC, Suarez G, Piazuelo MB, Whitaker ME *et al.* (2016): Pathogenic Helicobacter pylori strains translocate DNA and activate TLR9 via the cancer-associated cag type IV secretion system. *Oncogene* 35 (48):6262–6269.

Versalovic J, Osato MS, Spakovsky K, Dore MP, Reddy R, Stone GG *et al.* (1997): Point mutations in the 23S rRNA gene of Helicobacter pylori associated with different levels of clarithromycin resistance. *The Journal of antimicrobial chemotherapy* 40 (2):283–286.

Viala J, Chaput C, Boneca IG, Cardona A, Girardin SE, Moran AP *et al.* (2004): Nod1 responds to peptidoglycan delivered by the Helicobacter pylori cag pathogenicity island. *Nat Immunol* 5 (11):1166–1174.

Waksman G, Orlova EV (2014): Structural organisation of the type IV secretion systems. *Current Opinion in Microbiology* 17:24–31.

Wallden K, Rivera-Calzada A, Waksman G (2010): Type IV secretion systems: versatility and diversity in function. *Cellular Microbiology* 12 (9):1203–1212.

Wang D, Lippard SJ (2005): Cellular processing of platinum anticancer drugs. *Nat Rev Drug Discov* 4 (4):307–320.

Wang G, Alamuri P, Maier RJ (2006): The diverse antioxidant systems of Helicobacter pylori. *Molecular microbiology* 61 (4):847–860.

Wang G, Wilson TJ, Jiang Q, Taylor DE (2001): Spontaneous mutations that confer antibiotic resistance in Helicobacter pylori. *Antimicrobial agents and chemotherapy* 45 (3):727–733.

Wang X, Ling F, Wang H, Yu M, Zhu H, Chen C *et al.* (2016): The Helicobacter pylori Cag Pathogenicity Island Protein Cag1 is Associated with the Function of T4SS. *Curr Microbiol* 73 (1):22–30.

Ward JE, Akiyoshi DE, Regier D, Datta A, Gordon MP, Nester EW (1988): Characterization of the virB operon from an Agrobacterium tumefaciens Ti plasmid. *The Journal of biological chemistry* 263 (12):5804–5814.

Warnau J, Sharma V, Gamiz-Hernandez AP, Di Luca A, Haapanen O, Vattulainen I *et al.* (2018): Redox-coupled quinone dynamics in the respiratory complex I. *PNAS* 115 (36):E8413-E8420.

Warren JR, Marshall B (1983): Unidentified curved bacilli on gastric epithelium in active chronic gastritis. *Lancet (London, England)* 1 (8336):1273–1275.

Wen Y, Huang H, Tang T, Yang H, Wang X, Huang X *et al.* (2021): AI-2 represses CagA expression and bacterial adhesion, attenuating the Helicobacter pylori-induced inflammatory response of gastric epithelial cells. *Helicobacter*:e12778.

Westerhausen S, Nowak M, Torres-Vargas CE, Bilitewski U, Bohn E, Grin I, Wagner S (2020): A NanoLuc luciferase-based assay enabling the real-time analysis of protein secretion and injection by bacterial type III secretion systems. *Molecular microbiology* 113 (6):1240–1254.

Wexselblatt E, Yavin E, Gibson D (2012): Cellular interactions of platinum drugs. *Inorganica Chimica Acta* 393:75–83.

Weyermann M, Rothenbacher D, Brenner H (2009): Acquisition of Helicobacter pylori infection in early childhood: independent contributions of infected mothers, fathers, and siblings. *The American journal of gastroenterology* 104 (1):182–189.

WHO (2019): Antibacterial agents in clinical development: an analysis of the antibacterial clinical development pipeline. Geneva: World Health Organization (Licence: CC BY-NC-SA 3.0 IGO).

Wilharm G, Lehmann V, Krauss K, Lehnert B, Richter S, Ruckdeschel K *et al.* (2004): Yersinia enterocolitica type III secretion depends on the proton motive force but not on the flagellar motor components MotA and MotB. *Infection and immunity* 72 (7):4004–4009.

Woon AP, Tohidpour A, Alonso H, Saijo-Hamano Y, Kwok T, Roujeinikova A (2013): Conformational analysis of isolated domains of Helicobacter pylori CagA. *PloS one* 8 (11):e79367.

Wotherspoon AC (1998): Helicobacter pylori infection and gastric lymphoma. *British medical bulletin* 54 (1):79–85.

Wroblewski LE, Peek RM, Wilson KT (2010): Helicobacter pylori and gastric cancer: factors that modulate disease risk. *Clinical Microbiology Reviews* 23 (4):713–739.

Wüstner S, Anderl F, Wanisch A, Sachs C, Steiger K, Nerlich A *et al.* (2017): Helicobacter pylori γ-glutamyl transferase contributes to colonization and differential recruitment of T cells during persistence. *Scientific Reports* 7 (1):13636.

Yamaoka Y, Kikuchi S, El-Zimaity HMT, Gutierrez O, Osato MS, Graham DY (2002): Importance of Helicobacter pylori oipA in clinical presentation, gastric inflammation, and mucosal interleukin 8 production. *Gastroenterology* 123 (2):414–424.

Yamaoka Y, Kwon DH, Graham DY (2000): A M(r) 34,000 proinflammatory outer membrane protein (oipA) of Helicobacter pylori. *Proceedings of the National Academy of Sciences of the United States of America* 97 (13):7533–7538.

Yao Y, Shen Y, Zhu L, Ni Y, Wang H, Shao S (2018): Preliminary study and bioinformatics analysis on the potential role of CagQ in type IV secretion system of H.pylori. *Microbial pathogenesis* 116:1–7.

Yeh YC, Kuo HY, Chang WL, Yang HB, Lu CC, Cheng HC *et al.* (2019): H. pylori isolates with amino acid sequence polymorphisms as presence of both HtrA-L171 & CagL-Y58/E59 increase the risk of gastric cancer. *Journal of Biomedical Science* 26 (1):4.

Yuan M, Chua SL, Liu Y, Drautz-Moses DI, Yam JKH, Aung TT *et al.* (2018): Repurposing the anticancer drug cisplatin with the aim of developing novel Pseudomonas aeruginosa infection control agents. *Beilstein J. Org. Chem.* 14 (1):3059–3069.

Yun NR, San KY, Bennett GN (2005): Enhancement of lactate and succinate formation in adhE or pta-ackA mutants of NADH dehydrogenase-deficient Escherichia coli. *Journal of applied microbiology* 99 (6):1404–1412.

Zabaleta J, McGee DJ, Zea AH, Hernández CP, Rodriguez PC, Sierra RA *et al.* (2004): Helicobacter pylori arginase inhibits T cell proliferation and reduces the expression of the TCR zeta-chain (CD3zeta). *Journal of immunology (Baltimore, Md. : 1950)* 173 (1):586–593.

Zarzecka U, Harrer A, Zawilak-Pawlik A, Skorko-Glonek J, Backert S (2019): Chaperone activity of serine protease HtrA of Helicobacter pylori as a crucial survival factor under stress conditions. *Cell communication and signaling : CCS* 17 (1):161.

Zeitler A, Gerrer K, Haas R, Jiménez-Soto L (2017): Host cell resistance to CagA translocation is as variable as Helicobacter pylori. *Matters* 3 (10):e201706000006.

Zhang L, Zheng Y, Callahan B, Belfort M, Liu Y (2011): Cisplatin inhibits protein splicing, suggesting inteins as therapeutic targets in mycobacteria. *J. Biol. Chem.* 286 (2):1277–1282.

Zhao Q, Busch B, Jiménez-Soto LF, Ishikawa-Ankerhold H, Massberg S, Terradot L *et al.* (2018): Integrin but not CEACAM receptors are dispensable for Helicobacter pylori CagA translocation. *PLOS Pathogens* 14 (10):e1007359.

Zhong Y, Anderl F, Kruse T, Schindele F, Jagusztyn-Krynicka EK, Fischer W *et al.* (2016): Helicobacter pylori HP0231 Influences Bacterial Virulence and Is Essential for Gastric Colonization. *PloS one* 11 (5):e0154643.

Zhou Y, Joubran C, Miller-Vedam L, Isabella V, Nayar A, Tentarelli S, Miller A (2015): Thinking outside the "bug": a unique assay to measure intracellular drug penetration in gram-negative bacteria. *Analytical Chemistry* 87 (7):3579–3584.

Zimmermann S, Pfannkuch L, Al-Zeer MA, Bartfeld S, Koch M, Liu J *et al.* (2017): ALPK1- and TIFA-Dependent Innate Immune Response Triggered by the Helicobacter pylori Type IV Secretion System. *Cell reports* 20 (10):2384–2395.

Acknowledgment

My sincere thanks are given to Prof. Dr. Rainer Haas for providing me the opportunity to work on this exciting project. Thank you for your continuous scientific support. I enjoyed being part of your working group from the first day on.

Equally, I would like to express my huge thanks to PD Dr. Wolfgang Fischer. Thank you very much for supervising my thesis! Thank you for always having time for constructive and instructive discussions and sharing your knowledge. Thank you for your excellent scientific input and advice, and the continuous support to elaborate and implement my own ideas.

I could not have completed my thesis in such a pleasant way without Barbara and Evelyn. I want to thank you for all the lively conversations on various (scientific) topics and on how to solve technical issues in the lab. Thank you for always having a sympathetic ear for me and for supporting me. Thank you for the good time and the funny hours.
My thanks go to all current and former colleagues of the AG Haas, and the employees of the MVP who always helped with words and deeds. Particularly, I want to thank Nikola and Steffi for the diligent lab work during the development of the HiBiT-CagA translocation assay and the characterization of HiBiT-CagB. Furthermore, I wish to thank Dr. Franziska Schindele who started the inhibitor projects. Thank you all for the friendly and cooperatively working atmosphere and the very entertaining lunch breaks.

It is my pleasure to give thanks to all cooperation partners who were substantially involved in the success of my thesis:
Thank you, Thomas and Prof. Dr. Wolfgang Eisenreich, for the enjoyable and highly reliable collaboration on the *H. pylori* metabolism.
Thank you, Dr. Matthias Witschel, Prof. Dr. Ursula Bilitewski, and Prof. Dr. Rainer Schobert, for continuous supply with novel inhibitors and the valuable scientific input.
Thank you, Prof. Dr. Bärbel Stecher and Diana, for providing the opportunity to test “my” compounds, and the excellent technical assistance.
Thank you, Prof. Dr. Ruth Brack-Werner, Prof. Dr. Gerd Hummer, and Reza, for helpful discussions, support with molecular modelling algorithms and additional small molecule inhibitors, and especially for providing your knowledge on the respiratory chain complex I.

Above all, I wish to thank my family and friends, especially my parents, Elias, Jacob, Rainer, and Michael. You are the ones I can always rely on and ask for help. Thank you for encouraging, supporting, and cheering up.